STATISTICAL DESCRIPTION OF TURBULENT REACTING MEDIA

by
Kexin Liu
MSc, BEng

Submitted in accordance with the requirements for the degree of
Doctor of Philosophy

University of Leeds
School of Mechanical Engineering

March, 2002

The candidate confirms that the work submitted is his own and that appropriate credit has been given where reference has been made to the work of others.

ABSTRACT

Present work concerns the interaction of chemistry and turbulence in a turbulent reacting flow. Both self-ignition and flame propagation are studied.

For self-ignition study, the combined effects of temperature/concentration inhomogeneities and turbulence were studied numerically. For this purpose two statistic turbulent combustion models, namely Linear Eddy Model (LEM) and Reference Scalar Field (RSF), were applied for simulations of statistically homogeneous reacting media, because these two models allow the calculation of the averaged reaction rates in fluctuating media from the first principles. Self-ignition delays, species concentration and temperature evolutions were computed for three kinds of initial conditions, where temperature pdfs were given as Dirac's δ peak pdf, rectangular and bimodal shapes. The results obtained from the two models mentioned above were compared. The effect of heat loss on ignition delay was also studied with the RSF model.

For the study of turbulent flame propagation, RSF model was applied to the problem of 1-D flame propagation in a spherical fan-stirred bomb. This problem is selected because of its simplest possible flow field, hence reduced computation cost and easy implementation. For turbulent convection different conditionally averaged velocity models were introduced and evaluated. Pressure during gas explosion, and averaged mean values such as temperature and species concentration were calculated. The evolution of temperature pdf was also obtained from statistics of the reference scalar field. Flame radii and turbulent mass burning rates were determined from the calculated pressure rise and the mass burning rates were compared with two existing correlations of Bradley *et al.* and Zimont as well as with measurements.

Two types of reactive mixtures were studied, one was the methane/air flame and the other one was DTBP/N_2 decomposition flame. Experiments with both mixtures were carried out in a spherical fan-stirred bomb. In particular, pressure trace during explosion was recorded and this provided reference data for the modelling studies. Methane/air combustion was simulated with a reduced two-step chemical kinetics mechanism instead of the single-step kinetics commonly used for turbulent reacting flows modelling. The two-step kinetics employed was developed according to the

experimental observations of two-stage oxidation of hydrocarbons, in which the first stage is related to the consumption of the fuel and the second stage represents the oxidation of CO and H_2. Firstly, the kinetics was "calibrated" in the laminar situations to produce a reasonable agreement with measured flame speed. Then the kinetics was used with turbulent models to simulate the turbulent explosions. While DTBP/N_2 decomposition flame is described by a single step kinetics and the reaction constants have been well-studied. So for simulation of DTBP/N_2 flame, any ambiguity resulting in uncertainties in chemical mechanism is avoided.

ACKNOWLEDGEMENTS

I would like to express my sincere thanks to my supervisor Dr. A.A. Burluka, for his insight, guidance and friendship throughout my PhD study and more recently for his advice during the writing up period, and for his patience reading my drafts. I would also like to thank Prof. C.G.W. Sheppard for his guidance during the work.

I am grateful to Dr. R. Woolley for his friendship, his help for the experiments, also for his kindness providing some measurement data for comparisons; Dr. M. Lawes for reading Chapter 3 and 4; and Professor D. Bradley for useful discussions.

Big thanks are due to Prof. J.F. Griffiths, School of Chemistry, Leeds University, for the numerous discussions about the auto-ignition, chemical kinetics and more recently for providing the chemical kinetics data for DTBP, and DTBP fuel itself.

I thank the former and current PhD students: Drs. J. Yu, M. Perkins, Mr, A. Smallbone, M. Ormsby and C. Wu for their friendship.

Financial assistance from the schemes of ORS (Overseas Research Studentship), Tetley/Lupton, and the School of Mechanical Engineering is gratefully acknowledged.

Finally I would like to express my thanks to my parents and my wife for their endless support and love.

FIGURES

TABLES

NOMENCLATURE

a		Coefficient for discretised equations
A	cm^2	Flame surface area
A		Model constant in Eq. (4.15)
A_i		Pre-exponential coefficient for k_i
c		Progress variable
c_1		Model constant
c_2		Model constant in Eq. (4.2)
c_p	$J/mole \cdot K$	Specific heat at constant pressure
D		Diffusion flux
D	cm^2/s	Diffusivity
Da		Damköhler number
D_M	cm^2/s	Molecular diffusivity
D_T	cm^2/s	Turbulent diffisivity
E	$J/mole$	Activation energy
F		Convection flux
$H(c)$		Heaviside fuction
ΔH^0_{298}	$kJ/mole$	Standard enthalpy of formation
k_i		Chemical reaction constants for step i
k	m^2/s^2	Kinetic energy
	$ergs/K$	Boltzmann constant
K		Karlovitz number
Le		Lewis number
L_b	mm	Markstein length
l_k	cm	Kolmogorov length scale
l_t	cm	Turbulence integral length scale
P	bar	Pressure
P		Probability
Pe		Numerical Peclet number

Pr		Prandtl number
Q	*kcal/mole*	Heat release
R_b	*cm*	Bomb radius
Re_t		Turbulent Reynolds number
R_u	*J/mole*	Universal gas constant
r	*cm*	Spherical coordinate, distance
S_n	*m/s*	Flame speed with stretch
S_s	*m/s*	Flame speed with zero stretch
S_t	*m/s*	Turbulent flame speed
T	*K*	Temperature
T_b	*K*	Boiling point
T_W	*K*	Wall temperature
t	*s*	Time
u	*m/s*	Gas velocity
u'	*m/s*	rms turbulent velocity
u_k'	*m/s*	Effective rms turbulent velocity
u_L	*m/s*	Laminar burning velocity with zero stretch
u_n	*m/s*	Laminar burning velocity with stretch
u_t	*m/s*	Turbulent burning velocity
V_b	cm^3	Bomb volume
w_i	*mole/mole·s* or *mole/*cm^3*·s*	Formation/disappearing rate due to chemical reaction for species *i*
W_i	*mole/mole·s* or *mole/*cm^3*·s*	Chemical reaction rate
	g/mole	Molecular weight
W_{mix}	*g/mole*	Mixture molecular weight
X		Statistical coordinate
x		Physical coordinate, distance
Y_i	*mole/mole*	Mole fraction of species *i*

Greek symbols

α	$1/s$	Flame stretch rate
$\delta(c)$		Dirac delta function
δ_L	mm	Laminar flame thickness
ε	m^2/s^3	Dissipation rate of kinetic energy
	$ergs$	Potential-energy constant
ϕ		Fuel/air equivalence ratio
ϕ		General property, may refer to velocity, temperature, or species concentration
γ_u		Ratio of specific heats
κ	cm^2/s	Thermal diffusivity
λ	mm	Taylor micro length scale
λ_{mix}	$g\text{-}cal/cm\cdot s$	Mixture thermal conductivity
ν	cm^2/s	Kinetic viscosity
ρ	kg/m^3	Density
σ	$\dot{A}$	Characteristic collision cross-section
τ_a	s	Character time scale related to scalar field
τ_c	s	Chemical time scale
τ_{ign}	s	Ignition delay
τ_k	s	Kolmogorov time scale
τ_t	s	Turbulence integral time scale
τ_w^*	s	Time scale related to heat loss
ω		Acentric factor
Ω		Dimensionless molecular diffusion collision integral

Subscripts

0	Initial condition
E	East node

e	East face
u	Unburnt gas stage
b	Burnt gas state
c	Critical state
eq	Equilibrium state
t	Turbulent condition
L	Laminar condition
N	North node
n	North face
P	Node P
S	South node
s	South face
W	West node
w	West face

Superscripts

0	Initial condition
n	n-th moment

Introduction

In this thesis the main effort is concentrated on the combustion in turbulent medium where the chemical compounds are mixed prior to combustion. This combustion regime is commonly termed as turbulent premixed combustion. Its prominent feature is that turbulence increases heat and mass transfer rate, and hence increases the chemical energy release rate and the power output. Unlike laminar premixed combustion where all fundamental principles are well understood, see *e.g.* Zel'dovich *et al.* (1985), the basic theory of turbulent premixed combustion is still to be built. It will be a very practical theory because turbulent combustion, more generally turbulent reacting flows, is encountered frequently in many practical applications, for example, in the internal combustion engines, chemical transformation in atmosphere, etc. To understand and predict the turbulent combustion is important in various aspects of economics, safety and environment.

It is very commonly assumed that similarly to laminar flame, within quite thick turbulent flame brush there may be distinguished thin reaction zones, sometimes called flame fronts. Following those ideas originating in Damköhler's (1940) theory, turbulence may affect combustion through two different mechanisms in a premixed medium: (1) the large-scale (compared to laminar flame thickness) wrinkling the flame front, thus increasing flame surface and promoting combustion, (2) small scale enhancing the heat and mass transfer.

However, when strength of fluctuations is above a certain level, a further increase in turbulence intensity would result only in a very moderate increase in combustion rate, and, ultimately flame quenching. All this is best illustrated in Borghi's (1984) diagram, representing various combustion regimes, including possible extinction, see below.

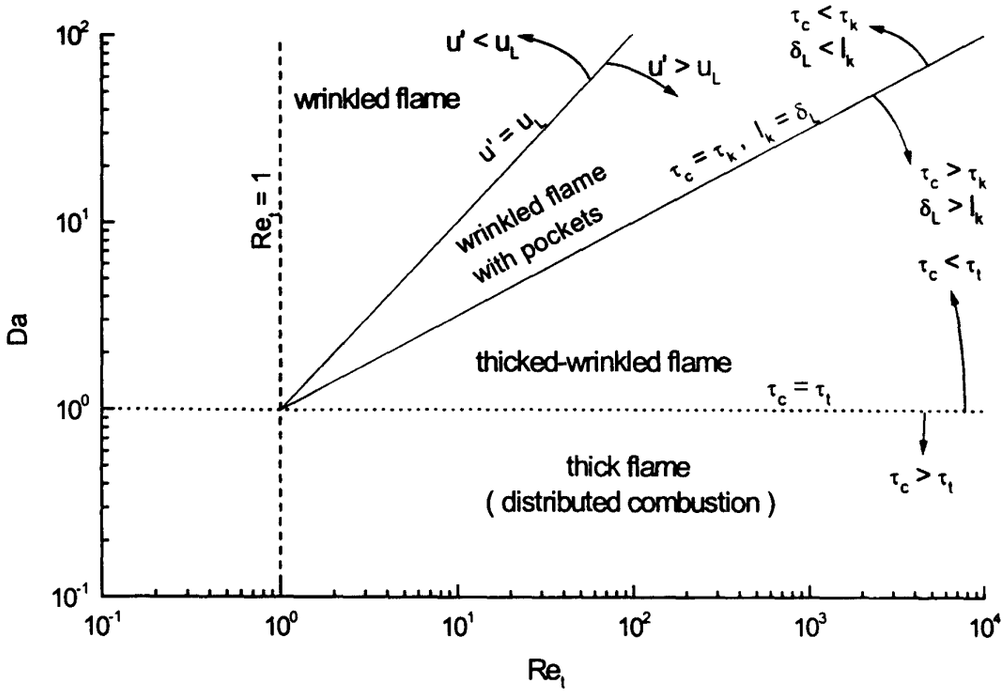

Premixed turbulent combustion regimes according to Borghi (1984)

It is obvious that in order to successfully predict turbulent burning velocity one needs a consideration of dynamic coupling between the turbulent flow and chemical reactions. This coupling may be summarised by stating that the turbulent flow field affects the structure and transport rate inside the flame, while concurrently heat release from the chemical reactions affects the turbulent flow field.

Some Important Parameters

In turbulent combustion, one can distinguish nondimensional parameters in terms of which various combustion regimes may be characterised. These important nondimensional parameters are the ratios of length-time-scales for velocity and scalar fields.

The length scales are:

1) turbulence integral length scale, l_t, roughly corresponding to a large eddy size
2) Kolmogorov length scale, l_k, characterises small scale turbulence, it can be estimated as $l_k = \left(\frac{\nu^3}{\varepsilon}\right)^{\frac{1}{4}}$, where ν is kinematic visicosity and ε is the turbulent

kinetic energy (TKE) dissipation rate expressed as $\varepsilon = \frac{u'^3}{l_t}$, where u' is the *rms* velocity fluctuation.

3) Laminar flame thickness δ_L

Any other characteristic length which may be encountered in the literature, *e.g.* Gibson or Taylor scales, may be expressed in terms of these three and Reynolds and Damköhler numbers. In definition of these numbers one can consider two characteristic magnitudes of velocity field: turbulence intensity u', which is *rms* fluctuation velocity, and laminar burning velocity u_L.

Characteristic time scales are:

1) Turbulence integral scale, τ_t, represents the large eddy turnover time, and it can be deduced from the integral scale and intensity as $\tau_t = l_t / u'$
2) Kolmogorov time scale, τ_k, which can be shown to be $\tau_k = (\nu/\varepsilon)^{1/2}$
3) Chemical time, τ_c, which can be estimated as $\tau_c = \frac{\delta_L}{u_L}$

Several dimensionless parameters can be defined from the variables introduced above, the most important being:

1) Reynolds number Re_t, $\mathrm{Re}_t = \frac{u' l_t}{\nu} = \frac{l_t}{\delta_L}\frac{u'}{u_L} = \left(\frac{l_t}{l_k}\right)^{\frac{4}{3}}$, where kinematic visicosity ν is expressed with laminar flame thickness and burning velocity as $\nu = \delta_L u_L$
2) Damköhler number *Da*, the ratio of integral time scale to chemical time scale, as $Da = \frac{\tau_t}{\tau_c} = \left(\frac{l_t}{\delta_L}\right) \Big/ \left(\frac{u'}{u_L}\right)$. This criterion serves to identify whether chemistry is "fast" or not. If *Da* >> 1, chemistry is termed as "fast", *Da* << 1 chemistry is "slow".
3) Karlovitz number *K*, which is a flame stretch factor, expressed as $K = \frac{u'}{u_l}\frac{\delta_L}{\lambda}$ where, λ is Taylor microscale related to integral length scale and Reynolds number as: $\frac{\lambda}{l_t} = c_1 \mathrm{Re}_t^{-0.5}$, c_1 is a constant for which Taylor (1935) gave $c_1 = \sqrt{\frac{15}{A}}$ where *A* is a

constant of the order of unity. Abdel-Gayed and Bradley *et al.* (1984) recommend $c_1 = \sqrt{40.4}$ for isotropic turbulence in bomb. So, $K = \frac{1}{c_1}\left(\frac{u'}{u_L}\right)^2 \mathrm{Re}_t^{-0.5} = \frac{1}{c_1}\frac{\tau_c}{\tau_K}$.

Pre-Mixed Turbulent Combustion Regimes

Turbulent reacting flow in a premixed medium has been studied for many years and much effort has been devoted to finding the flame structure and rate of combustion. Various premixed turbulent combustion regimes have been identified as function of l_t/δ_L and u'/u_L, *e.g.* Barrère (1974), or in terms of Re and Da, *e.g.* Borghi (1984). Following Borghi's work, the figure shown above is a graphical representation of different turbulent combustion regimes. There are four principal regimes: 1) wrinkled flame, 2) wrinkled flame with pockets, 3) thickened-wrinkled flame and 4) thick flame (or distributed reaction zone). It has to be noticed that the boundaries in this figure are only approximative, besides usually within a single device turbulence is non-uniform, therefore one can hardly attribute a point to a " practical device ". More detailed discussions about the regimes can be found in Borghi (1985, 1988). Also there are many modifications of this diagram, *e.g.* Peters (1986); these modifications however do not alter any essential physical idea.

Scope of This Thesis

It is clear that any general combustion model has to embrace quite a substantial range of l_t/δ_L and u'/u_L ratios in order to be successful. Thus, one cannot really rely upon the models where a particular flame structure is presumed, such as Bray (1990), Peters (1986) or Zimont (1979); instead one would need some kind of statistical description, *e.g.* O'Brien (1980).

The objective of present work is a statistical study of premixed turbulent reacting flow. Two statistical turbulence models have been tested, one is Linear Eddy Model (LEM) of Kerstein (1988), second is Reference Scalar Field (RSF) of Burluka and Borghi *et al.* (1997). These were used to study the turbulence effects on self-ignition as well as flame propagation in premixed mixture of methane-air. Finite chemical reaction rate was calculated with two-step kinetic scheme.

Chapter 1 introduces generalities on the modelling turbulent reacting flow. Emphasis is put on the laminar flamelet models, joint pdf models and the two statistical models of LEM and RSF.

Chapter 2 is auxiliary, it studies the laminar flame structure of premixed hydrocarbon mixture. Its main purpose is to assess the reduced two-step chemical kinetic mechanism used throughout this work for premixed methane/air flame. Calculations of self-ignition development and spherical laminar flame propagation are presented.

Chapter 3 is devoted to the interaction of turbulence and chemistry studied for self-ignition delays with this reduced two-step kinetics. Both LEM and RSF are used, and their predictions are analysed.

Chapter 4 presents a study of interaction of turbulence with chemistry as revealed in 1-D turbulent flame propagation in a spherical fan-stirred bomb. Only RSF model is used with the reduced two-step kinetics, and various expressions for conditionally averaged velocity.

Chapter 5 studies DTBP/N_2 decomposition flames, chosen due to their simple and clearly defined chemical kinetics and its constants. Laminar and turbulent flames propagation is studied, turbulence model used is the RSF model.

Chapter 6 is devoted to study the KPP theory to justify the procedures and computer codes used in *Chapters 2*, *4* and *5*.

Experimental study of turbulent flame propagation in a fan-stirred bomb for methane/Air flames is presented in *Appendix A*. Presented in *Appendix B* is the derivation of pressure rise model during flame propagating in the bomb, *Appendix C* is the comparison of the numerical methods used to "initiate" a flame, and *Appendix D* is the comparison of how various ways of molecular transport modelling affect flame propagation. *Appendix E* is the description of transport coefficients calculation.

Chapter 1

Modelling of Turbulent Reacting Flow

1.1 Introduction

In turbulent reacting flow, the chemical reaction rate is a highly non-linear function of temperature and/or species concentrations. At the same time turbulence in the flow enhances mixing of non-uniformities in species and temperature fields. When the rate of small scale mixing is less than the rates of chemical reaction, strong spatial and temporal fluctuations occur in the scalar quantities. The main question is then how to describe the influence of these fluctuations on the average rate of chemical transformations and heat release. In other words, turbulent combustion modelling should account for the interactions between the different range of length and time scales present in the flow. These turbulence-chemistry interactions are extremely important for the phenomena controlled by chemical kinetics, *e.g.* pollutant productions, ignition and extinction. The interaction between turbulence and chemical reaction is non-linear, that is why it is difficult to consider within moment closure method or large eddy simulation (LES). One thus needs a turbulent combustion submodel to treat the averaged reaction rate. A number of methodologies are suggested to overcome this special difficulty, such as flamelet approach (Peters, 1986, Cant and Bray, 1988, Bray and Peters, 1994), pdf method (O'Brien, 1980, Pope, 1985, Dopazo, 1994), conditional moment closure (CMC) (Klimenko and Bilger, 1999) *etc.* Of all the computational approaches, Direct Numerical Simulation (DNS) is particularly useful in increasing the basic understanding of the problem. However, DNS is still limited to simple geometries and low to moderate Reynolds number because of tremendous computation resources needed for.

1.2 Laminar Flamelet Approach

Laminar flametlet approach (Peters, 1986, Cant and Bray, 1988) has now been applied to most practical combustion systems using premixed combustion, such as petrol reciprocating engines, gas turbines and furnaces. Where the combustion occurs in the so-called flamelet regime, chemistry is fast compared to the turbulent transport process. As a result, the combustion occurs in thin layers, which separate the regions of unburnt reactants from fully burnt products. The principal assumption is that locally these layers are laminar flames, which propagate normally to itself, *i.e.* they follow Huygens principle. It is also sometimes admitted that these flamelets may be wrinkled and possibly torn by the turbulent motion. Formation of pockets of unburned mixture in the burnt gas is possible, while even stronger turbulence can cause flame extinction through high strain rates.

The laminar flamelet approach is based on the assumption that combustion rate and heat release in a turbulent flame can be calculated from the properties of an ensemble of the laminar flamelets embedded in the turbulent flow. The most difficult task in such modelling is then to establish a "library" of laminar flame properties (Bray, 1985, Cant and Bray, 1988), such as propagating speed, burning velocity, flame thickness, and reaction rate for a wide range of temperature, pressure and strain rates, *etc*, then turbulent reaction rate is calculated by building an appropriate ensemble of laminar flame properties from this "library". Such an establishment of the "library" is possible now because much achievement has been obtained in experimental as well as theoretical studies on the behaviour of laminar flames.

An alternative approach is to specify the form of an appropriate scalar probability density function, or pdf. For example, the presumed pdf in BM model (Bray and Moss, 1977) and its extension BML model (Bray *et al.*, 1981) as:

$$P(c;\vec{x}) = a(\vec{x})\delta(c) + \beta(\vec{x})\delta(1-c) + [H(c) - H(1-c)]\gamma(\vec{x})f(c,\vec{x}) \qquad (1.1)$$

where $\delta(c)$ and $H(c)$ are the Dirac delta and Heaviside functions, and the delta functions at $\hat{c}=0$ and 1 may be identified with the unburnt and fully burnt mixture, respectively. The function $f(c;\vec{x})$ is defined by the structure of the reaction zone and is conveniently normalized: $\int_0^1 f(\hat{c};\vec{x})\,d\hat{c}=1$. The coefficients $\alpha(\vec{x})$, $\beta(\vec{x})$ and $\gamma(\vec{x})$ are

the probabilities to meet the fresh mixture, burnt gas and the mixture undergoing the chemical transformation at the point x, respectively. It has been shown in the BML that the average rate of reaction is insensitive to a particular choice of $f(c;\bar{x})$ provided that $\gamma << 1$ and $f(c;\bar{x}) \neq \delta(c-\hat{c})$, $\hat{c} \neq 0,1$. This method can be used to study turbulent combustion phenomena where Damköhler number Da >> 1. One of the principle results obtained in the BML model is the recovery of the classical Eddy Break Up model of Spalding (Spalding, 1971) which is also formulated for the case of $\gamma << 1$, and which postulates that the average rate of heat release is proportional to the dissipation rate of temperature fluctuations. In terms of the progress variable $c(x,t)$ this reads:

$$\langle w \rangle = const\ \chi_c = const \frac{\langle c'^2 \rangle}{\tau_a}.$$

It has to be noted, however, that before any of the suggested flamelet theories could pretend to be general enough for practical purposes, it has to answer a number of currently un-addressed questions, such as effects of transient evolution of strain rate and flame surface curvature, or how to describe behaviour of compressed (*i.e.* subject to a negative strain) flamelets. Within this approach one particularly simple question also would be how to explain the effect of initial pressure on turbulent flame propagation. This means that in this approach $u_t \sim u_n$ for the same turbulence parameters and it results in u_t decreasing with initial pressure rise which contradicts the experiments which show that u_t either slowly increases with pressure rise or is independent on initial pressure, Kobayahsi *et al.* (1998).

1.3 Classical PDF methods

1.3.1 Methods Employing PDFs of Reactive Scalar

These methods do not presume a particular structure of the reaction zone, and the reaction rate terms are exact in resulting equations, see *e.g.* Pope (1985), O'Brien (1980). Below some general points of this approach are prescribed, for more details one may consult Pope (1985).

1.3.1.1 Probability Density Function (pdf)

Consider a stochastic variable ϕ and corresponding to it coordinate of phase space ψ, the probability $P(\phi)$ to meet an event of $\psi_1 \le \phi < \psi_2$ can be expressed as $P(\psi_1 < \phi < \psi_2) = F_\phi(\psi_2) - F_\phi(\psi_1)$, where $F_\phi(\psi)$ is the distribution function. The probability density function (pdf) of the stochastic variable $f_\phi(\psi)$ is defined as the derivative of the distribution function $F_\phi(\psi)$ as:

$$f_\phi(\psi) = \frac{d}{d\psi} F_\phi(\psi) \tag{1.2}$$

By integrating Eq. (1.2) between ψ_1 and ψ_2, another relationship between the pdf, and distribution function is obtained as:

$$\int_{\psi_1}^{\psi_2} f_\phi(\psi)\, d\psi = F_\phi(\psi_2) - F_\phi(\psi_1) = P(\psi_1 \le \phi < \psi_2) \tag{1.3}$$

In particular, for an infinitesimal region $d\psi$:

$$f_\phi(\psi)\, d\psi = F_\phi(\psi + d\psi) - F_\phi(\psi) = P(\psi \le \phi < \psi + d\psi) \tag{1.4}$$

Once the pdf is determined, other important parameters such as mean value, and its *rms* fluctuation can be calculated exactly.

The mean value known also as named mathematical expectation, is defined as:

$$\langle \phi \rangle = \int_{-\infty}^{\infty} \psi\, f_\phi(\psi)\, d\psi \tag{1.5}$$

More generally, the n-th moment is another important parameter which is defined as:

$$\langle \phi'^n \rangle = \int_{-\infty}^{\infty} \left(\psi - \langle \phi \rangle\right)^n f_\phi(\psi)\, d\psi \tag{1.6}$$

If n=1, one will find $\langle \phi' \rangle = 0$, that means the first moment about the mean value $\langle \phi \rangle$ is 0. The second moment $\langle \phi'^2 \rangle$ is so-called variance and $\sqrt{\langle \phi'^2 \rangle}$ is the so-called *rms* fluctuation.

1.3.1.2 Joint pdf

Similarly, consider another stochastic variable u and its coordinate V, the pdf $f_u(V)$ can be related to its distribution function $F_u(V)$ for an infinitesimal region dV as:

$$f_u(V)\,dV = F_u(V+dV) - F_u(V) = P(V \le u < V+dV) \tag{1.7}$$

The pdfs of $f_\phi(\psi)$ and $f_u(V)$ contain all the information of ϕ and u separately, but their knowledge does not contain sufficient information to find the probability of the simultaneous event of $\psi_1 \le \phi < \psi_2$ and $V_1 \le u < V_2$. This information can be provided by the joint pdf $f_{\phi,u}(V,\psi)$ which is defined as second derivative of its distribution function $F_{\phi,u}(\psi,V)$ as:

$$f_{\phi,u}(\psi,V) = \frac{\partial^2}{\partial\psi\partial V} F_{\phi,u}(\psi,V) \tag{1.8}$$

For an infinitesimal region ($d\psi$, dV), this has the form:

$$\begin{aligned} f_{\phi,u}(\psi,V)d\psi dV &= F_{\phi,u}(\psi+d\psi,V+dV) - F_{\phi,u}(\psi,V) \\ &= P(\psi \le \phi < \psi+d\psi, V \le u < V+dV) \end{aligned} \tag{1.9}$$

Some properties of joint pdf are:

$$\int_{-\infty}^{\infty}\int_{-\infty}^{\infty} f_{\phi,u}(\psi,V)\,d\psi dV = 1 \tag{1.10}$$

$$f_\phi(\psi) = \int_{-\infty}^{\infty} f_{\phi,u}(\psi,V)\,dV \tag{1.11}$$

$$f_u(V) = \int_{-\infty}^{\infty} f_{\phi,u}(\psi,V)\,d\psi \tag{1.12}$$

If the joint pdf is known, average value of any function of ϕ and u may be obtained. For example, if $Q(\phi,u)$ is a function of ϕ and u, then its mean value is calculated as:

$$\langle Q(\phi,u)\rangle = \int_{-\infty}^{\infty}\int_{-\infty}^{\infty} Q(\psi,V) f_{\phi,u}(\psi,V)\,d\psi dV \tag{1.13}$$

In particular, the covariance $\langle \phi' u' \rangle$ is defined as:

$$\langle \phi' u' \rangle = \int_{-\infty}^{\infty}\int_{-\infty}^{\infty} (\psi - \langle\phi\rangle)(V - \langle u\rangle)\,d\psi dV \tag{1.14}$$

1.3.1.3 Conditional pdf

The conditional probability $P(\phi|u)$ is the probability to meet the event ϕ at given condition of the event u occurs. It is defined through Bayes's theorem as:

$$P(\phi,u)=P(\phi|u)P(u) \tag{1.15}$$

The conditional pdf $f_{\phi|u}(\psi|V)$ can be expressed as:

$$f_{\phi,u}(\psi,V)=f_{\phi|u}(\psi|V)f_u(V) \tag{1.16}$$

Similarly, the mean value $\langle Q(\phi,u)|u=V\rangle$ at given event u is expressed as:

$$\langle Q(\phi,u)|u=V\rangle=\int_{-\infty}^{\infty}Q(\psi,V)f_{\phi|u}(\psi|V)d\psi \tag{1.17}$$

Also the unconditional mean values can be obtained as:

$$\begin{aligned}\langle Q(\phi,u)\rangle&=\int_{-\infty}^{\infty}\int_{-\infty}^{\infty}Q(\psi,V)f_{\phi,u}(\psi,V)d\psi dV\\&=\int_{-\infty}^{\infty}\int_{-\infty}^{\infty}Q(\psi,V)f_{\phi|u}(\psi|V)f_u(V)d\psi dV\\&=\int_{-\infty}^{\infty}f_u(V)\langle Q(\phi,u)|u=V\rangle dV\end{aligned} \tag{1.18}$$

1.3.2 PDF Models

If a pdf for scalars is needed, the simplest approach would be to guess its shape, and this approach is known as "presumed pdf" technique. In this method the shape of pdf is assumed to have a particular form, *e.g.* β-function, see Borghi (1985), parameterised by its first and second moments. These moments are calculated from their own transport equations in which the terms describing chemical reactions are closed with the help of the presumed pdf. This technique, in particular, has proved successful for diffusion flames, (Pope, 1990).

An alternative to presuming a pdf shape would be to solve a conservation equation for the pdf, sometimes it is this approach that is termed as pdf method. Various independent variables may be chosen, among most popular choices are: (1) joint pdf of scalars, (2)

joint pdf of velocity and scalars and (3) joint pdf of velocity, dissipation and scalar. These choices are briefly discussed below.

1.3.2.1 Joint pdf of Scalars

The transport equation for joint pdf of scalars is expressed as:

$$\frac{\partial \rho f_{\hat{c}}}{\partial t}+\frac{\partial \rho U_j f_{\hat{c}}}{\partial x_j}=-\frac{\partial}{\partial c_\alpha}\left(\left\langle \frac{\partial}{\partial x_i} J_i^\alpha \right\rangle_{\hat{c}} + \rho(\hat{c}) W_\alpha(\hat{c})\right) f_{\hat{c}} \tag{1.19}$$

where, $f_{\hat{c}}$ represents the joint pdf of scalars c_α, where α =1, 2,···n, and n is the number of scalars, $\frac{\partial}{\partial c_\alpha}$ represents the sum of $\sum_{\alpha=1}^{n}\frac{\partial}{\partial c_\alpha}$, J_i^α is the conditionally averaged diffusive flux of species α and $J_i^\alpha = -\rho D_\alpha \frac{\partial c_\alpha}{\partial x_i}$, W_α is the reaction rate for species α.

For details of the derivation of this transport equation, one may refer to Dopazo and O'Brien (1976), Pope (1976), O'Brien (1980). The term with J_i^α also known as the small scale mixing term is unclosed and its modelling is a serious challenge to the successful implementations of Eq. (1.19).

Such joint pdf of scalars provides a complete one-point statistical description of the scalars field. The advantage of this kind of pdf method is that it contains all the statistical information required to determine the mean reaction rates, because the chemical reaction terms in the pdf transport equation are in closed form. However, it contains no information about the velocity field, consequently, the fields of velocity and turbulence quantities have to be determined separately. As a consequence, a turbulence model, *e.g.* k-ε or Reynolds-stress model, is needed to determine the mean-velocity and turbulence fields (Pope, 1990).

1.3.2.2 Joint pdf of Velocity and Scalars

The transport equation for joint pdf of velocity and scalar may be obtained by different ways, for more details see O'Brien (1980), Pope (1985). Below is the transport equation in the form given by Pope (1985).

$$\rho(\hat{c})\frac{\partial f_{\bar{U},\hat{c}}}{\partial t}+\rho(\hat{c})U_j\frac{\partial f_{\bar{U},\hat{c}}}{\partial x_j}+\left(\rho(\hat{c})g_j-\frac{\partial\langle p\rangle}{\partial x_j}\right)\frac{\partial f_{\bar{U},\hat{c}}}{\partial U_j}+\frac{\partial}{\partial c_\alpha}\rho(\hat{c})W_\alpha(\hat{c})f_{\bar{U},\hat{c}}$$
$$=\frac{\partial}{\partial U_j}\left\langle-\frac{\partial\tau_{i,j}}{\partial x_i}+\frac{\partial P'}{\partial x_j}\middle|_{\bar{U},\hat{c}}\right\rangle f_{\bar{U},\hat{c}}-\frac{\partial}{\partial c_\alpha}\left\langle\frac{\partial J_j^\alpha}{\partial x_i}\middle|_{\bar{U},\hat{c}}\right\rangle f_{\bar{U},\hat{c}} \tag{1.20}$$

where, $f_{\bar{U},\hat{c}}$ is the joint pdf of velocity and scalars, g_j is the body force in the x_j direction, $\tau_{i,j}$ is the viscous tensor. In the left hand side, the first term is the rate of the joint pdf change with time; the second term is the convection of the joint pdf; the third one is due to the gravity and mean pressure gradient; the last term represents the chemical reactions. Mean pressure gradient can be calculated independently using the mean velocity field (Pope, 1985), the chemical reactions can be treated exactly for complex chemical kinetics, so in LHS, all the terms are closed. The unclosed terms are grouped in the right hand side, the first term in RHS relates to the transport of pdf in velocity space induced by viscous stresses and fluctuating pressure gradient; the second term is the scalar molecular mixing. Both terms in the RHS need to be modelled. For possible approaches to the first term closure one may refer to Pope (1985); closure models related to the scalar molecular mixing term are briefly discussed later.

The joint pdf of velocity and scalar completely chararterises the statistics of velocity and scalar and any functions of these random variables. By including the velocity into the formulation, the convective transport equations are treated exactly, since the corresponding term in the transport equation for the joint pdf of velocity and scalar is in closed form. However, it contains no information about the length scales or time scales of turbulence, such as turbulence time scale $\tau_t=\frac{k}{\langle\varepsilon\rangle}$ needed in many applications. While the kinetic energy can be obtained from the joint pdf, the mean dissipation rate is unknown because it is defined by two point statistics. As a proviso, however, it may be obtained by solving the standard dissipation equation.

1.3.2.3 Joint pdf of Velocity, Dissipation and Scalar

In contrast to the joint pdf of scalar and joint pdf of velocity and scalar, the joint pdf of velocity, dissipation and scalar (Pope and Chen, 1990, Pope, 1991) provides information for the characteristic time scale τ_t because both the dissipation rate and the

kinetic energy can be found from such joint pdf. So turbulent convection, mean pressure-gradient, straining/rotation and chemistry are completed closed, this leaves the fluctuating pressure gradient and the molecular diffusion unclosed. But it is argued that in this joint pdf, the equivalent time scale for the scalar field $\tau_\alpha = \frac{\langle c_\alpha'^2 \rangle}{2\langle \varepsilon_\alpha \rangle}$ is not provided, it only can be determined by the assumption that it is proportional to τ_t. For more details about this joint pdf one can refer to Pope (1990, 1991) and Dopazo (1994).

1.3.2.4 Numerical Solution of pdf Transport Equations

The pdf methods successfully overcome the closure problem related to non-linear chemical reaction rates. Once closure models are proposed for the pdf equations, it can be solved numerically. However, the transport equations of pdf can hardly be solved with any usual finite difference techniques because of large number of pdf dimensions. By this reason, following the pioneering work of Pope (1981), Monté-Carlo methods are currently employed for solving pdf equations. Monté-Carlo method consists in the representation of pdf with an ensemble of particles at each grid node. Statistics such as mean and variances can be determined from the properties of the particles ensemble.

Attractive side of Monté-Carlo technique is that the computational expense grows only linearly with the number of dimensions of the transport equation. The major drawback is that one has to use quite large number of particles for statistics to be represented accurately, because statistical error decreases only slowly with the number of particles N per cell. The error is proportional to $N^{-1/2}$.

1.3.3. Micro-Scale Mixing in pdf Methods

Pdfs methods overcome the difficulty related to the non-linear chemical reaction rates, so the chemistry terms in the pdf transport equation is in closed form. However, the major difficult problem is that the micro-scale mixing term associated with molecular diffusion is not in closed form and hence sub-models are needed to account for the effects of molecular diffusion. The micro-scale mixing term represents the effect of molecular diffusion in turbulent media and is responsible for pdf evolution in scalar space toward the perfect mixing state, or in other words, for smoothing out the temperature and concentrations non-uniformities under action of molecular diffusion.

This problem is particularly difficult in/near the flamelet regime of turbulent combustion, where the small scales of the composition field are strongly influenced by reaction.

Many models have been proposed for this small-scale mixing term, *e.g.* Coalescence Dispersion model of Curl (1963), IEM (Interaction of Exchange Mean) or LMSE (Least Mean Square Estimation) of Frost (1975), and somewhat close to Curl's ideology integral models (Frost, 1975, Dopazo, 1979, Pope, 1982).

1.3.3.1 Coalescence-Dispersion Models

Coalescence dispersion model presumes that the effects of molecular diffusivity may be represented through an exchange of concentrations and energy in pair-wise interaction of fluid parcels. Because every fluid parcel is represented by a Monté-Carlo particle, these models are well-suited for the Monté-Carlo simulation and they have been widely used in many studies of molecular mixing.

The basic version of this model is proposed by Curl (1963). In this version, n_p particles, randomly selected from an ensemble of N particles within a given grid cell, mix their values pairwise. During a time step Δt, two particles p and q with the concentrations (or properties) of $\psi^{(p)}(t)$ and $\psi^{(q)}(t)$ mix under some probability; after mixing the particles acquire new identical concentrations $\psi^{(p)}(t+\Delta t)$ and $\psi^{(q)}(t+\Delta t)$ as:

$$\psi^{(p)}(t+\Delta t)=\psi^{(q)}(t+\Delta t)=\frac{1}{2}\left(\psi^{(p)}(t)+\psi^{(q)}(t)\right) \tag{1.21}$$

n_p is selected according to $n_p = N\Delta t/\tau_\alpha$, remaining ($N$-$n_p$) particles do not change their values. Here, $\tau_\alpha = \dfrac{\langle c_\alpha'^2 \rangle}{2\langle \varepsilon_\alpha \rangle}$ is the characteristic time-scale related to the scalar field. Usually τ_α is set proportional to the turbulence integral time τ_t (Peters, 2000). Borghi *et al.* (1986) proposed that τ_α should follow from a turbulent time scale distributions which could be parameterized by the integral and Kolmogorov time scales. Unresolved remains the question of effects of chemical reactions and Schmidt number on τ_α.

This version does not result in Gaussian shape pdf for an inert scalar if the initial distribution itself is not Gaussian (Dopazo, 1994). There also exists a number of modified or extended versions of Curl's model such as those proposed by Dopazo (1979), Pope (1982).

1.3.3.2 IEM Model

The IEM (Interaction by Exchange with the Mean) mixing model was first proposed by Frost (1960) and later by Villermaux and Devillon (1972). It is also known as LMSE (Linear Mean Square Estimation) (see, Dopazo, 1975, O'Brien, 1980, Borghi, 1988). In this model, the scalar values relax toward the mean value as:

$$\frac{d\psi}{dt} = -\frac{\psi - \langle\psi\rangle}{\tau_\alpha} \tag{1.22}$$

Compared with Curl's model, LMSE is simpler but it has the drawback that the initial pdf shape is preserved. In particular, initially Gaussian distribution will remain Gaussian, but any Dirac δ-peak singularity in initial condition does not disappear during the mixing. Like Curl's model, this model is also unable to produce a relaxation towards a Gaussian pdf in homogeneous turbulence.

There are some other mixing models somewhat close to Curl's ideology, such as integral models of Frost (1975), Dopazo (1979) and Pope (1982), for details of these and other models one can refer to the review by Dopazo (1994). Recently, a number of new small-scale mixing models has been put forward. Among them are Mapping Closure for turbulent mixing of Chen *et al.* (1989), EMST (Euclidean Minimum Spanning Tree) of Subramaniam and Pope (1998). Also, some modifications of IEM model have been proposed, *e.g.* Valino and Dopazo (1991), Sabel'nikov *et al.* (2001), which try to mimic the randomness of the mixing process at the small scales.

Another interesting small-scale mixing description is given by the Multi-Fluid Model (MFM) developed by Spalding (see the lectures at the web site http://www.cham.co.uk for details) which may be regarded as an alternative to the pdf transport models introduced above. Basic idea behind this model is that a fluid mixture can be represented as some "Discretised population". Each member of a population is termed as a distinct fluid.

MFM model may be called "2-fluid", "4-fluid" etc according to the number of distinct fluids used. Volumetric fraction of a "fluid" at some point in MFM may be identified with a probability to meet the scalar value equal to that of this "fluid" at this point, if the latter is normalised to one. At the same time it is fairly obvious that mass fraction of this "fluid" equals the probability of its attribute, normalised to the medium density at the point. The small-scale mixing is represented with some values for changes of "fluid" concentrations within the same location. Unlike Monté Carlo method, MFM uses a conventional finite-volume method for computing the discretised pdfs. Simulations with "14-fluid" model for steady Bunsen burner, "100-fluid" model for stirred reactor have produced reasonable results (Spalding, 1998). MFM has several attractive properties such the fluid-attribute grids may be non-uniform, self-adaptive, and unstructured, and the number of fluids considered can vary in number and kind from one part to another in geometric domain.

1.4 Other Probabilistic Approaches

There are three distinct approaches of "classical" pdf method: LEM (Linear Eddy Model) proposed by Kerstein (1988), CMC (Conditional Moment Closure) by Kilmenko (1990) and Bilger (1993), and RSF (Reference Scalar Field) of Burluka *et al.* (1996, 1997). In all these models the use is made of some new stochastic independent variables, *i.e.* a N-dimensional pdf is split into N field possessing an extra dimension. For details of CMC, one can refer to the review by Kilmenko and Bilger (1999), LEM and RSF are introduced below.

1.4.1 Linear Eddy Model (LEM)

1.4.1.1 Principles of LEM

The mathematical formulation of LEM is essentially a set of equations:

$$\frac{\partial c}{\partial t} = D_M \frac{\partial^2 c}{\partial X^2} + W + Block\ Inversion \tag{1.23}$$

where X is the length along some extra dimension, sometimes argued to be aligned with the highest strain rate direction (Kerstein, 1988), D_M is molecular diffusivity, W is chemical reaction rates, c is scalar concentration. It should be noted at this point that X has never been given an exact definition, moreover it has been given different meanings

for different flows under consideration. This, in fact, reflects an heuristic character of the LEM model.

Block inversion event represents the effects of convection by turbulent velocity field and the following section considers various realisations of this event. This block inversions are implemented as a random rearrangements of the scalar field within a hypothetical eddy size. In fact, each rearrangement represents an individual eddy distortion of the instantaneous scalar profile along some line in an additional X direction, and the ensemble of these rearrangements is scaled according to the Kolmogorov's inertial interval 5/3 law.

As one can see from Eq. (1.23), the LEM model introduces separately the effects of molecular diffusion, turbulent advection and chemistry. This distinction between them is crucially important in combustion because chemical reactions proceed at the molecular level, at which reactants and heat diffusion should be taken into account. The rate of scalar diffusion is strongly affected by amplification of gradients induced by the small scale turbulent motion, and this mechanism is indeed what represents "turbulence-chemistry" coupling. The central assumption in LEM is that the evolution of the scalar field at small scales can be adequately captured with only one extra statistical coordinate. Hence it is argued that all turbulence scales should be resolved, in contrast to other mixing models, so that turbulent convection, the processes of molecular diffusion and chemistry at the smallest scales are captured. Because of this 1-D turbulence representation, simulations at high Reynolds, Damokhler, and Schmidt number are thus more affordable, compared with DNS where all turbulence spectrum has to be represented in all three dimensions.

In LEM, two principal physical mechanisms, turbulent micro- and macro-mixing, define a scalar statistics by virtue of their simultaneous action. The micro-mixing, in fact, is a principal problem addressed by LEM. Hence the micro-scale mixing is nothing but the molecular diffusion implemented deterministically according to Fick's law. The rate of diffusion is then changed with the block inversion event, representing straining action of turbulent eddies.

In applications of LEM for reacting flows, the system should be solved numerically on a computational grid that provides sufficient resolution in X to capture all physically relevant length-scales and allows one to conduct simulations for the values of the flow parameters such as Reynolds, Damköhler and Schmidt numbers as well as for more complex chemical kinetics higher than currently attainable with DNS. Since its original development, it has been applied to several types of flow field and it has been demonstrated to be able to yield reasonable predictions for various characteristics of turbulent mixing, Kerstein (1989, 1990, 1991), Frankel *et al.* (1995), Mcmurtry *et al.* (1992), Desjardin *et al.* (1996) and Debruynkops *et al.* (1998).

1.4.1.2 Realisations of LEM

So far, two kinds of realisations of the so-called block inversion have been proposed, one is the single mapping, the other one is the triplet mapping as shown in Fig. 1.1. The triplet mapping compresses the scalar field by a factor of three within the chosen eddy size, thus amplifying the integral magnitude of gradient over the entire eddy size. The original field within the chosen size is then replaced by three adjacent copies of this compressed field, with the middle copy mirror-inverted.

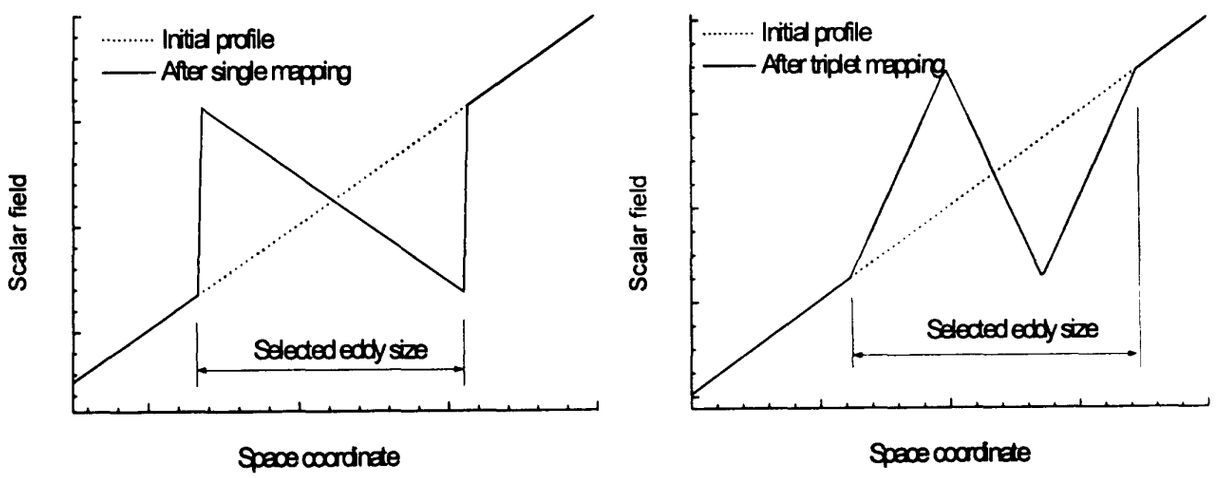

(a) Single mapping (b) Triplet mapping

Fig. 1.1 Mapping of block inversion

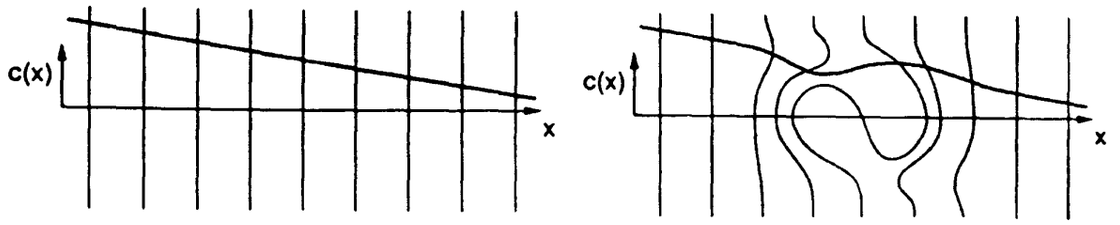

(a) initial profile (b) the distortion by an eddy

Fig. 1.2 Schematic illustration of the intuitive property of triplet mapping

The triplet mapping function for block inversion translates the scalar field $c_0(X,t_n)$, before the n-th inversion event, to a new field $c(X,t_n)$ after an inversion, according to Kerstein (1991, 1992) as:

$$c(X,t_n)=\begin{cases} c_0(3X-2x_0,t_n) & x_0 \le X \le x_0+\dfrac{l}{3} \\ c_0(-3X+4x_0+2l,t_n) & x_0+\dfrac{l}{3} \le X \le x_0+\dfrac{2l}{3} \\ c_0(3X-2x_0-2l,t_n) & x_0+\dfrac{2l}{3} \le X \le x_0+l \\ c_0(X,t_n) & \textit{the rest of the field} \end{cases} \tag{1.24}$$

where l is the chosen eddy size, x_0 is the eddy spatial location, and t_n is the instant of the *n-th* block inversion.

Compared to the single mapping of block inversion, the triplet mapping has the advantages of intuitive rationale. The intuitive picture is illustrated in Fig. 1.2. In this picture, the effect of a single, clock wise rotating eddy on a scalar field initially with a uniform concentration gradient and therefore with linear concentration isopleths as in Fig. 1.2(a) is presented. As illustrated, the eddy distorts these isopleths as indicated in Fig. 1.2 (b). Regarding the linear eddy computational domain as a line parallel to the initial gradient through the centre of the eddy, the initially linear concentration profile evolves to a form similar to the profile obtained by applying the triplet map as shown in Fig. 1.1(b).

One of the theoretical advantages of the triplet mapping is that the map increases the scalar gradient by a mechanism similar to the compressive strain mechanism in turbulent flow, without introducing discontinuities into the scalar field. The other

advantage is that the rearrangement of the triplet mapping during a simulated realisation induces exponential growth of isoplet area which is consistent with the classical theory of turbulence, thus resulting in an appropriate behaviour of viscous-convective range for high Schmidt fluids. These and other theoretical aspects of the triplet mapping use are presented in Kerstein (1991, 1992).

The complete algorithm for implementation of block inversion sequence is selection of

a) the eddy size according to some presumed pdf of eddy size. This pdf is chosen in such a way that the turbulence spectrum satisfy homogeneous and isotropic turbulence theory, see Batchelor (1953). The pdf, $f(l)$, of eddy size is expressed as:

$$f(l)=\frac{5}{3}\frac{1}{l_t}\frac{1}{(l_t/l_k)^{5/3}-1}\left(\frac{l}{l_t}\right)^{-8/3}=\frac{5}{3}\frac{l_t^{5/3}}{\mathrm{Re}_t^{5/4}-1}l^{-8/3} \tag{1.25}$$

for $l_k \le l \le l_t$, and $f(l)=0$ for others. Where, l is the selected eddy size, l_k is the Kolmogorov's length scale, l_t is the turbulent integral length scale. The numerical procedures are readily available for random selection with uniform pdf, the transformation of random variable y with such distribution to l having distribution given by Eq. (1.25) is:

$$l=\left[-\frac{y-a_2}{a_1}\right]^{-\frac{3}{5}} \tag{1.26}$$

where, y is a uniform distribution variable, y equals 0 at $l=l_k$ and 1 at $l=l_t$,

$$a_1=\frac{l_t}{\mathrm{Re}_t^{5/4}-1},\quad a_2=\frac{\mathrm{Re}_t^{5/4}}{\mathrm{Re}_t^{5/4}-1}.$$

b) the instant at which a block inversion occurs according to Poisson distribution. Because events of block inversion are independent, instant at which a block inversion occurs is selected distributed as a Poisson process with overall rate of $R=\lambda l_t$. Here λ is the frequency of block inversions occurring, which has the dimension of $(s\cdot cm)^{-1}$ and it can be expressed as (Kerstein, 1989):

$$\lambda=\frac{54}{5}\frac{D_t}{l_t^3}\frac{(l_t/l_k)^{5/3}-1}{1-(l_k/l_t)^{4/3}}=\frac{54}{5}\frac{D_t}{l_t^3}\mathrm{Re}_t^{5/4} \tag{1.27}$$

where D_t is turbulent diffusivity.

c) the eddy spatial location according uniform distribution over the calculated domain.

1.4.2 Reference Scalar Field Model (RSF)

RSF is a statistical model proposed by Burluka *et al.* (1997) for turbulent premixed combustion. The statistics of the reacting turbulent scalar field is described in terms of a new quantity, named the reference scalar field (RSF) possessing an extra probability dimension X. This procedure results in a allegedly simpler treatment of conditional scalar statistics needed for modelling and it allows to alleviate the problem of ill-posedness of the Cauchy problem for pdf transport equation (Burluka *et al.* 1997).

For a single scalar thermo-chemistry, RSF $c(X;\vec{x},t)$ is one-to-one reversed mapping $c(X;\vec{x},t)=X^{-1}(X(\hat{c};\vec{x},t))$ of cumulative density function (CDF). $X(\hat{c})$ defined as:

$$X(\hat{c})=1-\int_0^{\hat{c}} P(\hat{c})d\hat{c} \tag{1.28}$$

where $P(\hat{c})$ is concentration pdf, and $\hat{c}$ is an independent variable in concentration space. $X(\hat{c})$ may be expressed as the probability to meet the scalar value equal to or greater than $c(X;\vec{x},t)$ at a given point $(\vec{x},t)$ and, by definition, $0\le X\le 1$. The pdf $P(\hat{c})$ and rsf $c(X,t)$ contain the same amount of information on turbulent scalar field. It may be easily shown that Eq. (1.28) will allow to obtain all the statistics of scalars field in the term of rsf as $c(X;\vec{x},t)$. For example, the mean value and the *rms* fluctuation can be easily determined by Eq. (1.29).

$$\langle f(c)\rangle=\int_0^1 f(c(X))\,dX \tag{1.29}$$

$$\langle c'^2\rangle^{1/2}=\left[\int_0^1 (c(X)-\langle c\rangle)^2\,dX\right]^{1/2}$$

Such one-to-one reversed mapping $c(X)=X^{-1}(X(\hat{c}))$ for a nearly bimodal pdf may be sketched as:

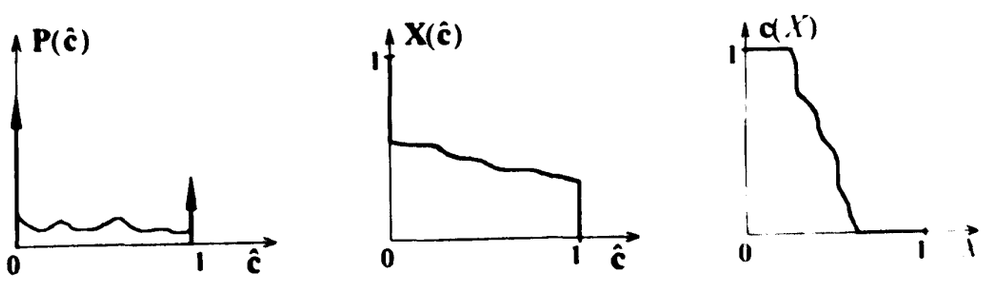

Fig. 1.3 Example of RSF construction, Burluka *et al.* (1997)

Once RSF $c(X,\vec{x},t)$ is known, the pdf $P(\hat{c};t)$ of scalar $\hat{c}$ may be found as:

$$P(\hat{c};t)=\begin{cases} -\left(\left.\dfrac{\partial c(X,t)}{\partial X}\right|_{c(X,t)=\hat{c}}\right)^{-1} & \text{if } \dfrac{\partial c(X,t)}{\partial X}\neq 0 \\ a\delta(\hat{c}-c(X,t)) & \text{if } \dfrac{\partial c(X,t)}{\partial X}=0 \end{cases} \tag{1.30}$$

where a is the length of interval where $c(X,t)=\hat{c}$. Example of the profile of $c(X,\vec{x},t)$ and its pdf is shown in Fig. 4.13 in terms of temperature.

The transport equation of RSF for statistically homogeneous situations may then be derived (Burluka *et al.*,1997) as:

$$\frac{\partial c}{\partial t}=\frac{D_M}{l_t^2}\frac{\partial^2 c}{\partial X^2}+\frac{\langle c\rangle-c}{\tau_t}+W \tag{1.31}$$

It is important to underline that X is not a physical coordinate but a dimensionless statistical coordinate. c is the scalar, W is the chemical reaction rate, D_M is molecular diffusivity, $\langle c\rangle$ is the mean value, τ_t and l_t are integral time and length scale, respectively. In Eq. (1.31) micro-scale mixing is represented by the first two terms which are derived from the conditionally averaged dissipation of a scalar, with more detail given in Burluka *et al.* (1997). The second term in Eq. (1.31) is similar to the well-known LMSE, or IEM (Internal Exchange Mean), model which is the simplest Lagrangian model. However, RSF has the advantage over IEM by including the effect of molecular diffusion, the first term on the RHS in Eq. (1.31). This advantage is demonstrated by Burluka and Borghi (1995) where substantial improvement may be obtained with adding an explicit term for molecular diffusion, compared to the IEM-LMSE model. So, similar to LEM, RSF can distinguish the effects of molecular diffusion, turbulent advection and chemical reaction.

The RSF model possesses a number of properties, such as :

(1) The computed pdf is always normalised and this normalisation simply follows from the fact that $X_{max}=1$

(2) In homogeneous turbulence, equations for mean values and *rms* fluctuations for a scalar c are consistent, as:

$$\frac{d\langle c\rangle}{dt}=\langle w\rangle \qquad (1.32)$$
$$\frac{d\langle c'^2\rangle}{dt}=-\langle\chi\rangle+\langle w'c'\rangle$$

where w is chemical reaction rate, χ is scalar dissipation rate

(3) The chemical terms are closed as they are in any pdf approach

(4) The Cauchy problem for Eq. (1.31) is well-posed

(5) It is well-posed for numerical simulation

Some preliminary assessment of the RSF model has been carried out for a single reactive scalar for several different flame configurations, *e.g.* V-flame with low turbulence, homogeneous case, see Burluka and Borghi *et al.* (1995) and a strongly turbulent flame in a duct, see Burluka (1996). The objective of the present work is to study the relative performance of the RSF model for the case where several reactive scalars have to be used, thus allowing for multiple-step chemical kinetics effects. Where possible, *i.e.* in homogeneous self-ignition studies, comparisons will be drawn with LEM.

Burluka (1996) demonstrated that it is possible to extend the RSF model to a reactive flow with multiple reacting scalars on the condition that all the flow-state trajectories in composition space form a single line connecting the initial and final states at each physical space at the same time. Such a limitation may be encountered in other models as well. Splitting of multi-dimensional pdf's into a number of one-dimensional lines implies obviously that the pdf carrier in the concentration (phase) can be described with only one parameter. An exact definition and physical meaning of that parameter varies from one model to another. For example, in LEM this parameter X in Eqs.(1.23) and (1.24) is assumed to be physical length aligned with one of the principal axes of the strain tensor; in RSF its exact meaning for the many scalars case is left so far open. Spalding's MFM with one parameter distinguishing the "populations" may also be qualified as belonging to this class; the parameter in this case being the progress variable. It is curious to note that it is possible to describe pdf's with one parameter base assumption, using the CMC model (Klimenko, 1990, Bilger, 1993) formulated for non-premixed flames.

Chapter 2

Chemical Kinetics, Auto-Ignition and Laminar Flame Propagation

2.1 Introduction

Both ignition and flame propagation are very important phenomena in most practical combustion systems. In laminar medium, flame propagation may be characterised by burning velocity, a global parameter which is governed by chemical kinetics and molecular transfer. In the problem of ignition, or flame initiation either from an incandenscent body or from a spark, there is no similar global parameter which similarly encompasses the details of the chemical reaction rates. In problems of self-ignition, an alternative parameter, namely ignition delay, appears. However, possibly with the exception of shock-tube studies, the ignition delay observed in experiments is subject to the influence of various physical factors (*e.g.* turbulence and heat losses) and the particular arrangement of the experimental rig, as well as the chemical kinetic mechanism.

It is well-established that for any practical fuel the chemical transformations proceed in a large number of elementary steps with participation of many intermediate agents. Turbulent fluctuations of species concentrations and temperature affect (a) the rates of these elementary steps and (b) the overall rate of fuel consumption and heat release. Hence, in study of turbulent combustion problems one needs to invoke a kinetic mechanism comprising more then one elementary step. With only one elementary step, many phenomena determined by the chemical effects are left out of consideration; in particular, the problem of pollutant formation.

A number of detailed chemical kinetic mechanisms for hydrocarbon combustion are now available (*e.g.* Kee *et al.*, 1985, Glarborg *et al.*, 1986, Westbrook *et al.*, 1979, 1984). They are also available at web sites (*e.g.* The Leeds methane oxidation

mechanism at *http://www.chem.leeds.ac.uk/Combustion/html* and GRI-MECH at *http://www.me.berkeley.edu/gri-mech/index.html*). The need for detailed chemical kinetics is more and more stressed in turbulent combustion problems (Smoot *et al.*, 1976, Westbrook and Dryer, 1980a) and there is a continuing need for small/reduced kinetic schemes having the capability to reproduce experimental phenomena over an extended range of operating conditions and to capture accurately major features such as ignition delay, burning velocity, temperature and important species profiles. Current *2-D* and *3-D* numerical simulations of practical combustion chambers can not include detailed chemical kinetic mechanisms, because the costs of computation are prohibitive. The computational costs of a given reaction mechanism depend primarily on the number of chemical species included, rather than on the number of reactions. The computer time requirements, for just the differential equations of the chemical kinetics themselves are roughly proportional to N^2 (Westbrook and Dryer, 1981); where N is the number of species. As an example Pope (1990) reported that it took 280 supercomputer hours to solve 40 stiff ordinary differential equations for calculation of a laminar flame using a Monté-Carlo technique employing 40 reactive compounds. The excessive computer time explains why one would be interested in the reduced chemical kinetic schemes; also, it is worth noting that there are many circumstances where the great amount of chemical information produced by a detailed reaction mechanism is unnecessary and simple mechanisms may suffice.

The need for small/reduced chemical kinetic mechanisms is most important for turbulent reacting flow modelling, where the fluctuating nature of turbulent flow and the associated turbulence-chemistry interactions introduce severe additional modelling difficulties, as discussed by Jones *et al.* (1982). The principal difficulty is that chemical reaction rates are highly non-linear functions of temperature and species concentrations. In consequence, the interaction of turbulence and chemistry induces large spatial and temporal fluctuations in scalar quantities such as composition, temperature and enthalpy. This results in the so-called "closure problem", *i.e.* how to calculate the average values of reaction rates necessary to calculate mean scalar fields.

In order to keep the numerical simulations feasible, the approach currently commonly adopted is to use reduced kinetic mechanisms involving 5 or less scalars (Pope, 1990, Jones & Kollmann, 1987). An alternative approach often encountered in turbulent

combustion studies (*e.g.* Bray, Libby and Moss, 1985, Cant and Bray, 1989) is to incorporate all the thermo-chemistry in terms of a single variable, *i.e.* a reaction progress variable, for premixed combustion. This variable equals *zero* in unburnt reactants, *one* in fully burnt products and has intermediate values in gas which is undergoing chemical reactions. In other words, all the chemistry is reduced to a single irreversible reaction.

In the present work, consideration has been restricted to two-step reduced chemistry. The justification for a two-step hydrocarbon oxidation mechanism is set out below. The two-step chemical kinetic scheme is intended to represent the combustion of methane and air. This scheme has been adopted for computation of ignition delay and 1-D spherical laminar flame propagation.

2.2 Chemical Kinetics

2.2.1 Premixed Laminar Flame Structure for Hydrocarbons

Following the seminal works by Zel'dovich, Semenov and Frank-Kamenetsky, (*e.g.* Zel'dovich *et al.*, 1985 and references therein), many varied descriptions of flame structure have been suggested. Over the last thirty years, very much attention has been paid to techniques based on the separation of flames into several distinctive zones on the basis of some criteria; approach also known as matched asymptotic development technique. To illustrate this approach, one may consult the studies of Peters and Williams (1987), Seshadri and Peters (1990) and Bui-Pham *et al.* (1992) who suggested that the structure of methane-air flame consists of three major distinct layers: preheat zone, oxidation layer and inner layer as shown in Fig. 2.1. Different combustion mechanisms appears in the three layers. In the preheat zone the balance between heat/mass convection and diffusion is dominant, the mixture is heated up by the conduction from the chemical heat release region. The inner layer is the zone where all hydrocarbon reactions are presumed to occur and the fuel is consumed and converted primarily to CO & H_2 with some CO_2 & H_2O. The oxidation layer is the zone where CO & H_2 are oxidized to form the products CO_2 & H_2O. Similar structure has been proposed by Jones and Lindstedt (1988) as shown in Fig. 2.2.

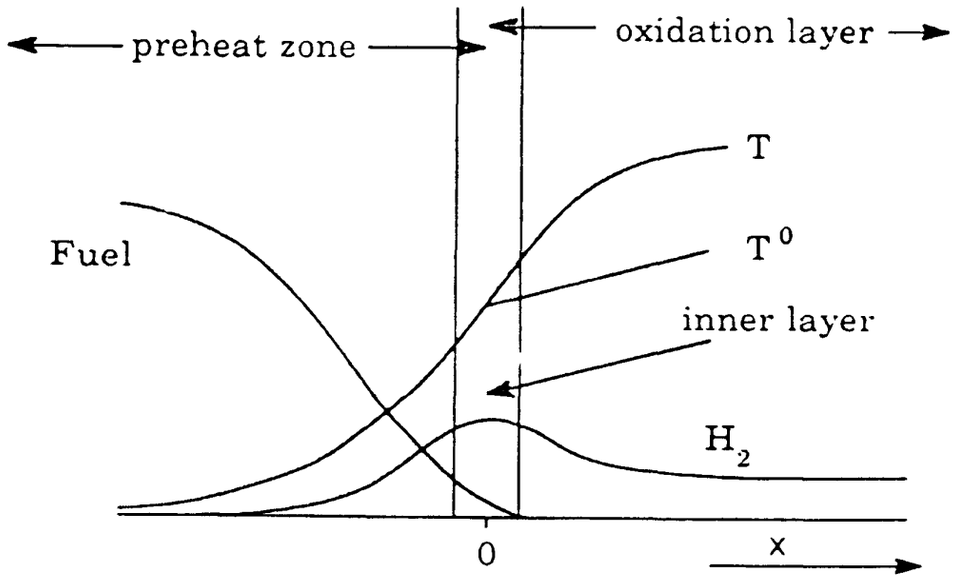

Fig. 2.1 Pre-mixed Hydrocarbon flame structure
proposed by Peters and Williams (1987)

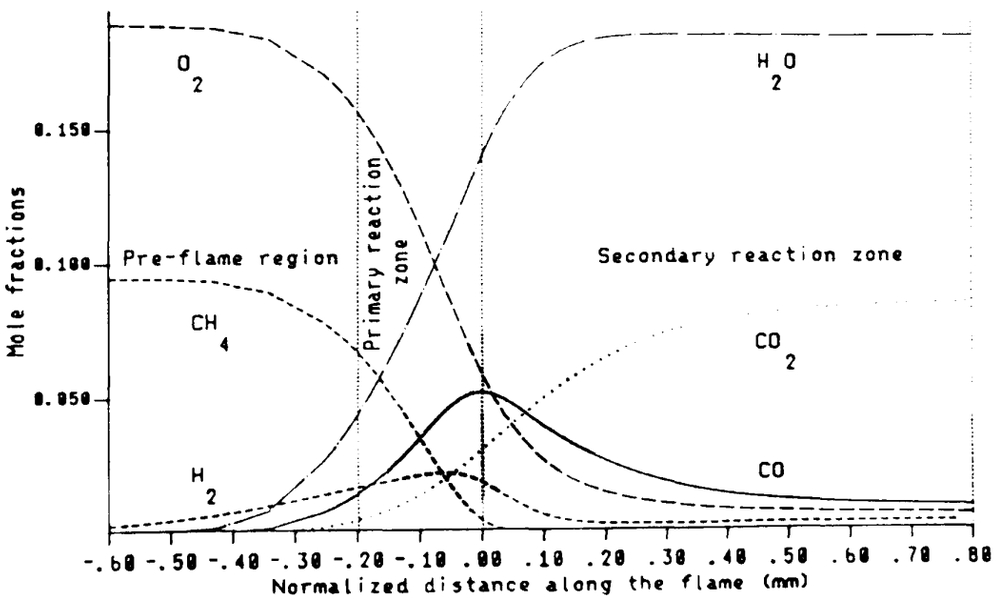

Fig. 2.2 Pre-mixed methane-air flame structure
proposed by Jones and Lindstedt (1988)

Comparing Figs. 2.1 and 2.2, it is seen that the inner and oxidation layer of Peters & Williams are similar to the primary and secondary reaction zones of Jones & Lindstedt, respectively.

This essentially two-stage oxidation has been confirmed by many experiments conducted by different research groups employing various experimental techniques. For example, Dryer and Glassman (1973), Peeters and Mahnen (1973) used a shock tube. All the above confirmed two stage hydrocarbon oxidation; the first stage essentially involving fuel oxidation to CO and H_2, the second stage combustion of CO and H_2 to CO_2 and H_2O.

Along with fuel oxidation to CO, a radical pool (including H_2, H_2O_2, HO_2, CHO *etc.*) is created in the first combustion stage. In the second reaction zone oxidation of CO is accompanied by consumption of the radical pool. Although oxidation of CO and the radical pool reactions can be solved by well-established H_2-O_2-CO chemical kinetics, such computations increase the number of species considered. This substantially restricts the use of full kinetic schemes in turbulent reacting flow analysis. The study of Jones and Lindstedt (1988) used a four-step global chemical kinetic scheme including 6 species (C_nH_{2n+2}, O_2, CO, CO_2, H_2, H_2O). Flame structures, as well as burning velocities, for alkanes up to butane agreeed well with experiments for a range of fuel air ratios.

On the basis of all the above, it is considered well established that oxidation of hydrocarbons takes place in two stages; the first essentially being conversion of fuel to CO and H_2, the second combustion of CO and H_2. This assumption is made in the computation reported in this thesis.

2.2.2 Quasi-Global Two-Step Chemical Kinetics

2.2.2.1 Global Two-Step Chemical Kinetics

Dryer and Glassman (1973) proposed a two-step chemical mechanism for methane-air combustion:

$$\begin{aligned} CH_4 + \frac{3}{2}O_2 &\Rightarrow CO + 2H_2O \\ CO + \frac{1}{2}O_2 &\Rightarrow CO_2 \end{aligned} \tag{2.1}$$

As discussed above this two-step mechanism should reflect the observed two-stage character of methane burning.

To take into account possible incomplete combustion, as well as to include (qualitatively) the chain nature of hydrocarbon oxidation, Westbrook and Dryer (1981) proposed a reversed two-step mechanism which considered CO_2 dissociation:

$$\begin{aligned} C_nH_m + \left(\frac{n}{2} + \frac{m}{4}\right)O_2 &\Rightarrow n\,CO + \frac{m}{2}H_2O \\ CO + \frac{1}{2}O_2 &\Leftrightarrow CO_2 \end{aligned} \tag{2.2}$$

Their simulations using the two-step mechanism yielded laminar burning velocities in good agreement with experiment and provided a more accurate estimation of flame parameters c.f. one-step chemical kinetics. Westbrook and Dryer (1981) also compared the results for single-step and two-step schemes with those employing the detailed kinetic mechanism of Westbrook and Dryer (1980b). This showed that, even though the most important radicals (such as *O*, *H*, *OH*) were not included in the two-step kinetics, the predictions of adiabatic temperature, and reactant and product species profiles were close to experimental observation. It is noteworthy that although the detailed kinetics and the two-step chemical kinetic approaches yield the same equilibrium *CO* level in the post-flame region, adoption of the detailed kinetics results in much higher *CO* concentration in the pre-flame and flame region, while the results wiht two-step kinetics (Eq. (2.2)) were in better agreement with the measured values.

Another mechanism of primary fuel breakdown to *CO* and H_2 was proposed by Edelman and Fortune (1969):

$$C_nH_{2m}+\frac{n}{2}O_2 \Rightarrow n\,CO+m\,H_2 \tag{2.3}$$

A similar mechanism was used by Duterque and Borghi (1981) for methane-air:

$$CH_4+\frac{1}{2}O_2 \Rightarrow CO+2H_2 \tag{2.4}$$

More recently, Peters and Williams (1987) proposed a two-step mechanism derived from their reduced four global reactions scheme as:

$$\begin{aligned} &CH_4+O_2 \Rightarrow \frac{2}{1+\alpha}(H_2+\alpha CO)+\frac{2\alpha}{1+\alpha}H_2O+\frac{1-\alpha}{1+\alpha}CO_2 \\ &\frac{2}{1+\alpha}(H_2+\alpha CO)+O_2 \Rightarrow \frac{2}{1+\alpha}H_2O+\frac{2\alpha}{1+\alpha}CO_2 \end{aligned} \tag{2.5}$$

where α denotes the ratio of CO to H_2 concentration at equilibrium of the water-gas shift reaction, through which CO is partially oxidised and H_2 is generated through the reaction of $CO+H_2O \Leftrightarrow CO_2+H_2$. The first reaction in Eq. (2.5) represents the primary fuel consumption and the second reaction describes the oxidation of CO and H_2. Peters and Williams (1987) assumed that the structure of the inner layer is affected by the rate of the first overall reaction and that in this layer the rates of the radical recombination reaction can be presumed small, as such, they termed the inner layer the "fuel consumption layer". In the oxidation layer downstream of the inner layer, the concentration of fuel was presumed to be zero, with the structure of this layer influenced primarily by the rate of the second overall reaction.

In fact, this two-step mechanism of Peters and Williams has some similarities to the generalised chemical kinetics proposed by Zel'dovich (1948). In Zel'dovich's two step mechanism, initial reactant A is transformed into a radical X by means of a first order autocatalytic reaction $A+X \Rightarrow 2X$ with a large activation energy and negligible heat release. In the second step the radical X recombines to form the final product P in a strongly exothermic reaction $X+X \Rightarrow P$.

The reaction rates for all the reactions presented above are usually expressed in Arrhenius form, the rate constants of which are considered below.

2.2.2.2 Global Reaction Rate of Methane

The reaction rates of the first stage oxidation in Eqs. (2.1) and (2.4) are the rates of methane destruction:

$$W_1 = -\frac{d[CH_4]}{dt} = k_1 [CH_4]^{\alpha_1} [O_2]^{\alpha_2} \tag{2.6}$$

where, generally, k_1 may be expressed as:

$$k_1 = A_1 \exp\left(-\frac{E_1}{R_u T}\right) \tag{2.7}$$

and square brackets denote molar concentration (*mole/cm*^{3}). Thus, the overall reaction rate has the dimension of *mole/cm*^{3}*-s* if using the units of *cm*, *mole*, *s*; such use is traditional in chemical kinetics. Values of various constants in Eq. (2.6) and Eq. (2.7), obtained by several research groups using different techniques (experimental as well as semi-theoretical analysis) are presented in Table 2.1. In that table, Westbrook and Dryer considered two kinds of CH_4 oxidation process, either to CO and H_2O or to CO and H_2, as expressed by Eqs. (2.1) and (2.4), respectively. One can notice that, for the same oxidation process, activation energies may be as different as 48.4 and 30 *kcal/mole*.

Table 2.1 Coefficients for global reaction rate of methane CH_4

Reference	A_1	α_1	α_2	E_1 (*kcal/mole*)	Experimental Method
Kozlov (1959)	7×10^8/T	- 0.5	1.5	60	Laminar Flow reactor
Edelman & Fortune (1969)	5.52×10^8 T	0.5	1.0	24.4 **	Jet-stirred Reactor
Dryer & Glassman (1973)	$10^{13.2\pm0.2}$	0.7	0.8	48.4±1.2 *	Turbulent-flow reactor
Duterque & Borghi (1981)	$(7\pm5)\times10^6$	1.0	1.0	47±2 **	Well-Stirred combustor
Westbrook & Dryer (1981)	2.8×10^9	-0.3	1.3	48.4 *	Semi-Theory
	1.5×10^7	-0.3	1.3	30 *	
	4.0×10^9	-0.3	1.3	48.4 **	
	2.3×10^9	-0.3	1.3	30 **	

Note: * for the process following Eq. (2.1)
** for the process following Eq. (2.4)

It is clear from Table 2.1 that there is considerable scatter in the proposed values for A_1, α_1, α_2 and E_1. For example, the activation energy value E_1 from Duterque & Borghi (1981) is the same as that from Westbrook & Dryer (1981), while all the other values

differ. Duterque & Borghi suggested that the difference in values of the constants may result from the use of different experimental techniques. It can also be seen from Table 2.1, that two different values have mainly been adopted for α_1 negative (close to -0.5) and positive (close to unity). Westbrook and Dryer (1981) showed that with α_1 taken as unity, serious overestimation of burning velocity and flammability limits results for fuel-rich mixture. Negative values of α_1 result in inhibition of methane oxidation with elevated concentrations of methane, the effect obviously being stronger in a rich mixture.

2.2.2.3 Global Reaction Rate for *CO* Oxidation

The second stage in the chemical kinetic schemes of Eqs. (2.1), (2.2) and (2.5) represents the oxidation of *CO*, the principal species formed from the primary fuel breakdown. For *CO* oxidation, the reaction rate can be expressed as:

$$W_2 = -\frac{d[CO]}{dt} = k_2 [CO]^{\beta_1} [H_2O]^{\beta_2} [O_2]^{\beta_3} \left(P/R_u T \right)^{\beta_4} \tag{2.8}$$

where the rate constant k_2 is commonly expressed as:

$$k_2 = A_2 \exp\left(-\frac{E_2}{R_u T} \right) \tag{2.9}$$

An unusual feature of this reaction rate expression is that it depends on water concentration, though water does not enter the left hand of Eqs. (2.1), (2.2) and (2.5). This reflects an experimentally well-established fact that the presence of water vapour accelerates *CO* oxidation. However, if the concentration of water vapour is above a certain threshold (1.5 ~ 3%*vol* by different estimations), *CO* oxidation is slowed down by increase in water concentration. Since first measured by Friedman and Cyphers (1956), the parameters of A_2, β_1, β_2, β_3, β_4 and E_2 have been the object of many studies, *e.g.* Dryer and Glassman (1973), Kozlov (1959), Hottel *et al.* (1965) and Williams *et al.* (1969). The values of A_2, β_1, β_2, β_3, β_4 and E_2, from different sources, are set out in Table 2.2.

As shown in Table 2.2, there is general agreement in the literatures that β_1 equals approximately 1.0 and β_2 is about *0.5*. There is considerably more divergence in the recommended reaction order for oxygen, which may be *0.2* or even *zero* at high oxygen concentration (*e.g.* $O_2 > 5\%$), or about *1.0* at lower concentrations ($O_2 < 5\%$) (Howard

et al., 1973, Sobolev, 1959). However, there seems to be general agreement for the values of $\beta_4=0$ *and* $\beta_3=0.25$.

Table 2.2 Coefficients for global reaction rate of *CO* oxidation

Reference	A_2	β_1	β_2	β_3	β_4	E_2 (*kcal/mole*)	Experimental method
Kozlov (1959)	$\frac{1.04\times10^{12}}{T^{2.5}}$	1.0	0.5	0.25	1.75	32	Laminar Flow reactor
Fristrom & Westenberg (1965)	4.0×10^{13}	1.0	0.5	0.25	0.0	45	Semi-theoretical
Hottel *et al.* (1965)	1.2×10^{11}	1.0	0.5	0.3	1.8	16	Well-stirred reactor
Lavrov *et al.* (1968)	1.8×10^{12}	1.0	0.5	0.25	0.0	28.3	Jet-Stirred reactor
Williams *et al.* (1969)	1.8×10^{13}	1.0	0.5	0.5	0.0	25	Stirred reactor
Dryer & Glassman (1973)	$10^{(14.6\pm0.25)}$	1.0	0.5	0.25	0.0	40 ± 1.2	Turbulent-flow reactor
Howard *et al.* (1973)	1.3×10^{14}	1.0	0.5	0.5	0.0	30	Continuous flow reactor
Lyon *et al.* (1985)	1.5×10^{10}	1.0	0.5	0.25	0.0	23.6	Continuos flow reactor

Comparison of the results of using the schemes suggested by Kozlov (1959), Hottel *et al.* (1965), Lavrov *et al.* (1968), Dryer and Glassman (1973) has been made by Yetter and Dryer (1991). They showed the variation in the computed values of $\left(d[CO]/dt\right)/\left([CO][H_2O]^{0.5}[O_2]^{0.25}\right)$ to be less than 50% of the averaged value.

2.2.3 Chemical Kinetics Used in Present Work

Based on the experimental observation of the two-stage character for hydrocarbon combustion, it was considered that a reduced two-step reaction mechanism would be adequate to capture the major features of the effects due to chemical kinetics in the modelling work presented in this thesis. Based on this observation, a scheme similar to that expressed by Eqs. (2.1) and (2.2) was adopted:

$$\begin{aligned} CH_4 + O_2 &\Rightarrow R + H_2O \qquad Q_1 = 66.4\,kcal/mole \\ R + O_2 &\Rightarrow CO_2 + H_2O \qquad Q_2 = 125.4\,kcal/mole \end{aligned} \tag{2.10}$$

where R is an equimolar mixture of H_2 and CO and considered to be the "chain propagation" agent; Q is the heat release. This scheme reflects the experimental observations above, in the sense that the first reaction represents the primary zone of fuel destruction and CO & H_2 formation, and the second reaction represents the secondary zone where CO & H_2 are slowly oxidised. In fact, Eq. (2.5) is identical to Eq. (2.10) when $\alpha = 1.0$.

The chemical reaction rates for the present two-step kinetics may tentatively be written as:

$$W_1 = A_1 [CH_4]^{-0.5} [O_2]^{1.5} \exp\left(-\frac{20000}{R_u T}\right)$$
$$W_2 = A_2 [R][H_2O]^{0.5} [O_2]^{0.25} \exp\left(-\frac{30000}{R_u T}\right) \qquad (2.11)$$

It may be seen that the first reaction in Eq. (2.11) coincides with that of Kozlov, with $\alpha_1 = -0.5$ and $\alpha_2 = 1.5$. The activation energy is set as $E_1 = 20$ *kcal/mole*. The second reaction in Eq. (2.11) corresponds to Eq. (2.9), with $\beta_1 = 1$, $\beta_2 = 0.5$, $\beta_3 = 0.25$ and $\beta_4 = 0.0$. Computations have been carried out for different values of E_2 in the range of 10 to 60 *kcal/mole* and it has been found that its value is not particularly critical for calculated burning velocity; but noting that good agreement with measurement has been obtained with a value of approximately 30 *kcal/mole* (Jones and Lindstedt, 1988). This value is also in agreement with the values given by Westbrook and Dryer (1981). So in the present work the value of E_2 is set to 30 *kcal/mole*.

The values of the pre-exponential factors A_1 and A_2 are given later in this Chapter. Different values are adopted for self-ignition and flame propagation modellings, as shown and discussed in the appropriate sections of this Chapter.

In Eq. (2.11), the square brackets [·] stand for molar concentration [*mole/cm*^{3}]. For computational convenience the dimension of W_i is converted to *1/s*, by transforming molar concentrations [·] to mole fraction (·) using the relationship:

$$[\,\cdot\,] = (\,\cdot\,)\frac{P}{R_u T} \qquad (2.12)$$

after the conversion, the expression of chemical reaction rates may be rewritten as:

$$W_1 = A_1 (CH_4)^{-0.5} (O_2)^{1.5} \exp\left(-\frac{20000}{R_u T} \right)$$
$$W_2 = A_2 (R)(H_2O)^{0.5} (O_2)^{0.25} \exp\left(-\frac{30000}{R_u T} \right)\left(P/R_u T \right)^{0.75} \tag{2.13}$$

where $(\cdot)$ represents mole fractions and W_i has units of *1/s*.

The rates of change of species concentrations are then calculated as:

$$\begin{cases} \dfrac{d(CH_4)}{dt} = -W_1 & \dfrac{d(O_2)}{dt} = -W_1 - W_2 & \dfrac{d(R)}{dt} = W_1 - W_2 \\ \dfrac{d(CO_2)}{dt} = W_2 & \dfrac{d(H_2O)}{dt} = W_1 + W_2 & \end{cases} \tag{2.14}$$

and the rate of change of temperature is calculated according to:

$$\frac{dT}{dt} = \frac{Q_1 W_1 + Q_2 W_2}{c_{P\,mix}} \tag{2.15}$$

where c_{pmix} is the specific heat of the mixture. It is calculated from the polynomial dependencies for the specific heats of the individual species as:

$$c_p = \begin{cases} a_0 + a_1 T + a_2 T^2 + a_3 T^3 & for\ a_3 \neq 0 \\ a_0 + a_1 T + a_2 / T^2 & for\ a_3 = 0 \end{cases} \tag{2.16}$$

where the polynomial coefficients are taken from JANAF thermochemical tables (1971) and are listed in Table 2.3. The unit of c_p is *cal/mole-K*.

Table 2.3 Coefficients for determination of c_P

Species	a_0	a_1	a_2	a_3
CH_4	4.17	14.45	0.267	-1.772
O_2	7.52	0.81	-0.90	0.0
CO	6.79	0.98	-0.11	0.0
H_2	6.52	0.78	0.12	0.0
H_2O	7.17	2.56	0.08	0.0
CO_2	10.55	2.16	-2.04	0.0
N_2	6.66	1.02	0.0	0.0

2.3 Simulation of Self-Ignition

In order to evaluate the two-step reaction kinetics introduced above, it was decided to study self-ignition phenomena in a laminar pre-mixture of methane and air at atmospheric pressure. The pre-exponential coefficients A_1 and A_2 were fixed from comparison with the ignition delays measured in a shock tube experiments, see below, for a stoichiometric mixture at an initial condition of temperature 800 K and pressure 1 *bar*. With the values so obtained, the reaction rates become:

$$W_1 = 0.125 \times 10^6 \, (CH_4)^{-0.5} \, (O_2)^{1.5} \exp\left(-\frac{20000}{R_u T} \right) \tag{2.17}$$

$$W_2 = 0.55 \times 10^{10} \, (R)(H_2O)^{0.5} \, (O_2)^{0.25} \exp\left(-\frac{30000}{R_u T} \right) \left(P/R_u T \right)^{0.75}$$

Ignition is revealed by a computed steep rise in temperature; here the instant at which ignition occurs is defined in terms of a rate of temperature rise greater than some threshold value:

$$\frac{dT}{dt} \geq 10^5 \quad K/Sec \tag{2.18}$$

The stiff system of ODE's for species concentrations and temperature were solved with a special computer subroutine "*EULSIM*" developed by Deuflhard *et al.* (1989). Self-ignition delays predicted with the two-step chemical kinetics scheme for various initial temperatures for stoichiometric mixture at initial pressure of 1 *bar* are shown in Fig. 2.3. The results are compared with the empirical expression proposed by of Spadaccini *et al.* (1994), which generalises the shock-tube experiments of Walker *et al.* (1969):

$$\tau_{ign} = 2.77 \times 10^{-12} \exp\left(\frac{20012}{R_u T} \right) [O_2]^{-1.0} \tag{2.19}$$

Although the pre-exponential coefficients were fixed from comparison of measured and calculated ignition delays at 800 K, Fig. 2.3, the calculated ignition delays agree quite well with measured values in the range of 800 to 1400 K. When initial temperature is higher than 1400 K, the ignition delays predicted by the present kinetic scheme are shorter than the experimental values.

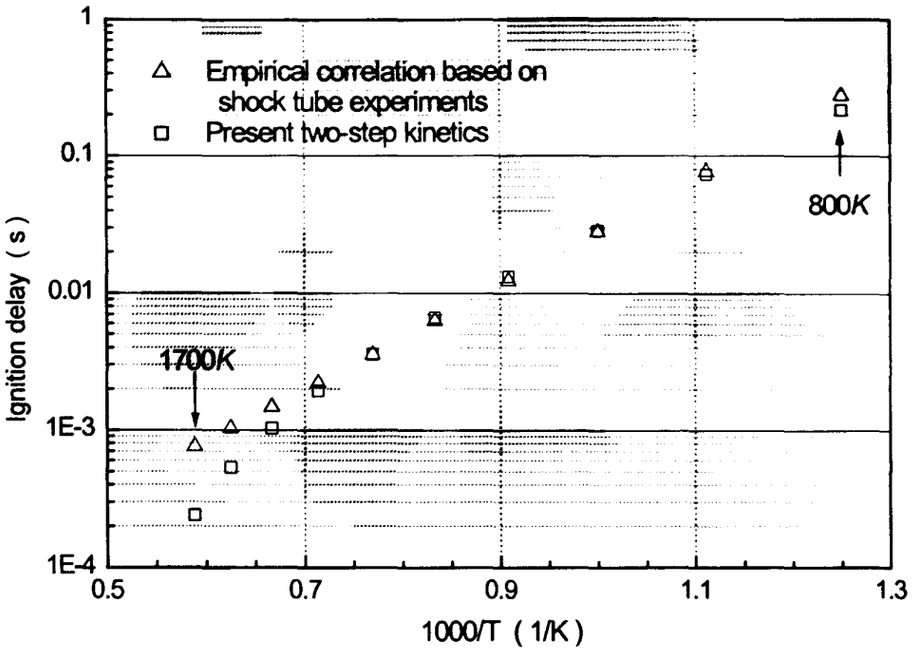

Fig. 2.3 Ignition delays as a function of initial temperature, $P_0 = 1$ *bar*, $\phi = 1.0$

The temporal dependencies of species concentrations and temperature for initial temperature 800 *K* are shown in Fig. 2.4(a) and (b), respectively. The output data are similar to produced by other chemical kinetic scheme (Jones and Lindstedt, 1988).

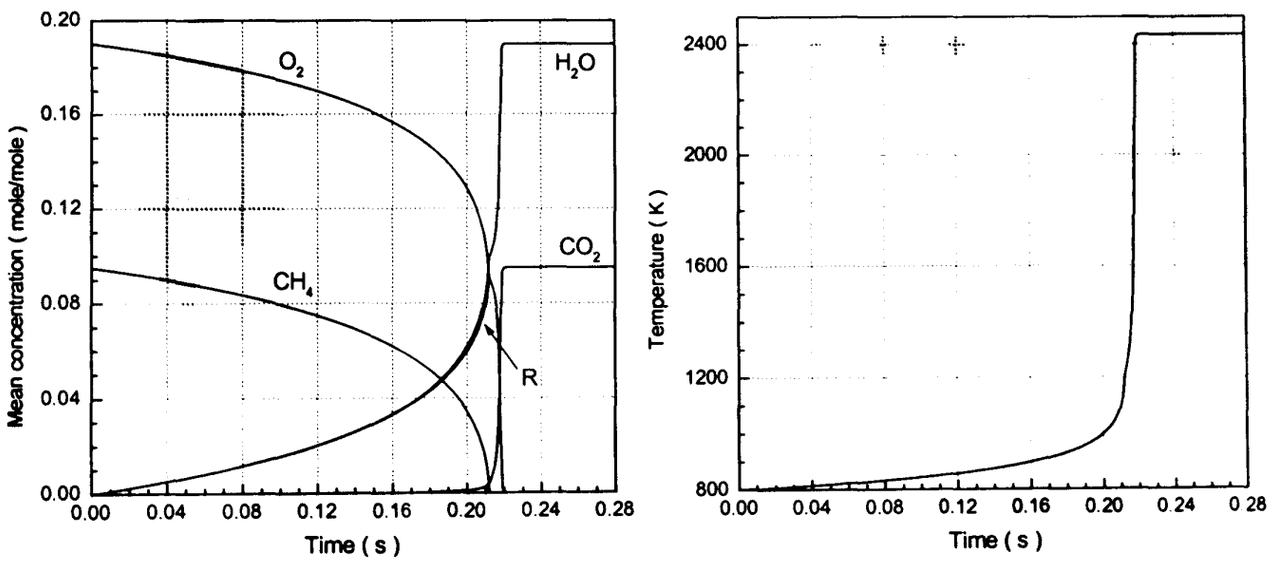

(a) Species profile (b) Temperature evolution

Fig. 2.4 Species profile and temperature evolution for T_0=800 *K*, $\phi = 1.0$

2.4 Kinetics Applied to Spherical Laminar Flame Propagation

2.4.1 Governing Equations

Propagation of spherically symmetrical flame in an initially quiescent mixture is described by the following system of equations:

$$\frac{\partial Y_i}{\partial t}+\frac{1}{r^2}\frac{\partial\left(r^2u(r,t)Y_i\right)}{\partial r} = w_i+\frac{1}{r^2}\frac{\partial}{\partial r}\left(r^2D_M\frac{\partial Y_i}{\partial r}\right)+S_M \tag{2.20}$$

$$\frac{\partial \rho}{\partial t}+\frac{1}{r^2}\frac{\partial\left(\rho r^2u(r,t)\right)}{\partial r}=0 \tag{2.21}$$

Here, Eq. (2.20) is the transport equation for scalars, *i.e.* concentrations and temperature. Chemical source terms are given by Eqs. (2.14) and (2.15). In these equations three basic mechanisms are reflected: convection --- the second term in the left hand side, chemical reaction and molecular diffusion --- the first and second term in the right hand side, respectively. The symbol Y_i represents mole fraction of species i, w_i is formation/destruction rate of species i due to chemical reaction (Eqs. (2.14) and (2.15)), D_M is molecular mass diffusivity and $u(r,t)$ is the gas velocity at radius r in term of mass velocity. S_M is the source term related to the change of mixture molecular weight W_{mix} arising upon the transformation of the transport equation from mass fraction to mole fraction in term of Y_i. For temperature $S_M = 0$, and for species S_M is expressed as:

$$\begin{aligned} S_M =& -Y_i\frac{\partial \ln(1/W_{mix})}{\partial t}-u(r,t)Y_i\frac{\partial \ln(1/W_{mix})}{\partial r} \\ &+D_M\frac{\partial Y_i}{\partial r}\frac{\partial \ln(1/W_{mix})}{\partial r}+\frac{W_{mix}}{r^2}\frac{\partial}{\partial r}\left(r^2D_MY_i\frac{\partial(1/W_{mix})}{\partial r}\right) \end{aligned} \tag{2.20a}$$

Throughout present work, the effect of change of mixture molecular weigh is neglected due to its slow change rate.

To find the gas velocity, the continuity Eq. (2.21) is rewritten in the form:

$$u(r,t)=-\frac{\int_0^r\frac{\partial \rho}{\partial t}r^2dr}{\rho r^2} \tag{2.21a}$$

which allows an explicit calculation of $u(r,t)$ once ρ and $\partial\rho/\partial t$ are known.

The temperature variation of molecular diffusivity D_M is taken into account as:

$$D_M = D_0\left(T/T_0\right)^n \tag{2.22}$$

where D_0 is the diffusion coefficient at temperature T_0 ($T_0 = 300\ K$ in the present study); recommended values for n vary from 1.5 to 2.0, here adopted is $n = 2.0$ according to the data from Walker and Westenberg (1960).

To have a convenient variable for comparison with measurements, the explosion is assumed to occur in a closed combustion vessel and pressure rise is calculated. The advantage of comparison with explosion pressure rather than flame radius is that the processing of experimental data is rather trivial and free from the various assumptions necessary to derive a flame radius. However, constant volume explosions are subject to rising temperature and pressure in the unburnt, fresh mixture; to avoid complications related to this effect, the present study is limited to the so-called pre-pressure period when the pressure rise $\Delta P << P_0$. In practice this means that for initial atmospheric pressure the study is limited to times such that $P(t) < 1.5\,bar$, for initial pressure of $P_0 = 5.0\ bar$, $P(t) < 1.2P_0 = 6.0\ bar$.

Consideration of only the pre-pressure period is also justified in the present case as the kinetics of methane (and, for that matter any other hydrocarbons) is much less studied and understood at higher pressures, especially those greater than 10 *bar*. In particular, the rates of trimolecular recombination reactions change most with pressure rise; and it is doubtful that the present two-step kinetics would reproduce this effect reliably. It has been found that the pre-exponential factors A_1 and A_2 have to be changed (compared with Eq. (2.17)) in order to match computed and measured burning velocity at $\phi = 1.0$, $T_0 = 300K$, $P_0 = 1.0\,bar$. This necessity reflects the fact that self-ignition is governed by (slow) radical accumulation, that is by the reactions of chain initiation; while for flame propagation, the diffusion of active particles from the flame reaction zone eliminates the chain initiation rates influence on the flame speed. In other words, τ_{ign} is associated with chain initiation, while u_n is associated with chain branching and propagation for hydrocarbon-air mixtures. Because these phenomena are not properly reflected in the present two-step kinetic scheme, it proved necessary to adjust the values

of the pre-exponential coefficients A_1 and A_2. The reactions rates, after these adjustments, are:

$$W_1 = 0.625 \times 10^7 [CH_4]^{-0.5} [O_2]^{1.5} \exp\left(-\frac{20000}{R_u T}\right)$$
$$W_2 = 2.5 \times 10^{11} [R][H_2O]^{0.5} [O_2]^{0.25} \exp\left(-\frac{30000}{R_u T}\right) \quad (2.23)$$

It should be noted that a literature search failed to reveal any reduced kinetic scheme with rate constants jointly optimised for both flame propagation and self-ignition. The principle objective of the currently reported work is to develop a model by which any chemical kinetic scheme behaviour could be included into a turbulent combustion simulation, creation a "universal" reduced chemical kinetic scheme for methane-air oxidation is beyond its scope.

Assuming low Mach number and neglecting acoustic effects, one may show that the pressure is uniform within the combustion vessel (hereafter also referred to as " bomb"). Then, for fixed mass, the pressure increment within the bomb may be defined from a discrete form as:

$$P^{n+1} = \frac{\int_0^R \rho^n r^2 dr}{\int_0^R \frac{W_{mix}^{n+1}}{R_u T^{n+1}} r^2 dr} \quad (2.24)$$

where W_{mix} is the molecular weight of mixture, the upper-scripts "n" and "n+1" relate to the current time and current time plus one time increment, respectively. The derivation of Eq. (2.24) is given in *Appendix B*.

2.4.2 Numerical Solution Method

The expression given by Eq. (2.20) is a typical unsteady convection-diffusion equation and it may be integrated with a classical *Finite Volume Method* to yield a finite-difference algebraic equation. As shown in Fig. 2.5, the control volume of a general node P is bounded to its west and east side faces, referred to as w and e, respectively. The neighbouring nodes are identified by W, E and WW, EE.

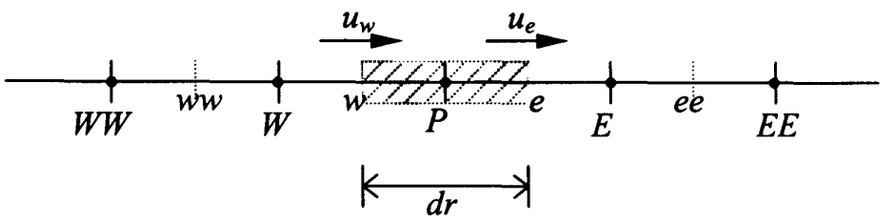

Fig. 2.5 Control volume of general node P

Both sides of Eq. (2.20) are multiplied by elementary volume $dV = r^2 dr$, then Eq. (2.20) is integrated over the control volume. Thus, ϕ_P, the property of node P at time t (*i.e.* either species concentrations or temperature), can be related to its neighbour nodes properties of ϕ_W, ϕ_{WW}, ϕ_E, ϕ_{EE} at the same instant and the property ϕ_P^0 of P at time t_0 as:

$$(a_P + a_P^0)\phi_P = a_{WW}\phi_{WW} + a_W\phi_W + a_E\phi_E + a_{EE}\phi_{EE} + a_P^0\phi_P^0 + S_0 \qquad (2.25)$$

where $a_P^0 = \frac{1}{\Delta t} dV$ comes from the unsteady term, $\Delta t = t - t_0$ is time increase, S_0 is the source term related to chemical reactions.

In Eq. (2.25), the crucial issue is the formulation of suitable expressions for values of coefficients a_{WW}, a_W, a_E, a_{EE} when accounting for the convective contribution in this equation. Different discretisation schemes may be used to treat the convection term. A good numerical method should have the properties a) high accuracy, b) conservativeness, c) boundedness, d) transportiveness, e) stability (see Patankar, 1980, Versteeg and Malalasekera, 1995).

There are several schemes in common use: Central Differencing, Upwind Differencing, Hybrid, Power law, Exponential and the QUICK scheme; more details, see Patankar (1980) and Versteeg & Malalasekera (1995). The resulting coefficients for different schemes are listed in Table 2.4.

Table 2.4 coefficients a_i for different numerical schemes

scheme	a_W	a_E	a_{WW}	a_{EE}
Central Differencing	$D_w + F_w/2$	$D_e - F_e/2$	0	0
Upwind Differencing	$D_w + \max(F_w, 0)$	$D_e + \max(0, -F_e)$	0	0
Hybrid Differencing	$\max\left[F_w, \left(D_w + F_w/2\right), 0\right]$	$\max\left[-F_e, \left(D_e - F_e/2\right), 0\right]$	0	0
Power Law	$D_w \max\left[0, (1-0.1\lvert Pe_w\rvert)^5\right] + \max(F_w, 0)$	$D_e \max\left[0, (1-0.1\lvert Pe_e\rvert)^5\right] + \max(F_e, 0)$	0	0
Standard QUICK	$D_w + \frac{6}{8}\alpha_w F_w + \frac{1}{8}\alpha_e F_e + \frac{3}{8}(1-\alpha_w)F_w$	$D_e - \frac{3}{8}\alpha_e F_e - \frac{6}{8}(1-\alpha_e)F_e - \frac{1}{8}(1-\alpha_w)F_w$	$-\frac{1}{8}\alpha_w \times F_w$	$\frac{1}{8}F_e \times (1-\alpha_e)$
Hayase *et al.* QUICK	$D_w + \alpha_w F_w$	$D_e - (1-\alpha_e)F_e$	0	0

In Table 2.4, D_e, D_w are diffusion fluxes at cell faces e and w, F_e, F_w are convection fluxes at these cell faces; Pe is non-dimensional cell Peclet number, defined as the ratio of diffusion flux to convection flux at cell faces, α_e, α_w are taken either 1 or 0 according the sign of F_e, F_w. In Eq. (2.20) and Table 2.4 these values are calculated as:

$$
\begin{aligned}
&D_e = \left(\frac{r^2 D_M}{\Delta r}\right)_e \qquad D_w = \left(\frac{r^2 D_M}{\Delta r}\right)_w \\
&F_e = \left(ur^2\right)_e \qquad F_w = \left(ur^2\right)_w \\
&Pe_e = \frac{F_e}{D_e} = \left(\frac{u\Delta r}{D_M}\right)_e \qquad Pe_w = \frac{F_w}{D_w} = \left(\frac{u\Delta r}{D_M}\right)_w \\
&\alpha_e = 1, \ for\, F_e > 0, \quad \alpha_e = 0, \ for\, F_e < 0 \\
&\alpha_w = 1, \ for\, F_w > 0, \quad \alpha_w = 0, \ for\, F_w < 0
\end{aligned}
\tag{2.26}
$$

Then a_P is calculated as:

$$a_P = a_{EE} + a_E + a_W + a_{WW} + \left(F_e - F_w\right) \tag{2.27}$$

Although the central scheme is of second order in space and it has high accuracy when numerical Peclet number is smaller than 2, when Peclet number is greater than 2 this scheme suffers the problem of unboundedness. As a results it yields physically spurious oscillating solutions. Neither this scheme has the property of transportiveness.

The upwind scheme has the properties of boundedness and transportiveness, but it is based on backward differencing; so its accuracy is only of the first order in space. This also may be easily shown with the Taylor series truncation error analysis. This scheme results in "false diffusion" problems when *Pe* is large, see Patankar (1980).

The hybrid scheme exploits the favorable properties of the upwind and central schemes. It switches to the upwind scheme when the central scheme produces inaccurate results at high Pe number. The scheme is fully conservative and unconditionally bounded. It satisfies the transportiveness requirement by using an upwind formulation for large values of Peclet number. This scheme produces physically realistic solutions and is highly stable when compared with higher order schemes. The hybrid scheme has been widely used in various CFD procedures and has been proved to be very useful for predicting practical flows, Versteeg and Malalasekera (1995). The disadvantage is that its accuracy in terms of Taylor series truncation error is only of the first order in space.

Quadratic Upstream Interpolation for Convective Kinetics, the QUICK scheme, has the third order accuracy. The cell face values of fluxes are always calculated by quadratic interpolation between two bracketing nodes and an upstream node. This scheme has the properties of conservativeness and transportiveness, but boundedness and stability are problems when Peclet number is greater than 8/3. There are several improvements to the QUICK scheme, such as QUICKC, Hayase *et al.* (1992). The Hayase *et al.* (1992) QUICK scheme overcomes the boundedness and stability problem suffered by general QUICK. In this scheme, there is an extra source term in the RHS of Eq. (2.25):

$$\begin{aligned}\bar{S} = &\frac{1}{8}(3\phi_P - 2\phi_W - \phi_{WW})\alpha_w F_w + \frac{1}{8}(3\phi_W - 2\phi_P - \phi_E)(1-\alpha_w)F_w \\ &+ \frac{1}{8}(\phi_W + 2\phi_P - 3\phi_E)\alpha_e F_e + \frac{1}{8}(2\phi_E + \phi_{EE} - 3\phi_P)(1-\alpha_e)F_e\end{aligned} \tag{2.28}$$

where, the values of α_w, α_e are determined from Eq. (2.26). It should be noted that all variants of QUICK scheme give the same solution upon convergence. Another advantage offered by modification Eq. (2.28) is that resulting discrete equations corresponding to a tri-diagonal matrix and henceforth may be solved with the help of TDMA algorithm, unlike the original QUICK.

In the present work, Hybrid, and the QUICK scheme of Hayase *et al.* are used. The solution algorithm is as follows:

1) at time 0, set initial values for $u(r,0) = 0$ and Y_i;
2) use subroutine " EULSIM " to obtain chemical reaction rates w_i;
3) solve Eq. (2.20) by TDMA method to get Y_i^{n+1};
4) calculate P^{n+1} according to Eq. (2.24);
5) calculate ρ^{n+1} from the ideal gas equation of state;
6) calculate $u(r,t)$ according to Eq. (2.21a);
7) repeat steps 2) to 6)

In simulation, the independence of solution upon grid size and time step have been tested with both differencing schemes. Different grid sizes (with 1000, 2000, 5000 and 8000 nodes in the r direction) have been tested, it was found that a mesh of 5000 nodes in the r direction provided sufficient resolution as a further mesh-refinement produced no change in results. Time steps of 1.0×10^{-4} and 1.0×10^{-6} s have been tested with 5000 nodes in the r direction and it was found that a time step of 1.0×10^{-4} s proved adequate.

2.4.3 Simulations and Results

2.4.3.1 Parameters for Simulations

Spherical laminar flame propagation for three different equivalence ratios (ϕ = *0.8*, *1.0* and *1.2*) for the initial temperature of 300 K with initial pressures of both P_0=1.0 *bar* and 5.0 *bar*, have been simulated.

In the simulations, the radius of combustion chamber was taken as an equivalent radius given by $R_b = \left(\frac{3V_b}{4\pi}\right)^{1/3}$ for the Leeds quasi-spherical bomb, namely R_b= 193 *mm*. The initial flame kernel produced by the spark was considered as a flame ball of hot products with 2.0 *mm* radius. The numerical study of Bradley *et al.* (1996b) confirmed that such a procedure, dependent (in principle) on the spark discharge energy, will have an effect on the flame speed only for flame radius smaller than 5.0 *mm*. In the 1-D simulations of spherical flame by Bradley *et al.* (1996b), the numerical setting of the initial flame ball size was 1.7 *mm* and the grid size was 40 nodes/*mm*; cf the 27 nodes/*mm* in the present work. In *Appendix C*, flame propagation is shown to be independent of the method of flame kernel initiation (either by hot spot or by pre-defined energy deposit) and also independent of initial energy deposit after some short initial period.

2.4.3.2 Determination of Flame Radius and Mass Burning Velocity

To compare the results of modelling with Schlieren imaging of the flame, one needs to calculate what is commonly called flame radius. Here flame radius has been calculated using two procedures. One was to assume a flame radius equal to the position of on isotherm at T = 305 K. The other technique was to calculate flame radius from the pressure rise. The flame radius and mass burning rate determined from the pressure rise were calculated adopting the relationships proposed by Lewis and von Elbe (1951). This procedure may be summarised in modified form (Zel'dovich *et al.*, 1985) as follows:

$$r(t) = R_b \left[1 - \frac{P_{eq} - P(t)}{P_{eq} - P_{ini}} \left(\frac{P_{ini}}{P(t)} \right)^{1/\gamma_u} \right]^{1/3} \qquad (2.29)$$

$$u_n = \frac{R_b^3 - r^3(t)}{3r^2(t)(P_{eq} - P(t))} \frac{dP}{dt} \qquad (2.30)$$

where P_{eq} is the thermodynamic equilibrium pressure at the end of combustion, P_{ini} is the initial pressure, $P(t)$ is the pressure at time t, $r(t)$ is equivalent flame radius at time t, γ_u is the ratio of specific heat at constant pressure to that at constant volume for unburnt gas. The equilibrium pressure and γ_u were calculated using the chemical equilibrium

code named Gaseq, for details see the web site *http://www.c.morley.ukgateway.net*. Computed values are listed in Table 2.5.

Table 2.5 Computed parameters used to determine flame radius and burning velocity

	$P_0 = 1.0\ bar$		$P_0 = 5.0\ bar$	
	γ_u	$P_{eq}\ (bar)$	γ_u	$P_{eq}\ (bar)$
$\phi = 0.8$	1.389	7.952	1.389	40.105
$\phi = 1.0$	1.387	8.752	1.387	44.643
$\phi = 1.2$	1.385	8.874	1.385	44.805

2.4.3.3 Simulation Results

Profiles of temperature and species concentration for various conditions, calculated for spherical laminar flame propagation using the numerical methods described above, are presented in Figs. 2.6 to 2.9. It can be inferred that the flame attains rapidly a steady regime of propagation. This observation is further supported by the "magnified" flame structure shown in Figs. 2.10 to 2.12, for various equivalence ratios at an initial pressure of 1.0 *bar*. Similar results are represented in Figs. 2.13 to 2.15 for an initial pressure of 5.0 *bar*.

Shown in Fig. 2.16 is the comparison of flame structure predicted with present two-step scheme with that computed by Dixon-Lewis (1990) using detailed kinetic shceme for ϕ = 1.0, P_0 = 1.0 *bar*. For convenience, in Fig. 2.16 the space coordinate is rescaled and zero point is taken at the position of peak value of *CO* concentration. The kinetic scheme used by Dixon-Lewis is the CH_4/C_2H_6 oxidation scheme of Warnatz (1981) and modification is made for CH_4/air flame with pyrolysis reaction truncated at entylen stage. This scheme is successful for computating laminar burning velocity as well as flame structure for several lean and slightly rich premixed CH_4/air flames (Dixon-Lewis, 1990). This scheme gives u_L = 36.7 *cm/s* for ϕ = 1.0, P_0 = 1.0 *bar*, T_0 = 295 *K*, and the prediction of flame strurce is shown in Fig. 2.16.

The thickness of reaction zone predicted by present scheme is approximately 4 time thicker than that of Dixon-Lewis. One reason is that present scheme uses lower activation energy for the first reaction (Eq. (2.23)). Except the flame thickness, several common properties of the flame have been predicted by the two scheme: 1) two-stage combustion mode; 2) at the position of peak value of *CO* concentration all the CH_4 has disappeared; 3) particularly, a temperature (T_i specified by Dixon-Lewis) is coincident with the peak value of *CO* concentration, which characterises the start of a very fundamental part of overall flame progress similar to ignition temperature of thermal therories of flame propagation (Dixon-Lewis, 1990). The radical pool is considered as $H+2O+OH+CH_3+C_2H_5+HO_2+HCO$, and Dixon-Lewis showed that the net radical production only occurs at the temprature higher than T_i. The comparison in Fig. 2.16 confirms that presented two-step kinetic scheme can capture the properties of flame structure althogh radical pool is neglected.

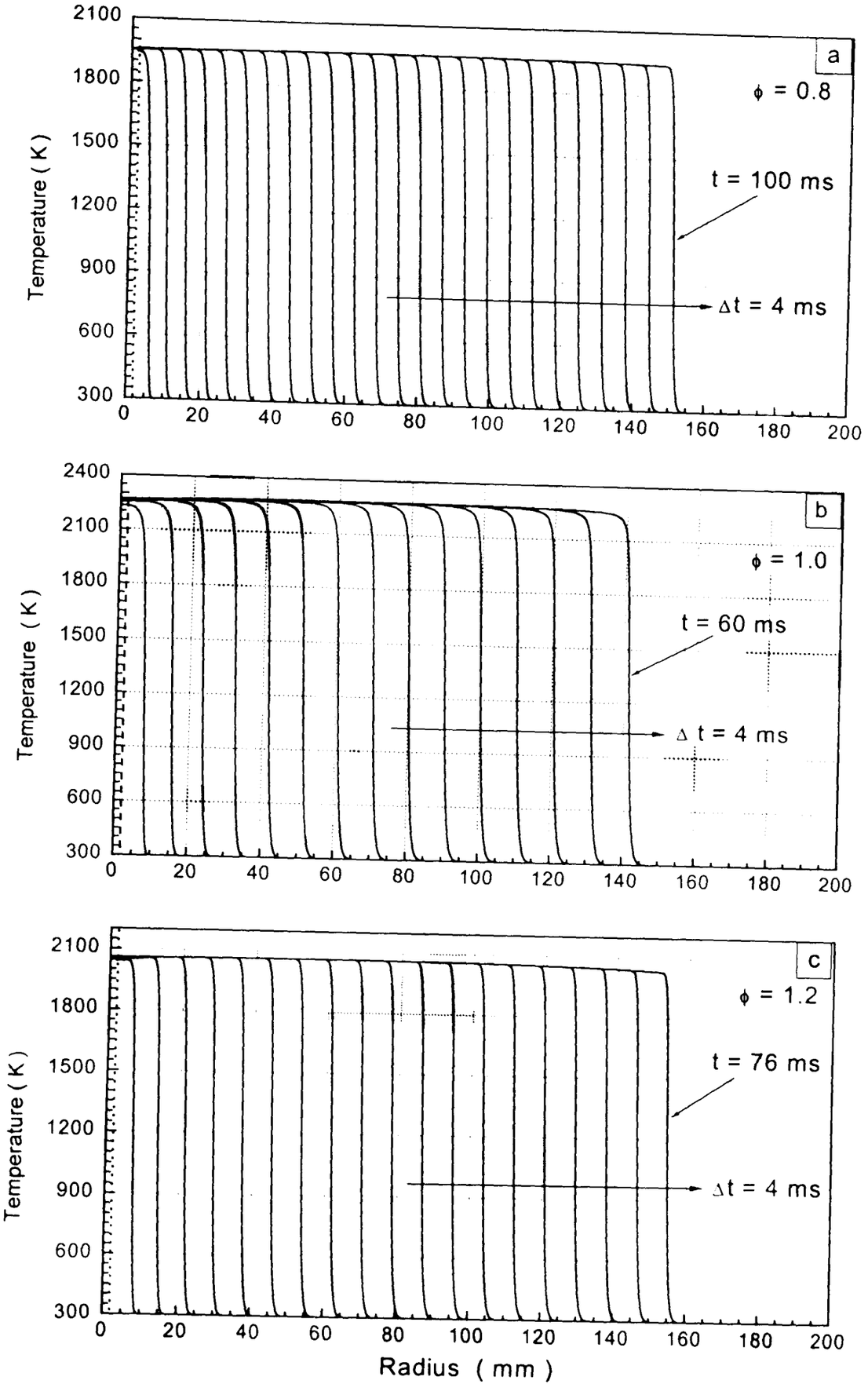

Fig. 2.6 Simulated temperature profiles at $T_0 = 300\ K$, $P_0 = 1.0\ bar$

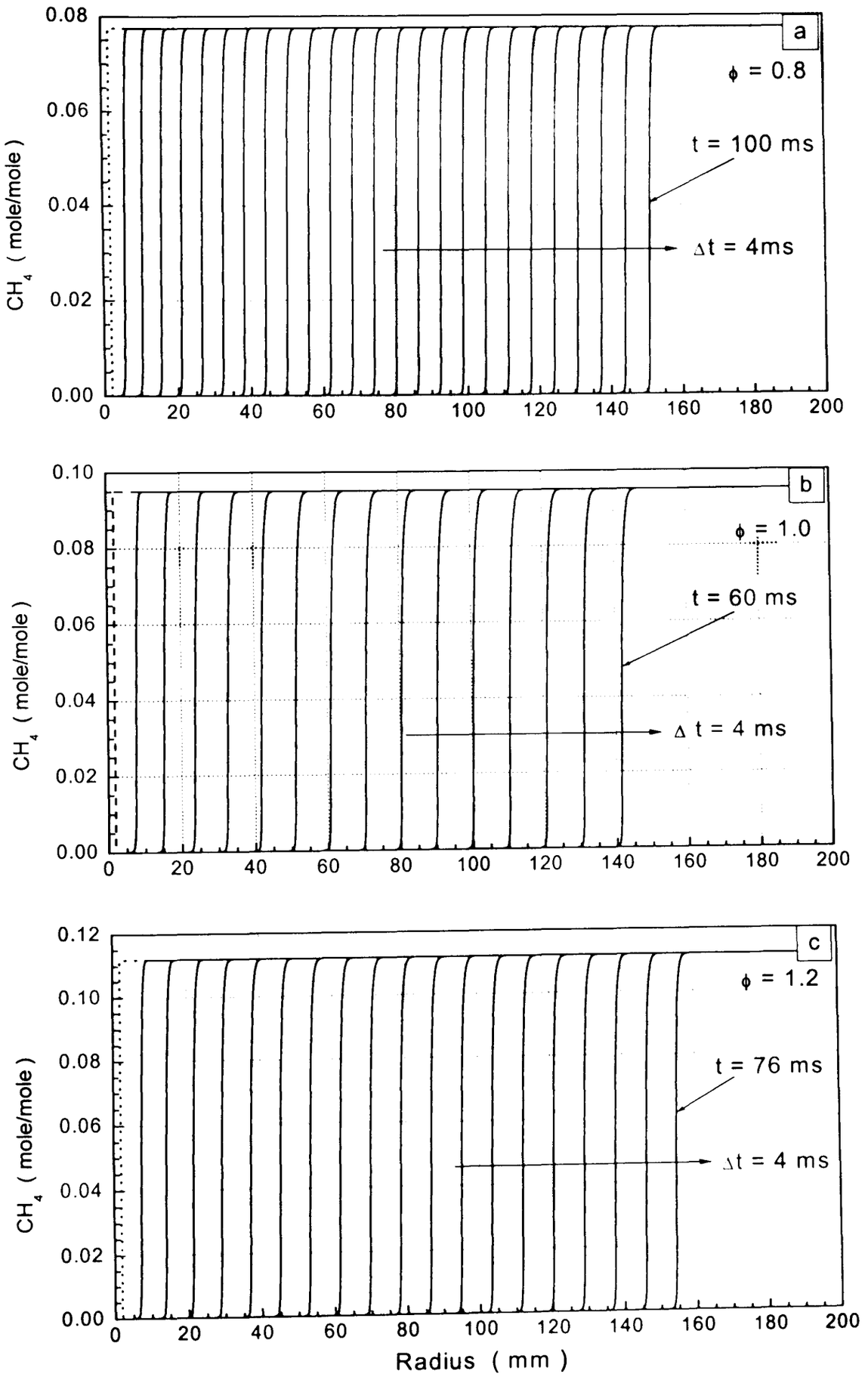

Fig. 2.7 Simulated CH_4 profiles at $T_0 = 300\ K$, $P_0 = 1.0\ bar$

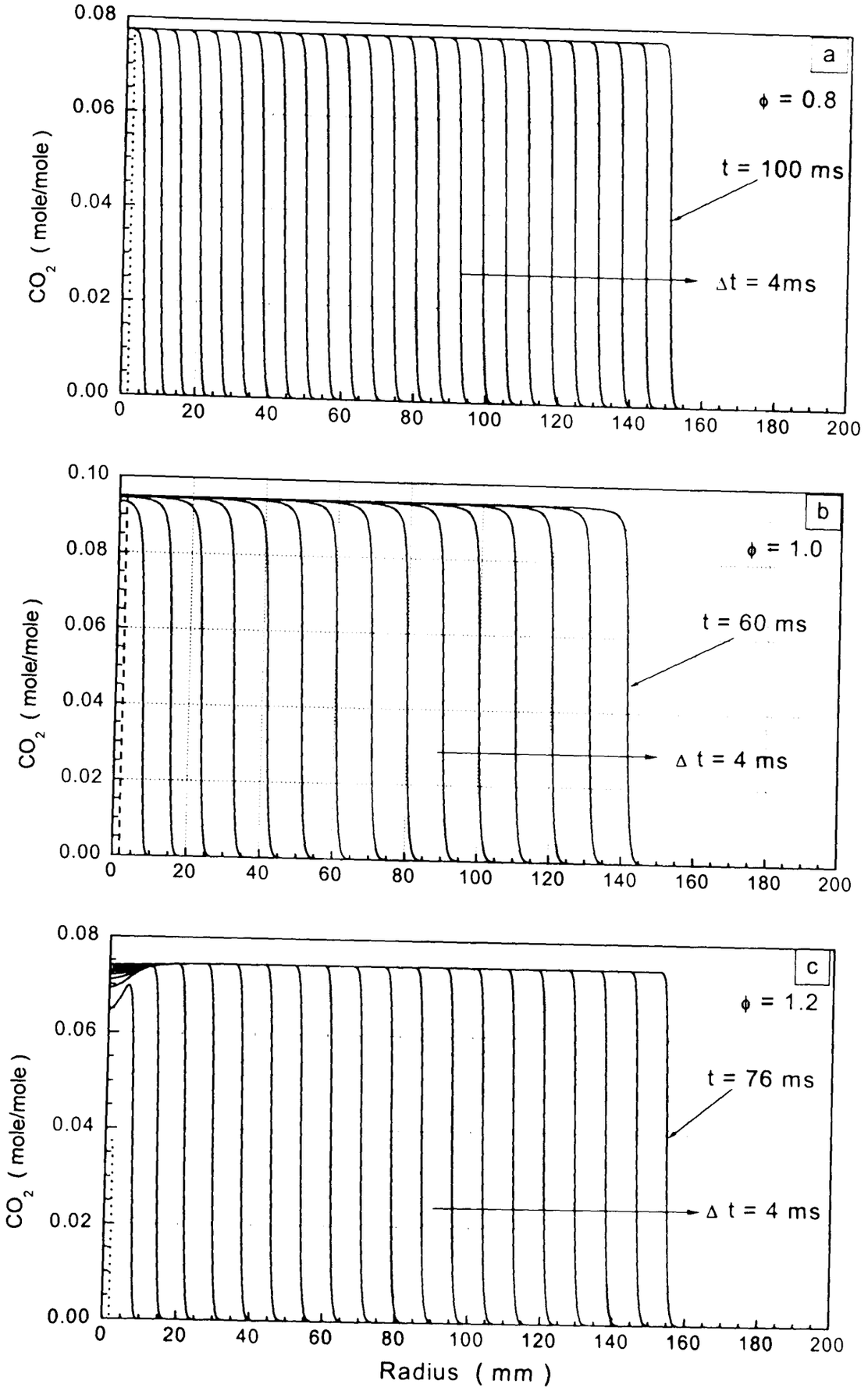

Fig. 2.8 Simulated CO_2 profiles at $T_0 = 300\ K$, $P_0 = 1.0\ bar$

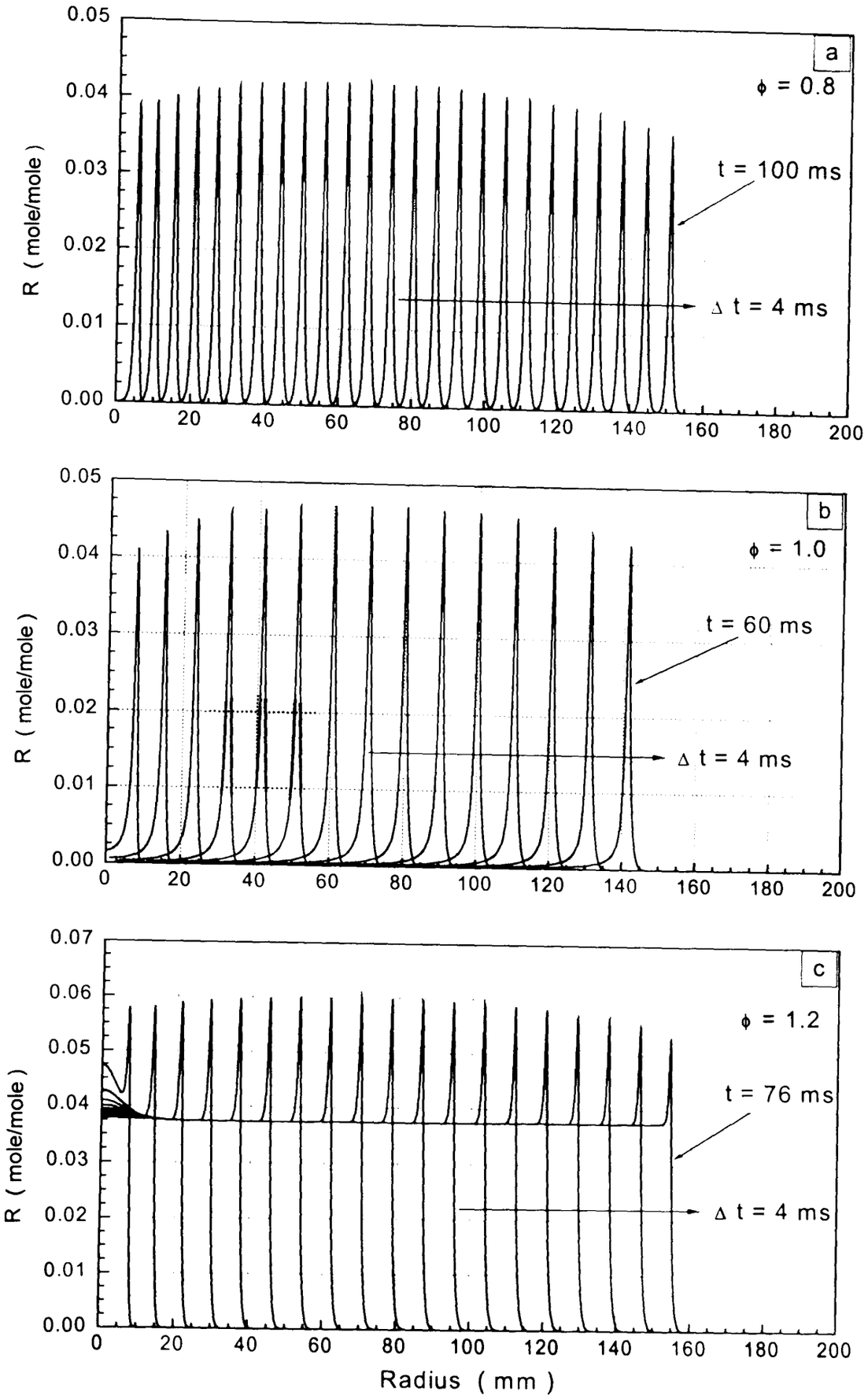

Fig. 2.9 Simulated intermediate profiles at $T_0 = 300\ K$, $P_0 = 1.0\ bar$

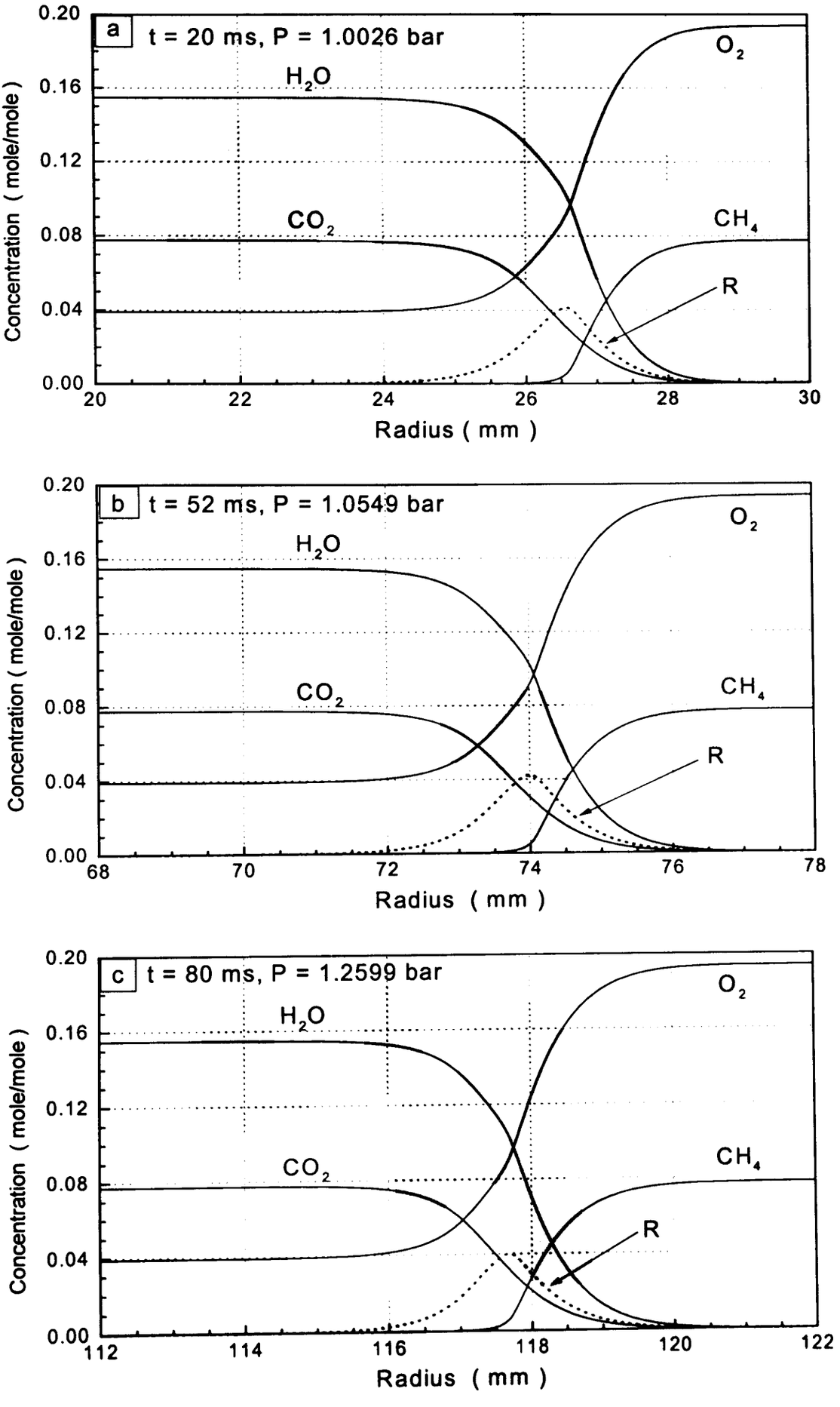

Fig. 2.10 Flame structure for mixture of $\phi = 0.8$ at $T_0 = 300\ K$, $P_0 = 1.0\ bar$

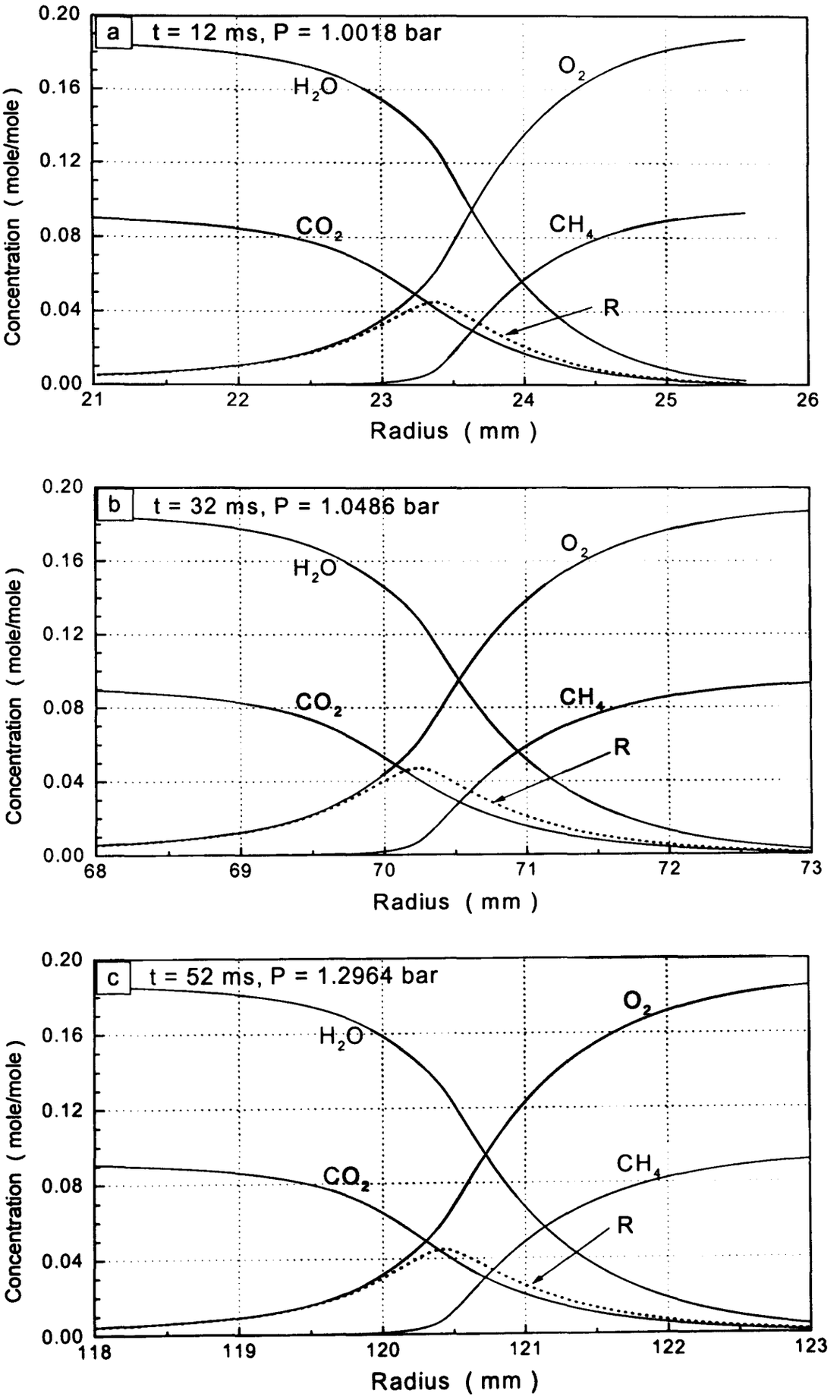

Fig. 2.11 Flame structure for the mixture of $\phi = 1.0$ at $T_0 = 300\ K$, $P_0 = 1.0\ bar$

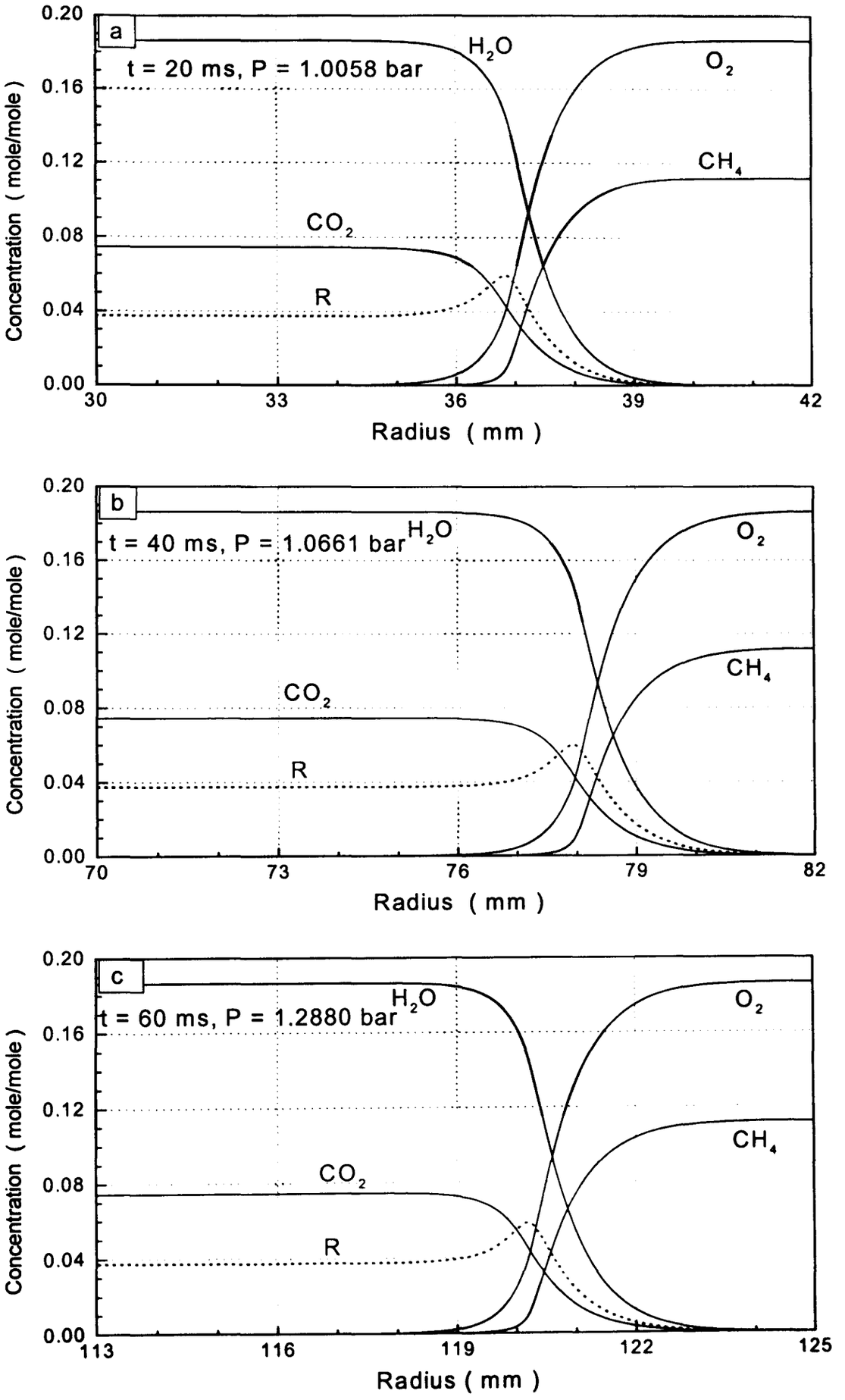

Fig. 2.12 Flame structure for the mixture of $\phi = 1.2$ at $T_0 = 300\ K$, $P_0 = 1.0\ bar$

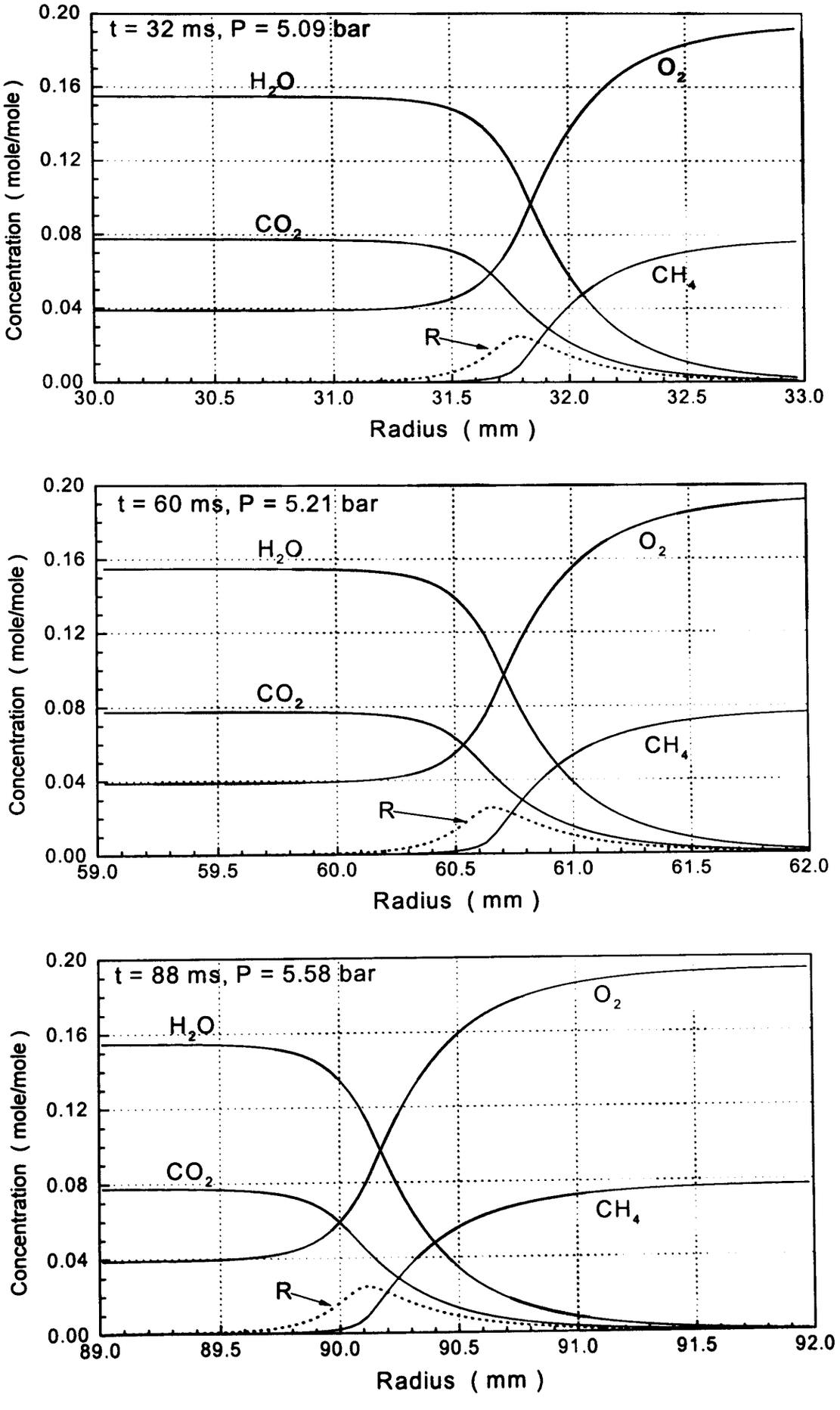

Fig. 2.13 Simulated flame structure for $\phi = 0.8$, $T_0 = 300\ K$, $P_0 = 5.0\ bar$

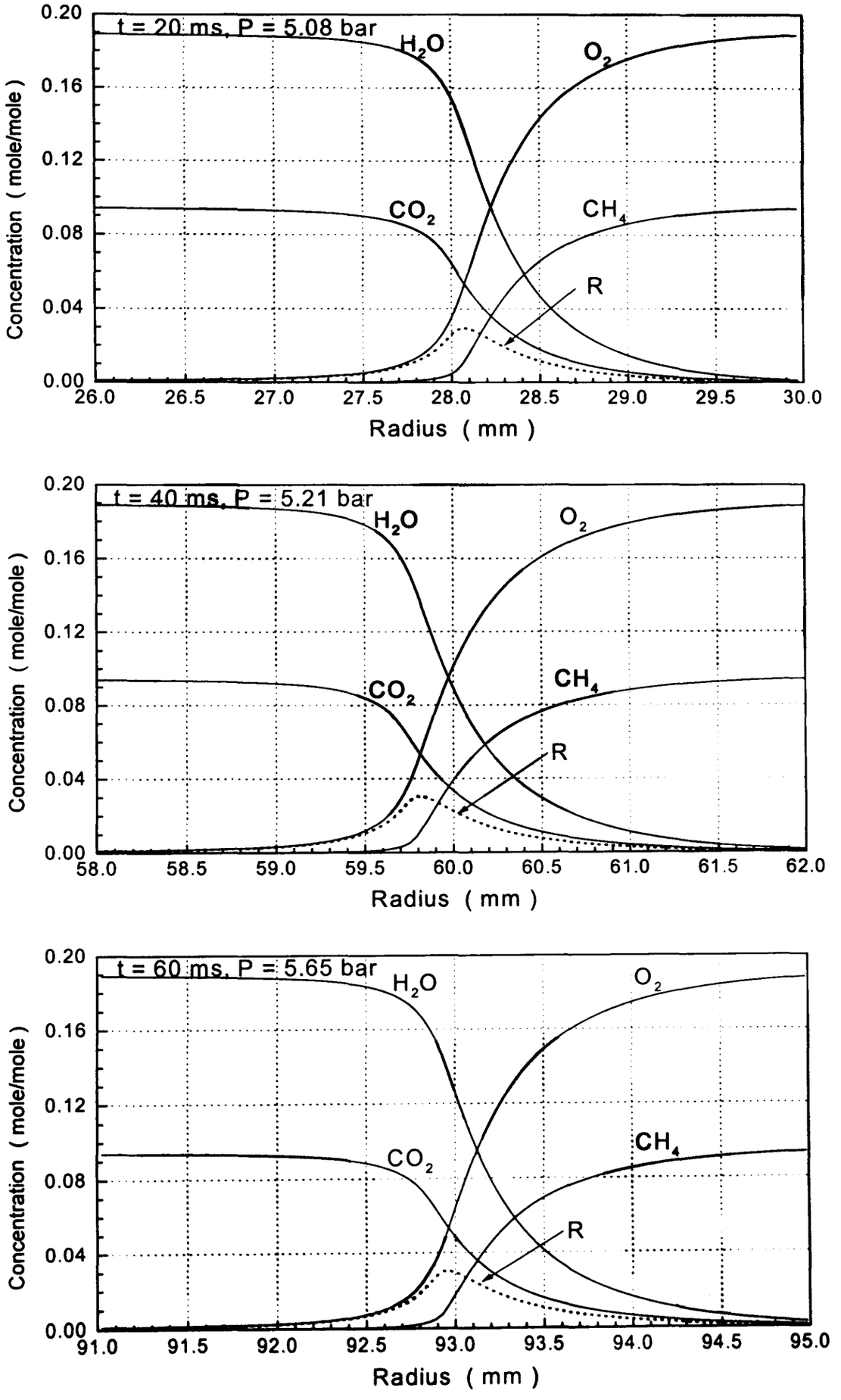

Fig. 2.14 Simulated flame structure for $\phi = 1.0$, $T_0 = 300\ K$, $P_0 = 5.0\ bar$

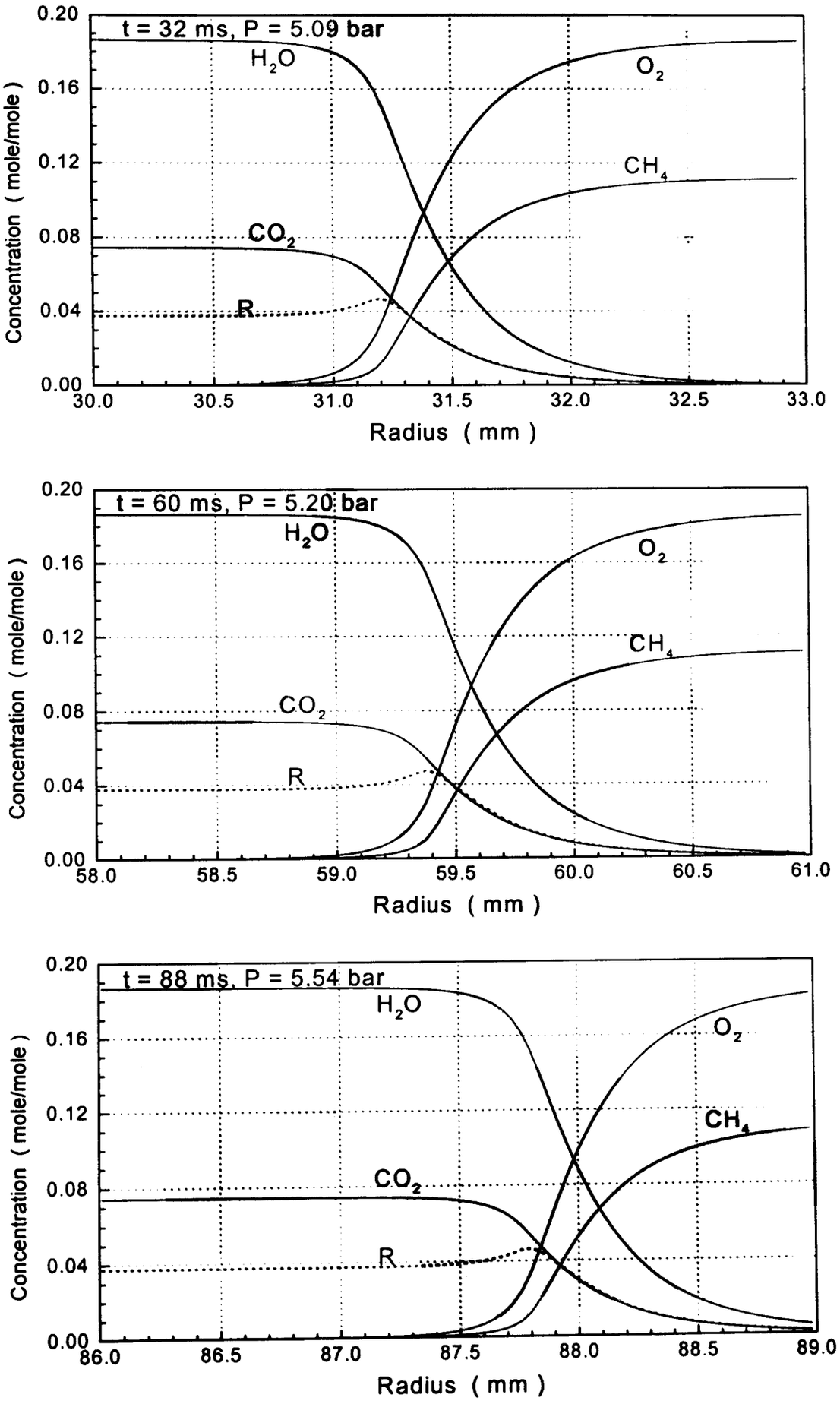

Fig. 2.15 Simulated flame structure for $\phi = 1.2$, $T_0 = 300\ K$, $P_0 = 5.0\ bar$

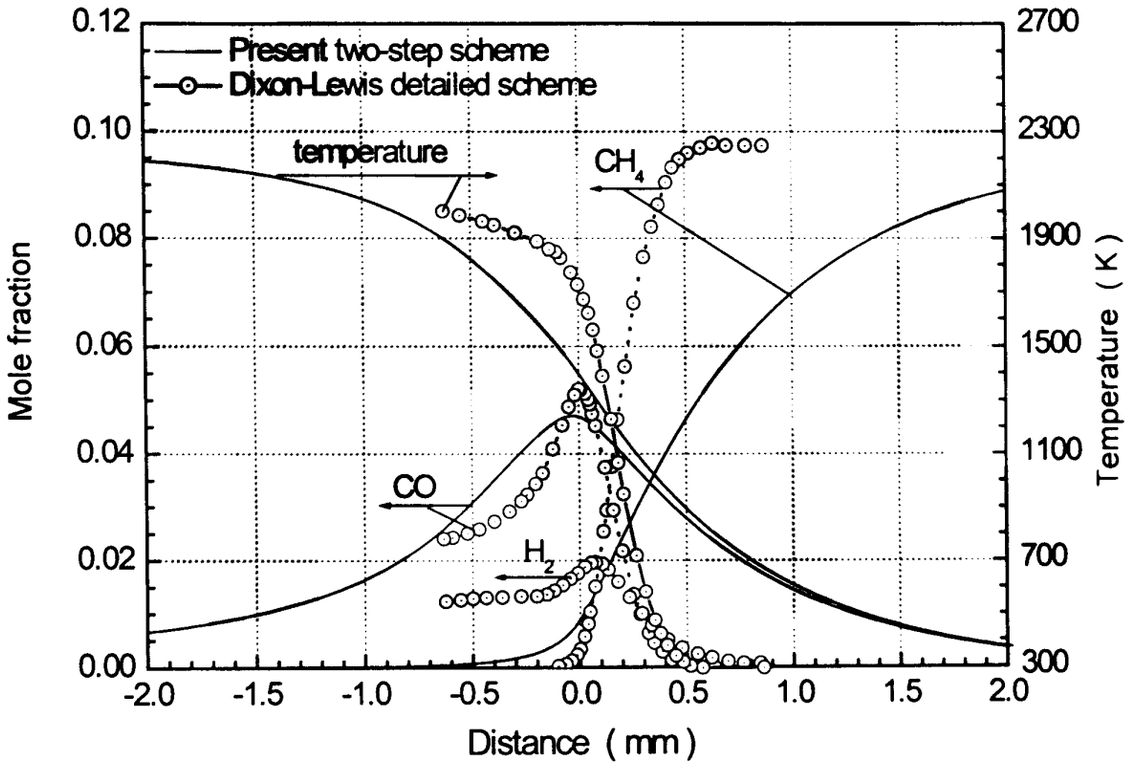

Fig. 2.16 Comparison of laminar flame structure between present two-step scheme simulation and detailed scheme computation by Dixon-Lewis (1990) for $\phi = 1.0$, $P_0 = 1.0$ *bar*

Shown in Figs. 2.17 to 2.22 are pressure, flame radii and mass burning velocity for various equivalence ratios. The results of the simulations are also compared with the measurements done by the author for initial pressure of 1.0 *bar*, the results for initial pressure of 5.0 *bar* done by Woolley, (Woolley, 2001). The purpose-conducted experiments were carried out using the Leeds quasi-spherical bomb, with central ignition system. Schlieren images during methane-air explosions were recorded by a fast camera (*5000 frame/s*) with simultaneous pressure record by Kistler 701A pressure transducer mounted flush to the wall. Details of the experimental arrangement are given in *Appendix A*.

Ideally, the results of simulation should be independent of choice of particular numerical procedures. To verify this, flame radii and burning velocity data for computed stoichiometric mixture using the Hybrid and the Hayase *et al.* version of the QUICK scheme were compared with measurement using pressure method. The results are shown in Fig. 2.17. As noted previously, calculated flame radius was determined either from the position of temperature isotherm corresponding to a 5 K rise or from pressure rise using Eq. (2.24). In the latter case, the burning velocity was calculated using Eq. (2.30). The results of simulations agree quite well with each other, as well as with measurements, for the two numerical schemes employed, although there exists a difference of about 1.0 *cm* of flame radius found from isothermal line position and from the pressure rise. From analysis of Fig. 2.17 one can infer that both finite-difference schemes used yield essentially identical results. Hereafter, unless otherwise stated, the results shown were obtained using the Hybrid finite-difference scheme.

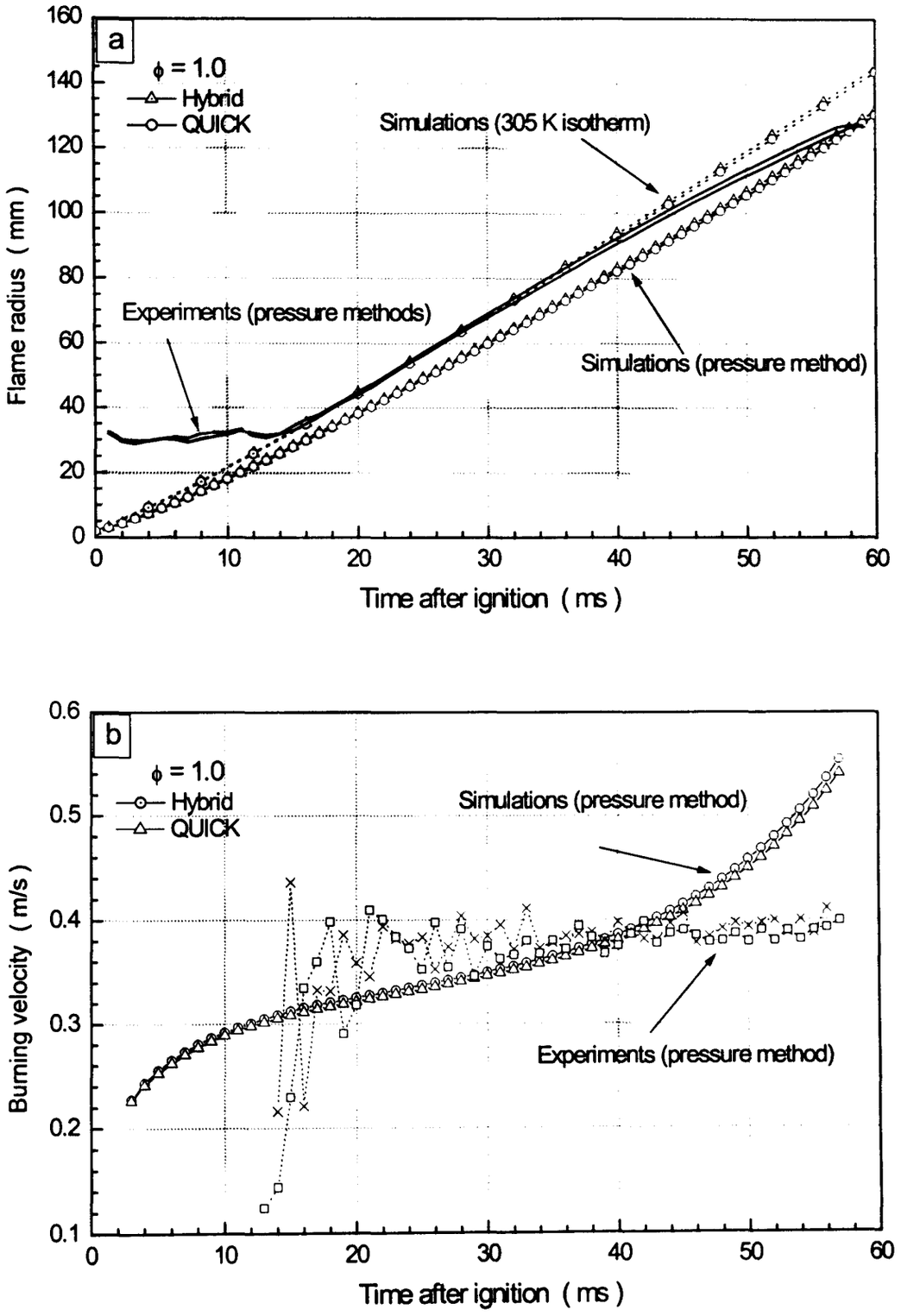

Fig. 2.17 Comparisons of results obtained with Hybrid and QUICK finite differencing schemes, $T_0 = 300\ K$, $P_0 = 1.0\ bar$

Presented in Fig. 2.18 are comparisons of the calculated flame radii (both on the basis of pressure rise and location of the 305 K isotherm) and the measured flame radii (from Schlieren filming and as calculated from the pressure record). The calculations show flame radius increasing nearly proportional to the time. The maximum radius for Schlieren derived experimental radius is limited by the bomb window size; the experimental pressure derived radii at the start of combustion are rendered unreliable by spark induced electrical interference. At intermediate stage, though, the radii derived from the two experimental methods agree well. For an equivalence ratio of 0.8, agreement between the two simulations and experimental data is good, particularly at small to moderate radii where neglect of effects of pressure and temperature rise in the unburnt mixture is justified. For stoichiometric and rich mixtures, measurements are closer to radii computed from 305 K isotherm than to those obtained from pressure. This may point to inadequacies in the simplified reaction rate modelling of Eq. (2.13). However, it has to be emphasised that the purpose of this work is to study the details of turbulence-chemistry interaction which can be predicted with the help of LEM and RSF models. By this reason, one may argue that the level of accuracy demonstrated in Figs. 2.18 to2.22 would be sufficient for this purpose.

This conclusion is further corroborated by analysis of Fig. 2.19, where are plotted the mass burning rates u_n calculated and measured from the pressure rise for different equivalent ratios and initial pressures. The history of the mass burning rate development is different, in experiments u_n attains nearly constant value at later stage of explosion, while in calculation u_n is steadily increasing (the rapid decrease in u_n at the later stage is explained with the flame approaching the wall). However, the rate of this increase is small, and for the most of explosion duration u_n values agree with the measurements within 30%. As demonstrated in *Appendix D*, the steadily increasing u_n in simulation is due to the modelling of molecular diffusivity, current model did not include the pressure effect on molecular diffusivity, only temperature effect was considered. With pressure rise in the bomb, molecular diffusivity is reduced, so one can expect u_n to be reduced as well.

To check this aspect, a series of computations for initial pressure of P_0 = 5.0 *bar*, T_0 = 358 *K* has been undertaken and the results are presented in Figs. 2.20(b), 2.21 and 2.22 for comparisons with measurements at the same conditions for pressure, flame radius and burning velocity. The present model is able to reproduce qualitatively decrease in u_n for elevated pressures which is due to greatly reduced molecular transport coefficients, though for rich mixture the agreement is not as good as for 1.0 *bar*. The corresponding results for turbulent mass burning rate are presented later in this thesis.

As previously noted, the data derived from Schlieren imaging of spherical explosions, here and for experiments elsewhere, is limited to flame kernel radii inferior to the size of the observation windows; this is usually not greater than a few centimeters. Within this time (or flame size) interval, the present oversimplified kinetics deliver performance comparable with (if not superior to) much more complicated "full" kinetics schemes (such as various variants of GRI-Mech mechanism). As noted previously, it is not practicable yet to use a kinetic scheme of several dozens/hundreds elementary step reactions for turbulent combustion modelling, so the present approach, with the use of only two step chemical kinetics, is considered justified.

The ultimate assessment of any combustion model is its ability to predict the effects of pressure on the (average) heat release rate. One of the most serious drawbacks of the so-called laminar flamelet approach, considered above, is that it results in u_t decreasing with initial pressure rise, because in this approach $u_t \sim u_n$ for the same turbulence parameters. At the same time, the experiments show that u_t either increases with or is independent on initial pressure rises, while u_n is markedly decreasing.

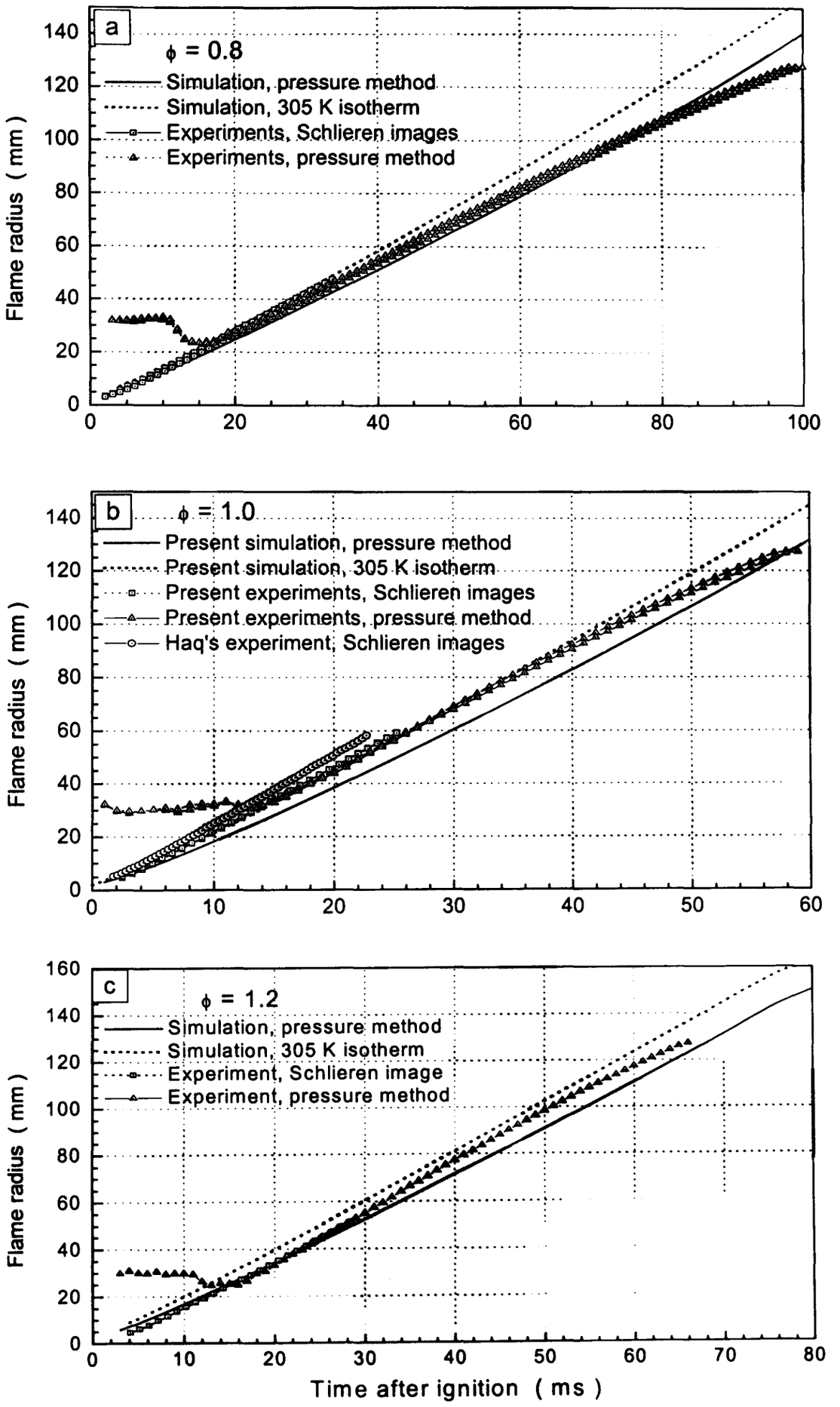

Fig. 2.18 Laminar flame growth, initial conditions of $T_0 = 300\ K$, $P_0 = 1.0\ bar$

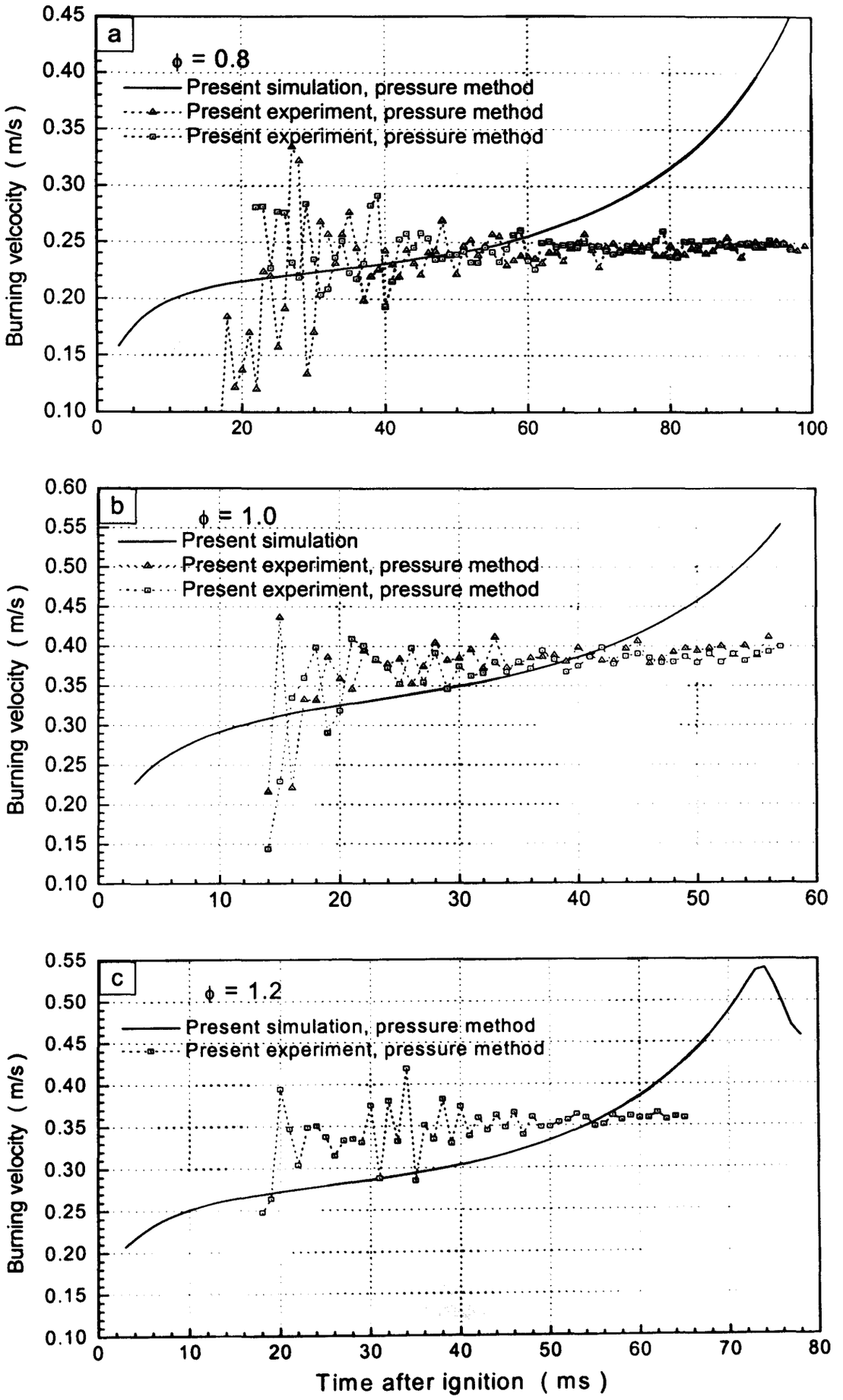

Fig. 2.19. Burning velocity simulated by pressure tracing method

$T_0 = 300\ K$, $P_0 = 1.0\ bar$

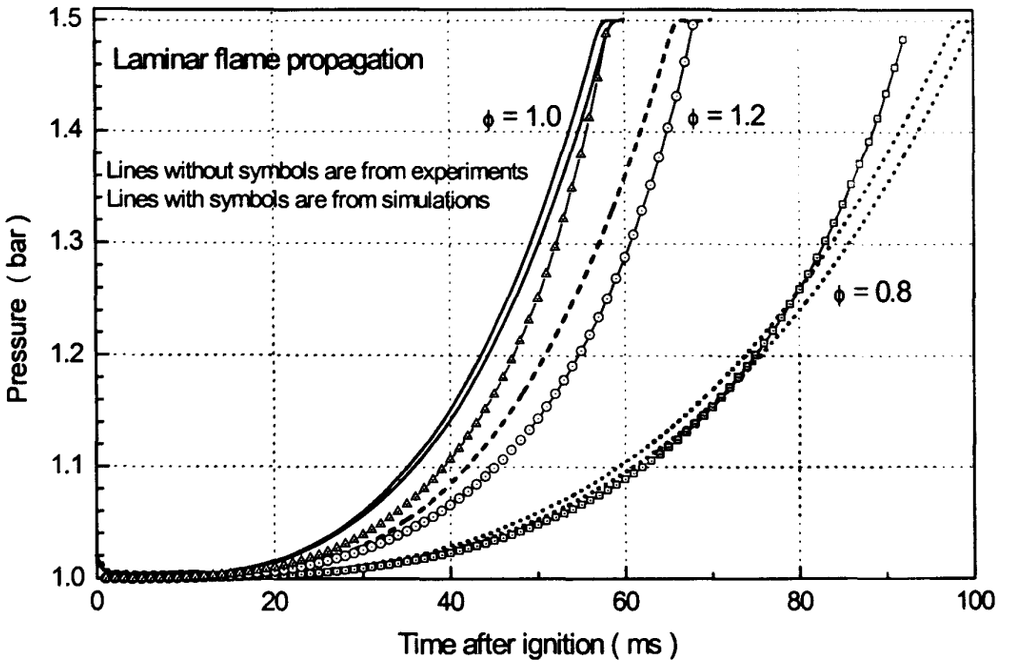

Fig. 2.20(a) Comparison of pressure history between experiments and simulations for laminar flame propagation of $T_0 = 300\ K$, $P_0 = 1.0\ bar$

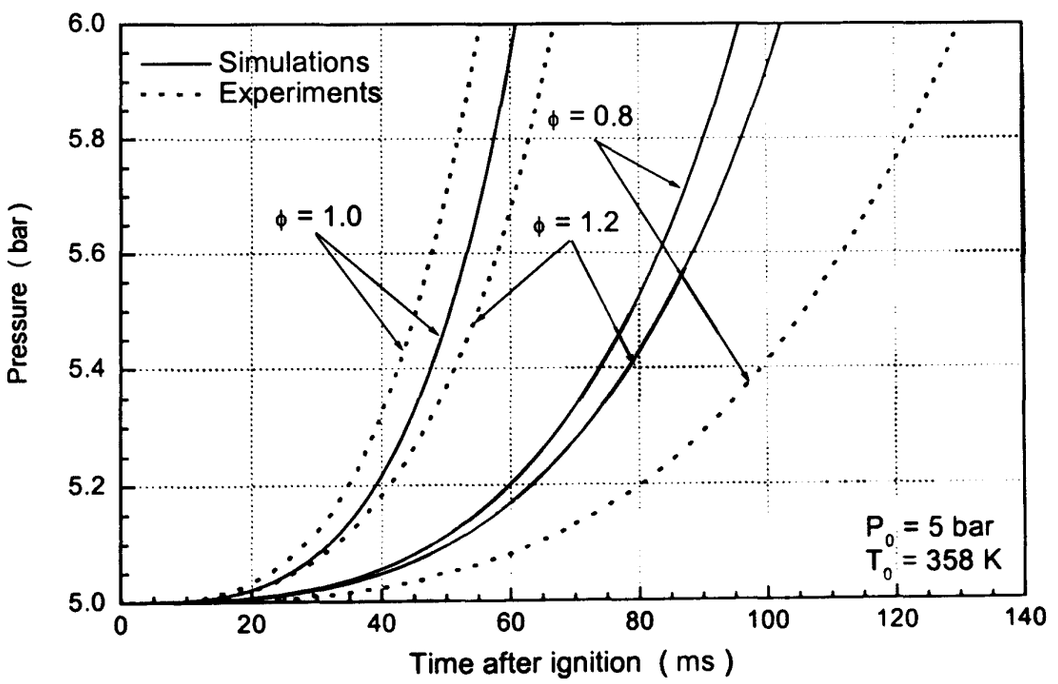

Fig. 2.20(b) Comparison of pressure history between experiments and simulations for laminar flame propagation of $T_0 = 358\ K$, $P_0 = 5.0\ bar$

Fig. 2.20 Pressure history for laminar flame propagation

More specifically, observation of Figs. 2.21 and 2.22 shows the present chemical kinetics applied to higher pressure yields, for a stoichoimetric mixture, a good agreement in terms of flame radius and burning velocity. However, it also predicts faster flame propagation than measurements for lean mixtures and much slower flame propagation for rich mixtures. One also can notice from these three figures that the present chemical kinetic scheme results in slower flame propagation for $\phi=1.2$ than for $\phi=0.8$, at contradiction with the measurements. This is an obvious deficiency of the present chemical kinetic scheme, which needs to be extended for rich mixtures and high pressures. Nevertheless, it must be noted that rich hydrocarbon-air mixtures involve notoriously complicated chemical kinetics; and no reliable literature data has been found for accurate simulation of laminar flame propagation in rich mixtures at high pressures.

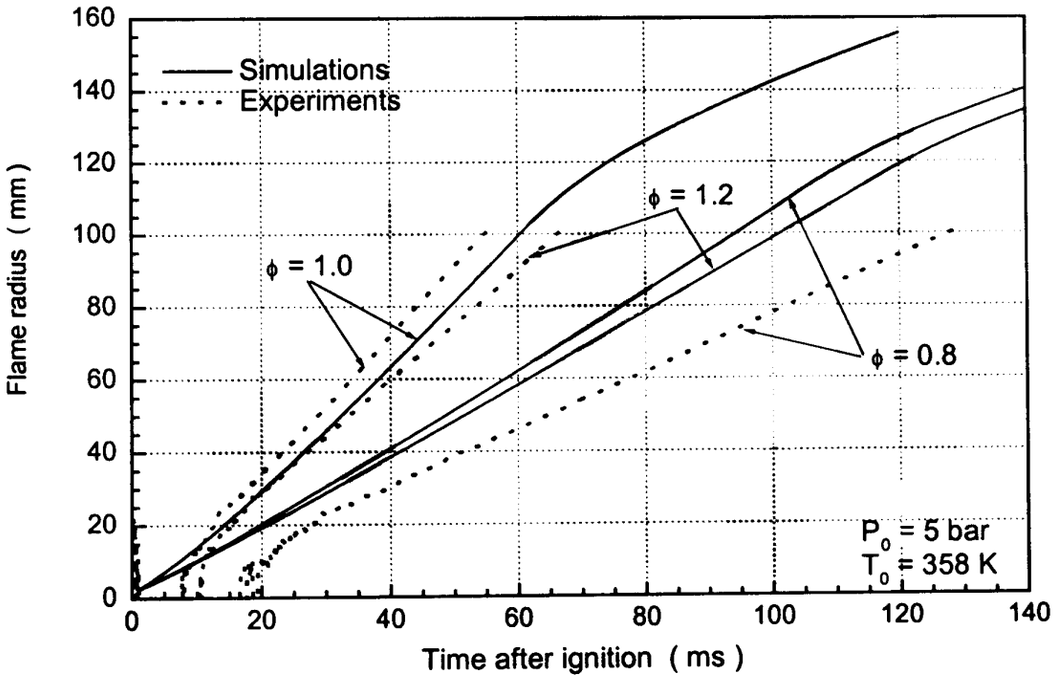

Fig. 2.21 Comparison of flame radius between experiments and simulations for laminar flame of $T_0 = 358K$, $P_0 = 5.0$ *bar*

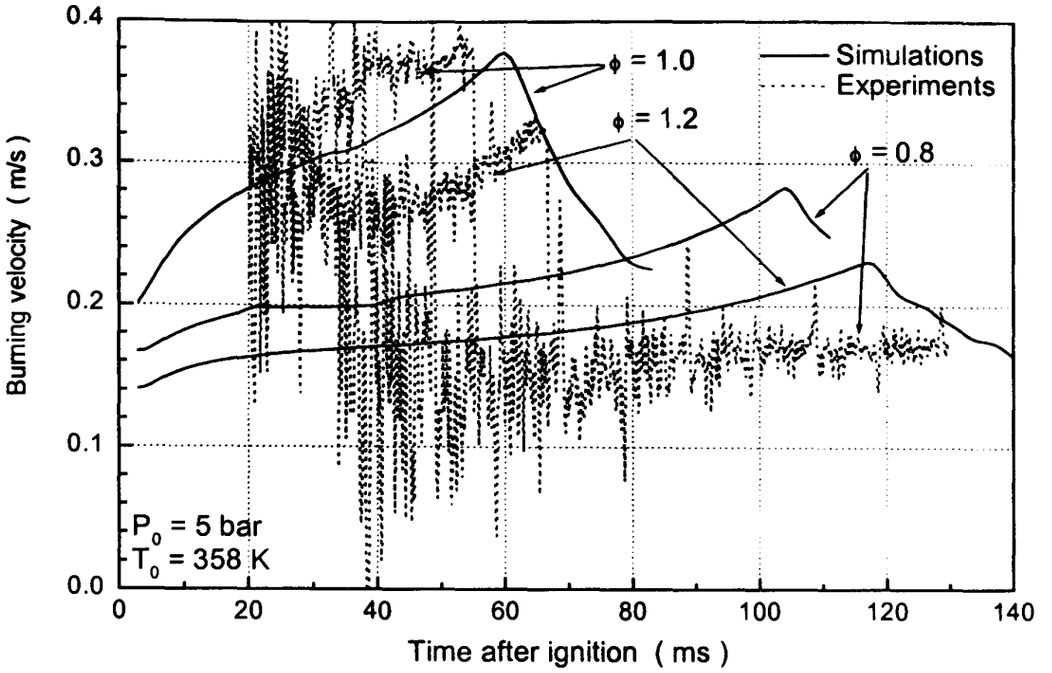

Fig. 2.22 Comparison of burning velocity between experiments and simulations for laminar flame of $T_0 = 358K$, $P_0 = 5.0$ *bar*

2.5 Summary

The work reported in this chapter, a foundation for what follows, has been concerned with the selection of a two-step chemical kinetic scheme and its assessment for cases of self-ignition and 1-D spherical laminar flame propagation. In simulation of self-ignition, the autoignition delay times predicted using the two-step reduced chemical kinetic mechanism agreed well with empirical correlation derived from shock tube experiments, over a wide range of initial temperatures. In the simulation of 1-D flame propagation, the profile of species and temperature, flame structure and flame kernel developments have been computed for lean, stoichiometric and rich fuel and air ratio mixtures. The scheme was able to reproduce the two-stage combustion character as well as the chemical time scales pertinent to CH_4 oxidation.

Chapter 3

Study of the Effects of Turbulence on Self-Ignition

3.1 Introduction

The spontaneous or self-ignition of hydrocarbon fuels is an important phenomenon playing a role in many practical applications. For example, it is the principle mode of ignition in Diesel engines. Conversely, in petrol engines, self-ignition is believed to be responsible for the highly non-desirable phenomenon of knock. Whether the effects of self-ignition are desirable or not, it is often necessary to know, quantitatively, the various sub-processes that control the self-ignition of a combustible mixture.

There are two distinctly different contributions to self-ignition: chemical and physical. For nearly every practical fuel the chemical kinetics of oxidation is extremely complex. However, their details may be represented in terms of a sole parameter, the so-called chemical ignition delay, or induction time, τ_c, defined by the finite rates of chemical reactions, or more precisely, by the rate of accumulation of radicals *i.e.* by the chain-initiation reactions. The ignition delay may be calculated once details of the chemical kinetics reaction mechanism are known.

In practice, experimentally observed ignition delays vary from one set of experiments to another and are usually greater than calculated chemical delays. The difference is called the physical ignition delay and it may be provoked by various processes, such as heat losses, vaporization, mixing and turbulence. Obviously, this physical delay would be different for a continuos flow device, *e.g.* as one used in the work of Mullins (1953) and the rapid compression machines (RCMs) of Beeley (1980), Griffiths and co-workers (1993, 2001).

The interaction of chemistry and flow motion may also be one of the reasons why the self-ignition phenomenon is believed complicated and is not fully understood, in spite of numerous studies devoted to it. There are also some intrinsically stochastic features,

e.g. spatial location of ignition sites cannot, in principle, be predicted, because of the statistical nature of the phenomenon.

Although studies of auto-ignition have been performed for many years, there are still many questions to be answered which are worth further study. For example, problems do exist in nearly every experimental study whether it be a continuous flow device, shock tube or Rapid Compression Machines, see below.

A continuous flow reactor (see Mullins (1953) for realisation of a classical example of this technique) is an apparatus, in which fuel is injected into a high temperature air stream and the combustible mixture ignites at some distance downstream of the injection location. In the continuous flow device, the time necessary for small-scale mixing processes and vaporisation may play a key role in ignition delay and it is hard to calculate precisely. An indication of this is that ignition delays determined by this method are usually longer than those measured by other methods.

A shock tube may as well be used to produce a high temperature gas under well-controlled test conditions. It is the only experimental facility that can produce sufficiently short compression and heat-up times. It possesses some definitive advantages, such as cleanliness, wide pressure and temperature ranges accessible without the necessity to change the composition of the inert fractions of the charge. The mixtures under investigation are generally diluted with a large fraction of inert gas (heat bath) (Ciezki and Adomeit, 1993). This has an additional advantage that temperature and pressure stay almost constant throughout the experiment, which allows a direct kinetic evaluation of reaction rates. However, because of very short residence times, the shock tube technique is ordinarily limited to times of measurement below 10 *ms*.

A rapid compression machine is used to study the autoignition of hydrocarbon and air mixtures in conditions similar to those in the combustion chamber of an IC engine. This facility consists of a well-sealed piston, and a closed cylindrical combustion chamber. During compression, the temperature and pressure of the mixture inside are increased. At the end of compression, the temperature of the mixture between the cylinder bottom and the piston is high enough for mixture to undergo self-ignition. The complete pressure-time history is measured throughout and used to verify proposed chemical

kinetic mechanisms for the auto-ignition of the reacting mixture. The advantages of the RCM is that it allows a direct measurement of induction time and a wide range of achievable pressures and concentrations. However, accurate temperature measurement is problematic (Desgroux *et al.*, 1996). In addition, difficulties in characterising the state of the reacting mixture have caused disconcerting discrepancies between measurements of ignition delays in different RCMs even at the same nominal conditions. In a RCM, the mixture motion, especially in the piston corner vortex, may produce quite strong non-uniformity in temperature and concentration. This phenomenon may strongly affect ignition and this has been studied by Tabaczynski *et al.* (1970), Green *et al.* (1997), Daeyup *et al.* (1998) and Shinjin *et al.* (1993). Heat loss is another factor that may affect ignition delay, and this aspect has been studied by Griffiths *et al.* (1992) and Frank *et al.* (1986) in relation to RCMs.

Compared with experimental studies, modelling studies with known chemical kinetics may be a good way to study the interaction between chemistry and physical factors such as flow motion, in particular, turbulence effects. In this chapter, the combined effects of temperature and concentration inhomogeneities and turbulence on self-ignition delays in methane/air mixtures are studied numerically. For this purpose two models are selected which allow the calculation of averaged reaction rates in fluctuating media, namely LEM and RSF described in *Chapter 1*. Both models have the advantage of being able to distinguish between the different physical processes of molecular diffusion, chemical reaction and turbulent convection. These two models are applied for simulations of statistically (in the mean) homogeneous reacting media. Self-ignition delays and species concentrations as well as temperature evolution are computed.

3.2 Modelling of Self-Ignition

3.2.1 Governing Equations for Turbulence Models

The turbulence models used here are LEM and RSF. For multiple species and statistically homogenous mixtures, the governing equations of the two models are:

$$LEM \qquad \frac{\partial Y_i}{\partial t} = D_M \frac{\partial^2 Y_i}{\partial X^2} + w_i + Block\ Inversion \tag{3.1}$$

$$RSF \qquad \frac{\partial Y_i}{\partial t} = \frac{D_M}{l_t^2} \frac{\partial^2 Y_i}{\partial X^2} + w_i + \frac{\langle Y_i \rangle - Y_i}{\tau_t} \tag{3.2}$$

Here, Y_i is the mole fraction of species i, other symbols as well as the details of the reaction rates, w_i, are given in *Chapters 1* and *2*.

3.2.2 Initial Conditions

Three different types of initial conditions, which are described below, have been used.

(1) Dirac's δ- peak pdf

Initially, temperature and concentration fields are homogeneous, there being no fluctuations in the mixture. Thus, the profiles in terms of temperature $T(X)$ and species concentrations $Y_i(X)$ are uniform, and the corresponding pdfs are Dirac's δ-peak functions.

(2) Rectangular pdf

Initially, species concentrations are uniform, temperature is not uniform but temperature gradient is statistically uniform, and the initial temperature profile in X is given by:

$$T(X) = \langle T \rangle + \sqrt{12} \sqrt{\langle T'^2 \rangle} \left(X - \tfrac{1}{2} \right) \tag{3.3}$$

where $\sqrt{\langle T'^2 \rangle}$ is the *rms* temperature fluctuation, $\langle T \rangle$ is the mean temperature. This profile in terms of $T(X)$ means that initial temperature is distributed according to a rectangular pdf, see Eq. (1.30).

(3) Bimodal pdf

In this case the initial state of the media is a homogeneous mixture of gas parcels, either completely burnt or fresh. The burnt parcels contain adiabatically equilibrium products. This means that initial temperature and concentrations are distributed according to a bimodal pdf.

For the simulations, the fresh gas temperature is 800 *K*; the *rms* temperature is set equal to 50 *K* for the rectangular pdf. For the bimodal pdf the burnt gas temperature is taken as 2400 *K* and its probability is 5%. With these initial settings, other parameters can be easily calculated. The initial parameters for the simulations are summarised in Table 3.1. The mixture is stoichiometric and the pressure is constant at 1.0 *bar*.

Table 3.1 Initial parameters for the simulation

Initial pdf	$\langle T \rangle$ (K)	$\sqrt{\langle T'^2 \rangle}$ (K)	Probability of burnt gas
δ-peak	800	0	0
Rectangular	800	50	0
Bimodal	800 for fresh gas 2400 for burnt gas	350	5%

3.2.3 Boundary Conditions

The boundary conditions for both models are:

$$\frac{\partial Y_i}{\partial X} = 0, \quad for \ X = 0,1 \tag{3.4}$$

3.2.4 Numerical Solution Method

Equations (3.1) and (3.2) are solved by the finite volume method. By integrating Eqs. (3.1) and (3.2) over the control volume, finite difference equations are obtained. The structure of these equations is such that it advances to a system of algebraic equations for each new time step and these equations may be solved implicitly with TDMA algorithm. The reaction rate terms are integrated over the time step with the help of the public domain code named EULSIM by Deuflhard *et al.* (1989) designed for integration of stiff systems of ordinary differential equations.

3.3 Effects of Initial Inhomogeneity

The effect of initial inhomogeities on ignition is studied first for a stagnant, "laminar", medium. In this situation, the turbulence terms in both RSF (relaxation) and LEM (the event of block inversion) equations disappear, and only molecular diffusion and chemistry remain to be modelled. The various initial conditions may be identified with the presence of initial inhomogeneities in temperature and/or concentration field.

Results of predictions for the evolution of temperature and concentrations are shown in Figs. 3.1 and 3.2, respectively. Shown in Fig. 3.2(a) is the history of species concentrations in the medium without any inhomogeneity, while Fig. 3.2(b) and Fig. 3.2(c) correspond to initial uniform temperature gradient and composed of burnt/unburnt patches, respectively.

Comparing Fig. 3.2(b), Fig. 3.2(c) with Fig. 3.2(a), and also comparing the three temperature profiles in Fig. 3.1, one can see that, in this case, initial temperature inhomogeneity induces subsequent variations of concentrations which may be strong enough to change the character of the chemical kinetics. This means that two consecutive reactions proceed now in parallel, which explains a simultaneous rise in concentrations of the intermediate agent R and final products of combustion, easily seen in Fig. 3.2(c). Especially for the case of initial temperature being distributed with rectangular pdf, the character of the chemical reaction is changed so greatly that even the definition of ignition becomes ambiguous, see Figs. 3.1 and 3.2(b). But for the case of bimodal pdf, these changes are not pronounced as much as it is in the case of the rectangular pdf, so that the definition of ignition delay is still clear. This may be explained as follows. For stagnant media, the ability of micro-scale mixing to smooth out the temperature gradients depends only on molecular diffusion. For the case of a rectangular pdf of initial temperature, temperature gradients exist everywhere, but for that of an initial bimodal pdf, in the unburnt area, it is still homogeneous at the beginning. Because molecular diffusion is a slow process, compared with chemistry, this effect is not much pronounced. Arguably, for this reason the character of chemical kinetics is changed much stronger for rectangular pdf than for the bimodal one.

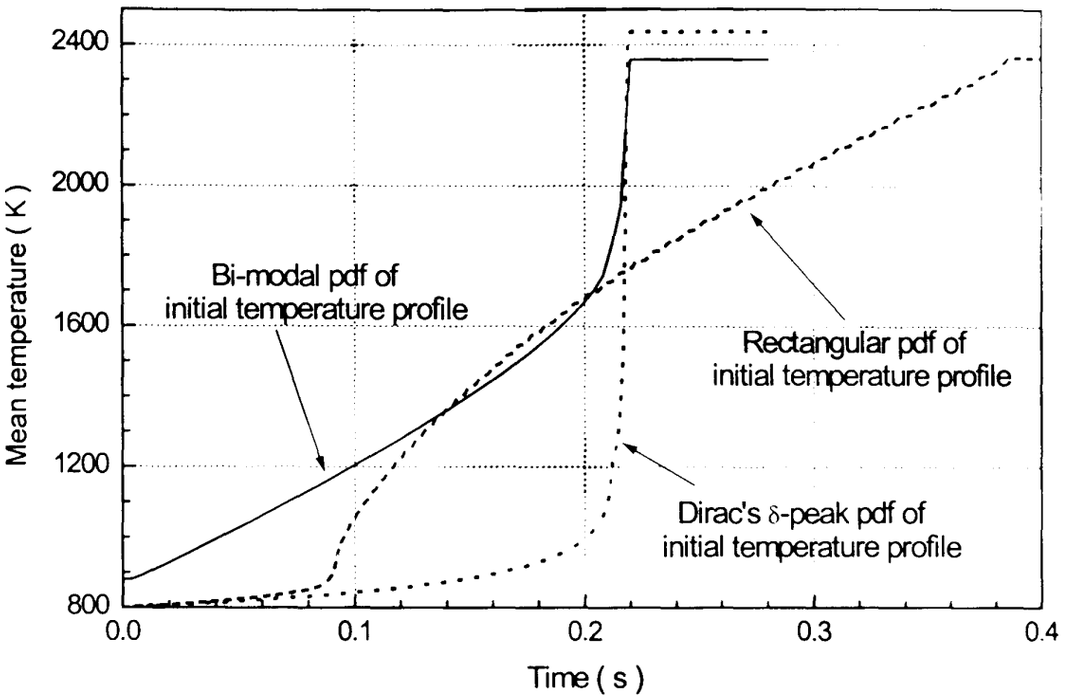

Fig. 3.1 Temperature evolution for the different initial pdfs in stagnant medium

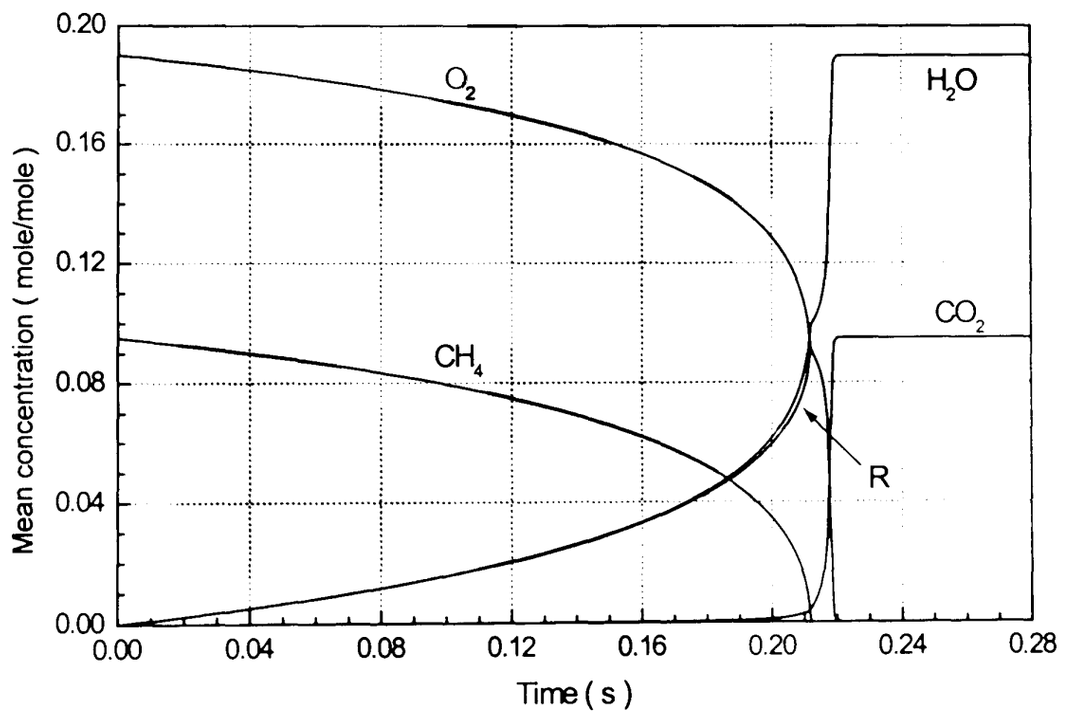

Fig. 3.2 (a) Initial composition and temperature are homogeneous, Dirac's δ peak pdf

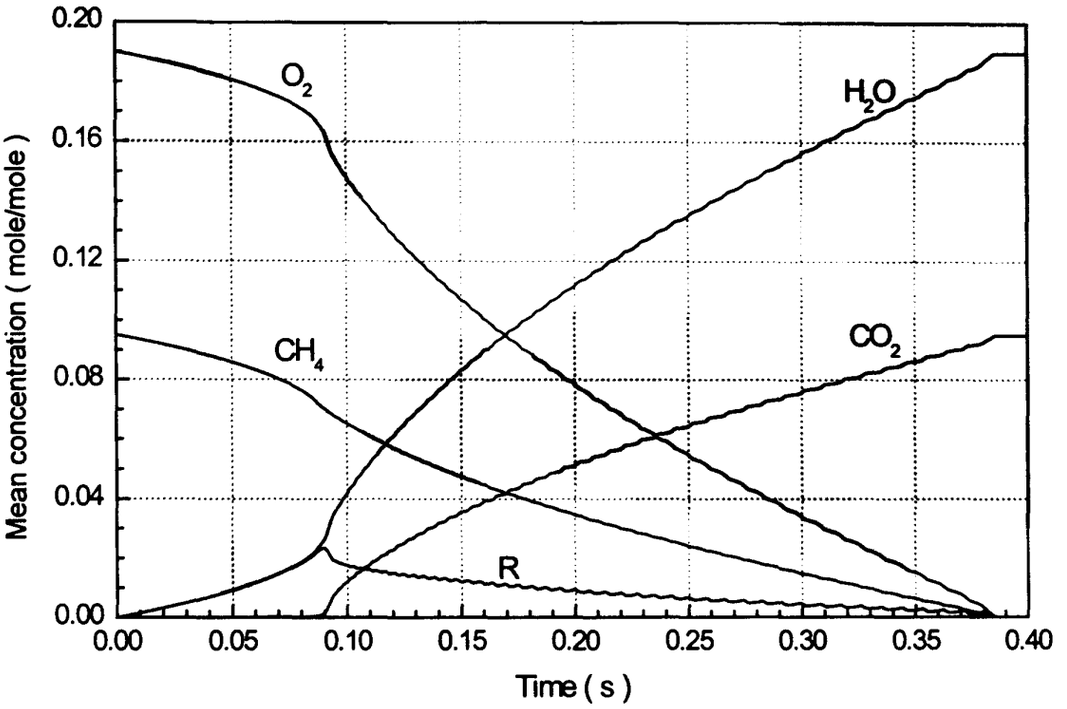

Fig. 3.2 (b) Initial temperature gradient is uniform, rectangular temperature pdf

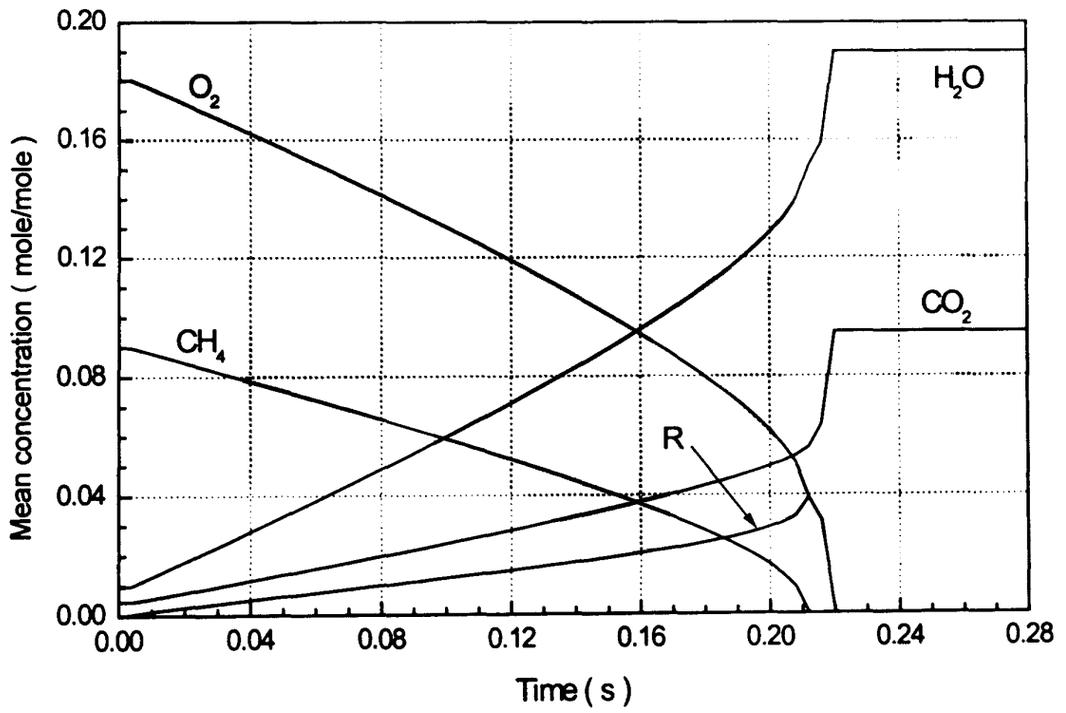

Fig. 3.2 (c) Initial mixture composed of burnt/unburnt parcels, bimodal temperature and concentration distribution

Fig. 3.2 Species evolution profiles for various types of initial conditions

3.4 Effects Induced by Turbulence in Inhomogenous Medium

The effects of turbulence on ignition delay have been simulated with LEM and RSF models. For the RSF model, simulations have been carried out for three turbulent Reynolds numbers, Re_t = 50, 500 and 2000, where $Re_t = \frac{u' l_t}{D_M} = \frac{l_t^2}{\tau_t D_M}$. For the LEM model, simulations have been carried out for two turbulent Reynolds number, Re_t = 50 and 500. Computer simulation had been attempted but stopped before the completion in the case of Re_t = 2000 after 7 days of computing, which limits at prohibitive computer time consumption of the LEM for high Re_t. In LEM simulations, the triplet map of block inversion (Eq. (1.24)) is used. Turbulence parameters used in the present simulations are listed in Table 3.2.

Table 3.2 Turbulence parameters (units are *cm, s*)

(a) Rectangular initial pdf

	l_t (*cm*)	Re_t=50	Re_t=500
LEM	*0.2*	τ_t = *0.04 s*	τ_t = *0.004 s*
RSF	*1.0*	τ_t = *0.1 s*	τ_t = *0.01 s*

(b) Bimodal initial pdf

	l_t (*cm*)	Re_t=500	Re_t=2000
LEM	*0.2*	τ_t = *0.004 s*	--------
RSF	*0.2*	τ_t = *0.004 s*	τ_t = *0.001 s*

The initial conditions for temperature and concentrations have been taken to be the same as in the previously described laminar stagnant medium case listed in Table 3.1.

Results of calculations for an initial rectangular pdf are shown in Figs. 3.3 to 3.7. Temperature evolutions predicted by LEM and RSF are shown in Fig. 3.3. Species concentration profiles predicted by LEM and RSF are shown in Fig. 3.4 for Re_t = 50 and in Fig. 3.5 for Re_t = 500. Fluctuations of methane concentration and temperature were calculated as well, and the results are shown in Fig. 3.6 for Re_t = 50 and Fig. 3.7 for Re_t = 500, respectively.

Presented in Figs. 3.8 to 3.12 are the predicted results for initial bimodal pdf, where, shown in Fig. 3.8 is the temperature evolutions predicted by LEM and RSF, shown in

Fig. 3.9 and Fig. 3.10 are species concentration profiles predicted by LEM and RSF. Presented in Fig. 3.11 is the *rms* fluctuations of methane concentration and temperature for Re_t=500 predicted by LEM and RSF. The predictions for Re_t=2000 by RSF are shown in Fig. 3.12.

The following conclusions can be deduced from analysis of Figs. 3.3 to 3.12 regarding the joint effects of initial inhomogeneity and turbulence. With the presence of initially non-zero temperature gradient, the ignition delay times are shorter than those defined in uniform media. This conclusion can be drawn from a comparison of the species concentration profiles in Figs. 3.4 with Fig. 3.2(b) as well as the temperature curves in Figs. 3.3 and 3.1. However, when turbulence intensity increases, according to common sense expectations, ignition delays become longer, and this conclusion is easily obtained by comparing the curves obtained for two different Reynolds number in Figs. 3.4 and 3.5 for Re_t=50, 500, and in Figs. 3.9 and 3.10 for Re_t=2000 and 500. These trends are predicted by both the LEM and RSF models. In quantitative terms, the predictions of these models differ at very low turbulence intensities, but become indistinguishable for moderate and strong turbulence. This difference, however, persists for another kind of initial conditions, bimodal pdf, see below.

The interaction between turbulence and initial temperature inhomogeneity affects the chemistry in a complex manner. Combined effects of turbulence and imhomogeneity may result in a pronounced segregation of mixture with strong fluctuations of temperature and species concentration as shown in Figs. 3.6 and 3.7 for fluctuations of methane concentration and temperature, respectively. An interesting feature displayed in these two figures is that the chemical reactions are effective in generating fluctuations in methane concentration, but unable to produce a corresponding fluctuation in temperature. Would this result be plotted in configuration/concentration-temperature/space, also called sometimes "phase" space in pdf-devoted literature, in comparison with the stagnant medium results, the trajectories characterising the system evolution will be different.

This result implies, in particular, that certain non-zero probability exists for meeting hot gas parcels which have not commenced the reactions or "quenched" partly reacted

parcels. Such situations are commonly neglected in construction of mixing models. Certainly, generality and extent to which this result is attributed to the deficiencies in small-scale mixing description within the used models have to be further assessed and carefully verified. Surprising though is the fact that both models produce essentially identical prediction in spite of radically different small-scale mixing representation.

From all the results presented in this section, one may say that turbulence may reduce the effects of variations in initial temperature and concentrations on the chemical kinetics by comparing Figs. 3.3 and 3.8 with Fig. 3.1. This means that turbulence fluctuations may be strong enough to smear out the hot kernels before they provoke the ignition of the adjacent gas layer. When turbulence is strong enough, it may smooth out the initial inhomogeniety from the very beginning as shown explicitly in Fig. 3.7 for Re_t = 500 as well as in Fig. 3.12 for Re_t = 2000.

Both LEM and RSF predict the same trends of temperature evolution, species concentration and fluctuation of species and temperature. As shown in Figs. 3.3 and 3.1, with initial uniform temperature gradient, the ignition delay is shorter than that in the initially homogeneous medium.

Last remark is that what concerns the computational cost, RSF is more economical than LEM. For example, for Re_t = 2000, the LEM model still had not yield a converged solution after 7 days computing while it took only 10 hours to produce a solution for the RSF model on the same Silicon Graphics work station.

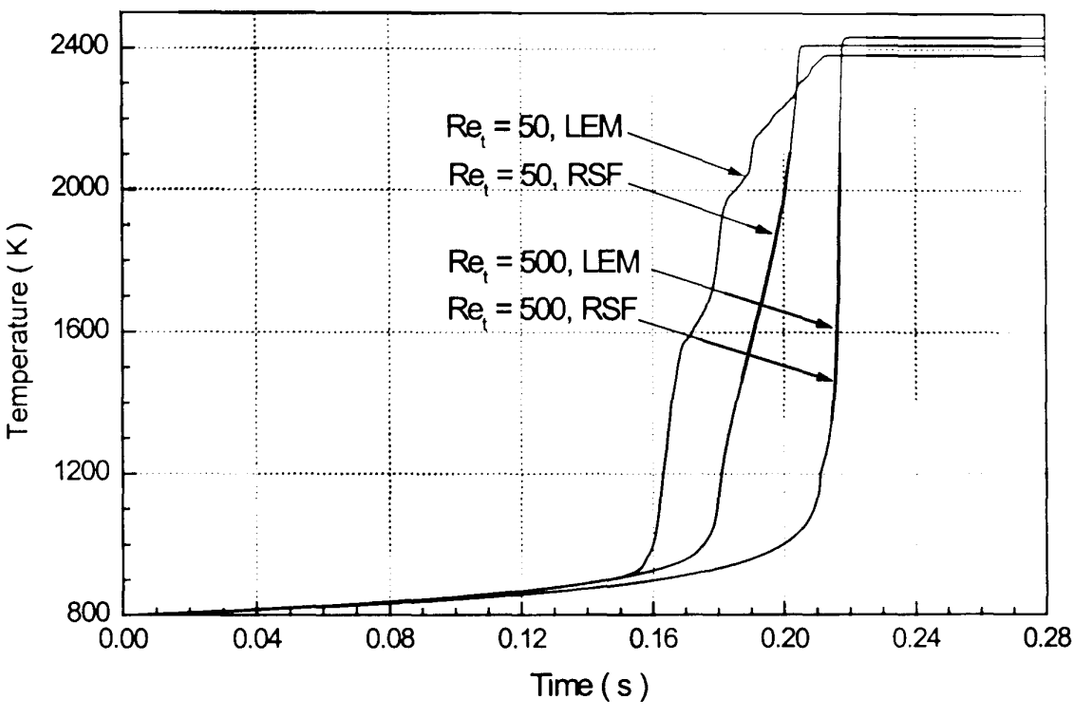

Fig. 3.3 Temperature evolutions for initial rectangular pdf for Re_t = 50, 500, predicted by LEM and RSF

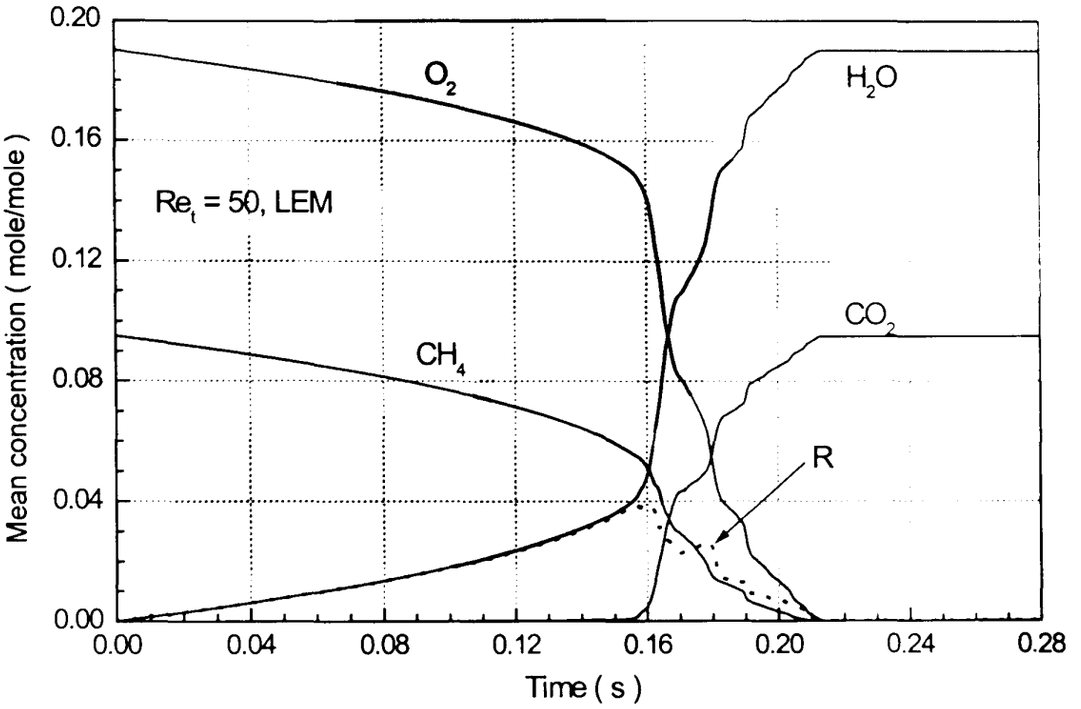

Fig. 3.4(a) Predicted by LEM

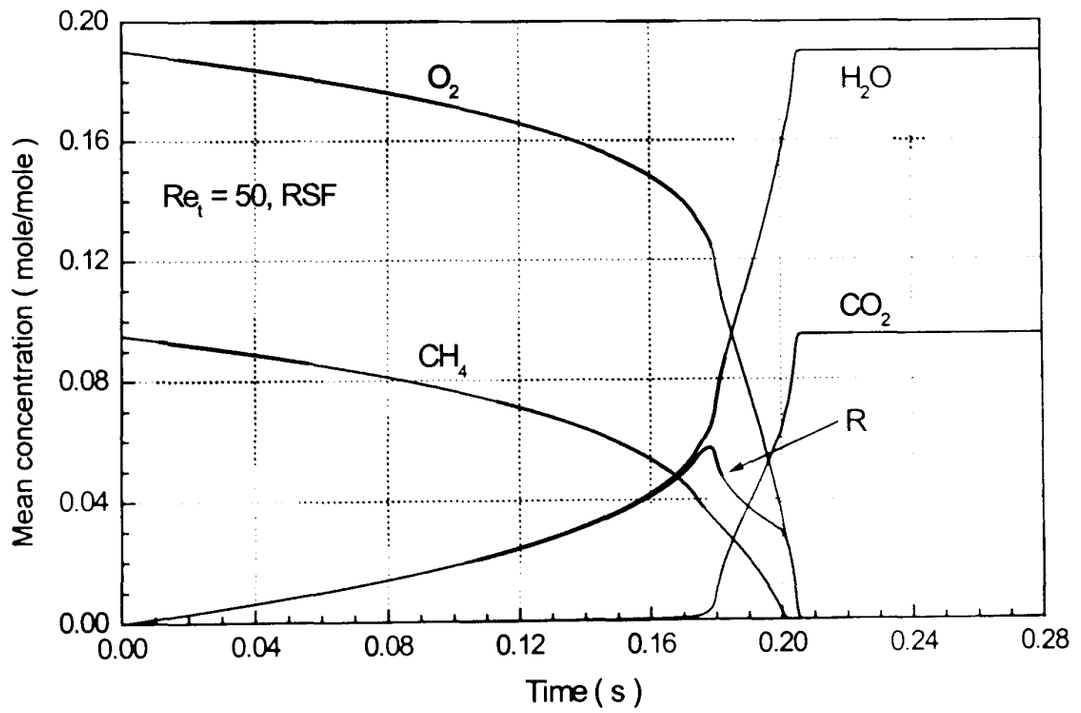

Fig. 3.4(b) Predicted by RSF

Fig. 3.4 Species profiles for initial rectangular pdf, predicted by LEM and RSF for Re_t = 50

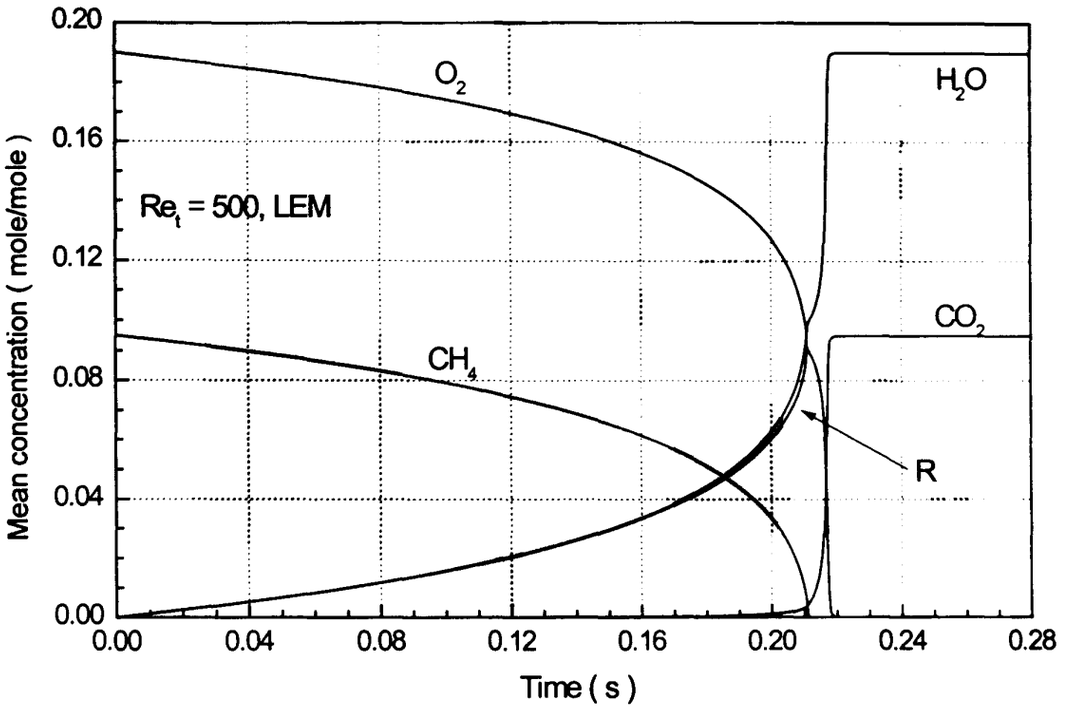

Fig. 3.5(a) Predicted by LEM

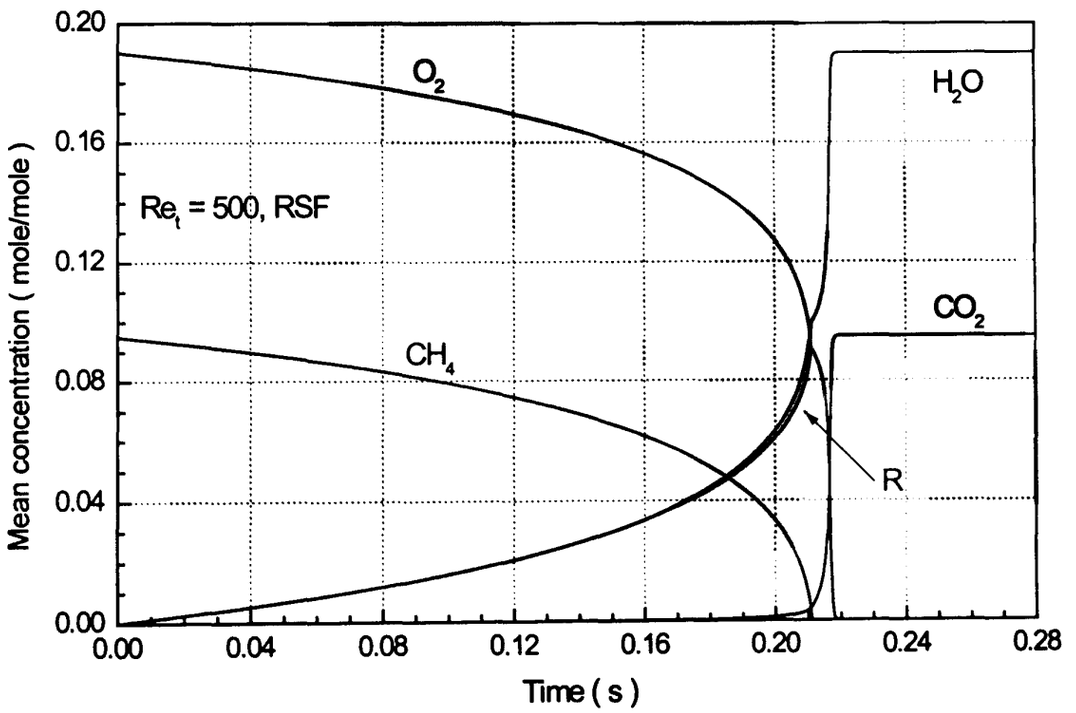

Fig. 3.5(b) Predicted by RSF

Fig. 3.5 Species profiles for initial rectangular pdf, predicted by LEM and RSF for Re_t = 500

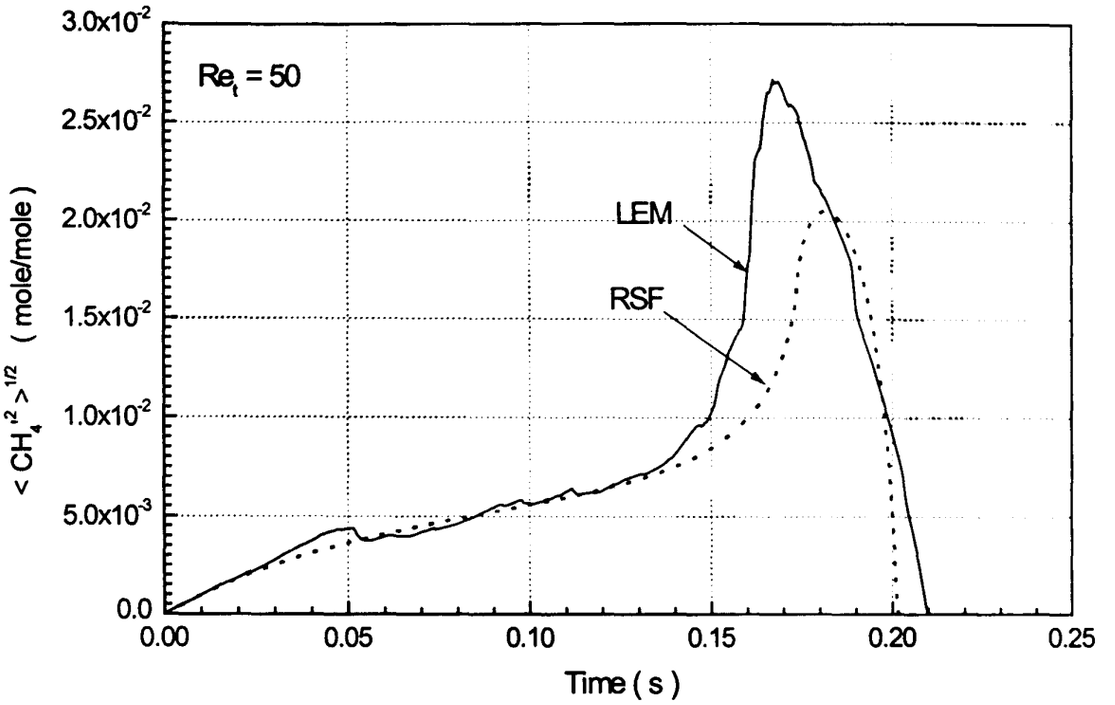

Fig. 3.6(a) Methane concentration fluctuations

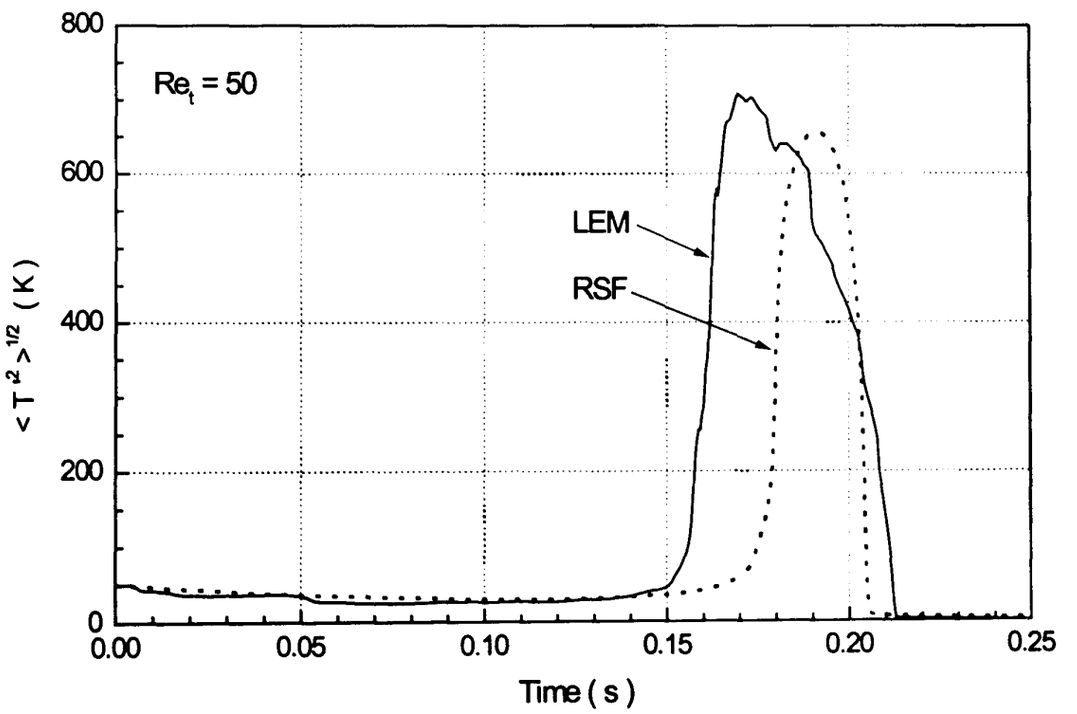

Fig. 3.6(b) Temperature fluctuations

Fig. 3.6 Fluctuations of methane and temperature predicted by LEM and RSF for initial rectangular pdf for $Re_t = 50$

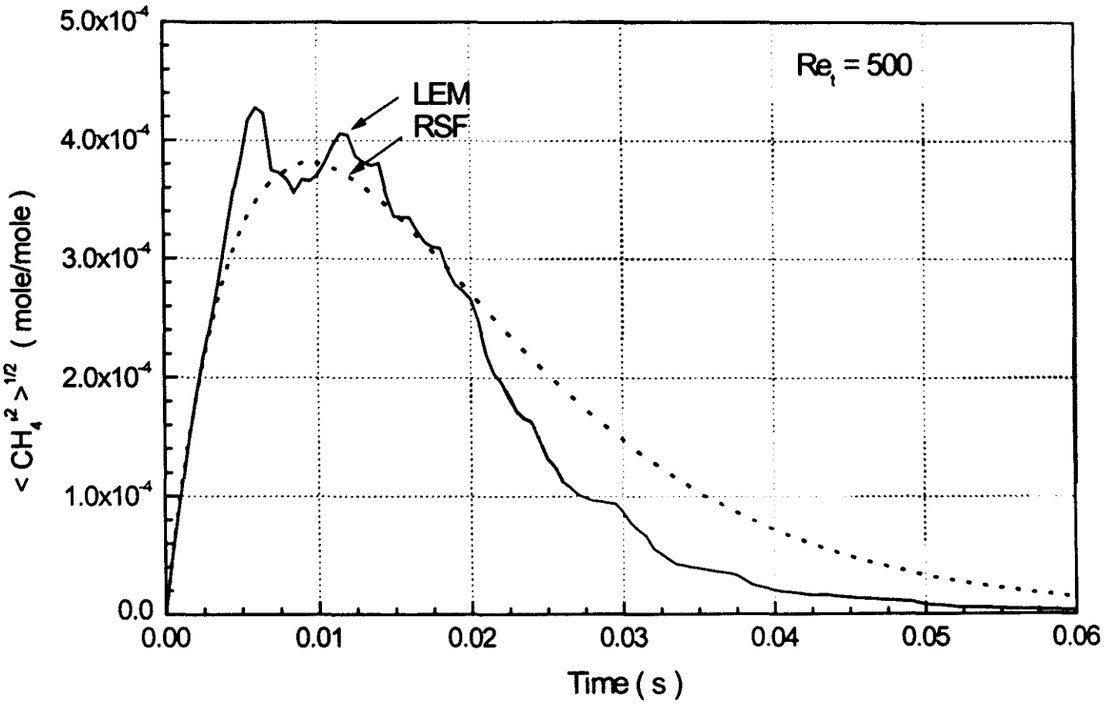

Fig. 3.7(a) Methane concentration fluctuations

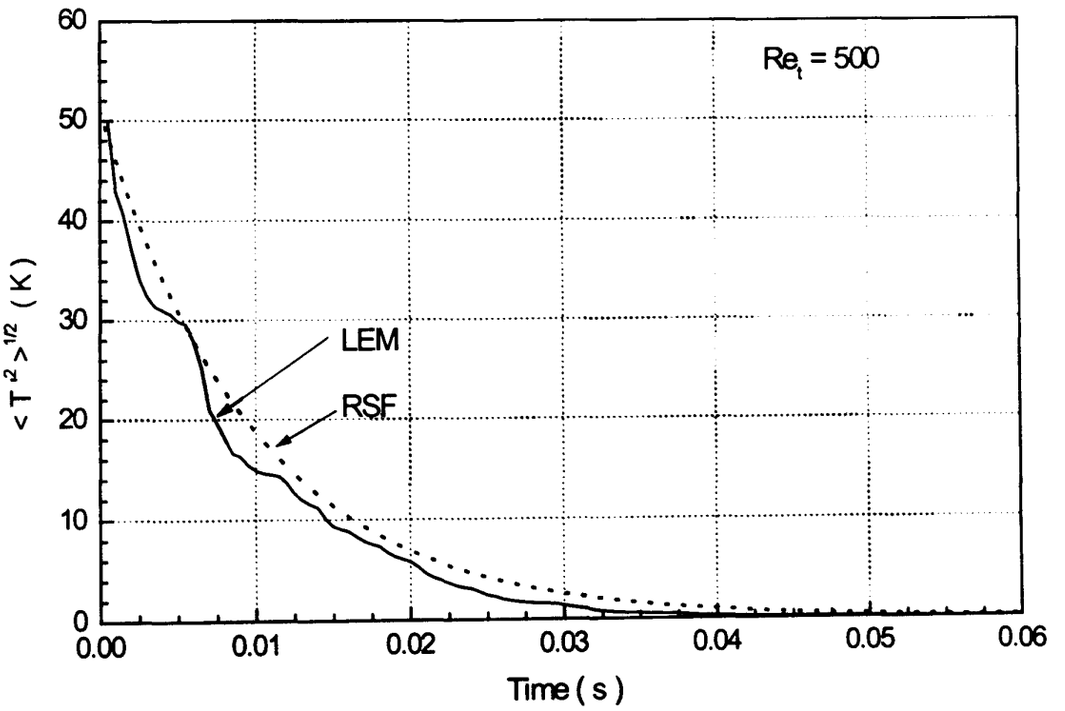

Fig. 3.7(b) Temperature fluctuations

Fig. 3.7 Fluctuations of methane concentration and temperature predicted by LEM and RSF for initial rectangular pdf for $Re_t = 500$

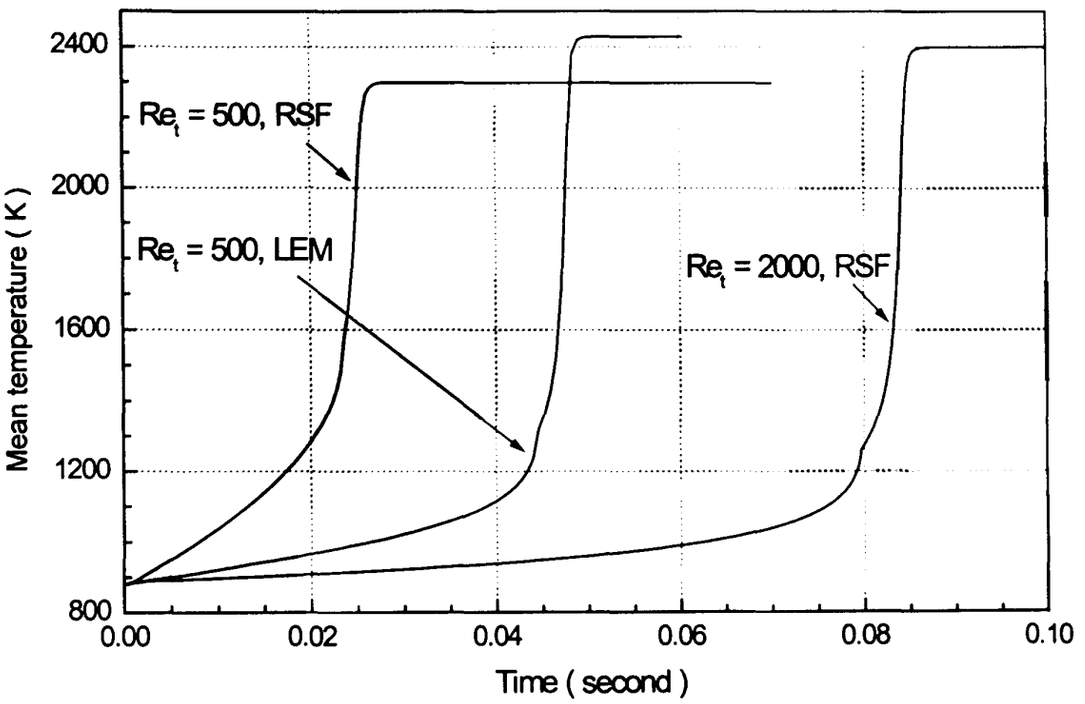

Fig. 3.8 Temperature evolutions for initial bimodal pdf for Re_t = 500, 2000 predicted by LEM and RSF

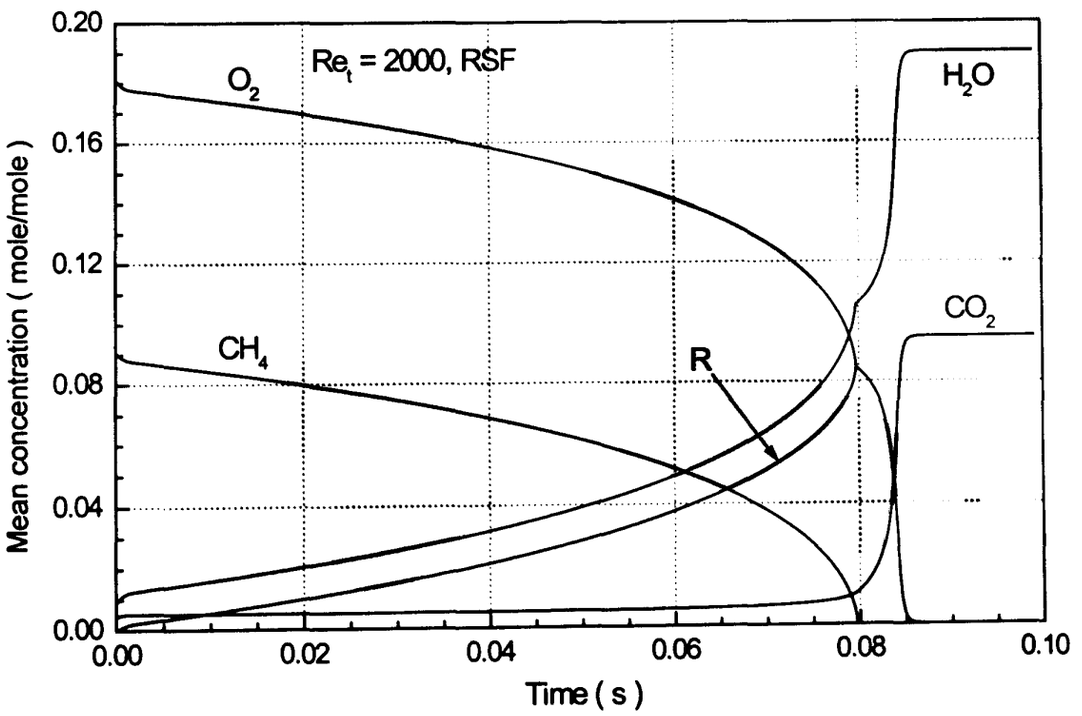

Fig. 3.9 Species concentration profiles for initial bimodal pdf predicted by RSF for Re_t = 2000

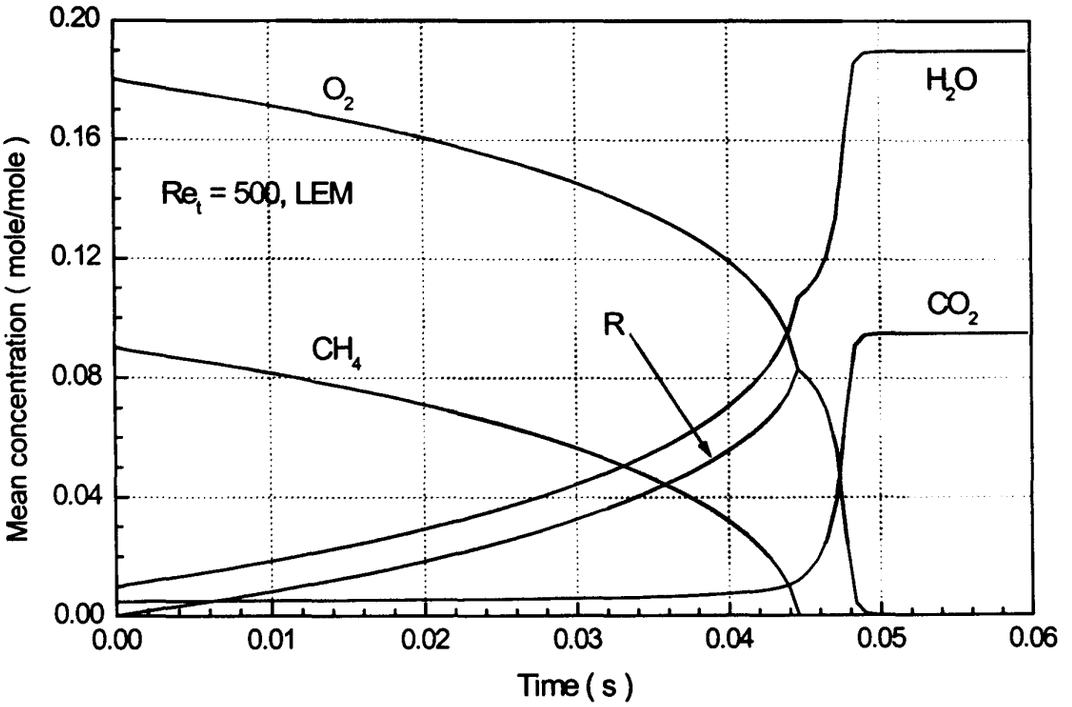

Fig. 3.10(a) Predicted by LEM

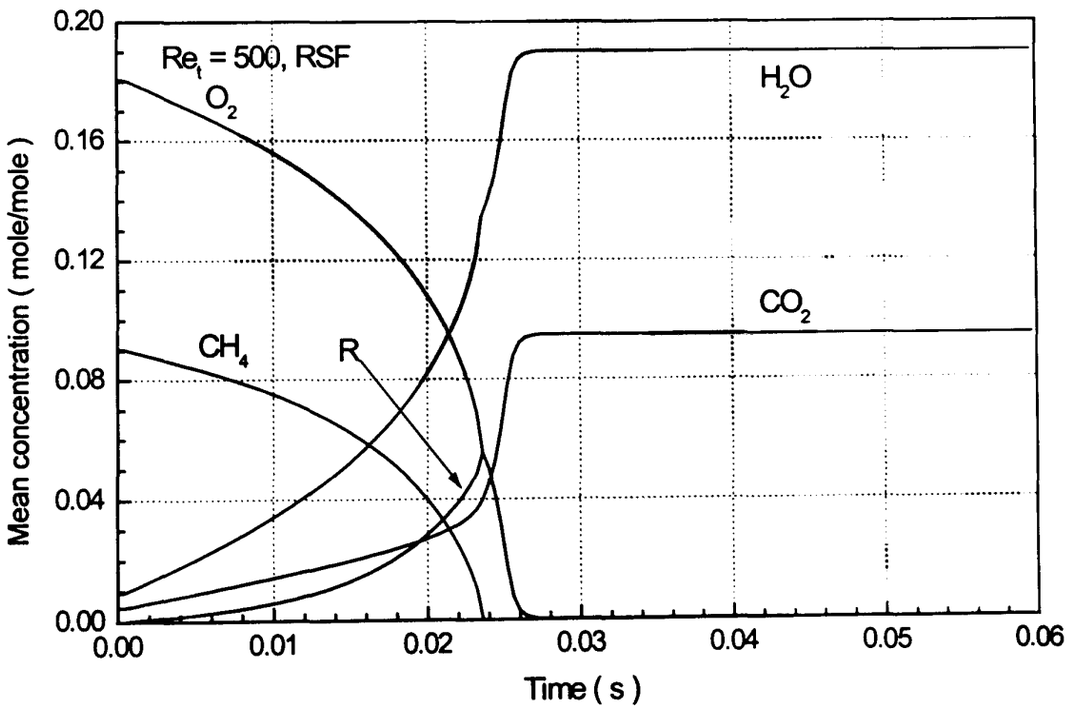

Fig. 3.10(b) Predicted by RSF

Fig. 3.10 Species concentrations profiles for initial bimodal pdf predicted by LEM and RSF for $Re_t = 500$

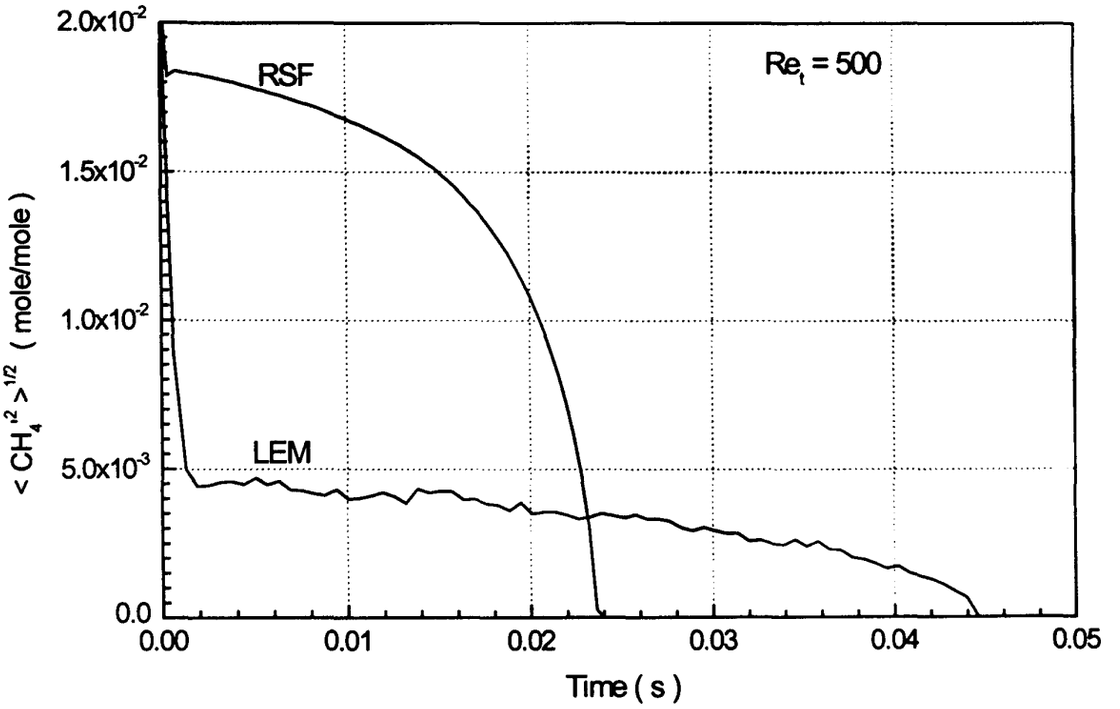

Fig. 3.11(a) Methane concentration fluctuations

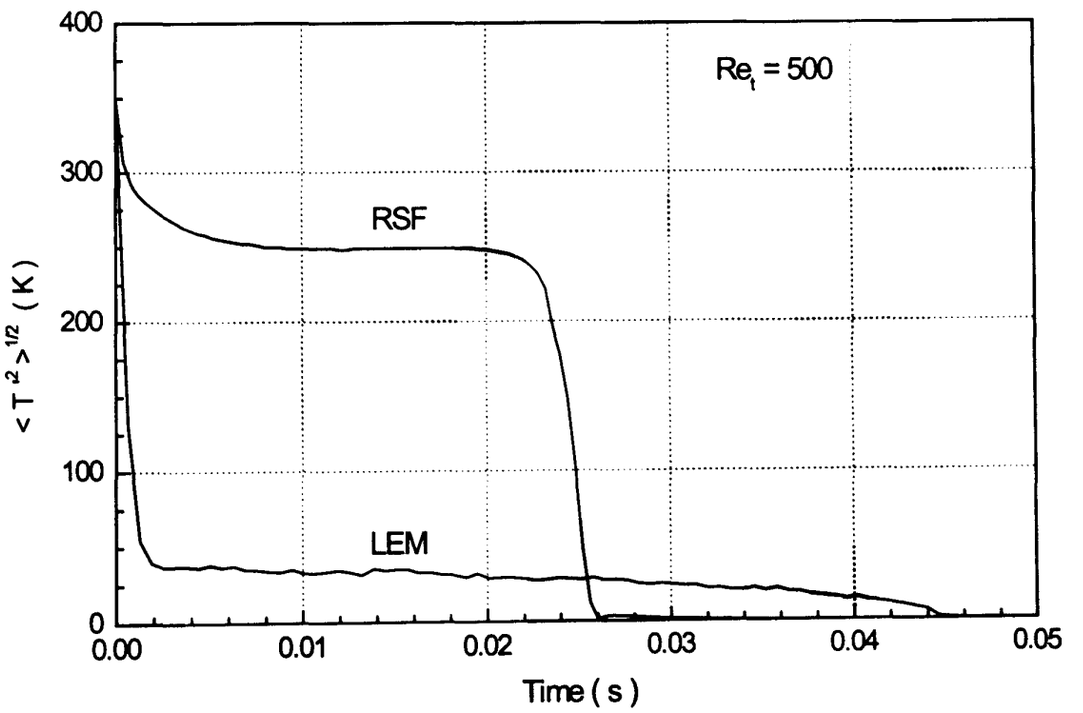

Fig. 3.11(b) Temperature fluctuations

Fig. 3.11 Fluctuations of methane concentration and temperature for initial bimodal pdf predicted by LEM and RSF for $Re_t = 500$

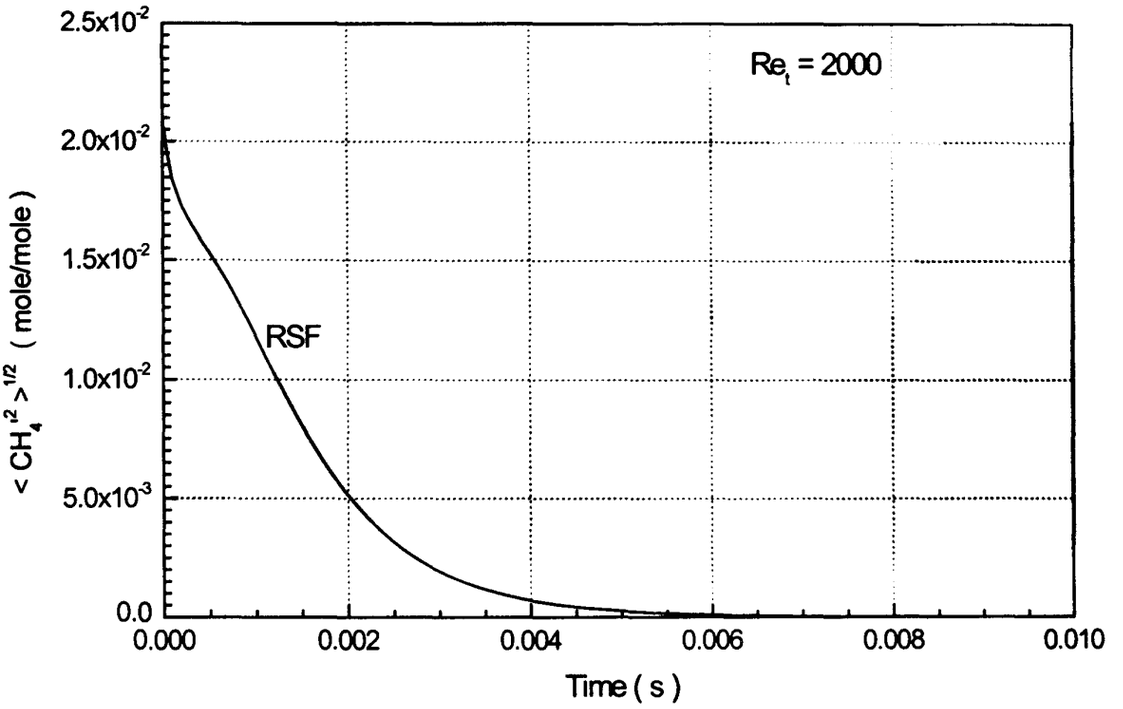

Fig. 3.12(a) Methane fluctuations

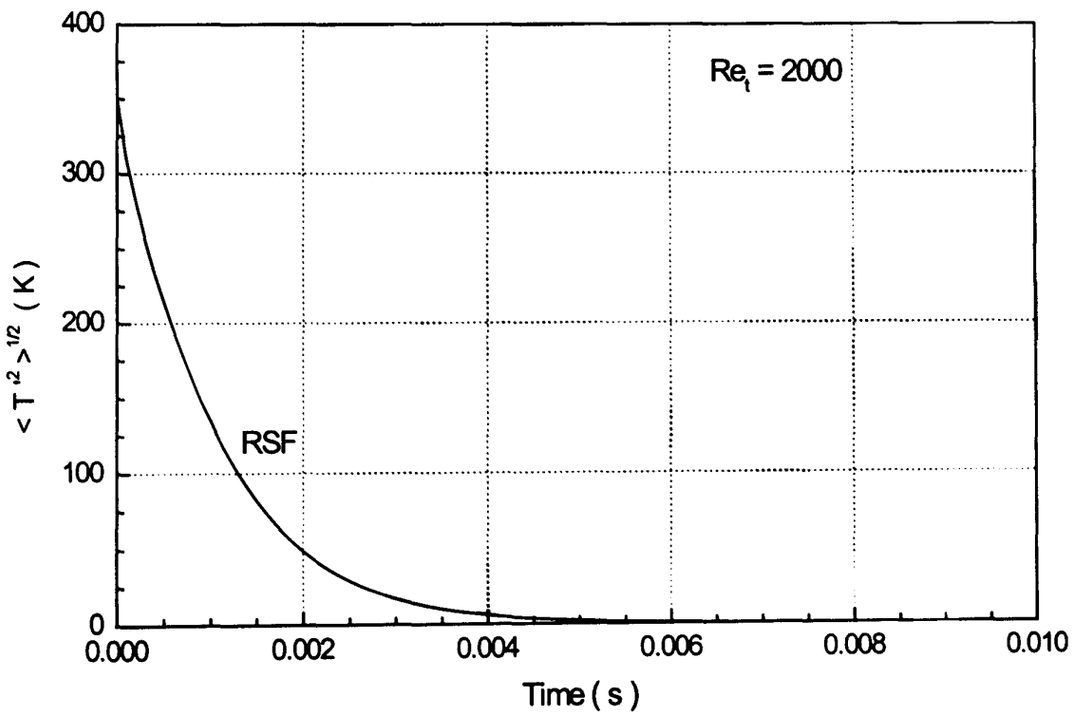

Fig. 3.12(b) Temperature fluctuations

Fig. 3.12 Fluctuation of methane concentration and temperature for initial bimodal pdf predicted by RSF for $Re_t = 2000$

3.5 Effects of Heat Losses

Many theoretical studies of combustion rely on assumption of adiabatic conditions. However, it may be argued that the effect of heat losses may be important for practical applications, such as IC engines. For example, Yeo (1994) studied the effect of heat losses on self-ignition delays during the final stage of compression in a rapid compression machine. It was found that when heat losses are stronger, the self-ignition delay time is longer. In particular, the heat losses have a great impact on the self-ignition delay for the temperature range from 650 *K* to 850 *K*. Also, stronger turbulence induces greater heat losses. Some very interesting research on the effect of heat losses on self-ignition delay was undertaken by Frank *et al.* (1986) in a rapid compression machine. They used grids with different hole sizes to control the turbulence intensity of the mixture at the end of compression. They found that when the turbulence is higher, the heat losses are greater and the minimum compressed gas temperature required for ignition is also raised. Considering heat losses during the ignition process, the mathematical description of temperature evolution is changed by adding a heat loss term, which is simply assumed to decrease the temperature with time scale calculated from the diffusion equation, while the equation for species remains the same:

$$\frac{\partial T}{\partial t}=\frac{D_M}{l_t^{\,2}}\frac{\partial^2 T}{\partial X^2}+\frac{\langle T\rangle - T}{\tau_t}+w_t+\frac{T_w - T}{\tau_t^{*}} \tag{3.5}$$

where w_t is temperature increase due to chemical reaction. T_w is the wall temperature taken to be 300 *K*. The characteristic time for heat losses, τ_t^*, is estimated from experiments of Voinov, described by Khitrin (1965), where a curve of $T(t)$ is given for non-reactive charge cooling in RCM. Here it is set to $\tau_t^* = 0.28\ s$.

For the rectangular pdf of initial temperature, two turbulent integral time-scales, τ_t = 0.028 and 0.28 *s* was simulated. For the bimodal pdf of initial temperature τ_t = 0.28 *s* was simulated. Other parameters remain the same as the simulations without heat loss. Comparisons of ignition delays are presented in Tables 3.3 and 3.4 for rectangular and bimodal initial temperature, respectively. Also the comparisons are drawn in Fig. 3.13. The ignition delays were found with Eq. (2.18).

Table 3.3 Comparison of ignition delays with and without heat losses in turbulent media for a rectangular pdf of initial temperature

T (K)	Ignition delay (s)			
	$\tau_t = 0.28\ s$		$\tau_t = 0.028\ s$	
	Without heat loss	With heat loss	Without heat loss	With heat loss
900	0.0422	∞	0.0656	∞
1000	0.0183	0.0230	0.0223	0.0321
1100	0.0093	0.0103	0.0100	0.0114
1200	0.0050	0.0053	0.0052	0.0056
1300	0.0029	0.0030	0.0030	0.0031
1400	0.0018	0.0018	0.0018	0.0018
1500	0.0010	0.0011	0.0010	0.0011
1600	0.0006	0.0006	0.0006	0.0006

Table 3.4 Comparisons of ignition delays with and without heat losses in turbulent media for bimodal pdf of initial temperature

T (K)	Ignition delays (s)	
	Without heat loss	With heat loss
900	0.0544	∞
1000	0.0263	0.0363
1100	0.0128	0.0150
1200	0.0064	0.0071
1300	0.0033	0.0035
1400	0.0017	0.0018
1500	0.0009	0.0010

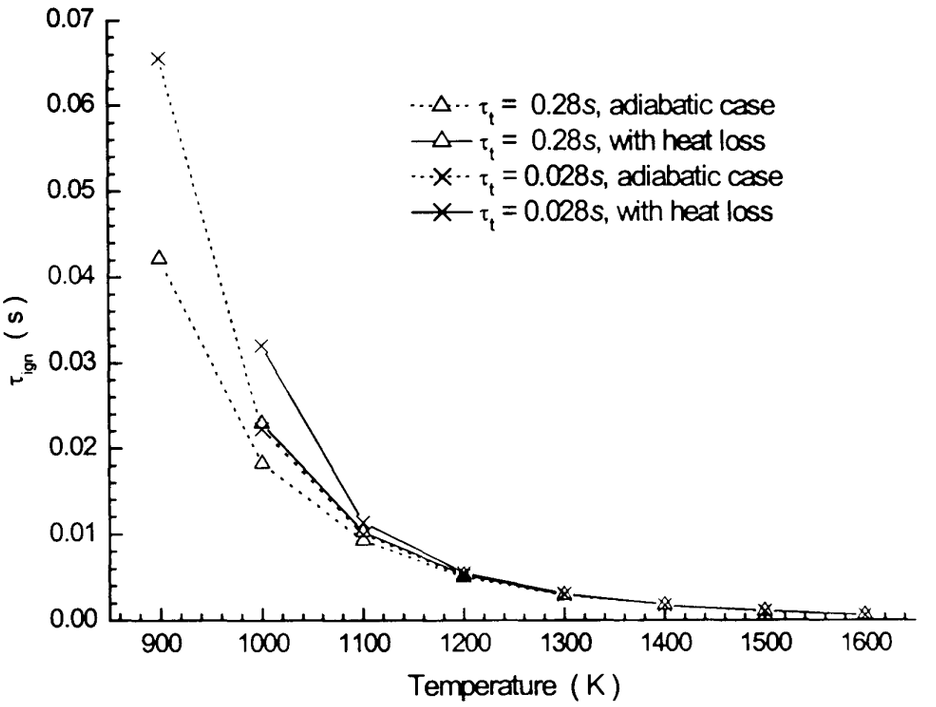

Fig. 3.13(a) Rectangular pdf

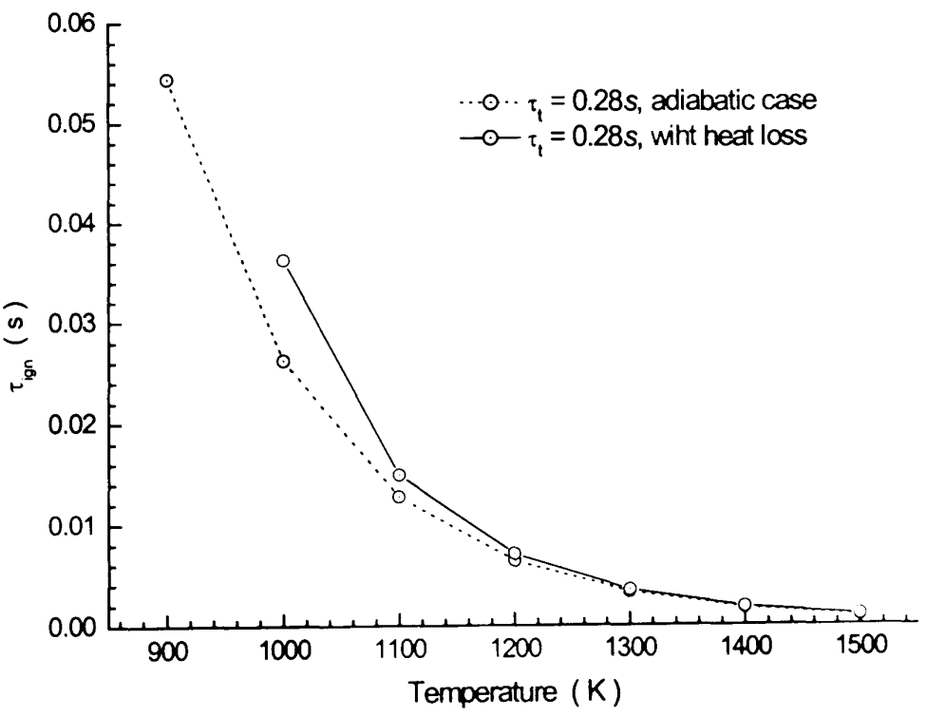

Fig. 3.13(b) Bimodal pdf

Fig. 3.13 Comparisons of ignition delays with and without heat losses

As shown in Tables 3.3, and 3.4, heat loss only affects the self-ignition delay for lower initial temperatures and makes ignition longer than that in adiabatic conditions. For higher initial temperature, the heat losses have practically no effect upon the ignition delay. This result seems to agree with Yeo's conclusions (1994) that the heat losses strongly affect the autoignition delay for lower temperatures. The effect of heat loss on self-ignition delay is more noticeable for higher turbulence intensity, see Fig. 3.13(a), and heat losses make ignition delay even longer for higher turbulence intensity, for example, for rectangular pdf of initial temperature with an initial temperature of 1000 *K*, the difference between the ignition delays with and without heat loss is 0.0098 second for τ_t=0.028 *s* and 0.0047 *s* for τ_t=0.28 *s*.

The comparisons of mean temperature evolution for the cases with and without heat loss are shown in Figs. 3.14 and 3.15 for an initial rectangular pdf of temperature and Fig. 3.16 for initial bimodal pdf of temperature.

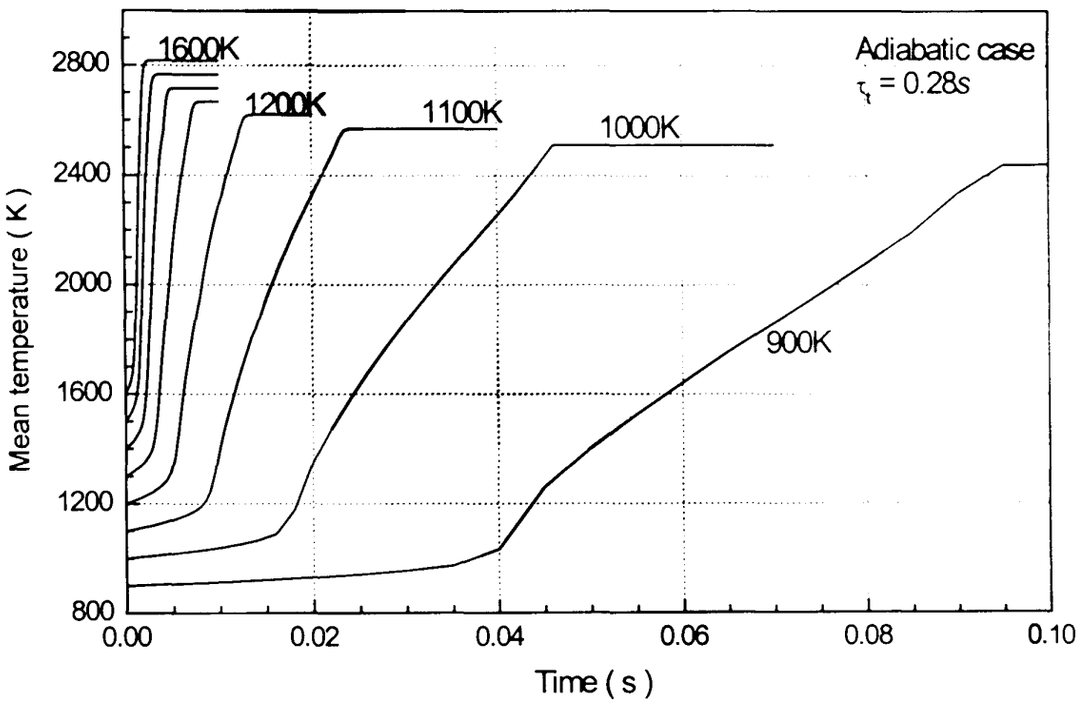

Fig. 3.14 (a) Without heat losses

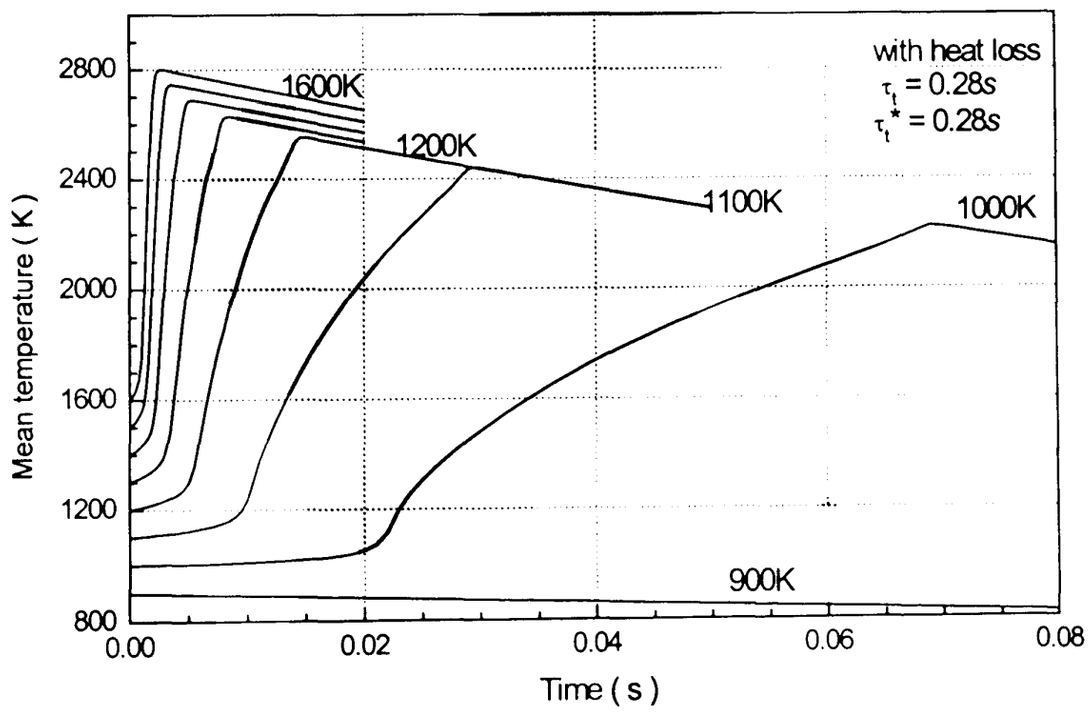

Fig. 3.14 (b) With heat losses

Fig. 3.14 Comparison of mean temperature evolutions for initial rectangular pdf for $\tau_t = 0.28\ s$ with and without heat losses

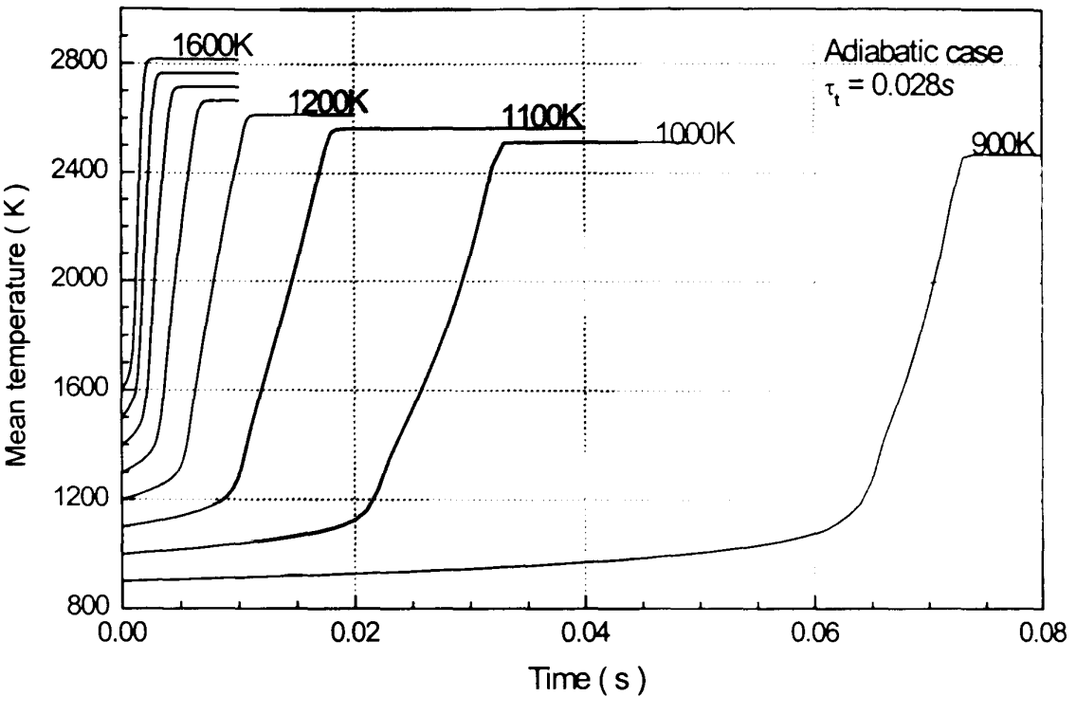

Fig. 3.15 (a) Without heat losses

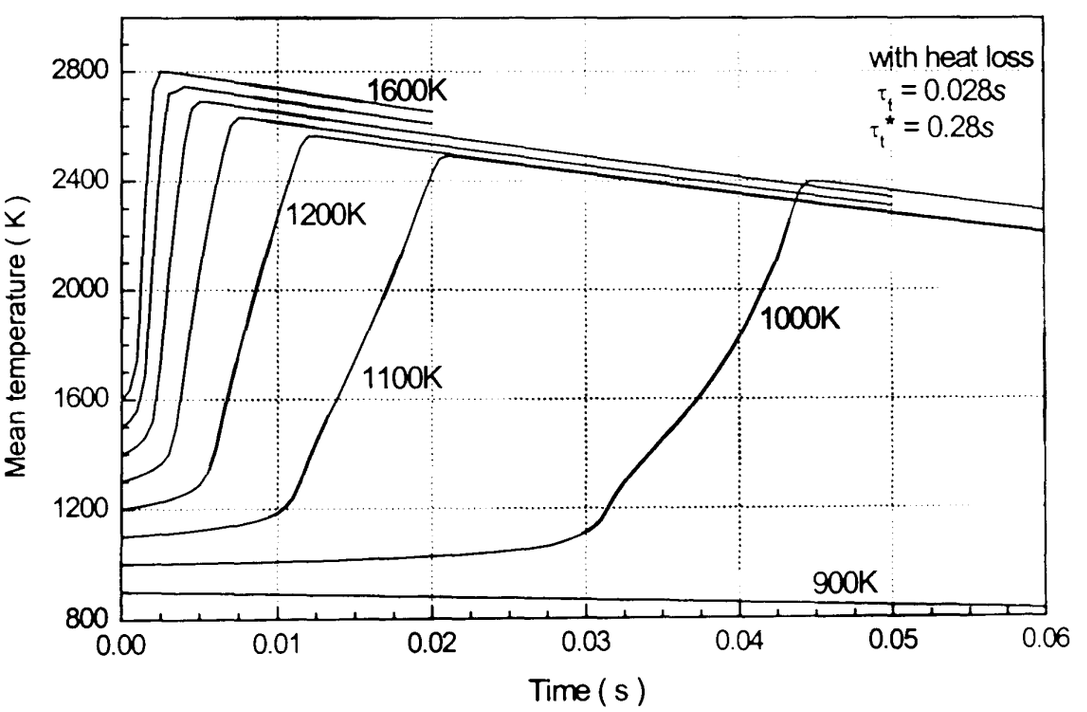

Fig. 3.15 (b) With heat losses

Fig. 3.15 Comparison of mean temperature evolutions for initial rectangular pdf for $\tau_t = 0.028$ *s* with and without heat losses

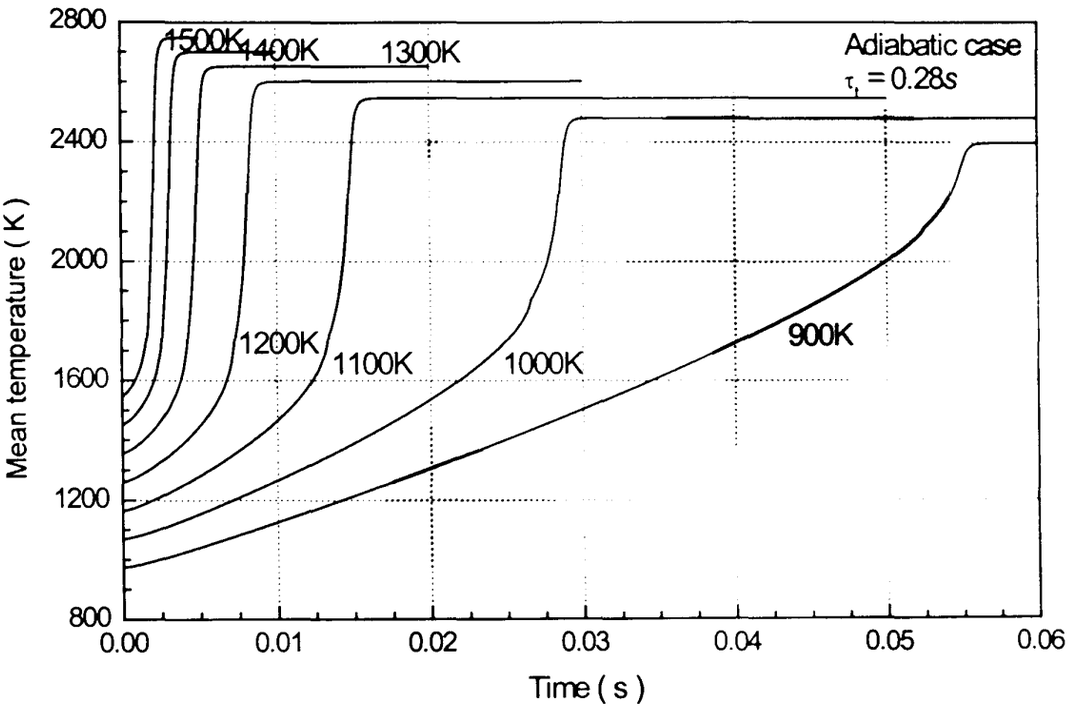

Fig. 3.16 (a) Without heat losses

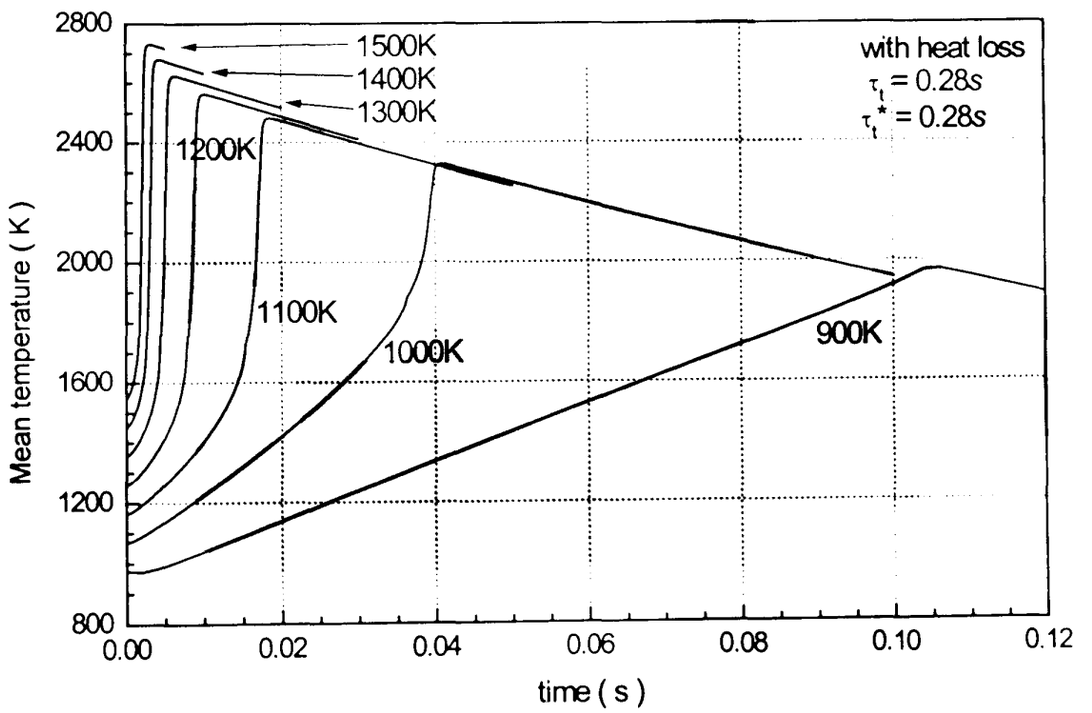

Fig. 3.16 (b) With heat losses

Fig. 3.16 Comparison of mean temperature evolutions for initial bimodal pdf for $\tau_t = 0.28\ s$ with and without heat losses

3.6 Conclusions

As shown in Fig. 3.2, initial temperature inhomogeneity induces non-uniformity of species concentration. A potentially very important result is that both temperature and concentration inhomogeneities may change the character of the chemical kinetics in such a way that reactions which occur consecutively in stagnant media may occur simultaneously if the fluctuations are strong enough. This conclusion is illustrated in Figs. 3.2(b) and Fig. 3.2(c). This affects the heat release rate and, in the limit, even the definition of an ignition delay event may become ambiguous, see Fig. 3.1. The interaction between turbulence and initial temperature inhomogeneities affects the chemistry in a complex manner. In particular, strong turbulence may reduce the effects of initial temperature and concentrations variations on the chemical kinetics. The results also show that in the presence of initial temperature gradients, the ignition delay time is shorter than that defined in a stagnant medium. However, when the turbulence intensity increases, the ignition delay becomes longer. These trends are predicted with both LEM and RSF models as shown in Figs. 3.3 and 3.8. In quantitative terms, the predictions of these models differ at very low turbulence intensities, but become indistinguishable for moderate and strong turbulence. It is noteworthy that RSF is computationally much less expensive.

Another result, relevant to the inhomogeneous conditions, is the heat losses only affect the self-ignition delay at lower initial temperatures. This is illustrated in Figs. 3.13, 3.14 and 3.15. This increase in the self-ignition delay due to heat losses is particularly strong for the temperature below 1000 K; in this temperature interval it is also very sensible to the turbulence intensity. These trends predicted with the RSF model are reasonable; however, no definitive answer can be given at this stage mainly because of a severe lack of experimental data on the ignition delays in a controlled turbulence environment.

Chapter 4

Study of 1-D CH_4/Air Turbulent Flame Propagation

4.1 Introduction

The Reference Scalar Field (RSF) model is introduced in *Chapter 1*. Since the RSF model was proposed (Burluka *et al.*, 1997), it has been applied to several flame geometries. However, in those previous RSF simulations mentioned above, the chemistry was reduced to a single progress variable undergoing an irreversible one-step reaction.

In *Chapter 3*, the RSF model is used to study the turbulence effects on auto-ignition delay in a statistically homogeneous premixed methane/air mixture. The chemical reactions are described with a reduced two-step scheme with 5 species. Simulation results are compared with predictions obtained with the Linear Eddy Model (LEM). For elevated turbulence intensity, the results given by the two models agree quite well. One can note, however, that the RSF model is more economic if considering the computation resource.

The RSF model with multiple reactive species in a pre-mixed turbulent reacting medium has not yet been tested with strong turbulence. To assess it a suitable set of experiments is needed. Because a fan-stirred bomb can generate very strong turbulence and the turbulence is nearly homogeneous and isotropic near the centre, it has been widely used to study strongly turbulent flames, *e.g.* Bradley *et al.*, (1996a). Also, such flames have the simplest possible flow geometry, so it has been chosen for the present work to test RSF model predictions. It allows also avoids uncertainties related to the description of a more complex flow field where turbulence properties vary strongly. In this simple case, for example, one can argue that a simple linear dependency for conditionally averaged velocity, Eq. (4.4), would be an acceptable approximation of turbulent advection.

This Chapter describes an application of the RSF model, as formulated by Eq. (4.1), to the modelling of spherical flames propagating in homogeneous turbulence. This case is an approximation of the experimental conditions in a fan-stirred bomb, and a special series of experiments were undertaken in parallel to provide validation data.

4.2 RSF Transport Equation for 1-D Spherical Flame

The transport equation of the RSF is obtained from its pdf $P(\hat{c};\vec{x},t)$, where $\vec{x}$ is the physical coordinate, $\hat{c}$ is the scalar space and hereafter, Y_k is used to denote the scalar, k. After some closure assumptions on conditional scalar dissipation (Burluka *et al.*, 1997), the RSF model for *1-D* turbulent spherical flame propagation can be written as :

$$\frac{\partial Y_k}{\partial t}+\frac{1}{r^2}\frac{\partial}{\partial r}\left(u(r,t;X)r^2Y_k\right)=\frac{D_M}{l_t^2}\frac{\partial^2 Y_k}{\partial X^2}+\frac{\langle Y_k\rangle-Y_k}{\tau_t}+w_k + \frac{1}{r^2}\frac{\partial}{\partial r}\left(D_M r^2\frac{\partial Y_k}{\partial r}\right)+S_M \tag{4.1}$$

The symbols in this equation are listed in the *Nomenclature*, and for convenience, they are also listed in the Table 4.1.

Table 4.1 Symbols used in Eq. (4.1)

Y_k	Species, k, (*mole/mole*)
t	Time, (s)
$u(r,t;X)$	Flow velocity, conditionally averaged at given scalar value, (*cm/s*), as $\langle u\|Y(r,t)=Y(r,t;X)\rangle$
D_M	Molecular diffusivity, (cm^2/s)
τ_t	Turbulence integral time scale, (s)
l_t	Turbulence integral length scale, (*cm*)
w_k	Production rate for species k due to chemistry, (*1/s*)
$\langle Y_k\rangle$	Mean value for species k, (*mole/mole*)
S_M	Source term due to change of mixture molecular weight

In Eq. (4.1), the second term on the left hand side (LHS) describes turbulent convection in terms of conditional velocity $u(r,t;X)$. On the right hand side (RHS), the first and second terms represent molecular mixing enhanced by turbulence, the third term describes the chemical reactions, represented here with the two-step scheme introduced

in *Chapter 2*, the fourth term is the molecular diffusion in the physical coordinate, r. The fourth term can be neglected when compared with turbulent convection and diffusion given by the second term on LHS, for high turbulent Reynolds number.

In Eq. (4.1), the Lagrangian time scale for turnover of energy-containing eddies, τ_t, may be expressed in terms of experimentally measurable quantities as:

$$\tau_t = c_2 \, l_t / u' \tag{4.2}$$

where u' is the *rms* turbulence velocity. The constant, c_2, is configuration-dependent, with an estimated value of 1.0 for grid turbulence (Snyder and Lumley, 1971) and 0.6 in certain geophysical flows (Pasquill and Smith, 1983). In the fan-stirred bomb this value is suggested as: $(\pi/8)^{1/2} \cong 0.627$ by Abdel-Gayed and Bradley *et al.* (1984). In present work the value of c_2, is adopted as 0.5.

Only one variable in Eq. (4.1), the conditional velocity $u(r,t;X)$, needs sub-modelling. Once a suitable expression for the conditional velocity is found, Eq. (4.1) is closed and it can be solved with usual CFD methods.

4.3 Modelling of Conditional Velocity

Conditionally averaged values such as chemical reaction rate and velocity are very important parameters in the models of CMC (Klimenko and Bilger, 1999), and *pdf* (O'Brien, 1985). One of the reasons of using conditionally averaged values is to improve the accuracy of turbulence modelling. In turbulent reacting flows, the chemical reaction rates are highly non-linear and if the turbulent mixing rate is much slower than chemistry reaction rates, then large fluctuations of temperature and species concentrations exist. If averages are taken over all values, then there exits large variations around the mean value. However, if averages are taken at a condition at which the temperature or species have a particular value, then the conditionally averaged values exhibit much smaller variations and the fluctuations have less influence on the accuracy.

4.3.1 Special Difficulty for the Exact Expression of Conditional Velocity

To model the turbulent convection in the scalar pdf transport equation, one must employ a term containing *conditionally averaged velocity* which is a priory unknown. At the time of writing it is still difficult to give a sufficiently sound description of the conditional velocity (Kuznetsov and Sabel'nikov, 1990). There may be two reasons for this: first, an extreme shortage of experiments with sufficient accuracy, although there exists some experiments such as those of Shcherbina (1982) and Tavoularis & Corrsin (1981); second, large errors may arise when measuring the conditional velocity in regions of large amplitudes of concentration fluctuations because of the effects of molecular transfer and large statistical errors of such rare events as large fluctuation amplitudes. Although there does exist an exact transport equation for the conditional velocity, it has not been put to practice. Here, a choice is made in favour of a simpler, algebraic, formula for the *conditionally averaged velocity,* such as the linear dependence of Kuznetsov (1972). Another alternative to it, the eddy diffisivity concept, though it may be acceptable for pdf approach, may be shown inadequate for RSF, Burluka (1996).

4.3.2 Gradient Transport Model

The gradient transport model is a widely used closure model in the modelling of turbulent flow, mainly because of its simplicity. The conditional velocity $\langle u \rangle_{\hat{c}}$ can be expressed with this model as:

$$\langle u_i \rangle_{\hat{c}} = \langle u_i \rangle - \Gamma_t \frac{\partial \ln c}{\partial x_i} \tag{4.3}$$

where $\langle u_i \rangle$ is unconditionally averaged mean velocity, Γ_t is turbulent diffusivity, c is a scalar variable, x_i is distance in i-th direction. The Prandtl number for the scalar c is defined from $\Gamma_c = \frac{\nu_t}{\mathrm{Pr}_c}$, where ν_t is the turbulent viscosity. In the framework of a classical $k-\varepsilon$ model, $\nu_t = c_\mu {k^2}/{\varepsilon}$, where k and ε are turbulent kinetic energy and its dissipation rate. In general, it has to be noticed that the existence of scalar turbulent

viscosity/diffusivity implies local homogeneity and isotropy of turbulence, a condition which is not always fulfilled, especially in reactive flows. This would also explain the limited experimental support for Eq. (4.3).

However, Eq. (4.3), partly because of historical reasons, partly because of its simplicity, served as a starting point for many simulations of turbulent flows, *e.g.* O'Brien (1980), Pope (1981), Bilger (2000) for pdf simulation, Swaminathan and Bilger (2001) for CMC simulation, Colucci *et al.* (1998) for LES simulation. The expression of Eq. (4.3) has also been used with the RSF model (Burluka *et al.*, 1997), for simulation of open V-flames in hydrogen-air and methane-air mixtures. Though averaged concentration and temperature were reasonablly well predicted, the second moments of scalar fields cannot be predicted when Eq. (4.3) is used with RSF (Burluka, 1996).

4.3.3 Algebraic Formula for Conditionally Averaged Velocity

When the joint velocity and scalar pdf is Gaussian, then it can be shown (Kuznetsov, 1972), that the conditionally averaged velocity is related to the mean velocity and concentration as:

$$\langle u \rangle_{\hat{c}} = \langle u \rangle + q\sigma^{-2}\left(\hat{c} - \langle c \rangle\right) \tag{4.4}$$

where $q = \left\langle \left(u - \langle u \rangle\right)\left(\hat{c} - \langle c \rangle\right) \right\rangle$ is the vector of mass flow flux; $\sigma^2 = \left\langle \left(\hat{c} - \langle c \rangle\right)^2 \right\rangle$ is the variance of concentration fluctuations. A similar dependency, under the name of Linear Mean Square Estimation (LMSE) was proposed by Dopazo (1975), and this model has been applied to predict the centerline evolution of the temperature pdf for an axisymmetrical turbulent heated jet (Dopazo, 1975). Kuznetsov and Sabel'nikov (1990) concluded that though the joint velocity-scalars pdf may deviate from a jointly normal distribution, Eq. (4.4) may still hold. However, when the scalar is normalised in such a way that it is bound between 0 and 1, then one may expect deviations of *conditionally averaged velocity* from the linear law of Eq. (4.4) especially at near the limit scalar values. Indeed, such deviations have been found in the measurements of Shcherbina (1982). However, big scatter in experimental data prevents a definitive conclusion on the character of these deviations. It has to be noticed that the experimental data available to Kuznetsov and Sabel'nikov (1990) concern nearly-constant density, slightly heated, jets in air.

Quite recently, a series of measurements in helium jets in air has been undertaken by Amielh *et al.* (2000). These jets have the density ratio more typical for combustion applications, $\rho_{jet}/\rho_{amb} \approx 7$, where subscriptions of *jet* and *amb* represent the jet and ambient. It has been found that a linear dependency is valid everywhere except at the jet boundaries, which are characterised by strong intermittency. However, no systematic study of *conditionally averaged velocity* behaviour in the intermittency regions has been carried out.

For the purpose of the present study, one can argue that Eq. (4.4) should be appropriate, because the turbulent field is homogeneous and isotropic. No external intermittency similar to that in turbulent jet boundaries is expected to occur in the fan-stirred bomb. Though no measurements of the higher order velocity moments, such as kurtosis or flatness factor, are available, it has been noted in Bradley *et al.* (1996a) that the velocity pdfs are close to Gaussian, in which case Eq. (4.4) is exact. For this reason, Eq. (4.4) is adopted for the simulations presented in this Chapter.

In a case where $\langle c'^2 \rangle \approx 0$, numerical realisation of Eq. (4.4) may be difficult, because of the necessity of finding the ratio $\frac{\langle u'c' \rangle}{\langle c'^2 \rangle}$ of two small values. A modification of Eq. (4.4), suitable for use in the RSF model, has been suggested for this case (Burluka, 1996):

$$u(r,t;X) = \langle u(r,t) \rangle + \sqrt{12}\, u'(X - 1/2) \tag{4.5}$$

This can be obtained as follows:

when the intensity of fluctuations is low, the scalar $c(X)$ can be approximated by $c(X) = \langle c \rangle + \alpha(X - 1/2)$ (Burluka, 1996), if $X \neq 0,1$. In this case the scalar variance is

$$\langle c'^2 \rangle = \int_0^1 \left(c(X) - \langle c \rangle\right)^2 dX = \int_0^1 \alpha^2 (X - 1/2)^2 dX = \frac{1}{12}\alpha^2 \tag{4.6}$$

so $\alpha = \sqrt{12}\sqrt{\langle c'^2 \rangle}$. Using this link in Eq. (4.4) one obtains Eq. (4.5) for the *conditionally averaged velocity* $u(r,t;X)$. Here, $\langle u(r,t) \rangle$ is the mean velocity at point r, at time t.

4.3.4 Directly Model Conditionally Averaged Velocity

A conditionally averaged velocity equation suitable for use in the RSF model could be obtained as:

$$\frac{\partial u(r,t;X)}{\partial t}+u(r,t;X)\frac{\partial u(r,t;X)}{\partial r}=-\frac{1}{\rho(r,t;X)}\frac{\partial\langle P\rangle}{\partial r}+\frac{\upsilon_m}{l_t^2}\frac{\partial^2 u(r,t;X)}{\partial^2 X}+\frac{\langle u(r,t)\rangle-u(r,t;X)}{\tau_t}+S_0(r,X,t)$$

where, $S_0(r,X,t)$ is the source term for the turbulence generated by the fans in the bomb. $S_0(r,X,t)$ can be randomly chosen from -1, 0, +1, the average of $S_0(r,X,t)$ on r and X is 0 because of the zero mean velocity in the bomb. An attempt has been made to solve this equation coupled with the RSF governing equations, Eq. (4.1), but for some unknown reason, no reasonable output has been obtained. Future work could be focussed on the better description of the turbulent convection for the RSF approach, in particular, in implementing a transport equation for conditionally averaged velocity similar to that displayed above.

4.4 Mean Velocity

In the expressions for *conditionally averaged velocity* mentioned above, information is needed on the unconditional mean velocity $\langle u(r,t)\rangle$. Here, instead of solving the equations of motion, it is found from the equation of continuity as follows. Firstly, the Reynolds decomposition:

$$\rho=\langle\rho\rangle+\rho', \quad u=\langle u\rangle+u' \tag{4.7}$$

commonly used in turbulence studies is applied to the continuity equation of Eq. (2.21). Upon neglecting the correlation $\langle\rho'u'\rangle$ one can obtain:

$$\frac{\partial\langle\rho\rangle}{\partial t}+\frac{1}{r^2}\frac{\partial\left(\langle\rho\rangle\langle u(r,t)\rangle r^2\right)}{\partial r}=0 \tag{4.8}$$

Secondly, by integrating Eq. (4.8) from 0 to r, the mean velocity $\langle u(r,t)\rangle$ at position r is determined by:

$$\langle u(r,t)\rangle = -\frac{\int_0^r \frac{\partial\langle\rho\rangle}{\partial t} r^2 dr}{\langle\rho\rangle r^2} \tag{4.9}$$

Because of the boundary condition $\langle u(r=0,t)\rangle=0$, Eq. (4.9) allows an explicit expression for velocity.

The pressure during a gas explosion is derived in *Appendix B*. By using a mean value, Eq. (B.6) is rewritten as:

$$P^{n+1} = \frac{\int_0^{R_b} \langle\rho^n\rangle r^2 dr}{\int_0^{R_b} \frac{W_{mix}^{\ n+1}}{R_u\langle T^{n+1}\rangle} r^2 dr} \tag{4.10}$$

4.5 Numerical Solution Procedure

The solution of Eq. (4.1) can be obtained with the finite volume method. The grid generation procedure is shown in Fig. 4.1, with a general grid node, *P*, and its four neighbours denoted with the upper case letters, *W* (west), *E* (east), *N* (north), *S* (south), and face boundaries denoted with the lowercase letters, *w*, *e*, *n*, *s*.

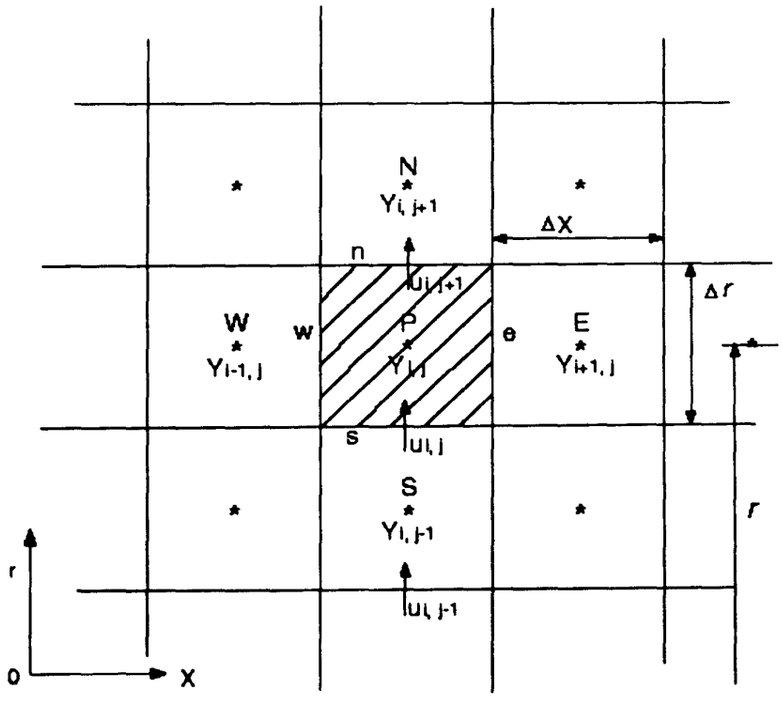

Fig. 4.1 Illustration of grid arrangement

By integrating Eq. (4.1) over a control volume, a system of algebraic discretised equations, one per each grid node, is obtained. These discretised equations form a tri-diagonal matrix in each coordinate, r and X, so the system can be solved by the iterative line-by-line method in X and r directions, in each line TDMA (tri-diagonal matrix algorithm) is used to get the solutions until the convergence criteria are satisfied (Patankar, 1980).

Details of the numerical algorithm are:

1) at time, 0, set initial values of Y_k^0 and $\langle u(r,0)\rangle$;
2) calculate conditional velocity, $u(r,0,X)$ from Eq. (4.5);
3) use subroutine " EULSIM " to obtain chemical reaction rates, w_i;
4) solve Eq. (4.1) to obtain new time step values of Y_k^{n+1} and T^{n+1}, using line-by-line and TDMA;
5) calculate pressure, p^{n+1}, with Eq. (4.10);
6) calculate ρ^{n+1} with the ideal gas equation of state;
7) calculate $\langle u(r,t+\Delta t)\rangle$ with Eq. (4.9);
8) calculate the conditional velocity, $u(r,t+\Delta t,X)$;
9) repeat steps 3) to 8) until the end.

Boundary conditions for species in the X coordinate are expressed by $\frac{d}{dX}(\cdot)=0$, when $X = 0, 1$, and in the physical coordinate, r, are expressed by $\frac{d}{dr}(\cdot)=0$, when $r = 0, R_b$, corresponding to the bomb centre and wall, respectively. The mean velocity, $\langle u(r,t)\rangle$, and conditional velocity, $\langle u(r,t,X)\rangle$, are set to zero at the boundaries of $r = 0$, and R_b.

Initial conditions correspond to quiescent mixture, $\langle u(r,t=0)\rangle$. The flame has been initiated either by numerically creating a hot kernel with radius of 2 *mm*, filled with adiabatically equilibrium combustion products or by depositing an energy within a given radius and at a given time. This last approach to flame initiation is described in more detail in *Appendix C*, where also a comparison is presented for these two ways of "ignition". Indeed, the results obtained are identical except for very short initial period.

Grid independence of the solutions has been checked with three series of calculations performed with different grid sizes in both X and r directions. They are: *100×500*, *200×500* and *200×1000*. It has been found that a grid size of *200×500* provides a sufficient resolution, and further refinement does not change the obtained solution.

4.6 Parameters for Simulations

Parameters have been chosen to describe explosions in the Leeds quasi-spherical bomb described in *Appendix A* and references given theerein. In this rig, for different fan speeds, the integral length scale remains approximately constant and equals to 20 *mm*, while the *rms* turbulence velocity may attain 9.52 *m/s*. A set of parameters including the calculated Reynolds and Damköhler numbers are given in Table 4.2.

Explosions in methane/air mixtures at different equivalence ratios, ϕ = 0.8, 1.0 and 1.2, are studied. The laminar burning velocities, u_L, are taken from Leeds experimental database (Bradley *et al.*, 1996b) as 0.25 *m/s* for ϕ = 0.8, 0.38 *m/s* for ϕ = 1.0 and 0.34 *m/s* for ϕ = 1.2. Simulations were carried out for two different initial pressures, P_0 = 1.0 *bar* with T_0 = 300 *K* and P_0 = 5.0 *bar* with T_0 = 358 *K*.

Presented in Fig. 4.2 is the present modelling and experimental conditions located in a Borghi's (1984) diagram. One can observe that the regimes of wrinkled flames with pocket formation and thickened-wrinkled flames are covered.

Table 4-2 Parameters used in simulations, P_0 = 1.0 *bar*, T_0 = 300 *K*

		u' (m/s)				
		0.595	1.19	2.38	4.76	9.52
Re_t		743.75	1487.5	2975	5950	11900
u'/u_L	ϕ = 0.8	2.38	4.76	9.52	19.04	------
	ϕ = 1.0	1.57	3.13	6.26	12.53	25.05
	ϕ = 1.2	1.75	3.50	7.00	------	------
Da	ϕ = 0.8	131.30	65.65	32.83	16.41	-------
	ϕ = 1.0	303.36	151.68	75.84	37.92	18.96
	ϕ = 1.2	242.86	121.43	60.71	-------	-------

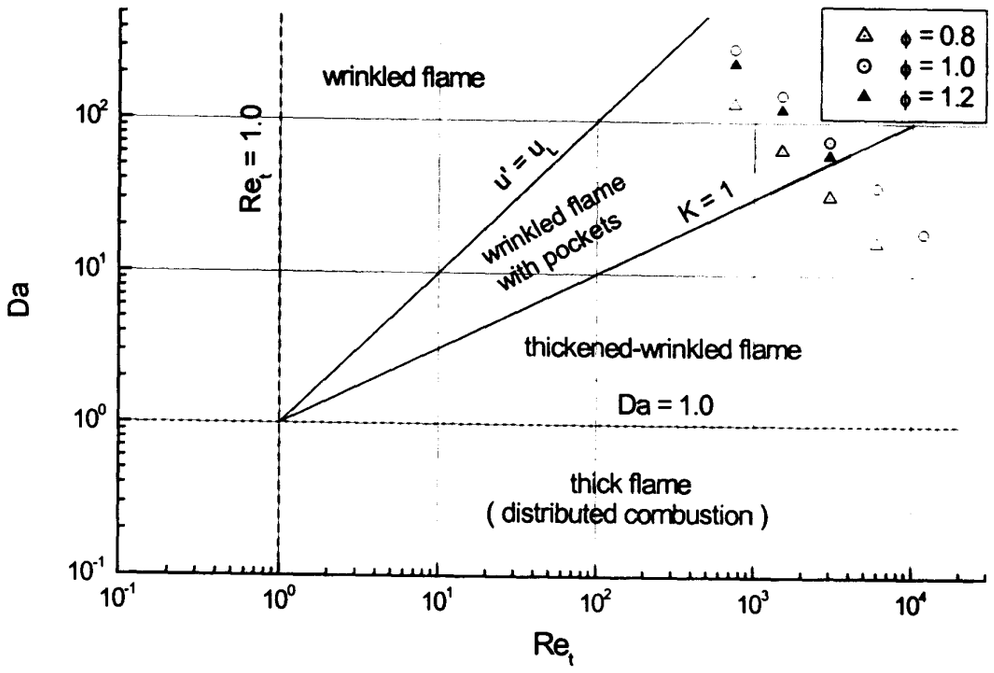

Fig. 4.2 Present conditions situated in a Borghi's diagram

4.7 Results and Discussions

Pressure histories during gas explosions in the bomb, mean species and temperature profiles, pdf evolution, and turbulent burning velocities were calculated and the results are presented and discussed in the following Sections.

4.7.1 Pressures

Calculated pressures for the three mixtures are presented in the Figs. 4.3, 4.4 and 4.5 for P_0 = 1.0 *bar*, T_0 = 300 *K*. In comparison with the measured values, one can see the simulated pressures are close to measurements at strong turbulence, but at lower turbulence intensities the simulated pressure rise is much slower than the measured one. The measurements also reveal a long initial period during which the pressure increase is quite slow, and this trend is not reproduced by the modelling.

The comparison for initial condition of P_0 = 5.0 *bar*, T_0 = 358 *K* is shown in Fig. 4.6, for lean (ϕ = 0.8) and stoichiometric mixtures at various turbulence intensities. The measurements are provided by Woolley (2001).

4.7.2 Mean Values and Fluctuations

Profiles of averaged temperature and species concentrations, including CH_4, CO_2 and R are presented in Figs. 4.7, 4.8 and 4.9 for the three mixtures at different turbulence intensities. The corresponding fluctuations are shown in Figs. 4.10, 4.11 and 4.12. As shown in these Figures, the magnitude of fluctuations for both temperature and species concentration reduced with increase in turbulence.

4.7.3 Temperature pdf Evolutions

The scalar pdf evolution can be determined from the extra statistical coordinate, X, through Eq. (1.30). Shown in Fig. 4.13 is an example of the link between temperature profile in X and its pdf evolution for $\phi = 0.8$, $u' = 4.76$ *m/s*, where $r = 2/6\,R_b$ represents the distance from the bomb centre at which the spark is located, R_b is the bomb radius.

The temperature pdf evolutions at different distances from the bomb centre are shown in Fig. 4.14, to 4.17 for the three mixtures. In these Figures, bimodal pdf evolution is clearly seen. By a comparison of Figs. 4.15 and 4.16, the effect of turbulence on the pdf evolution can be observed, higher turbulence results in faster flame propagation; however, the motion of a broadened peak corresponding to the fresh mixture is also visible. This is a clear deficiency of the model caused by simple IEM-like term in the RSF Eq. (4.1).

4.7.4 Turbulent Flame Development

Once the pressure is calculated, turbulent flame radius and mass burning rate can be obtained, for example, using the technique suggested by Lewis and von Elbe (1951) and described in *Chapter 2* and *Appendix A*. Knowledge of mass burning rate will provide immediately the possibility of quantitative comparison with suggested models and correlations. One such correlation, which is used to compare with the present modelling results, is the KLe correlation proposed by Abdel-Gayed *et al.* (1987). In this correlation, an effective *rms* velocity, u_k', is introduced, which characterises the

proposition of total turbulent intensity "felt" by the growing flame kernel (Abdel-Gayed and Bradley *et al.*, 1987, Bradley *et al.*, 1994, 2000). From measured power spectral density (PSD) functions, u_k' has been derived as:

$$u_k' = u'\left(1-\exp\left(-0.28\left(\frac{t}{\tau_t}\right)^{3/4}\right)\right) \tag{4.12}$$

where τ_t is the turbulence integral time scale, and t is the time elapsed after ignition.

The turbulent burning velocity growing with time is determined by:

$$u_t = 0.88u_k'(KLe)^{-0.3} \tag{4.13}$$

where K is the Karlovitz number calculated by:

$$K = 0.157\left(\frac{u'}{u_L}\right)^2 \mathrm{Re}_t^{-0.5} \tag{4.14}$$

where Re_t is turbulent Reynolds number ($\mathrm{Re}_t = \frac{l_t u'}{\nu}$).

Another model proposed by Lipatnikov *et al.* (2000) is based on an expression for u_t^0, derived by Zimont (1979) from an assumption that the instantaneous reaction zone is thickened by the turbulence:

$$u_t^0 = Au'^{0.75}u_L^{0.5}k^{0.25}l_t^{0.25} \tag{4.15}$$

Where k is molecular thermal diffusivity, and A is a constant of order unity, which is taken as 0.4 in the present study as suggested by Lipatnikov *et al.* (2000).

After that, if Eq. (4.15) is coupled with Taylor turbulent diffusion theory, one can obtain:

$$u_t = u_t^0\left(1+\frac{\tau_t}{t}\left(\exp\left(-\frac{t}{\tau_t}\right)-1\right)\right)^{1/2} \tag{4.16}$$

The comparison of turbulent burning velocity predicted by RSF model with these two models is shown in Fig. 4.18. Good agreement can be seen for all three mixtures, except for the very early period. For that period, it seems that the modelling results produce much higher turbulent burning velocities. However, during this early period combustion

is sensitive to initial conditions such as spark ignition energy, while after that period the initial conditions do not affect combustion. One can see in Fig. C.4 in *Appendix C*, that the turbulent burning velocity during some short initial period is much reduced when the combustion is initiated by depositing an amount of energy compared with combustion initiated by a hot spot.

Turbulent flame radii and burning velocities are also compared with the measurements (see description of the experimental technique in *Appendix A*), obtained at the same conditions, and the comparison is shown in Figs. 4.19 and 4.20 for P_0 = 1.0 *bar*, T_0 = 300 *K*, and in Figs. 4.22 and 4.23 for P_0 = 5.0 *bar*, T_0 = 358 *K*. The measurements at P_0 = 1.0 *bar* were carried out by the present author, and the measurements at P_0 = 5.0 *bar* were carried out by Woolley (2001).

General trends such as increasing burning velocity with increasing turbulence are well produced by the modelling, but there exists quite strong quantitative discrepancies due to the initial "incubation" period, when combustion is quite slow.

4.8 Conclusions

Statistically homogeneous turbulent flame propagation in a fan-stirred bomb has been selected as a test case to assess the RSF model. This problem is an ideal test case because 1) purpose-made experiments can be performed in the Leeds fan-stirred bomb, which can generate homogenous and isotropic turbulence, providing data of which collection and processing procedures are known entirely; 2) the geometry is simple and avoids uncertainties related to the description of a more complex flow field where turbulence properties could vary strongly.

In order to have a clear basis for comparison, experimental studies of turbulent methane/air flame propagation in a fan-stirred bomb were carried out. Pressure during gas explosion was recorded. Flame radius and turbulent mass burning rate were then obtained from pressure trace method. The measurements revealed a substantially long initial "incubation" period during which flame propagated quite slowly, and the

duration of this initial period seemed to increase for stronger turbulence as shown in Figs. 4.4, 4.5 and 4.6.

Turbulent methane/air flames propagating in a spherical bomb was simulated using the RSF model. Pressure in the bomb, averaged mean values of species concentrations and temperature were calculated for different conditions. Turbulent burning velocity was then determined from calculated pressure rise. The obtained turbulent mass burning rate was compared with experiments as well as the predictions of *KLe* correlation of Bradley *et al.* and Lipatnikov-Zimont's model. The comparisons showed that the results obtained with all three different models agreed quite well as shown in Fig. 4.18. However, when compared with measurements, the simulations could not reproduce the observed initial "incubation" period, and quantitatively, calculated turbulent burning velocities were much slower than those from measurements. General trends, such as increase in burning velocity and decrease in the magnitude of *rms* fluctuations of temperature/concentration for stronger turbulence, have been well-predicted by RSF .

The evolutions of corresponding pdfs were also obtained from the reference scalar fields. The RSF model predicted reasonably well the bimodal pdf evolution for the studied regimes of premixed turbulent flame. For example, the temperature pdf evolutions showed that the pdf evolution was bimodal as presented in Figs. 4.14 to 4.17 over the entire range of the varied parameters. However, the displacement of the (broadened) δ-peak, corresponding to the fresh mixture, is also visible. This means that the fresh gas immediately in front of the flame front is already heated-up. This is a clear deficiency of the model caused by the simple IEM-like term in Eq. (4.1) for micro-scale mixing.

It proved also that the methane-air flames simulations may suffer from an inadequate representation of the chemical kinetics mechanism. In particular, it is unclear yet whether the deviation of the initial period is sensitive to the details of chemical kinetics; the experiments do not allow us to draw a definitive conclusion and the simulations were unable to reproduce this phenomena at all! For this reason it was deemed necessary to find a combustion system with simple and unambiguous reaction mechanism.

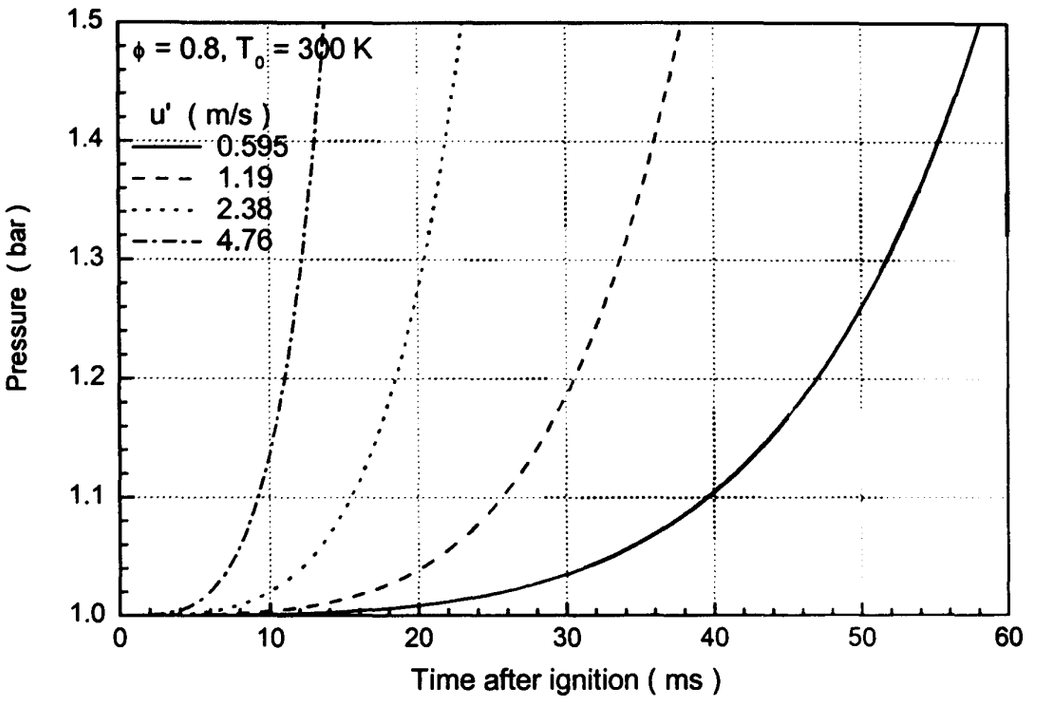

Fig. 4.3(a) Simulated pressures

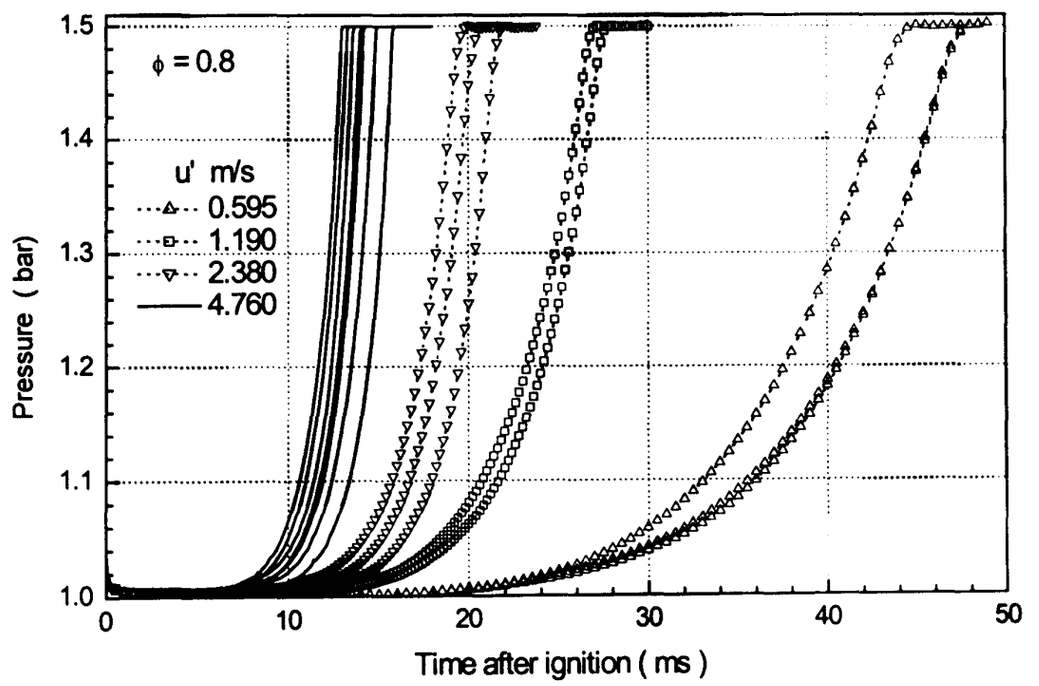

Fig. 4.3(b) Measurements

Fig. 4.3 Comparison of calculated and measured pressure traces for $\phi = 0.8$, $P_0 = 1.0$ *bar*, $T_0 = 300$ *K* at various turbulence intensities

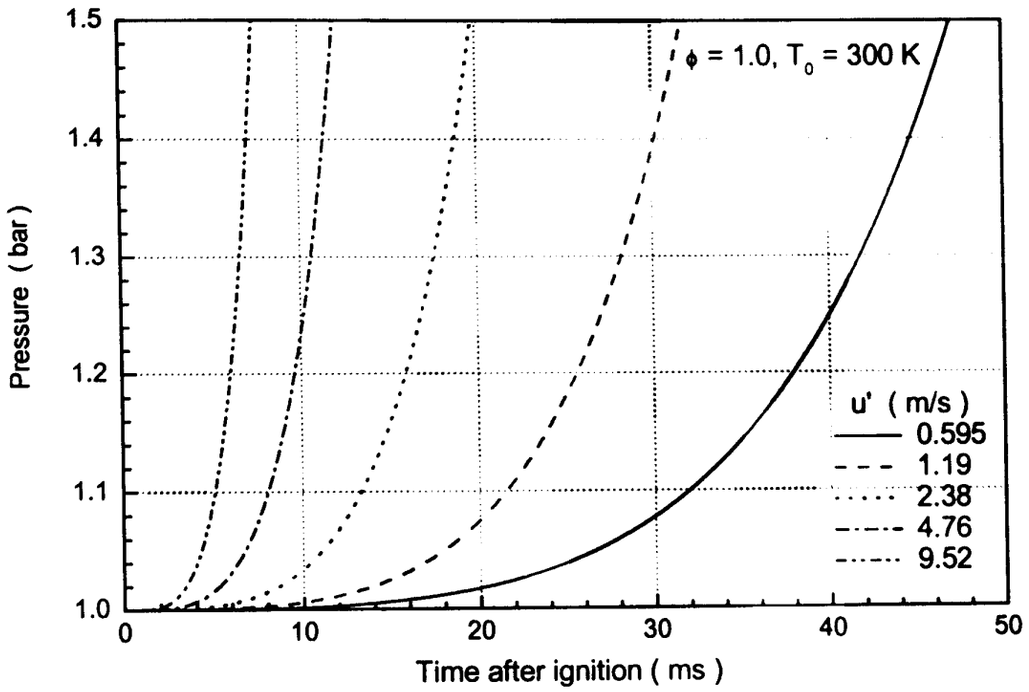

Fig. 4.4(a) Simulated pressures

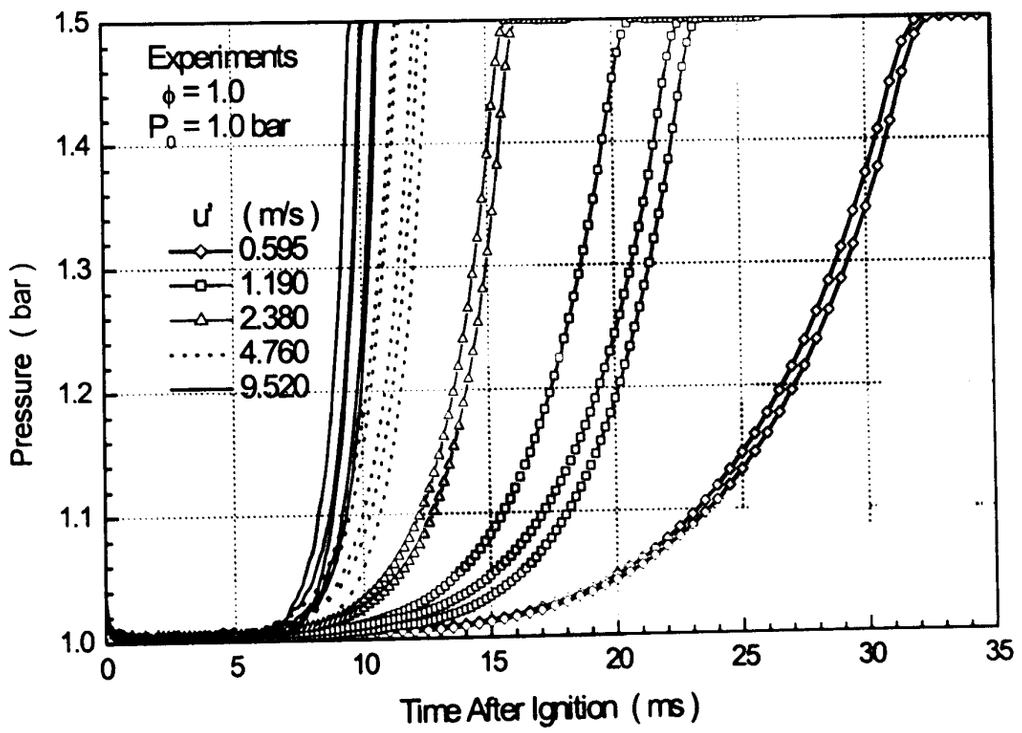

Fig. 4.4(b) Measurements

Fig. 4.4 Comparison of calculated and measured pressure traces for $\phi = 1.0$, $P_0 = 1.0$ *bar*, $T_0 = 300$ *K* at various turbulence intensities

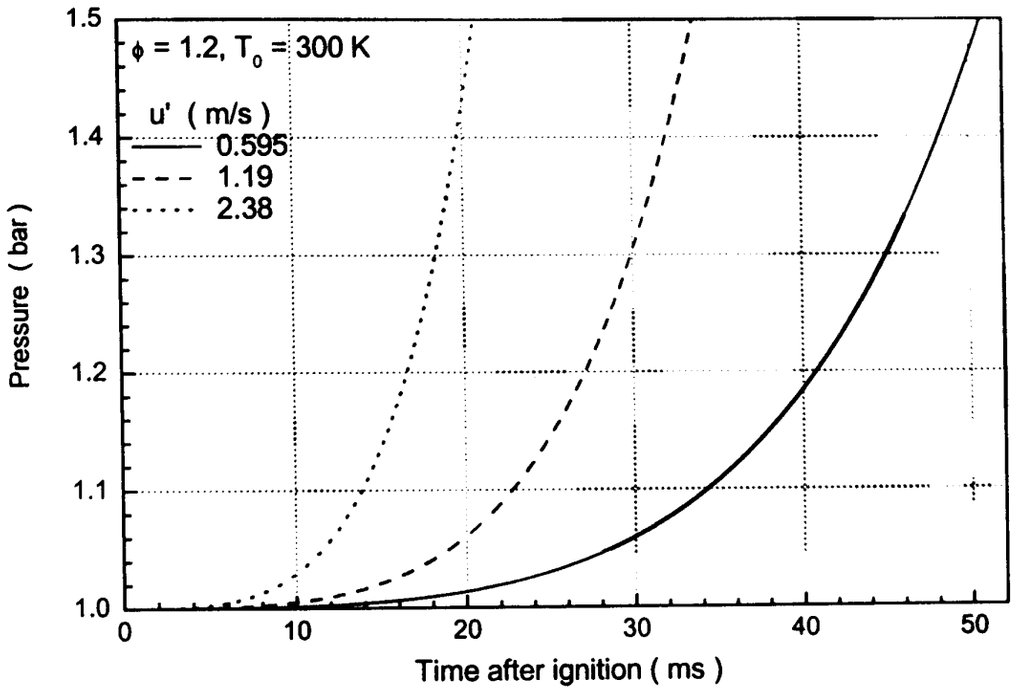

Fig. 4.5(a) Simulated pressures

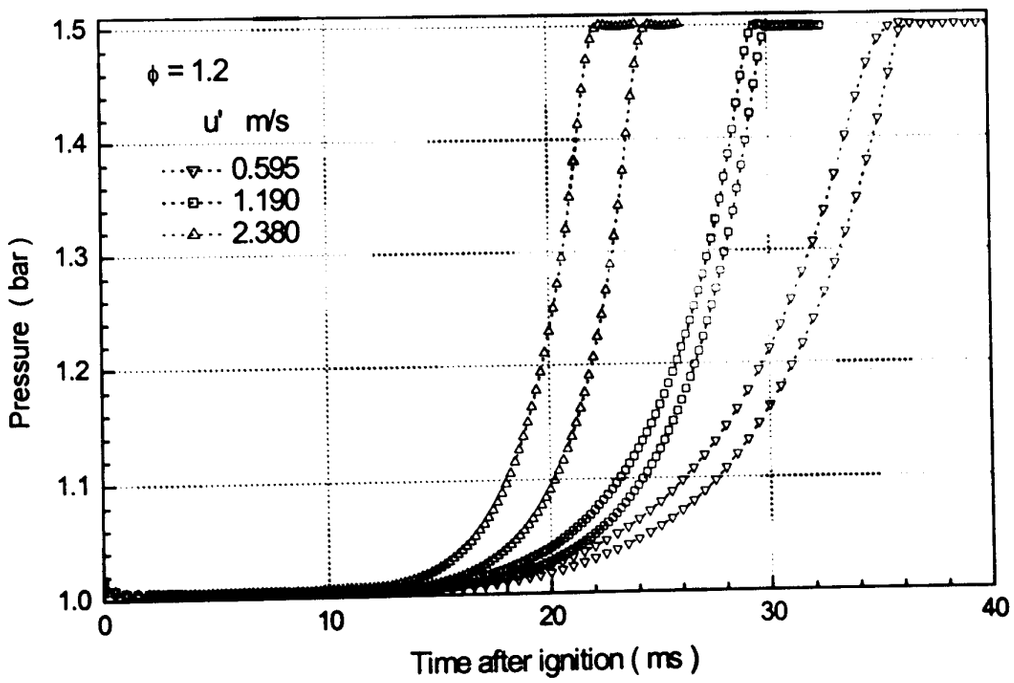

Fig. 4.5(b) Measurements

Fig. 4.5 Comparison of calculated and measured pressure traces for $\phi = 1.2$, $P_0 = 1.0$ *bar*, $T_0 = 300$ *K* at various turbulence intensities

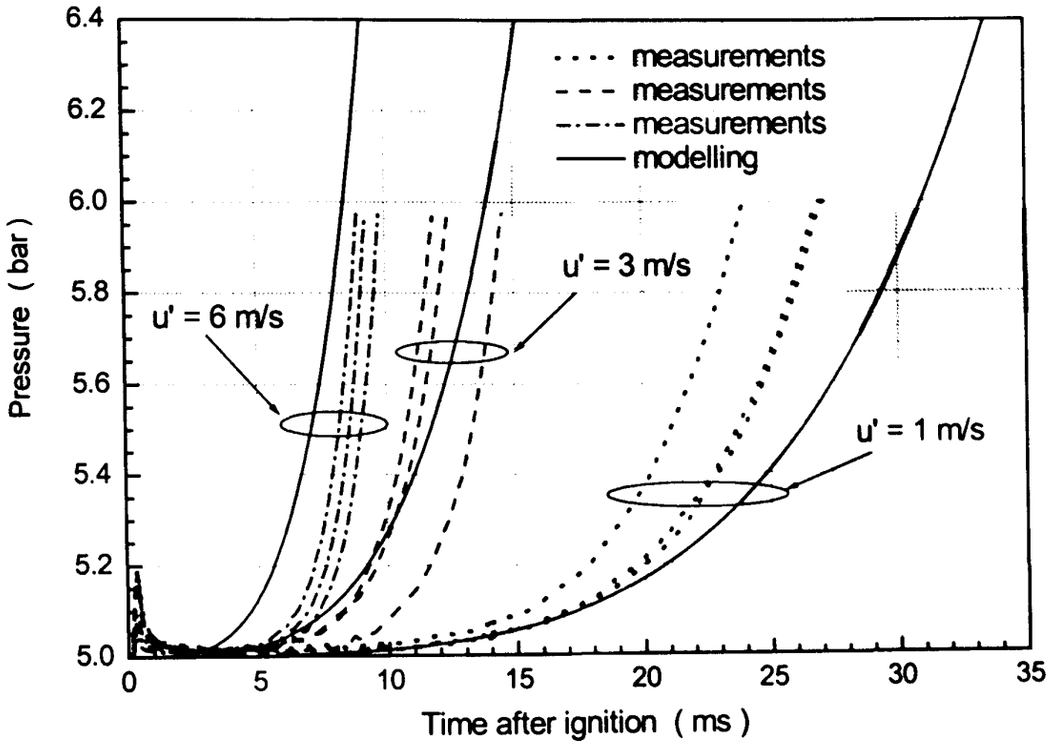

Fig. 4.6(a) $\phi = 0.8$

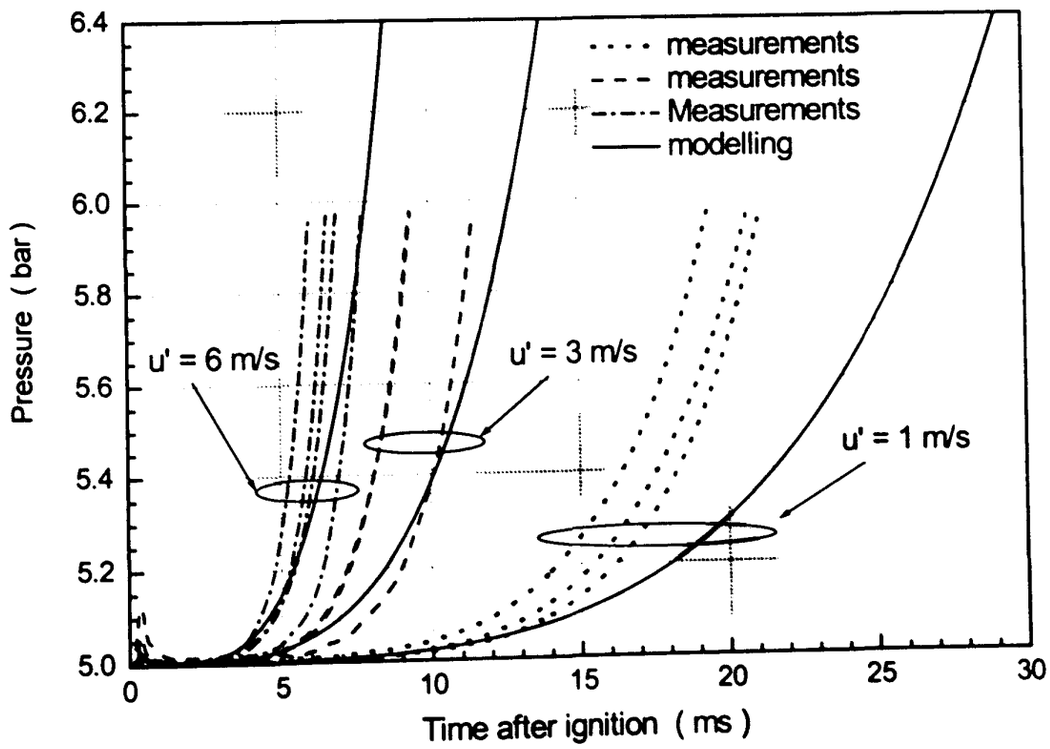

Fig. 4.6(b), $\phi = 1.0$

Fig. 4.6 Comparisons of calculated and measured pressure traces for lean and stoichiometric mixtures at $P_0 = 5.0$ *bar*, $T_0 = 358$ *K*

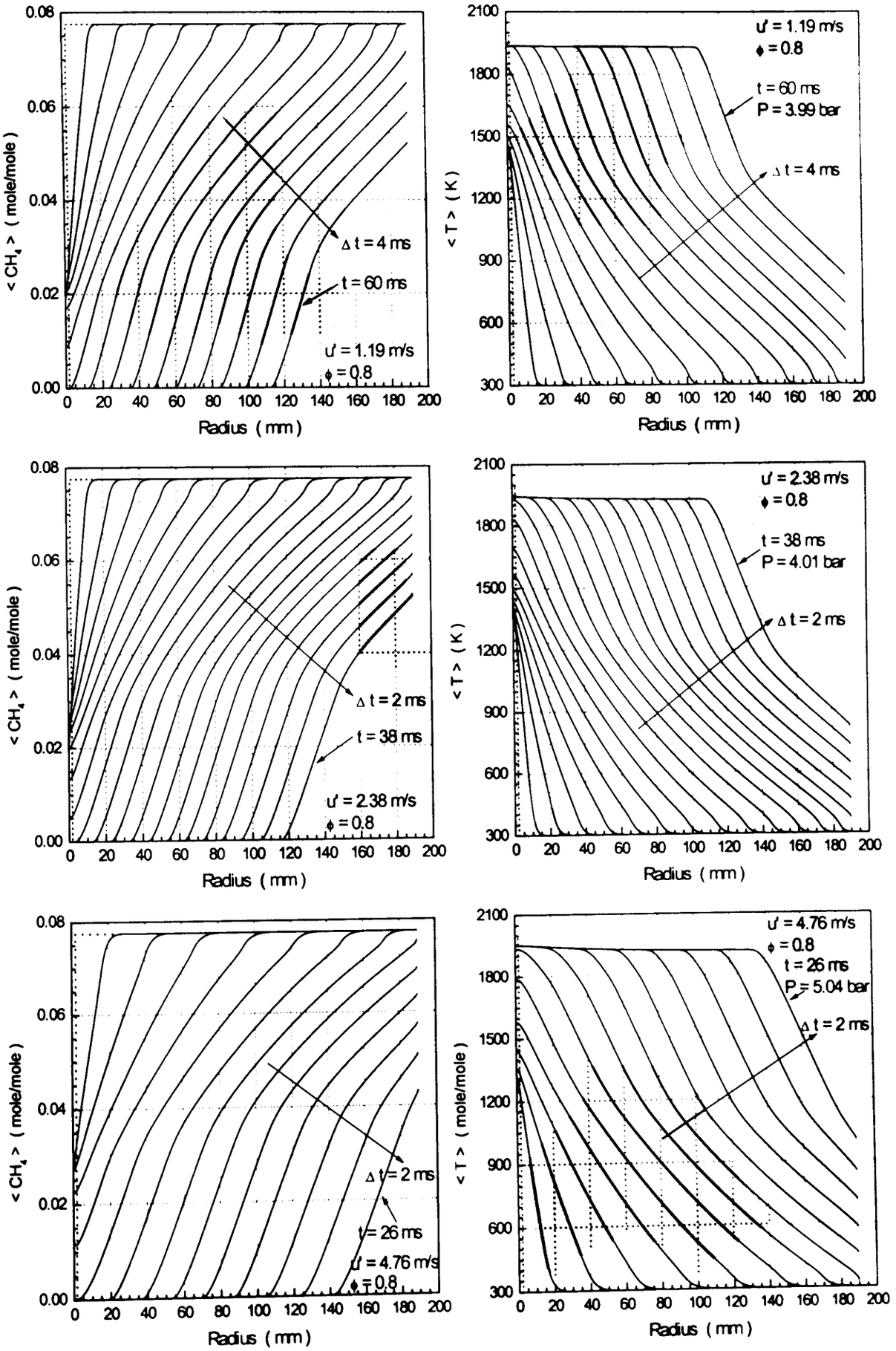

Fig. 4.7(a) CH_4 profiles

Fig. 4.7(b) Temperature profiles

Fig. 4.7 Mean value profiles for for $\phi = 0.8$, $P_0 = 1.0$ *bar*, $T_0 = 300$ *K* at various turbulence intensities

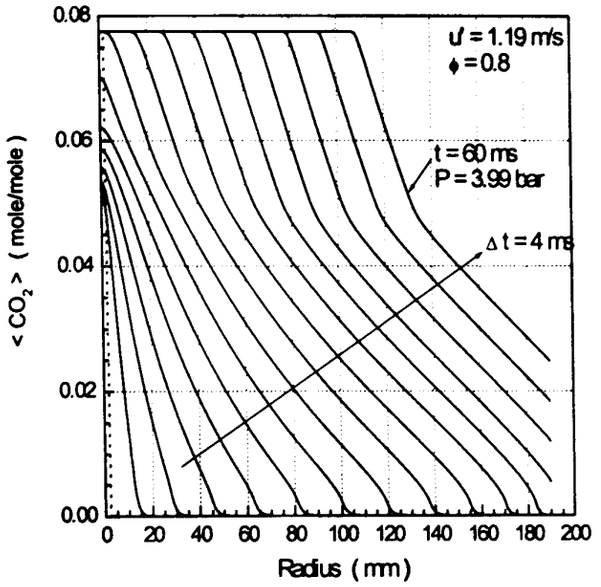

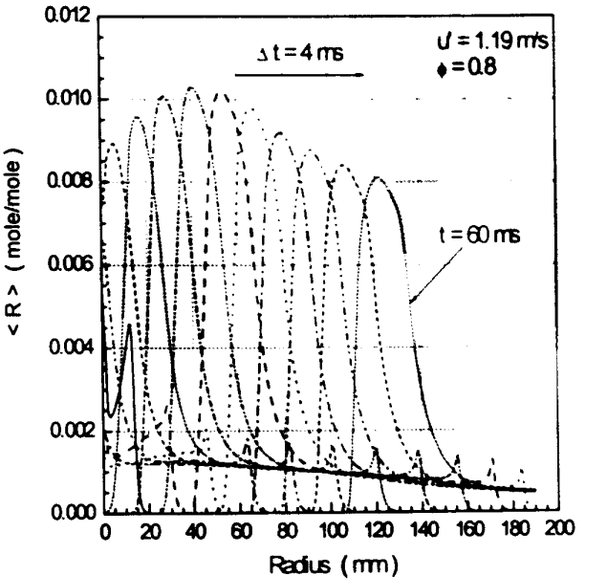

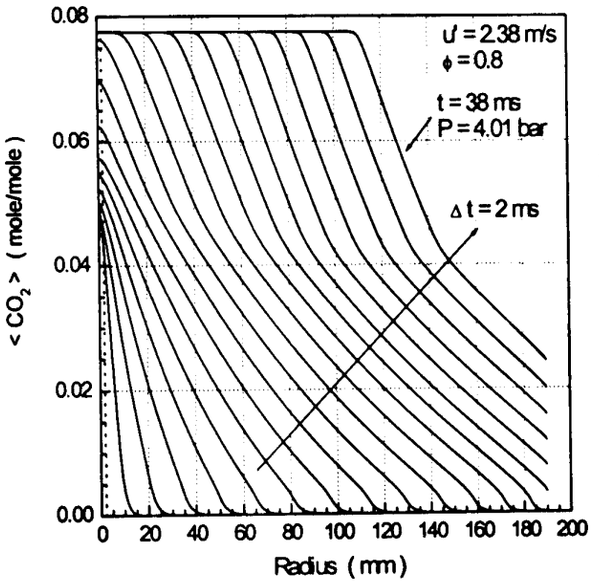

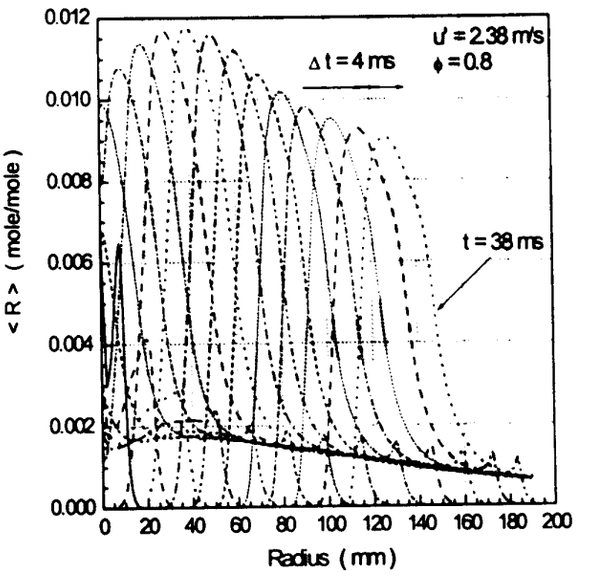

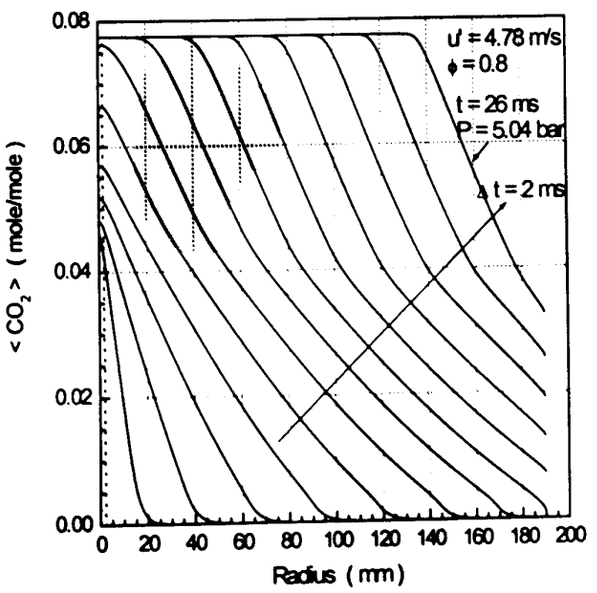

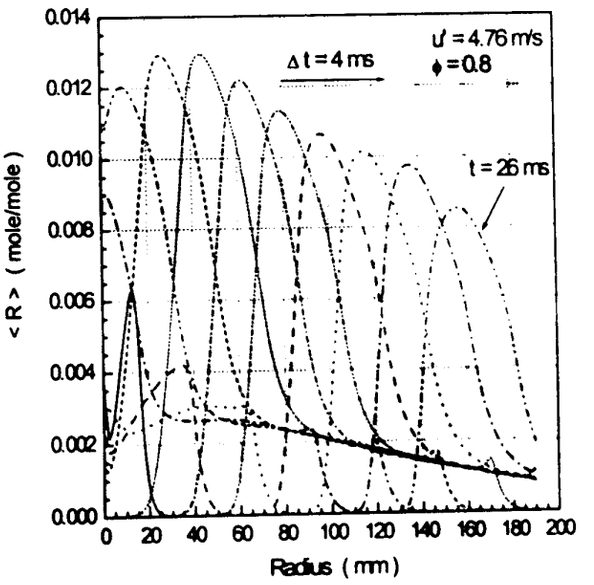

Fig. 4.7(c) CO_2 profiles

Fig. 4.7(d) R profiles

Fig. 4.7 Mean value profiles for for $\phi = 0.8$, $P_0 = 1.0$ *bar*, $T_0 = 300$ *K* at various turbulence intensities

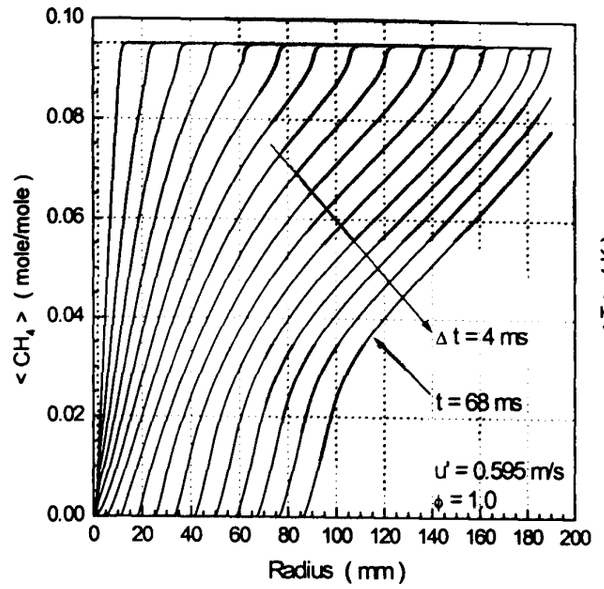

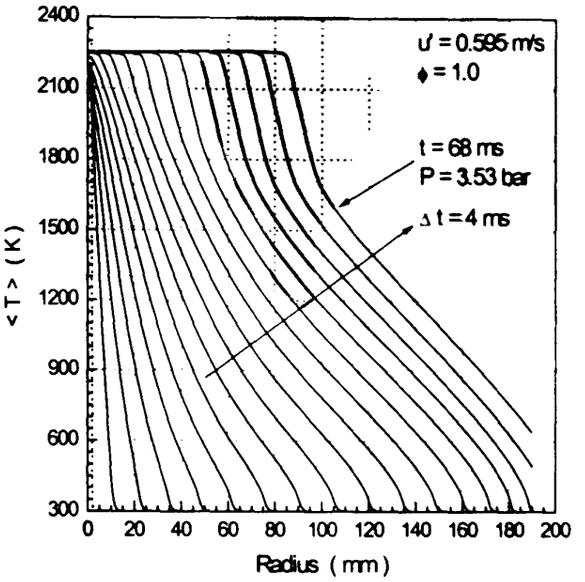

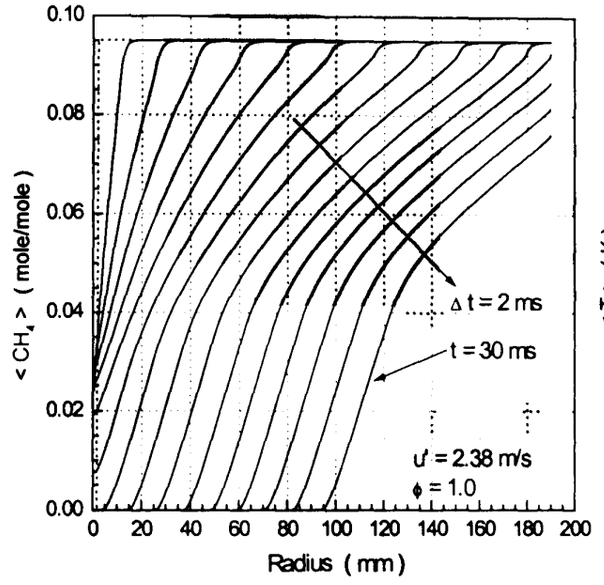

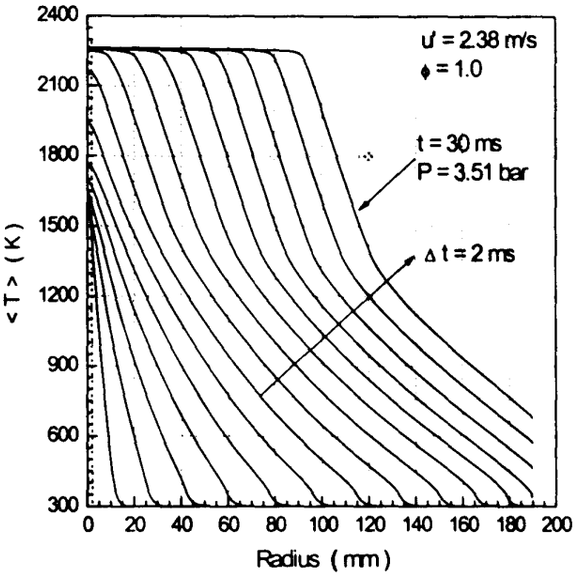

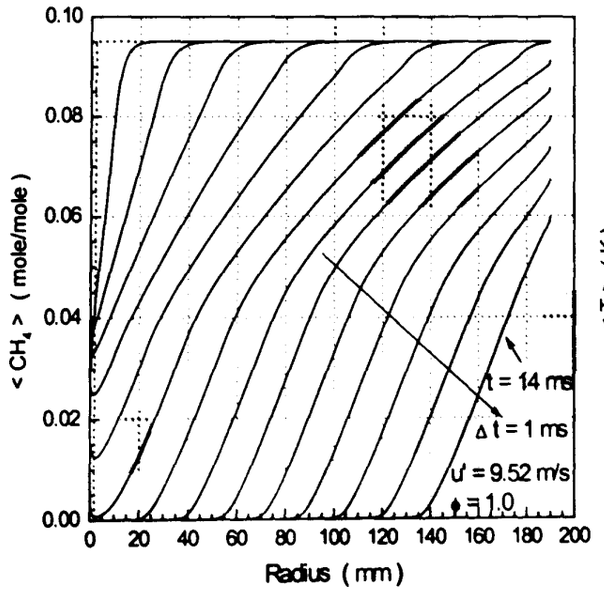

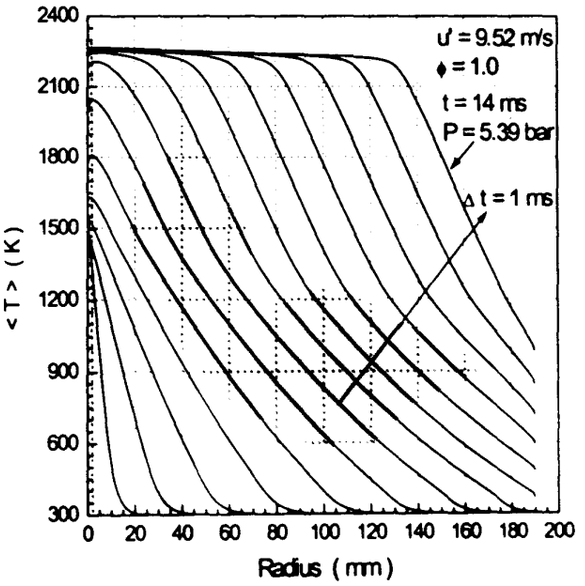

Fig. 4.8(a) CH_4 profiles

Fig. 4.8(b) Temperature profiles

Fig. 4.8 Mean value profiles for for $\phi = 1.0$, $P_0 = 1.0$ *bar*, $T_0 = 300$ *K* at various turbulence intensities

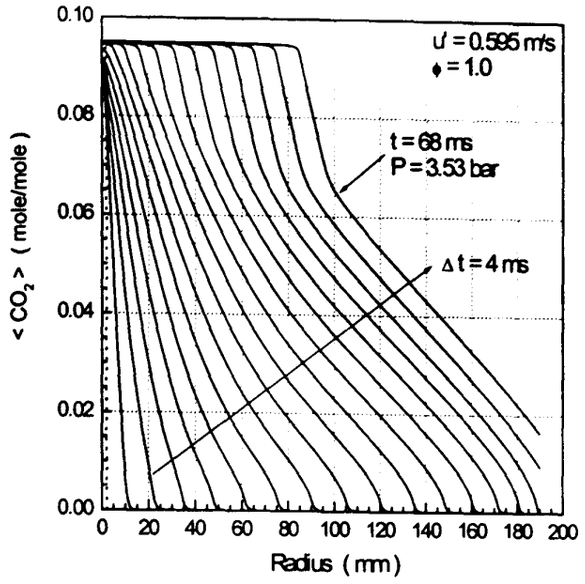

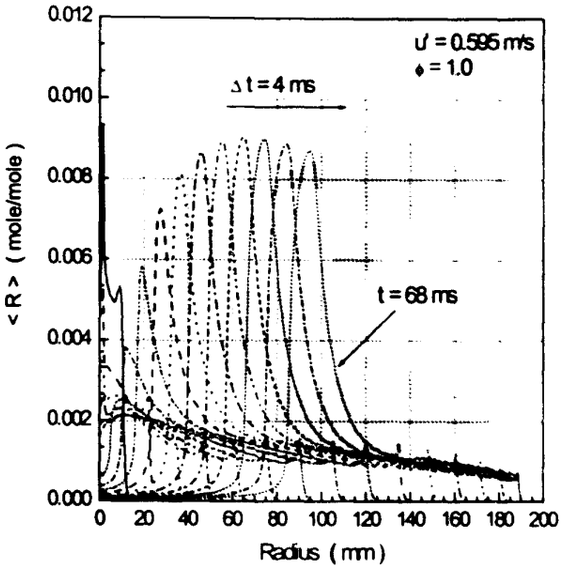

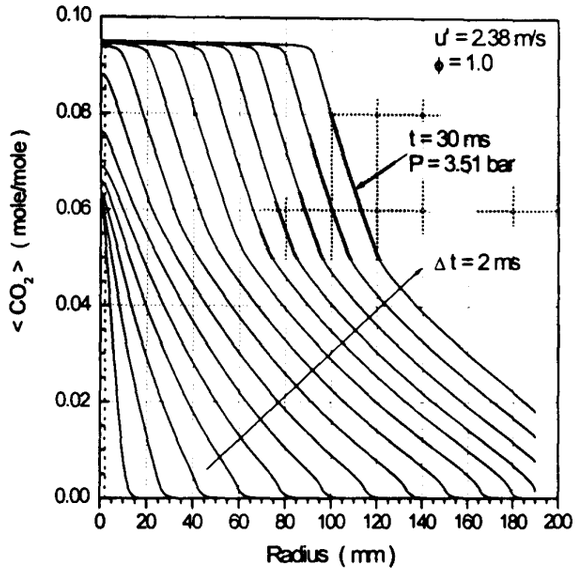

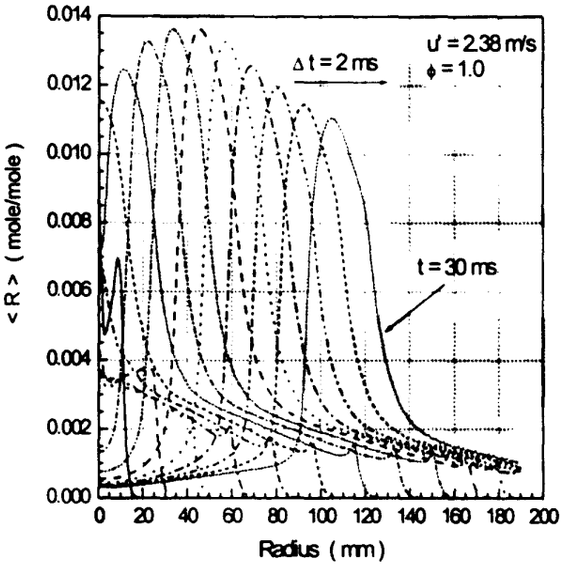

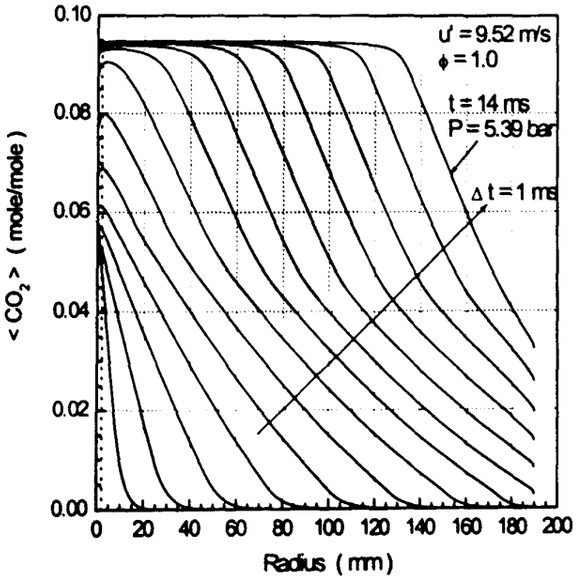

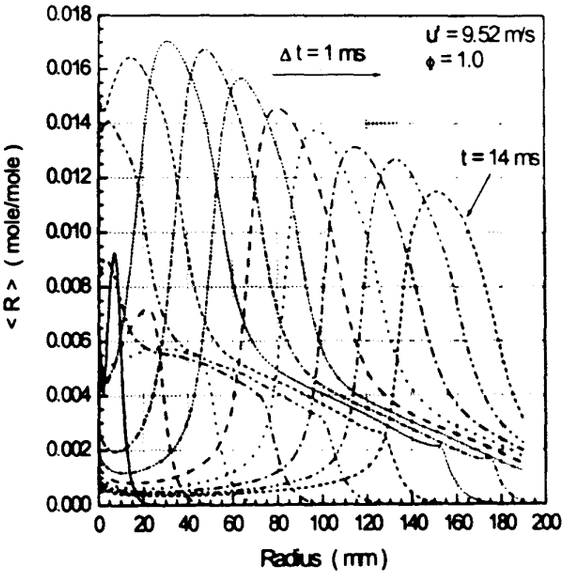

Fig. 4.8(c) CO_2 profiles

Fig. 4.8(d) R profiles

Fig. 4.8 Mean value profiles for for $\phi = 1.0$, $P_0 = 1.0$ *bar*, $T_0 = 300$ *K* at various turbulence intensities

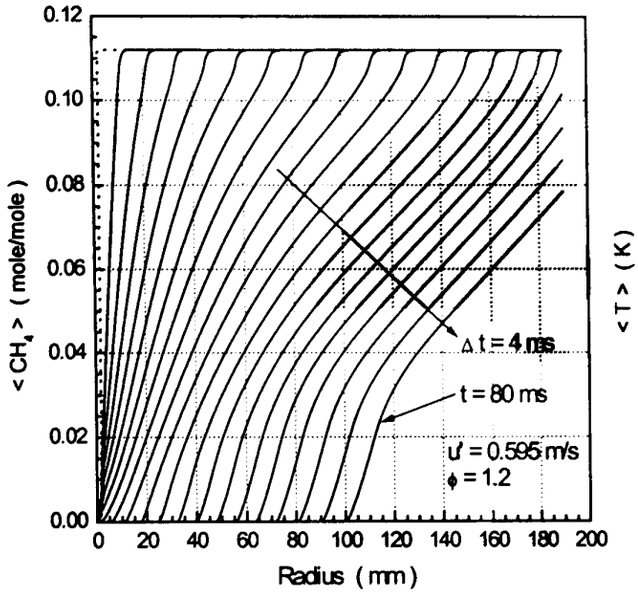

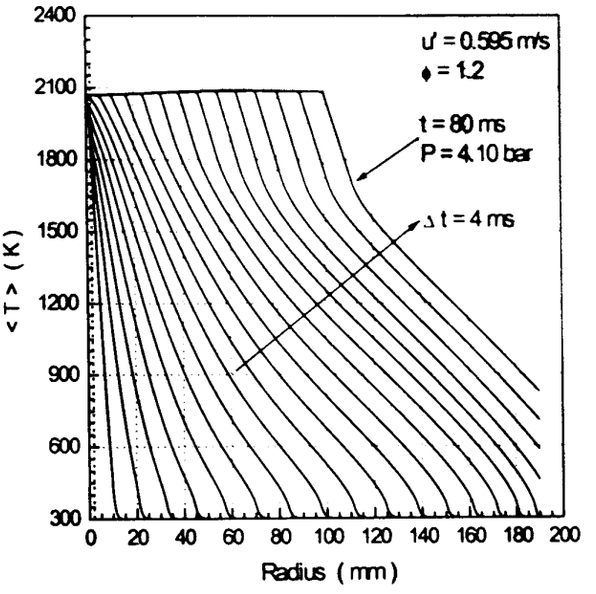

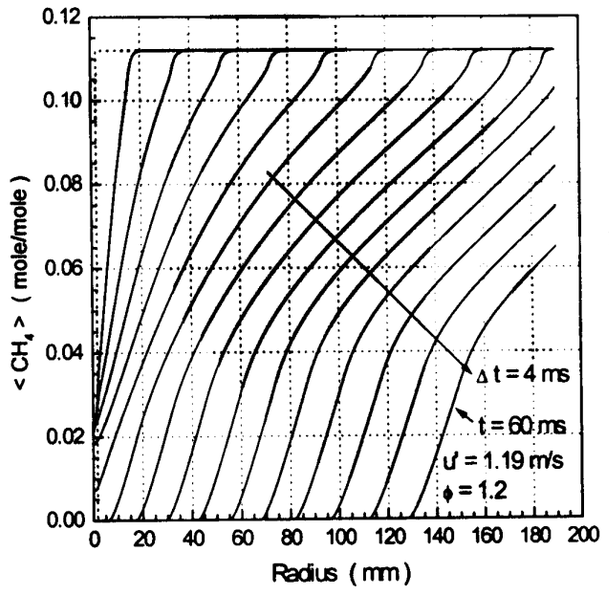

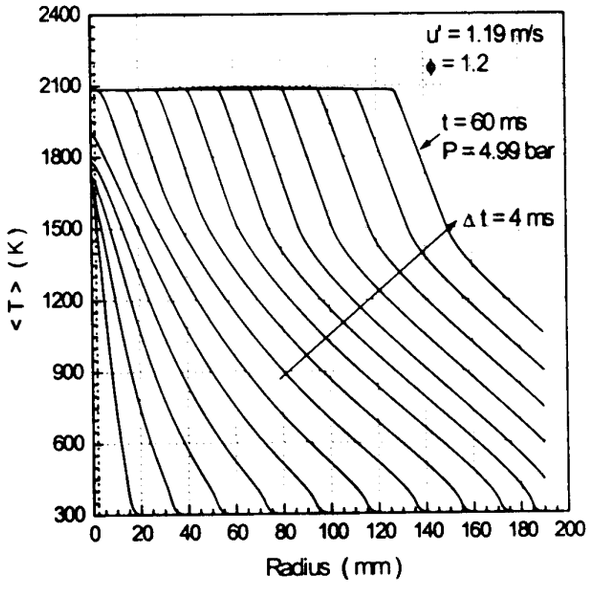

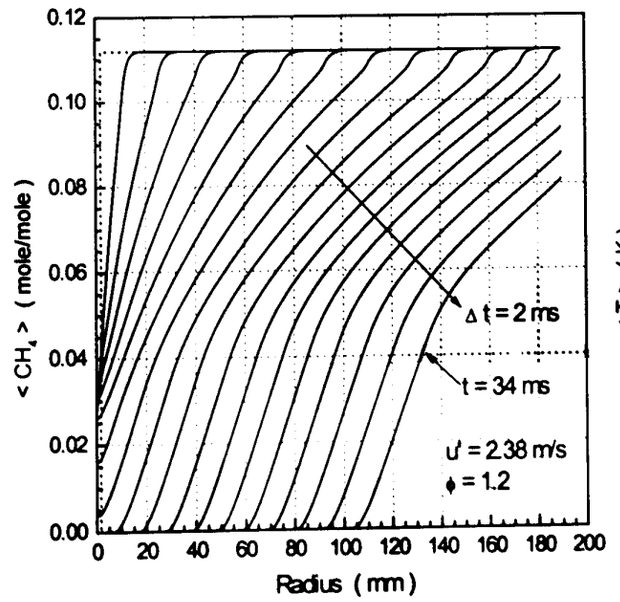

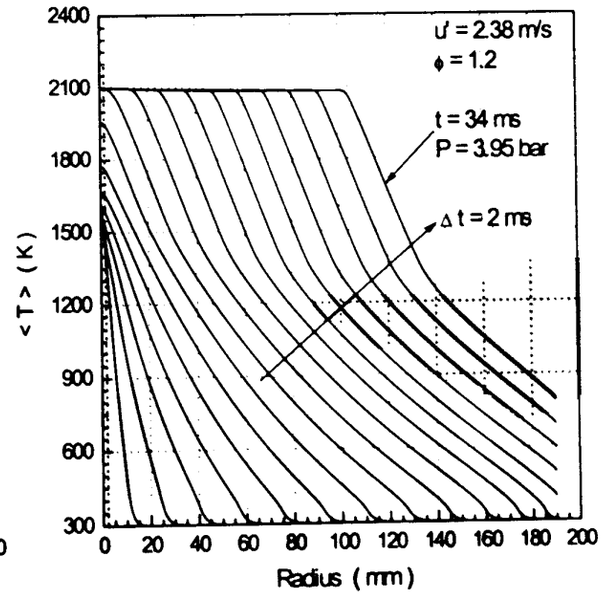

Fig. 4.9(a) CH_4 profiles

Fig. 4.9(b) Temperature profiles

Fig. 4.9 Mean value profiles for for $\phi = 1.2$, $P_0 = 1.0$ *bar*, $T_0 = 300$ *K* at various turbulence intensities

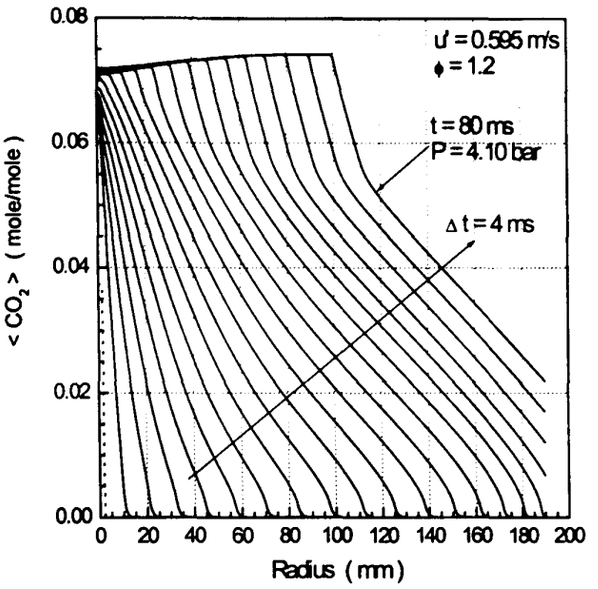

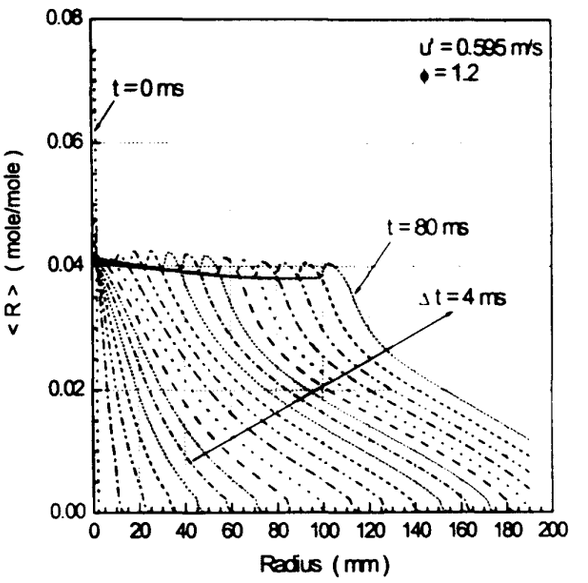

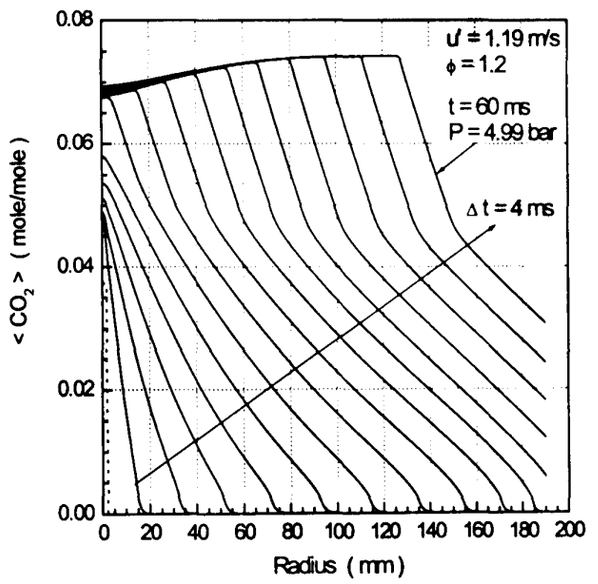

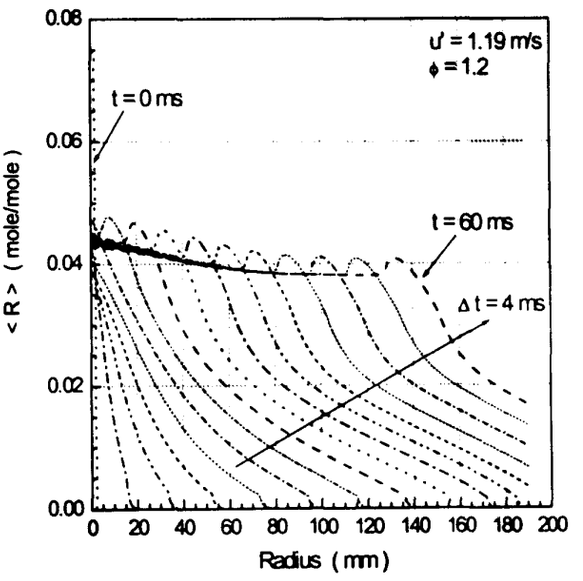

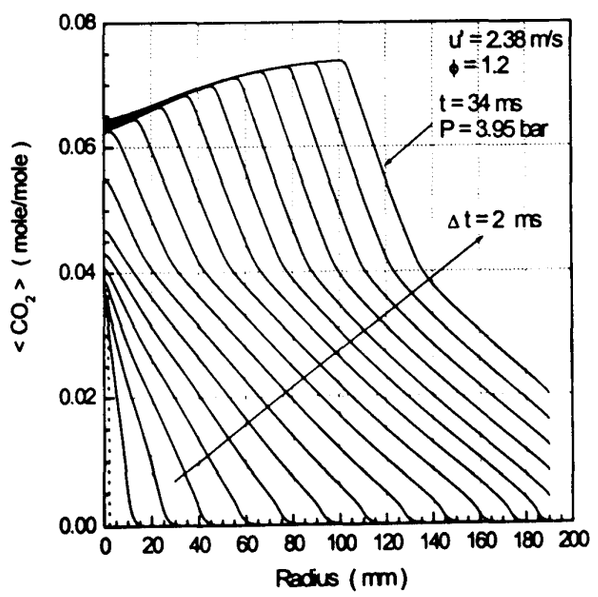

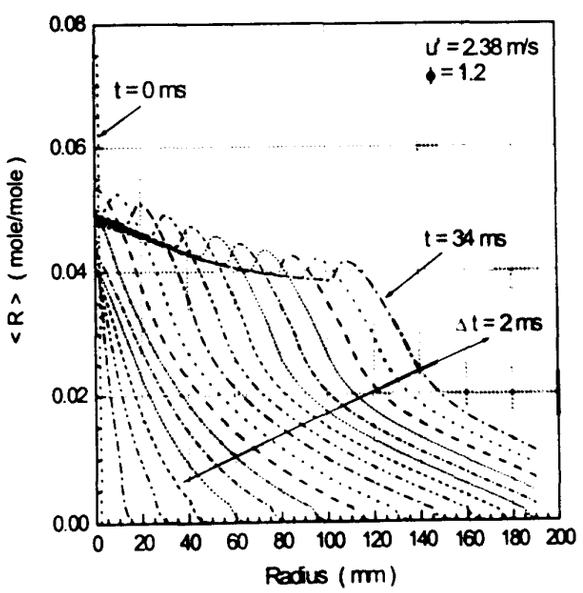

Fig. 4.9(c) CO_2 profiles

Fig. 4.9(d) R profiles

Fig. 4.9 Mean value profiles for for $\phi = 1.2$, $P_0 = 1.0$ *bar*, $T_0 = 300$ *K* at various turbulence intensities

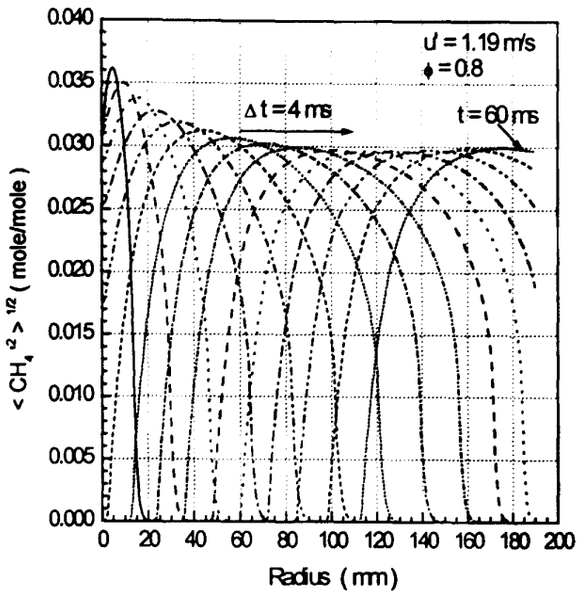

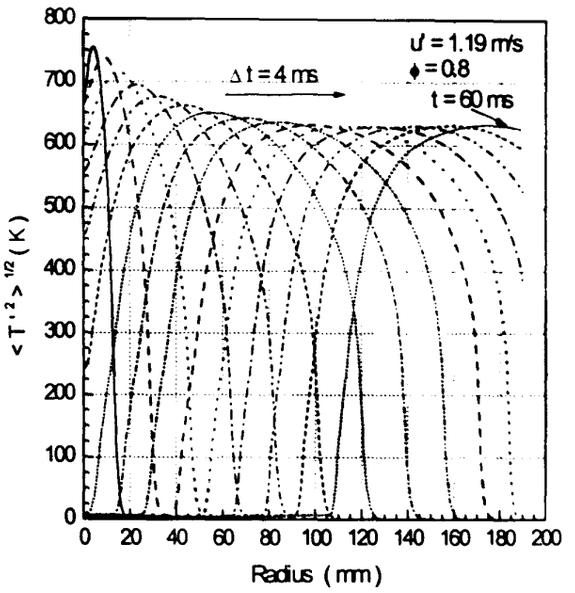

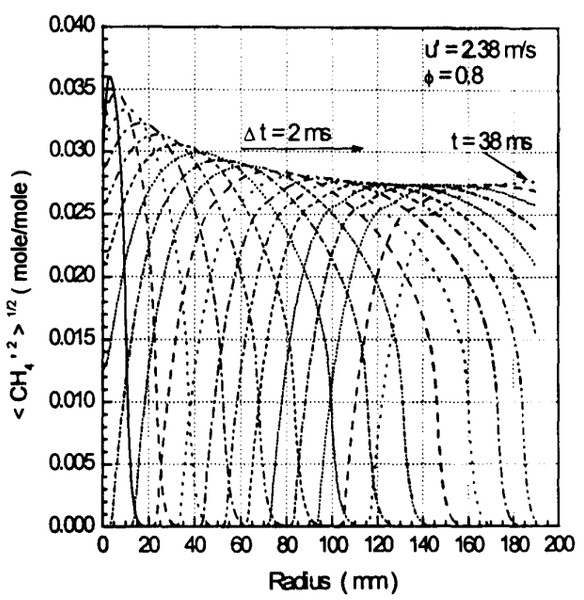

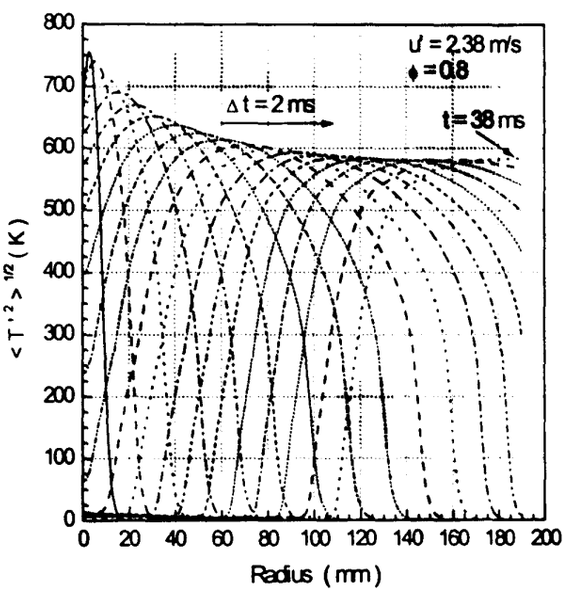

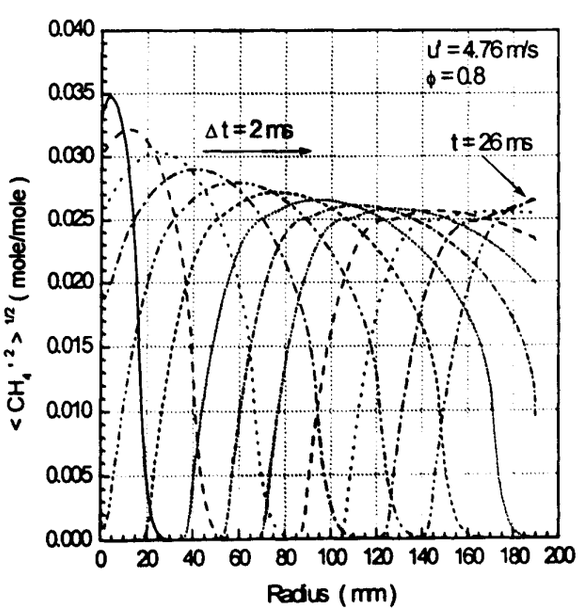

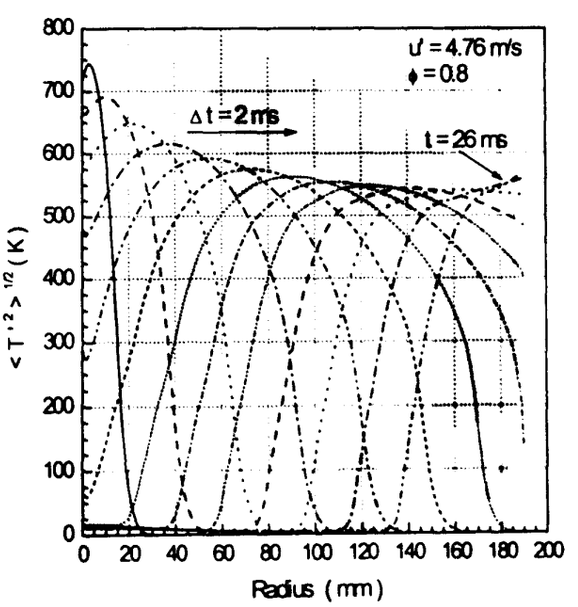

Fig. 4.10(a) CH_4 profiles

Fig. 4.10(b) Temperature profiles

Fig. 4.10 Fluctuation profiles for for $\phi = 0.8$, $P_0 = 1.0$ *bar*, $T_0 = 300$ *K* at various turbulence intensities

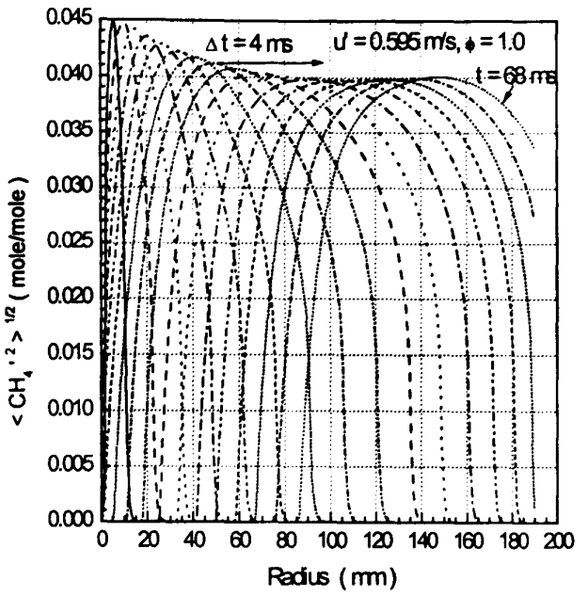

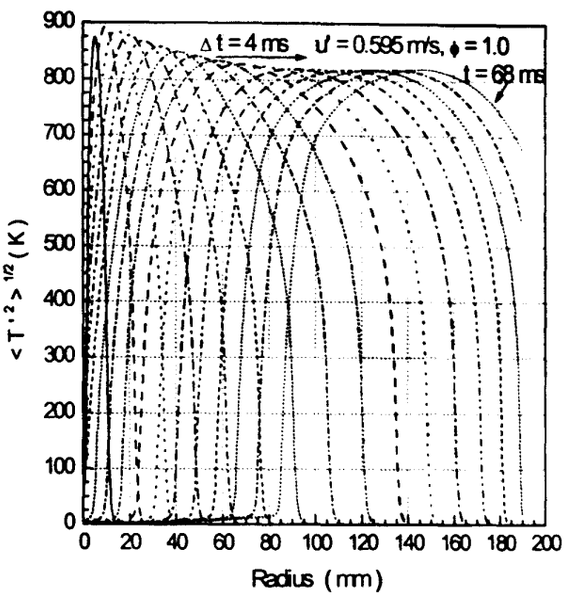

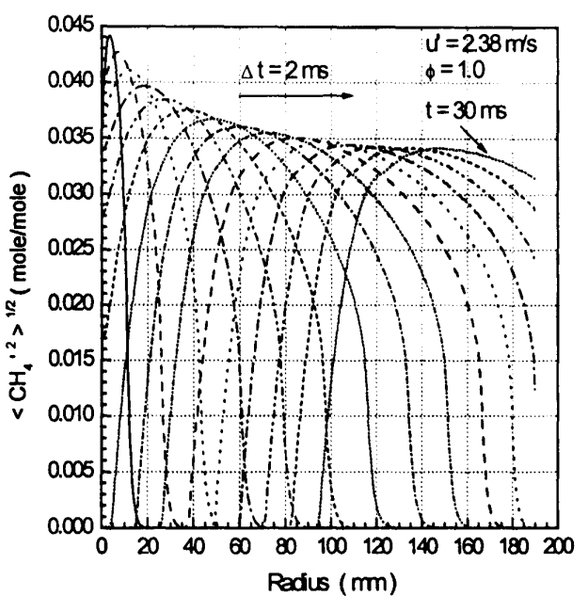

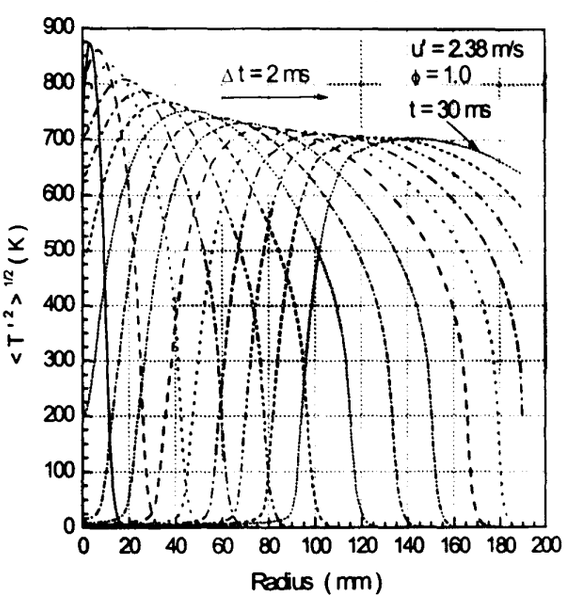

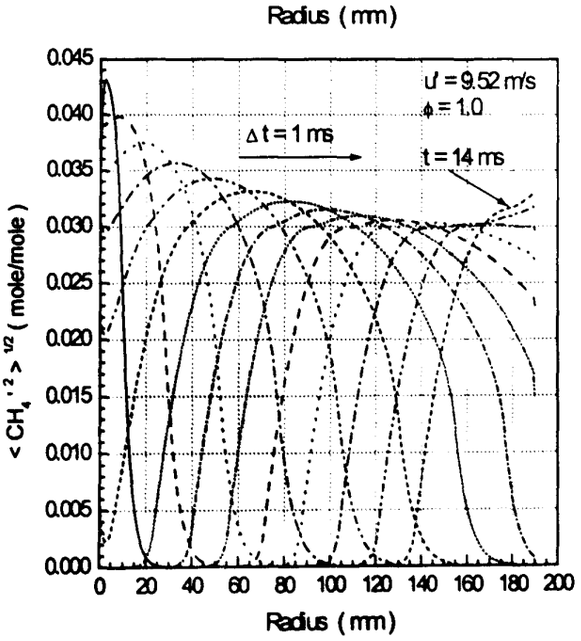

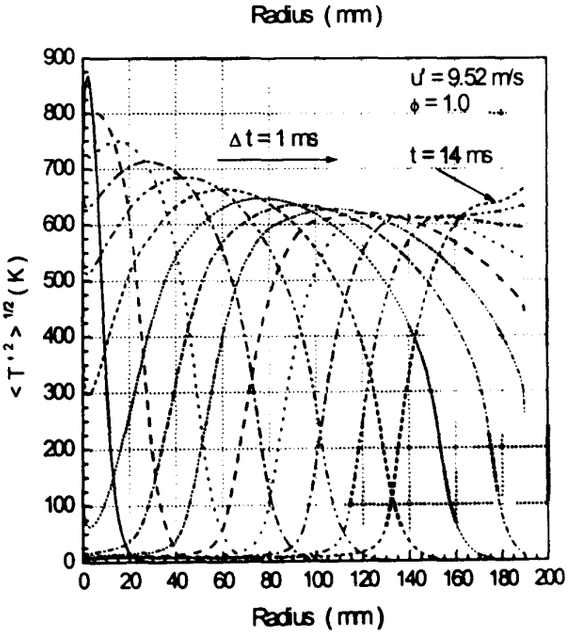

Fig. 4.11(a) CH_4 profiles

Fig. 4.11(b) Temperature profiles

Fig. 4.11 Fluctuation profiles for for $\phi = 1.0$, $P_0 = 1.0$ *bar*, $T_0 = 300$ *K* at various turbulence intensities

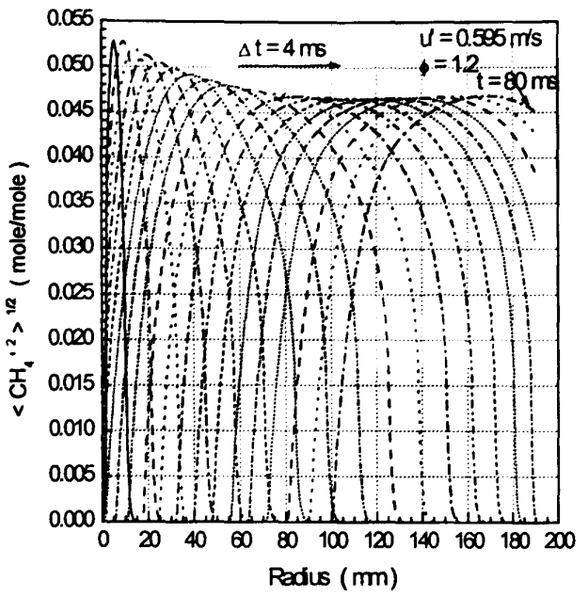

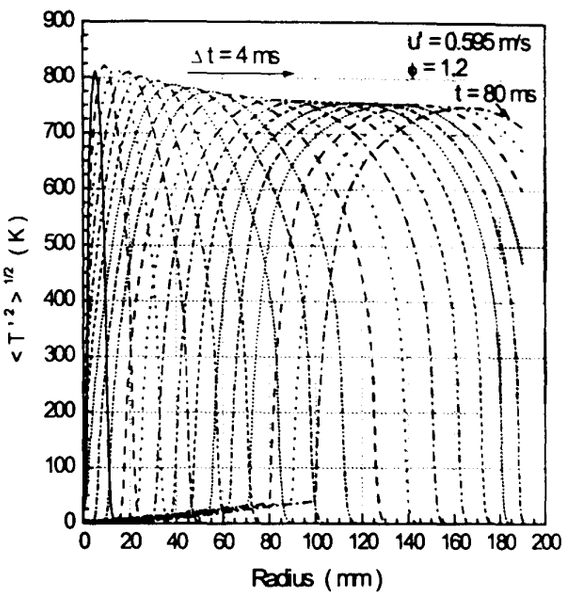

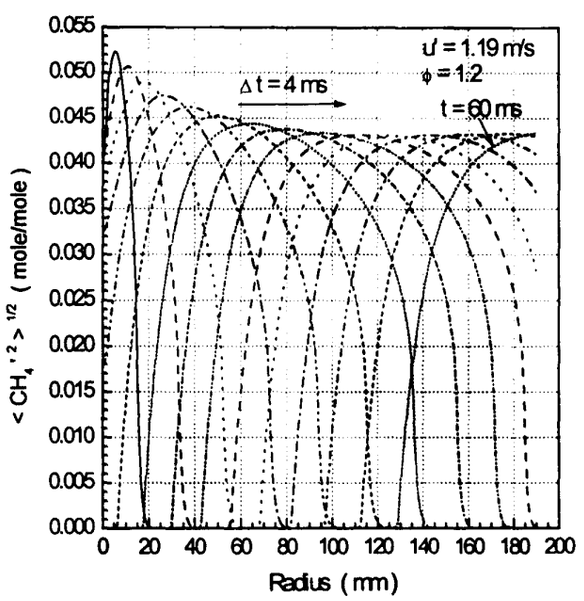

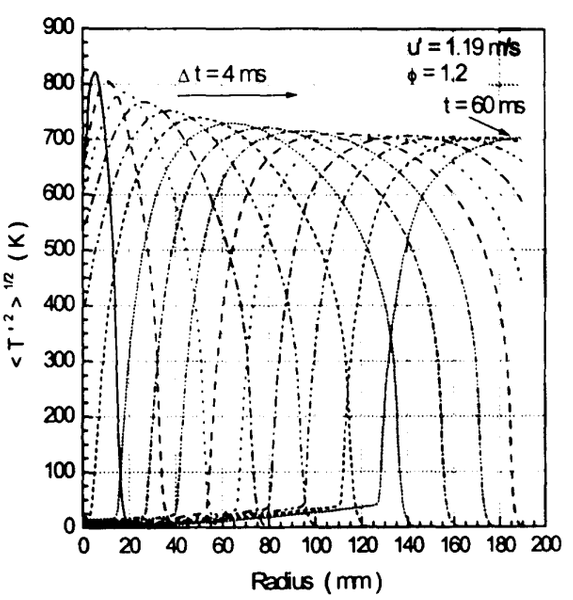

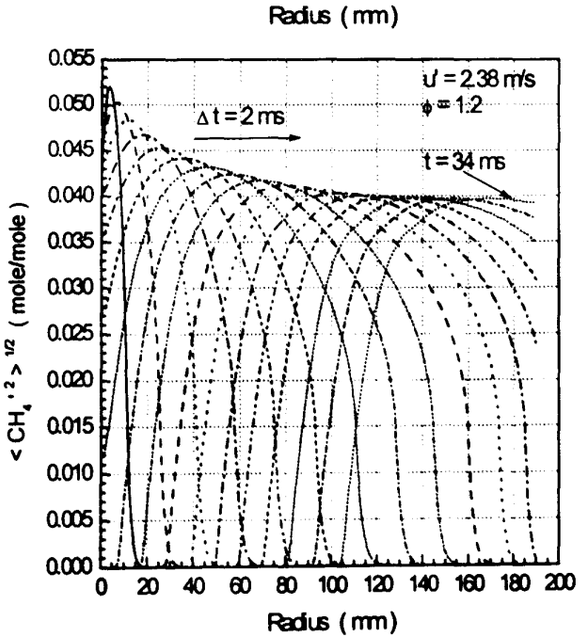

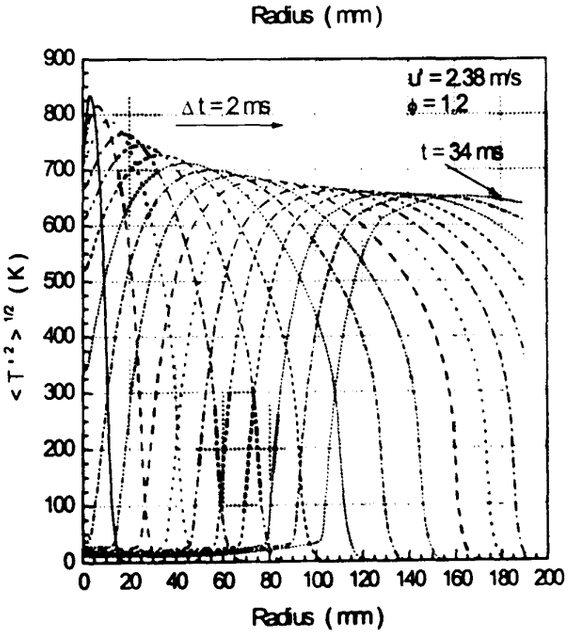

Fig. 4.12(a) CH_4 profiles

Fig. 4.12(b) Temperature profiles

Fig. 4.12 Fluctuation profiles for for $\phi = 1.2$, $P_0 = 1.0$ *bar*, $T_0 = 300$ *K* at various turbulence intensities

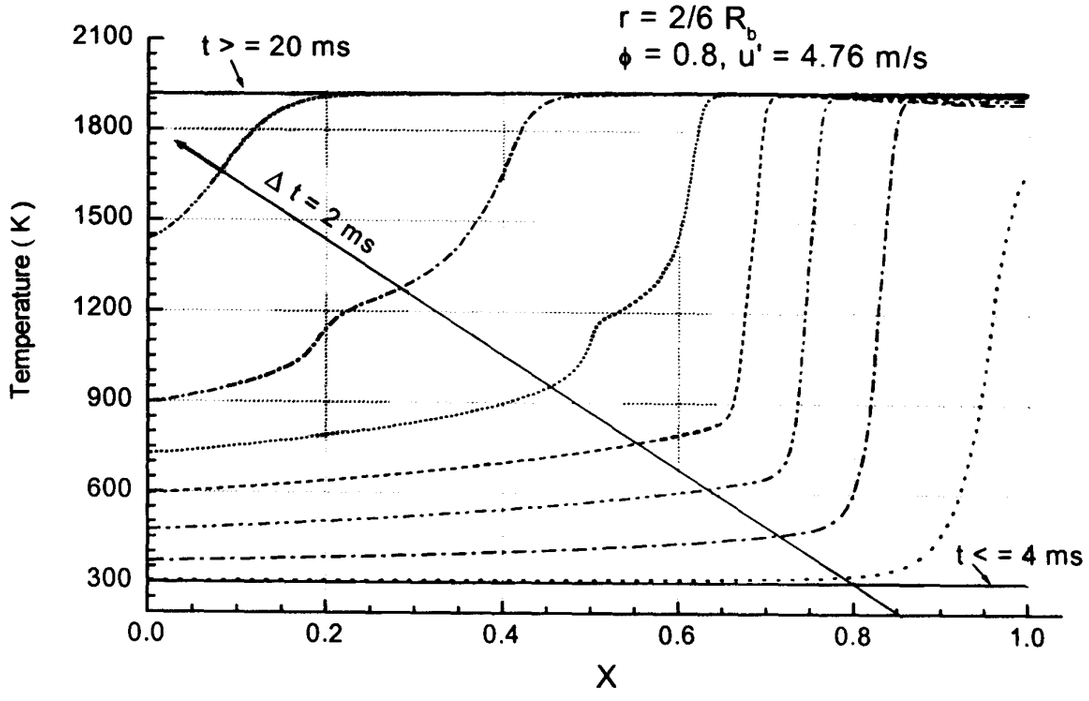

Fig. 4.13(a) Temperature profile in X coordinate

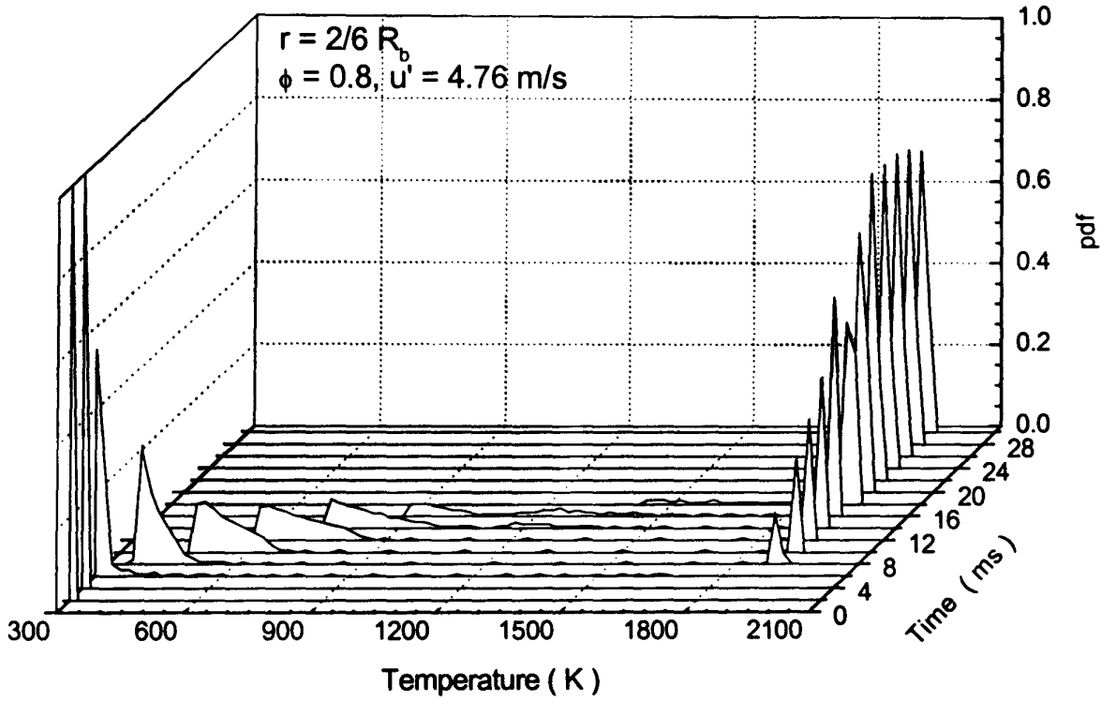

Fig. 4.13(b) Temperature pdf evolutions

Fig. 4.13 Example of the link between the profile in X coordinate and pdf evolution

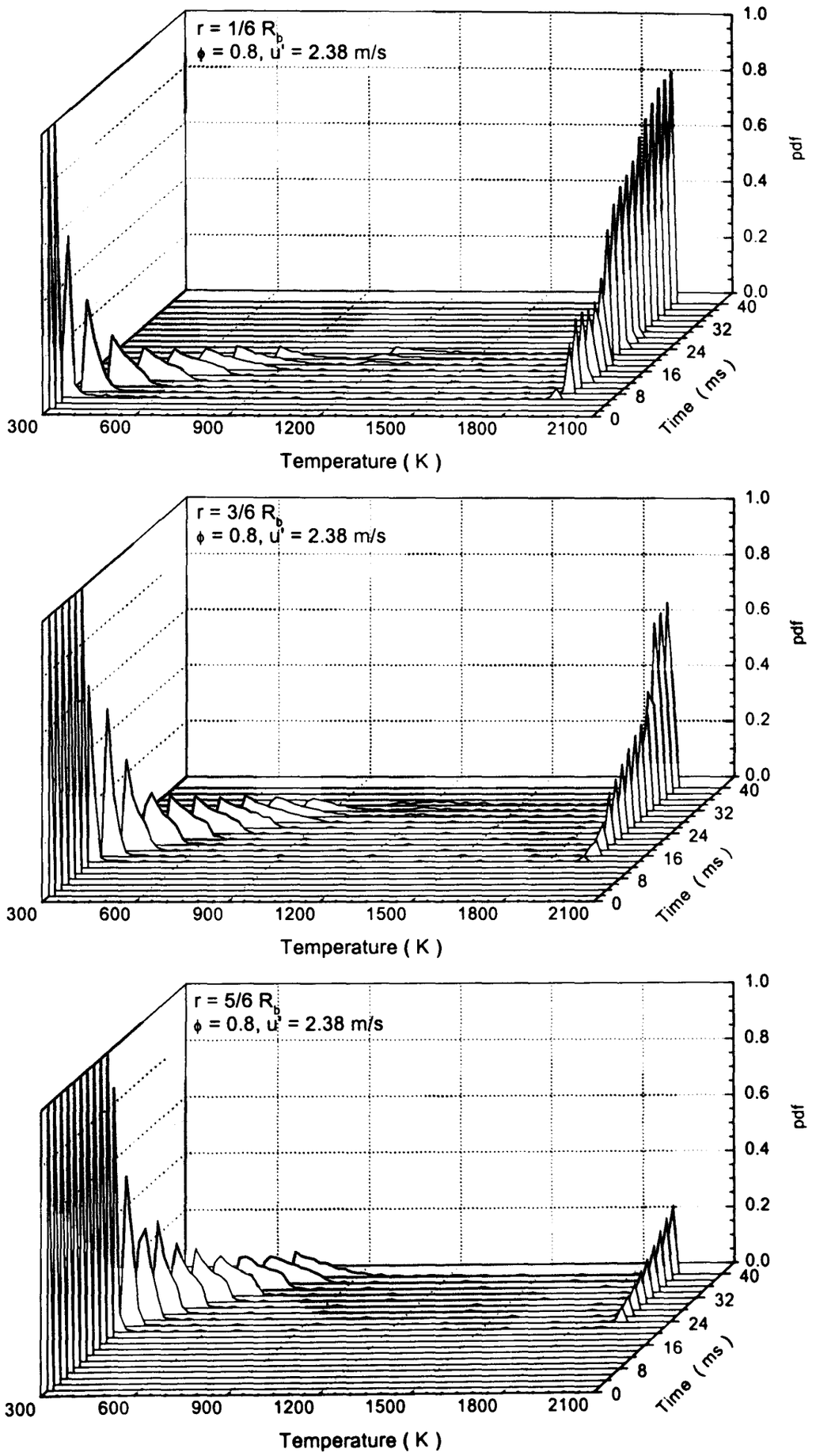

Fig. 4.14 Evolution of temperature pdf
for $\phi = 0.8$, $T_0 = 300\ K$, $P_0 = 1.0\ bar$ at $u' = 2.38\ m/s$

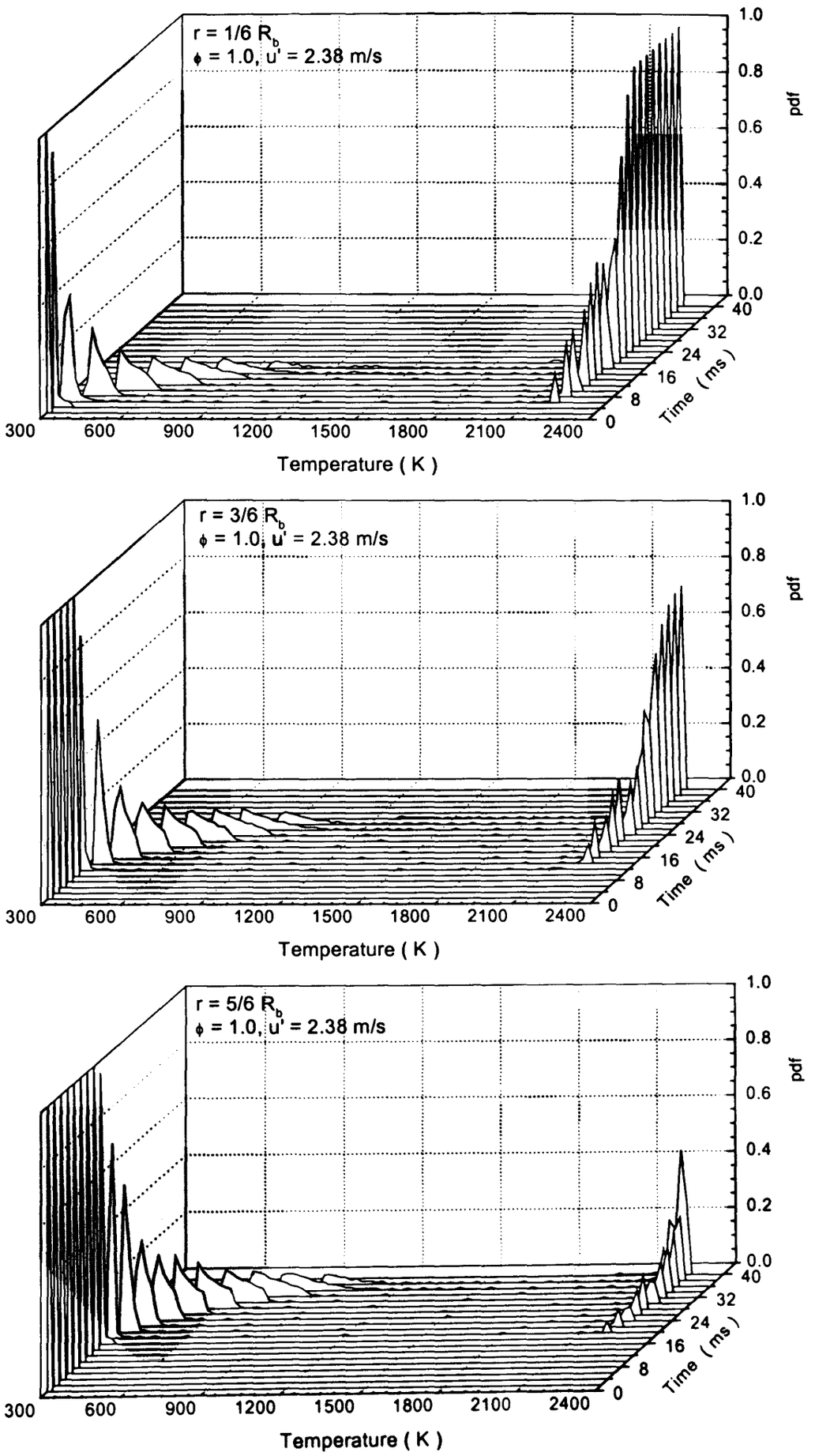

Fig. 4.15 Evolution of temperature pdf
for $\phi = 1.0$, $T_0 = 300\ K$, $P_0 = 1.0\ bar$ at $u' = 2.38\ m/s$

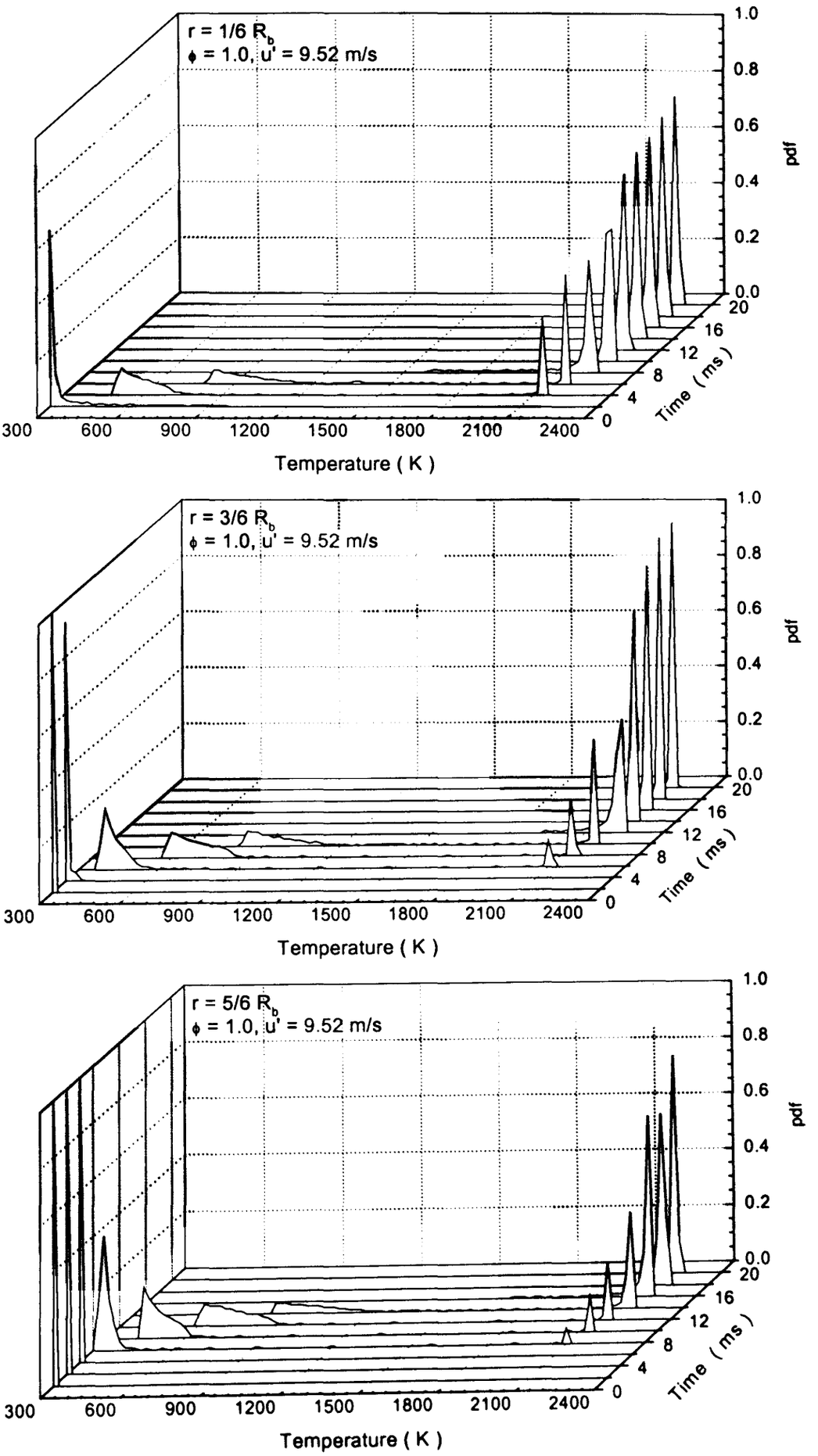

Fig. 4.16 Evolution of temperature pdf
for $\phi = 1.0$, $T_0 = 300\ K$, $P_0 = 1.0\ bar$ at $u' = 9.52\ m/s$

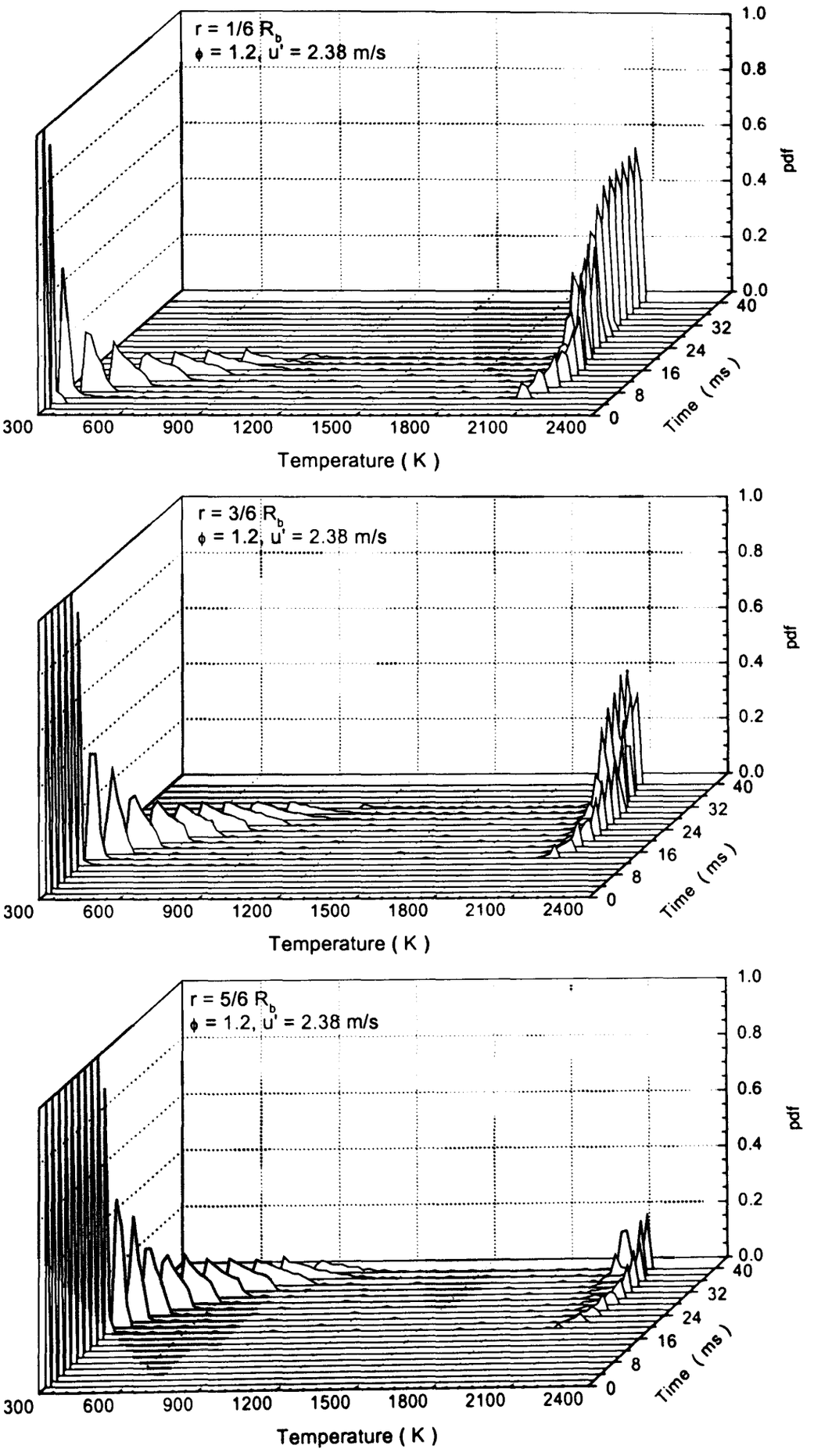

Fig. 4.17 Evolution of temperature pdf
for $\phi = 1.2$, $T_0 = 300\ K$, $P_0 = 1.0\ bar$ at $u' = 2.38\ m/s$

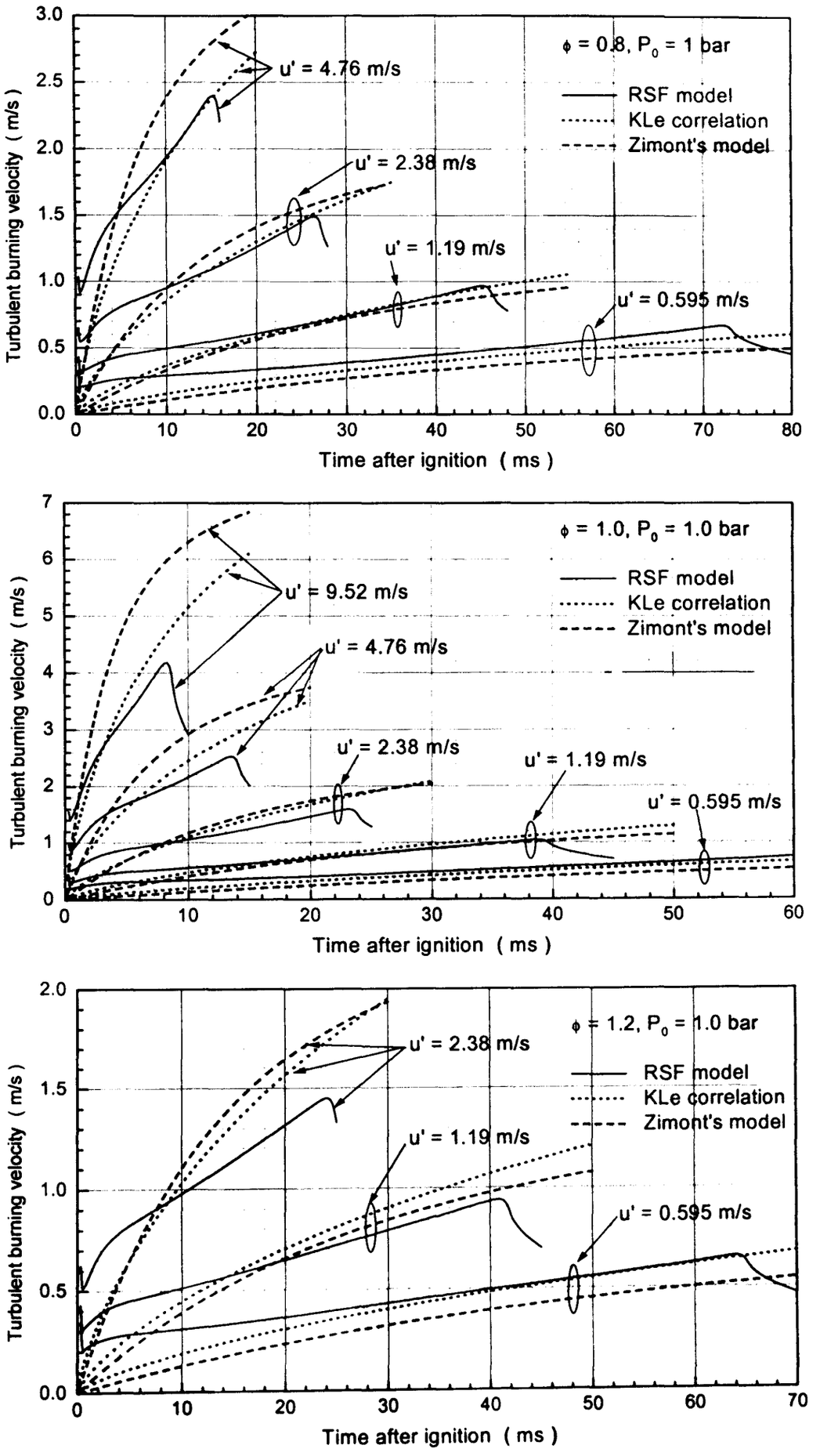

Fig. 4.18 Comparison of calculated burning velocities with KLe correlation and Lipatnikov-Zimont model for different mixtures at $P_0 = 1.0\ bar$, $T_0 = 300\ K$

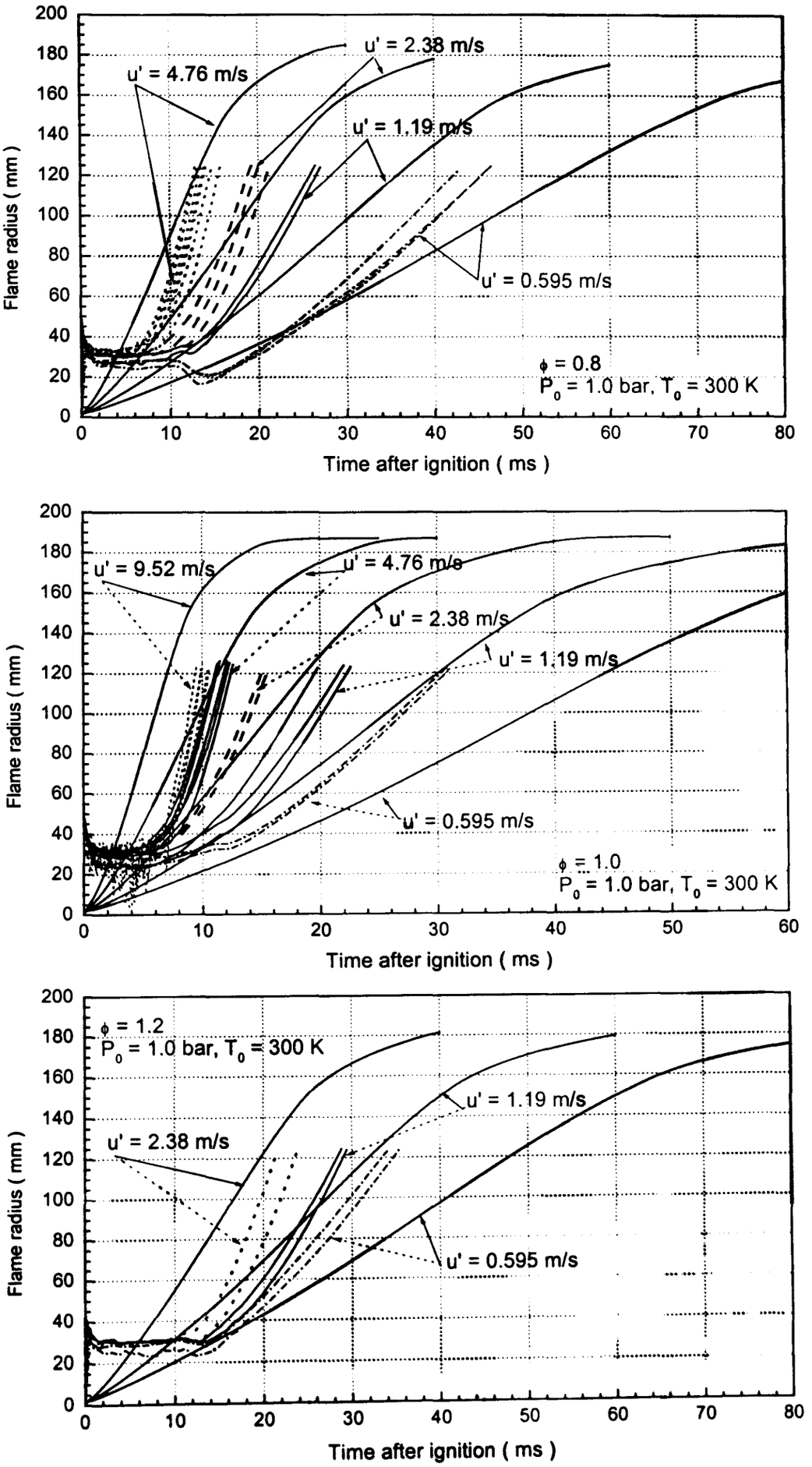

Fig. 4.19 Comparison of calculated flame radius with measurements for different mixtures at $P_0 = 1.0$ *bar*, $T_0 = 300$ *K*

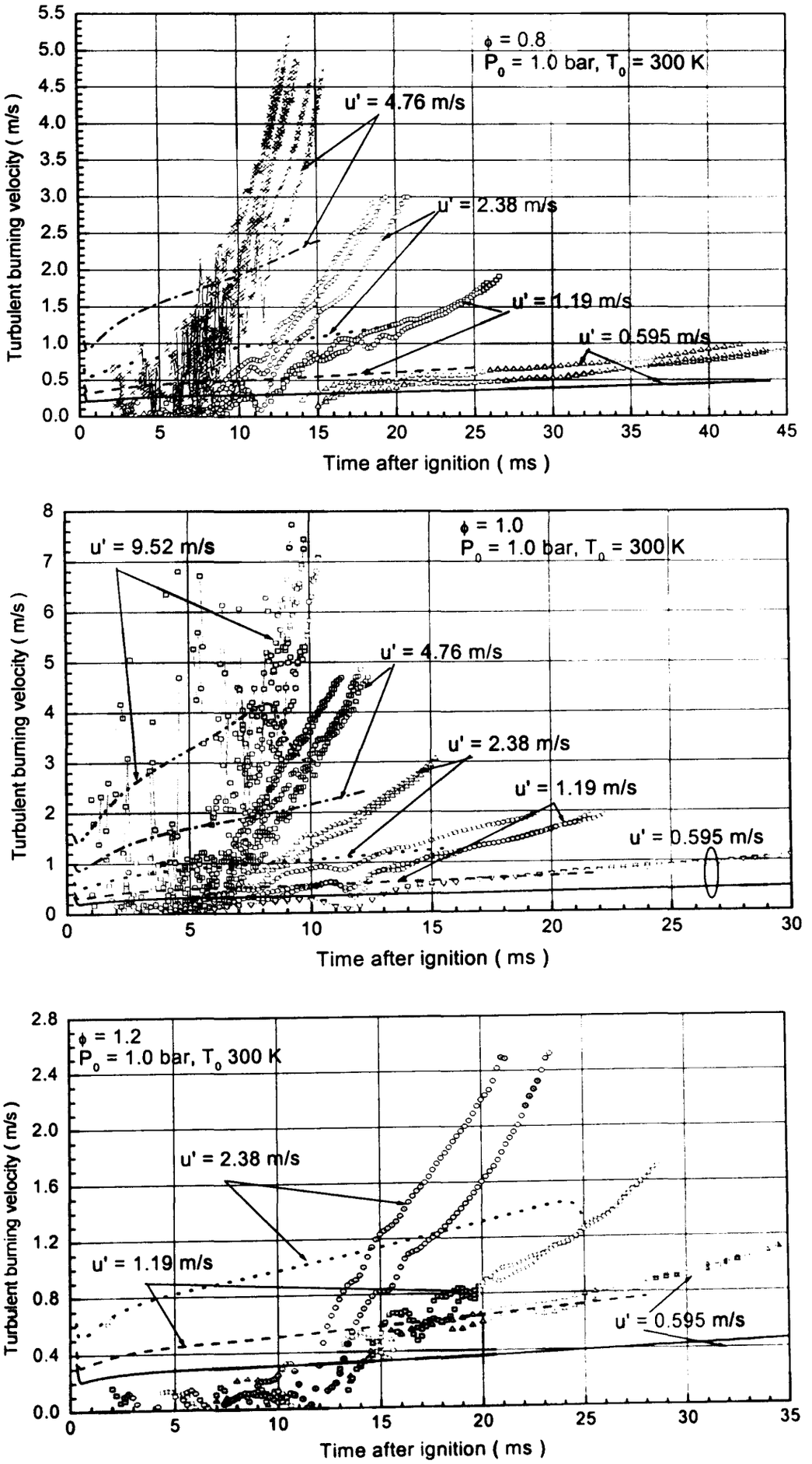

Fig. 4.20 Comparisons of calculated burning velocities with measurements for different mixtures at $P_0 = 1.0$ *bar*, $T_0 = 300$ *K*

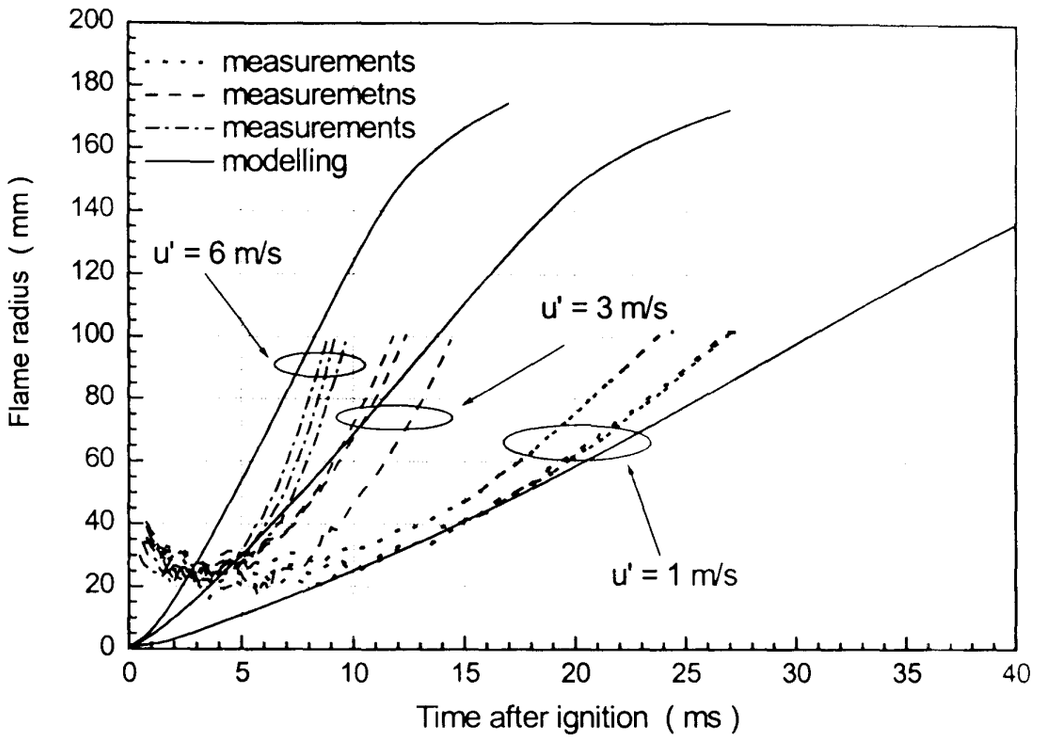

Fig. 2.21(a) ϕ = 0.8

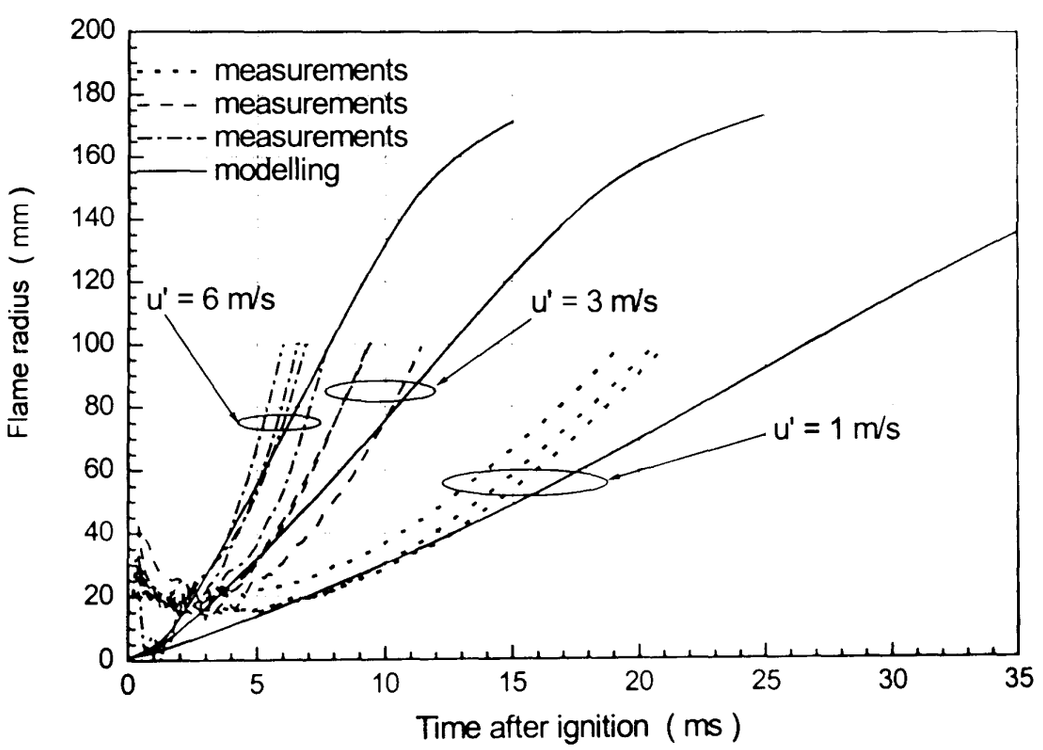

Fig. 2.21(b) ϕ = 1.0

Fig. 4.21 Comparisons of calculated flame radius with measurements for different mixtures at P_0 = 5.0 *bar*, T_0 = 358 K

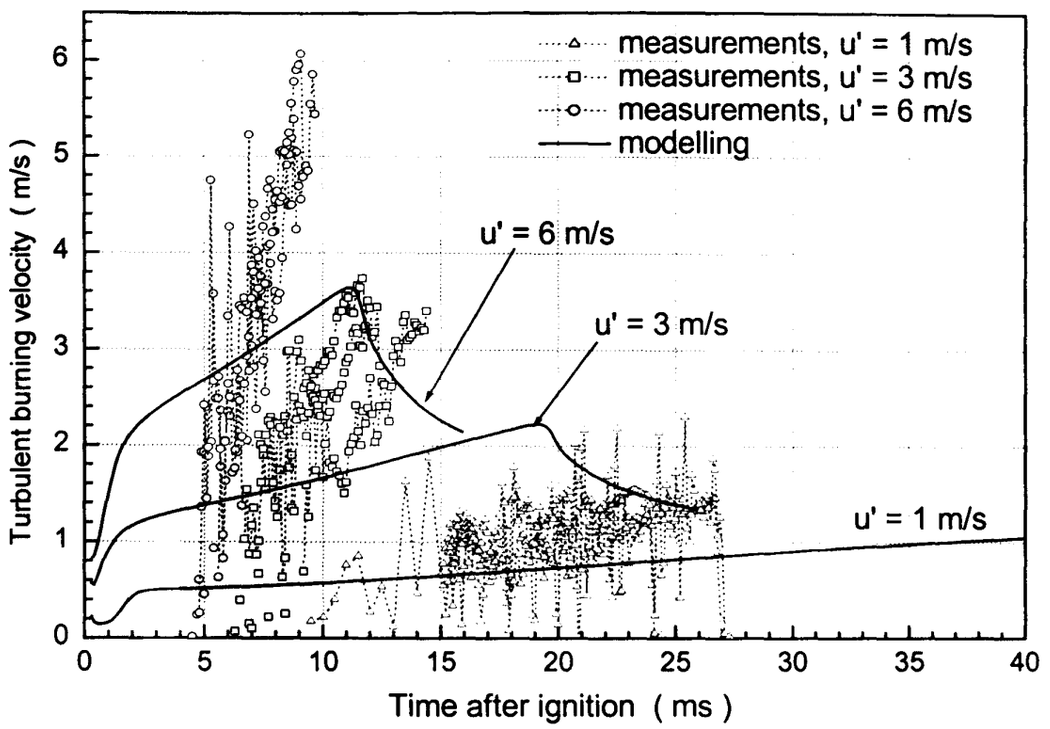

Fig. 2.22(a) $\phi = 0.8$

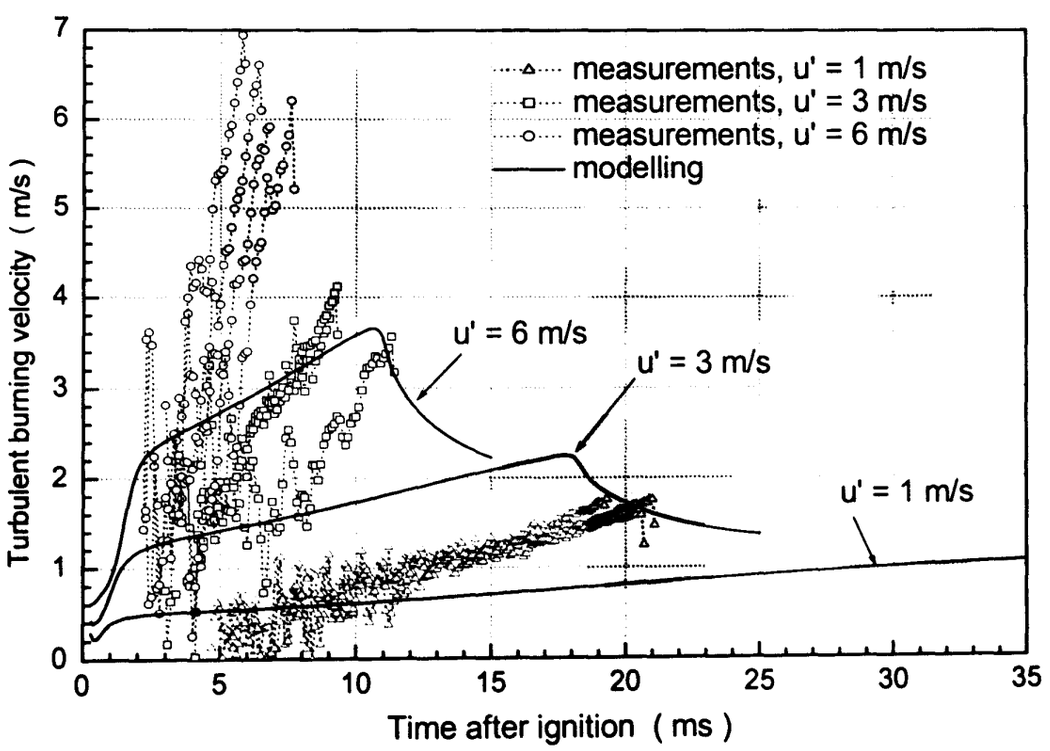

Fig. 2.22(b) $\phi = 1.0$

Fig. 4.22 Comparisons of calculated burning velocities with measurements for different mixtures at $P_0 = 5.0$ *bar*, $T_0 = 358$ *K*

Chapter 5

Study of Di-Tert-Butyl-Peroxide (DTBP)/N_2 Decomposition Flame

5.1 Introduction

For turbulent combustion modelling, reduced chemical reaction mechanisms are particularly useful in order to make calculations computationally affordable. However, some of the conclusions made from the studies of reduced chemical kinetics may be questionable due to the effects of more complex chemistry as demonstrated by Mantel *et al.* (1999). They showed an example: for DNS simulations of the interaction between two dimensional decaying isotropic turbulence and premixed H_2-air flame, Haworth and Poinsot (1992) used single-step Arrhenius chemistry and reported that the local flame structure was controlled by the curvature, a strong correlation was observed between the curvature and local flame speed for all three typical Lewis numbers (Le = 0.8, 1.0, 1.2), and significant correlation between the tangential strain rate and local flame speed existed only for Le = 1.0; however, for the same configuration, Baum and Poinsot (1994) used the detailed reaction mechanism of Millers (1982) with 9 species and 19 reaction steps, they found that local flame speed was better correlated with tangential strain rate than with local curvature. The conclusion based on single-step reaction kinetics partially contradicts those obtained using "full" kinetics.

Although a number of techniques have been established to get reduced chemical kinetics from the detailed ones (Seshadri and Williams, 1994), it is still very important to study turbulent combustion with unambiguous chemistry thus isolating the effects of inaccuracies in kinetics on the outcome of turbulence combustion modelling. For this purpose, Prof. Griffiths kindly pointed us towards di-tert-butyl-peroxide (DTBP) decomposition in an inert gas is used to study turbulence combustion model, because in an inert gas the decomposition of DTBP is described with a single-step reaction and parameters of which are well-established (Griffiths, 1985). The study of this flame thus would not thus suffer from any ambiguity related to reaction mechanisms in

hydrocarbon-air flames. The other attractive property of DTBP decomposition in an inert gas is its low overall heat release (ΔH^0_{298} = -169.8 *kJ/mole*, Griffiths, 1985), as compared with common hydrocarbon-air flames (802.3 *kJ/mole* for CH_4-air flame, 752.3 *kJ/mole* for C_4H_{10}-air flame, Glassman, (1996)).

Presented in this Chapter is the study of DTBP decomposition in N_2 atmosphere in a spherical bomb. Both laminar and turbulent conditions are experimental and numerical studied. Presented in this Chapter are the details and results of numerical study as well as comparison with the measurements. Turbulent combustion model studied here is the RSF model as introduced previously, see Eq. (4.1).

5.2 Kinetic and Thermochemical Properties of DTBP Decomposition

5.2.1 Mechanism of DTBP Decomposition in Inert Gas

The decomposition of DTBP in an inert gas medium is characterised with a simple chemical kinetics, the mechanism is studied in details by Griffiths (1985) and described below.

In the absence of oxygen, the chemical kinetics mechanism is reduced to an endothermic peroxide bond breakdown:

$$(CH_3)_3COOC(CH_3)_3 \rightarrow 2(CH_3)_3CO \tag{5.1}$$

followed by two rapid steps involving free radicals:

$$2(CH_3)_3CO \rightarrow 2(CH_3)_2CO + 2CH_3 \tag{5.2}$$

$$CH_3 + CH_3 \rightarrow C_2H_6 \tag{5.3}$$

the final products of decomposition being acetone and ethane.

The initial degradation of Eq. (5.1) is the rate-determining step with the overall reaction rate constrant:

$$k_{overall} = 10^{15.3} \exp\left(-\frac{18282}{T}\right) \tag{5.4}$$

in the "high" pressure limit (Griffiths *et al.*, 1982). Hydrogen atom abstraction from the reactant by methyl radicals plays only a very minor role and, as a result, the propagating flame of DTBP pyrolysis is described with a single-step chemical kinetics:

$$(CH_3)_3COOC(CH_3)_3 \rightarrow 2(CH_3)_3CO + C_2H_6 \qquad (5.5)$$

The chemical reaction rate constants given by Eq. (5.4) have been accurately measured by Griffiths (1985). Hence, the study of this flame is free of the effect of any possible drawback originating in complexities or inaccuracies of chemical kinetics scheme.

5.2.2 Thermochemical Properties

The standard enthalpies of formation, $\Delta H_f^0(298)$, given by Griffiths (1985) are listed in Table 5.1, where f refers to different species, l, g, refers to liquid and gas state, respectively.

Table 5.1 Standard enthalpies of formation for DTBP, acetone and ethane

$\Delta H_f^0(298)$ (*kJ/mole*)		
DTBP (l)	$(CH_3)_2CO$ (g)	C_2H_6 (g)
-380.4	-216.8	-84.6

The enthalpy of DTBP vaporisation, ΔH_{vap}^0, is 31.9 *kJ/mole*. With this data set, the enthalpy of formation for gaseous DTBP is $\Delta H_f^0(298)$ = -348.5 *kJ/mole*, quite close to the value of -340.6 *kJ/mole* given by the Benson group contribution method (Benson, 1976). Hence, the heat release of DTBP decomposition is 169.8 *kJ/mole* at 350 *K* according to the data of Griffiths (1985).

The specific heat is obtained by a polynomial fit to estimated values as:

$$c_p(T) = 9.25 + 0.8592T - 4.5 \times 10^{-4} T^2 - 8.33 \times 10^{-8} T^3 \quad (kJ / mole \cdot K) \qquad (5.6)$$

These data together with the data for acetone and ethane from Reid *et al.* (1977) yield the adiabatic flame temperature 799.3 *K* for initial temperature 350 *K*, pressure 1 *atm*. The corresponding density ratio ρ_u / ρ_b is 3.57, and adiabatic pressure is 3.53 *atm* for constant volume combustion.

For DTBP, the initial temperature 350 *K* corresponds to saturated vapour pressure of 0.273 *atm* which is equivalent to the mixture of 0.376DTBP+N_2 at the initial pressure of

1 *atm*. It is this mixture that was used in the simulations and measurements presented below.

5.3 Laminar Flame Propagation

Laminar flame propagation of 0.376DTBP+N_2 in a spherical bomb at initial temperature 350 *K* and initial pressure 1 *atm* was simulated. The governing equation and solution procedure are described in *Chapter 2*. For DTBP, no measured values of the heat and mass diffusivities were found in the available literature, so they were estimated by using Lydersen's method (Reid *et al.*, 1977) as described in *Appendix E*. The mass and thermal diffusivities of each species are temperature and pressure dependent. For this mixture, calculated binary mass diffusivity is D_m (350 *K*) = 0.057 cm^2/s, D_m (800 *K*) = 0.212 cm^2/s, and heat or thermal diffusivity is κ(350 *K*) = 0.070 cm^2/s, κ(800 *K*) = 0.537 cm^2/s. Hence the cold gas Lewis number $Le = \kappa/D$ is 1.24.

Pressure during flame propagation in the bomb was simulated by the method described in *Chapter 2* and the result is presented in Fig. 5.1. The calculated final pressure is 3.5 *bar*, agrees with the adiabatic pressure 3.53 *atm* calculated based on the thermodynamical properties. In this figure, the comparison with measurement in the bomb is also presented, and the agreement is quite good.

Since pressure history has been recorded, flame radius and burning velocity can be calculated from it using the method of Lewis and von Elbe (1951) described in *Appendix A*. Presented in Fig. 5.2 are flame radii as function of time, the symbols represent the flame radius measured from Schlieren filming, and the solid line is the result of the simulation. The simulation reveals a good agreement with measurement, except the very beginning period which is presumably spark sensitive.

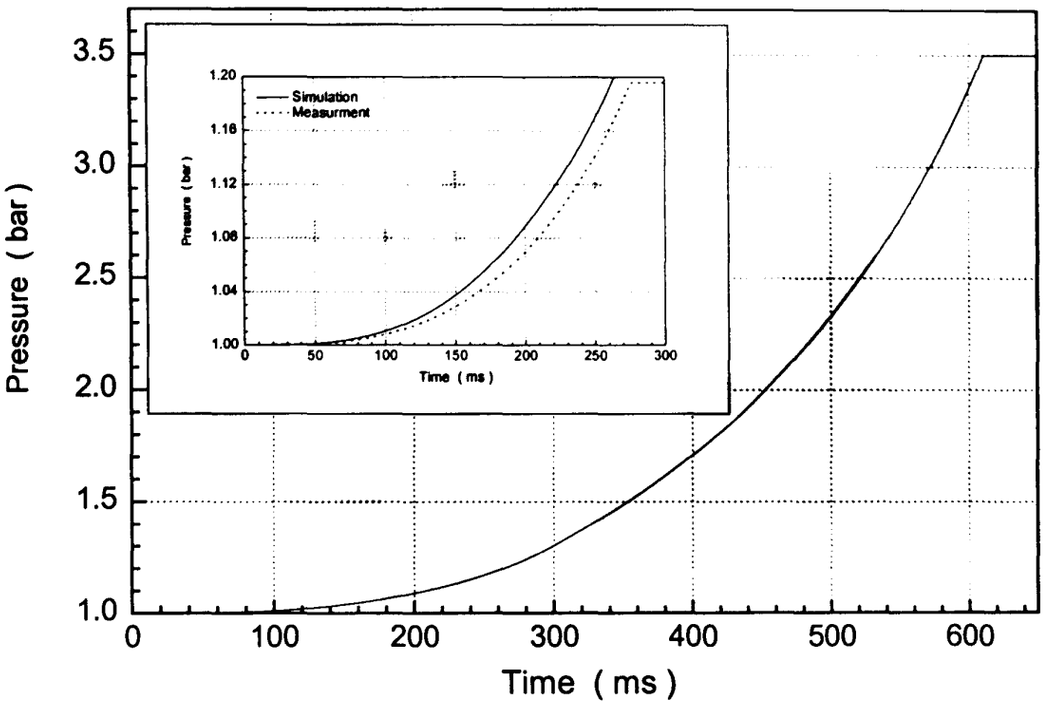

Fig. 5.1 Pressure records of DTBP decomposition in laminar medium

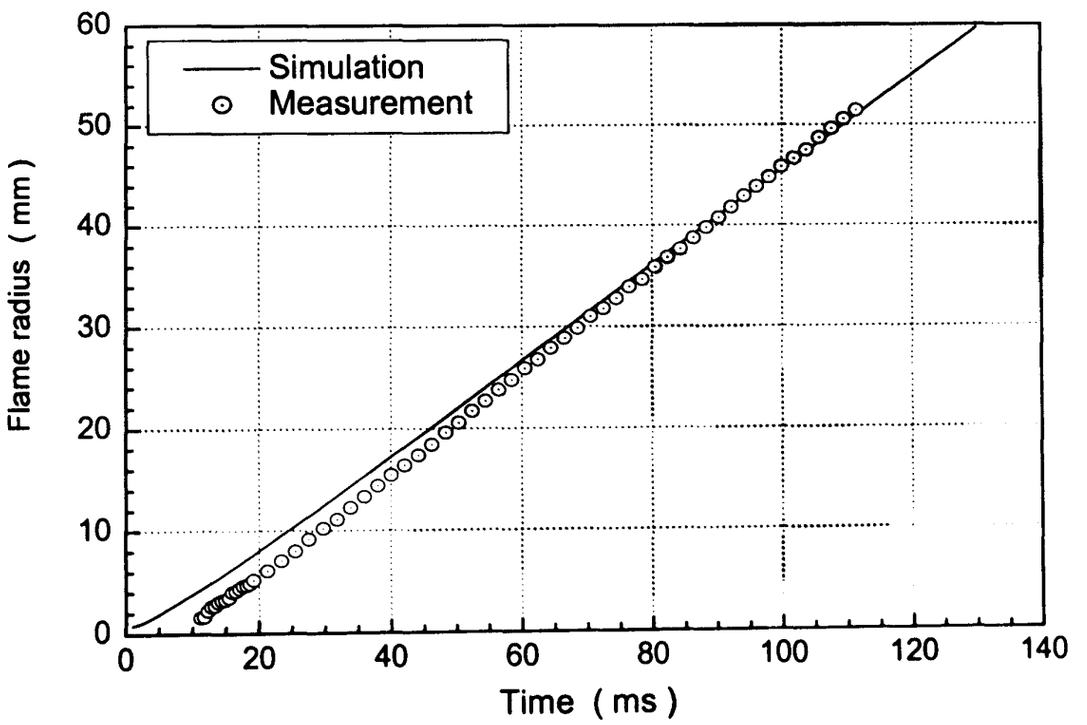

Fig. 5.2 Laminar flame radius

Once the flame radius, r, has been determined, flame propagation speed, S_n, relative to the burnt gas can be found from flame radius versus time as:

$$S_n = \frac{dr}{dt} \tag{5.7}$$

Flame stretch rate may affect flame speed, for a spherical flame the total stretch rate, α, acting on the flame is defined , Bradley *et al.* (1996b), as:

$$\alpha = \frac{1}{A}\frac{dA}{dt} = \frac{2}{r}S_n \tag{5.8}$$

where A is flame surface area. There supposedly exists a linear relationship between flame speed and the total stretch rate, quantified by Markstein length, L_b, (Bradley *et al.*, 1998):

$$S_s = S_n + L_b\alpha \tag{5.9}$$

where S_s is unstretched flame speed, when $r \to \infty$, and $S_n \to S_s$. This yields S_s as the intercept value of S_n at $\alpha = 0$. The slope of the straight line $S_s(\alpha)$ gives the L_b. The unstretched laminar burning velocity, u_L, is deduced (Bradley *et al.*, 1998) as:

$$u_L = S_s\frac{\rho_b}{\rho_u} \tag{5.10}$$

Least square procedure was applied to Eq. (5.7) and flame speed so obtained is shown in Fig. 5.3 as function of flame radius for both simulation and measurement. One can see that the calculated flame speed is slightly lower than the measured one. But the agreement is quite good. Flame speed versus flame stretch rate is shown in Fig. 5.4. To compare with measurement, the range of flame size shown in Fig. 5.4 is selected from 5 to 50 *mm*, when $r < 5$ *mm* it is affected by the spark effect discharge (Bradley *et al.*, 1998), and when $r > 50$ *mm* the flame edge is outside the bomb windows. As presented in Fig. 5.4, the agreement between measurement and simulation is quite good, the measurement gives $S_s = 0.52$ *m/s*, $L_b = 0.352$ *mm*, and simulation gives $S_s = 0.485$ *m/s*, $L_b = 0.379$ *mm*. Hence, unstretched laminar burning velocity, $u_L = 0.146$ *m/s* for measurement, $u_L = 0.136$ *m/s* for simulation. The possible reasons for the difference may come from both experimental errors (e.g. possible presence of traces of oxygen in the bomb) and calculation procedure (*e.g.* necessity to estimate the transport properties of DTBP).

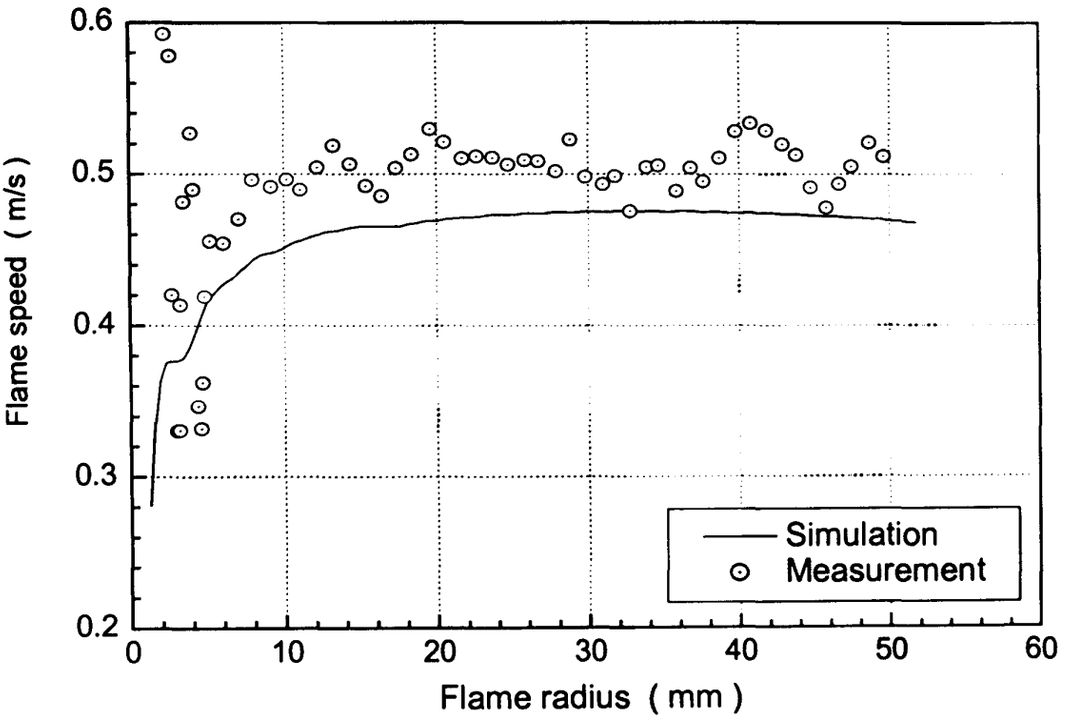

Fig. 5.3 Laminar flame speed

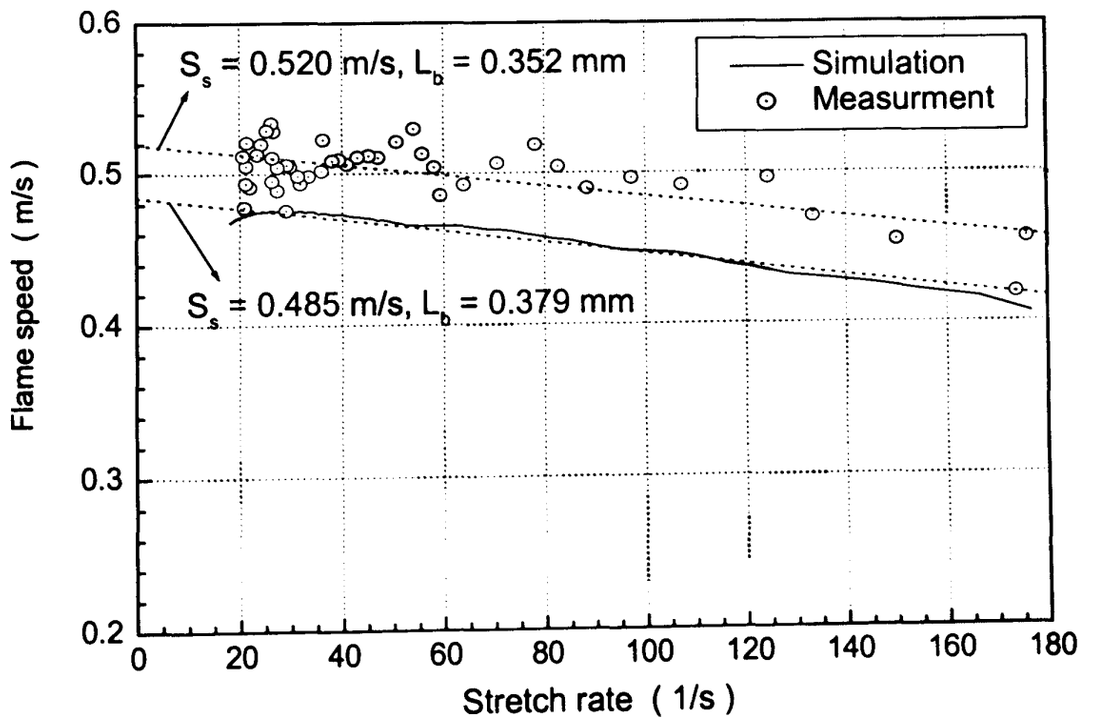

Fig. 5.4 Laminar flame speed *vs.* stretch rate

Shown in Fig. 5.5 is the simulated laminar burning velicity (with stretch effect), u_n, versus flame radius, where the burning velocity was obtained from pressure method. In this figure, the initial increase of burning velocity is due to the initial flame development, after that, burning velocity remains nearly constant for some time, after which u_n is decreasing as the flame grows further. For example, one can see in Fig. 5.5 that when r increased from 40 to 100 *mm*, pressure in the bomb changed from P = 1.007 *bar* to 1.125 *bar* and burning velocity decreased from u_n = 0.146 *m/s* to 0.129 *m/s*. Thus a 11.72% increase in pressure is accompanied with 11.64% decrease in u_n. Probably the easiest explanation is that the transport properties, such as thermal diffusivity, used in the simulation, depend on pressure as $1/P$ and value of laminar burning velocity is highly dependent on these transport properties. However, in measurements, this phenomenon never has been found, one of the reasons may be the flame unstability problem such as flame cracks. Leisenheimer *et al.* (1996) distinguished three stages of flame evolution in a constant volume bomb: first stage is stretched laminar flame which is same as the pre-pressure period used widely elsewhere (Bradley *et al.*, 1998); the second stage is cellular flame with approximately linear acceleration due to flame cracks; the third period is self-turbulent flame where unburnt gas is highly compressed. However, any further discussion about unstability effects would be beyond the scope of the present work.

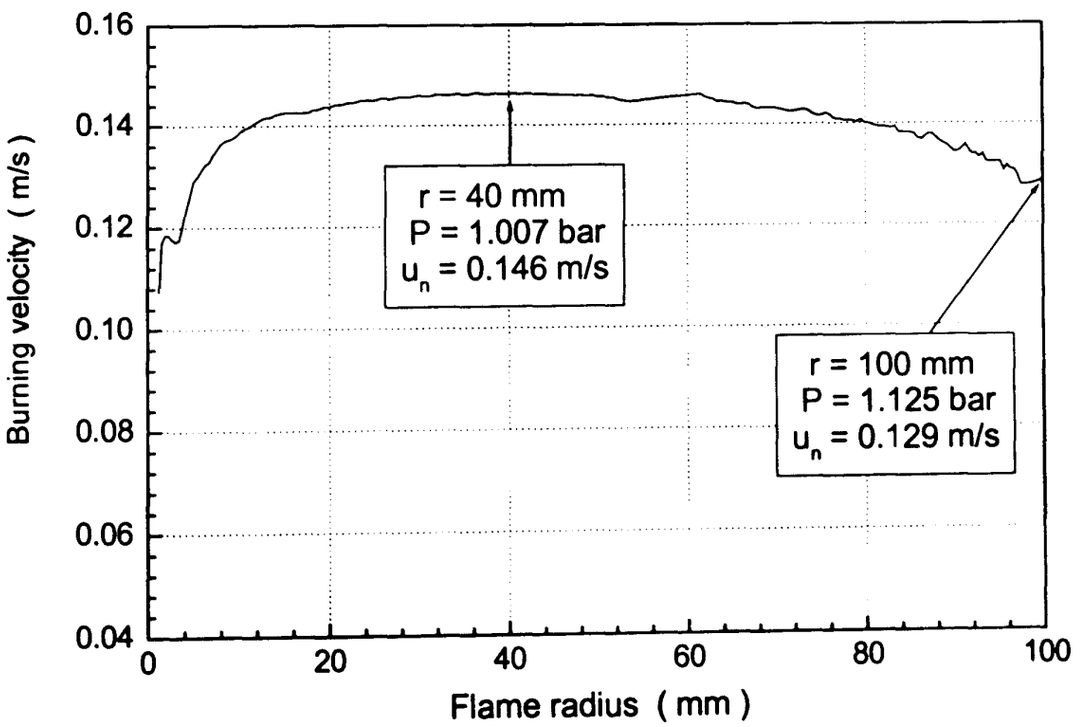

Fig. 5.5 Simulated laminar burning velocity *vs.* flame radius

Calculated temperature profile for flame propagation in the bomb is presented in Fig. 5.6. It can be inferred that the flame attains a self-similar nearly steady regime of propagation. This observation is further supported by the "magnified" flame structure shown in Fig. 5.7. In Fig. 5.7 temperature, species concentrations at different time are shown, from that figure one can estimate that the flame thickness is about 0.5 *mm*, which is close to thermochemical calculation of thermal flame thickness κ_b/u_L = 0.37 *mm*, where u_L is taken from present simulation.

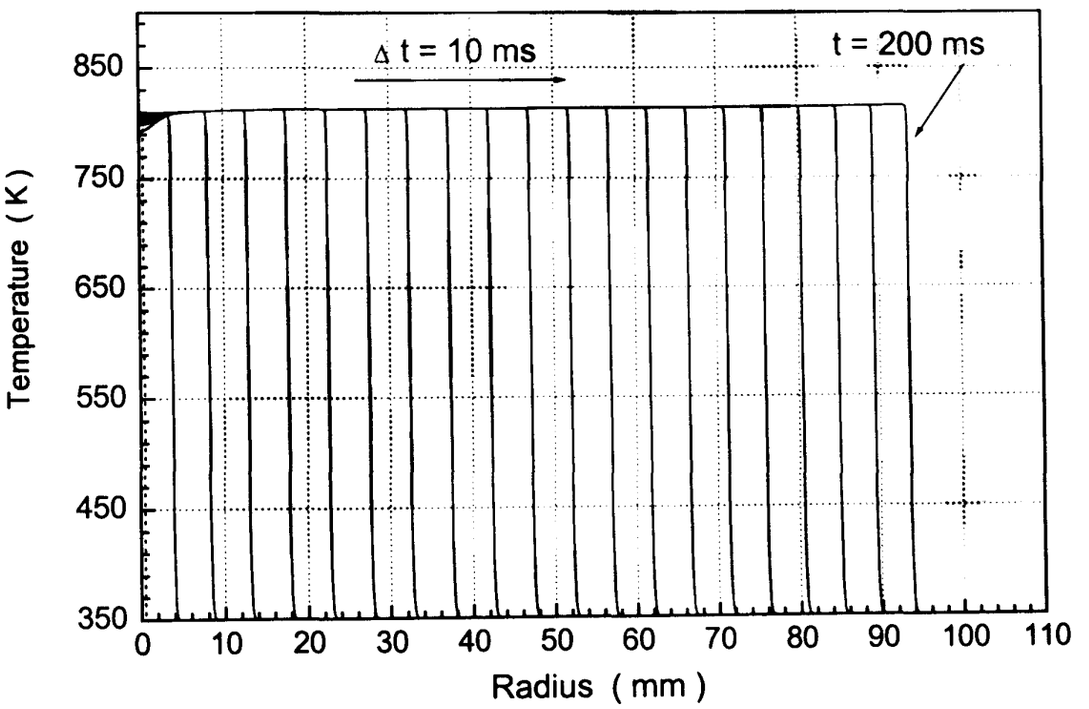

Fig. 5.6 Temporal evolution of temperature profile

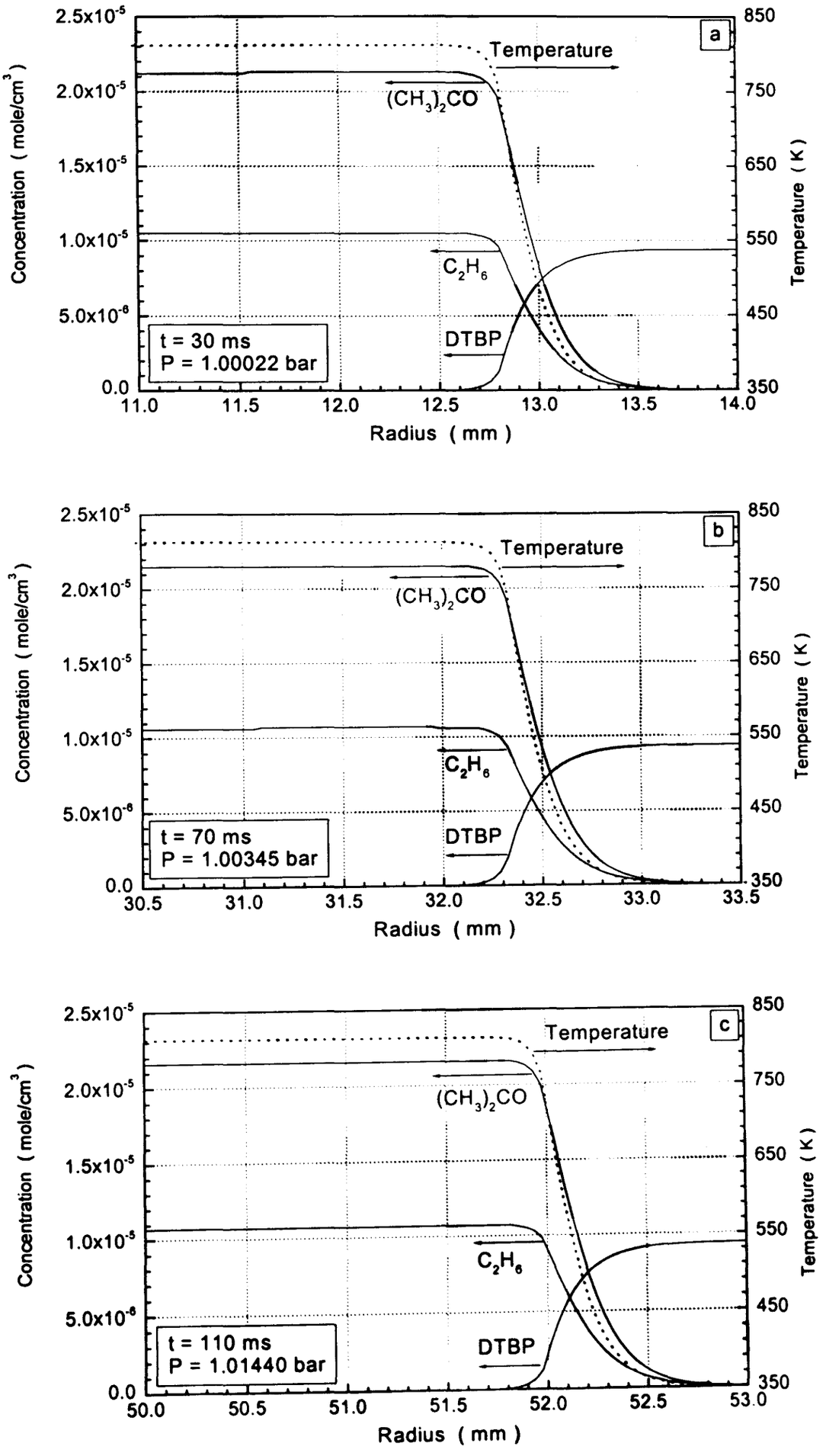

Fig. 5.7 Laminar flame structure of DTBP/N_2 decomposition flame

5.4 Turbulent Flame Propagation

RSF model was used to simulate turbulent flame propagation of DTBP/N_2 in the bomb. The equation governing the RSF evolution is Eq. (4.1); conditional velocity is calculated with Eq. (4.5); pressure in the bomb during flame propagation was simulated with the formulae presented in *Appendix B*, solution procedure was exactly the same as that used in the simulations of turbulent methane-air flame described in *Chapter 4*. The only difference is now a different fuel in the bomb.

Presented in Fig. 5.8 are pressure records with different turbulence intensities for RSF simulations and measurements. For measurement, similarly to methane-air turbulent flame, there exists quite long initial "incubation" period during which pressure rise is too small to be detected. Hence the simulation results shown in Fig. 5.8(b) can not be directly compared with the measurements shown in Fig, 5.8(a). However, it is reasonable to consider this long initial period is about 30 *ms* as presented in Fig. 5.8(a), then the duration from 30 *ms* at its initial value to 20% rise can be compared. For example, for u'=0.5 *m/s*, the duration from initial pressure to its 20% rise is about 85 *ms* for simulation and about 90 *ms* (120-30) for measurements; for u'=1.0 *m/s*, the duration is about 50 *ms* for simulation and 35 *ms* for measurement. For this two turbulence intensities, the simulations are "close" to measurements, this is further supported by the comparisons of simulations and measurements for turbulent burning velocity versus flame radius as presented in Fig. 5.10. For u'=2.0 *m/s*, comparison is more difficult because the measurements suffered from poor ignition problem: with 50% probability to ignite the mixture successfully big scatter arises in behaviour of subsequent flame development.

From the pressure records turbulent flame radius and burning velocity can be determined. Shown in Figs. 5.9 and 5.10 are flame radius and burning velocity which were calculated by the method of Lewis and von Elbe (1951). From these figures, one can see that the initial "incubation" period in measurements affects all subsequent flame develepment and as a consequence in this period burning velocity is quite small. This initial period has been noticed previously in the methane-air flame, see *Chapter 4* and Liu *et al.* (2001) as well as *Appendix A*. Similar to the methane-air turbulent flame (*Appendix A*) the duration of this initial "incubation" period with slow burning rate may

vary greatly from one explosion to another, and is most noticeable for higher turbulence, for example, for u'=2.0 *m/s* shown in Figs. 5.9 and 5.10.

As shown in Fig.5.10(a), agreement between RSF predictions and measurements is improved if one compares u_t taken at the same flame size. Except for the long initial period, flame acceleration is apparent both in predictions and measurements. Burning velocity is approximately linearly proportional to the flame radius except the very early and later stages. This linear growth of turbulent burning velocity with flame size is in direct contradiction to a number of experimental observation, *e.g.* Karpov *et al.* (1980). They reported that in a constant volume bomb, turbulent burning velocity was approximately constant for the flame radius at the interval of 15 $mm \leq r \leq 45$ *mm*, corresponding pressure rise being in the range of $1.005 \leq P(t)/P_{ini} \leq 1.16$. The combustion vessel volume they used was 3800 cm^3, for the same pressure increase the equivalent flame radius in the present bomb would be in the range of 25 $mm \leq r \leq$ 95 *mm*. For this flame size range, approximately linear profile is thought to represent well the results of current study both for measurements and simulations as shown in Fig. 5.10.

For measurements, there was no visible trend that the burning velocity reaches any constant value for the whole period of measurement. Neither it was found in the simulations. However, flame acceleration, observed at the late stages of explosions, was greater in measurements than that calculated. Reasons for this deviation are unclear at the present time.

As can be seen in Fig. 5.10(a) for u' = 2.0 *m/s*, the scatter between different explosions in terms of turbulent burning rate against flame radius is quite large. In particular, one of the measurements is quite close to another one obtained at u' = 1.0 m/s. Arguably this scatter originates at the ignition instant and persists for the whole duration of the explosion. It has to be stressed that at u' = 2.0 *m/s* the probability of successful ignition is only 50%. As generally recognised, flame extinction is characterised by Karlovitz number, K, near unity, for u' =2.0 *m/s*, l_t =20 mm in current study, Karlovitz number is: $K = 0.157(u'/u_l)\,\mathrm{Re}^{-0.5} \approx 0.35$. As suggested by Abdel-Gayed and Bradley (1985), the extinction criterion is $u' = 3.1 u_L\, \mathrm{Re}^{1/4}\, Le^{-1/2}$. So the expected extinction limit for current

study is about u' =3.5 *m/s*. Strictly speaking, what is observed in the present measurement is not the extinction of flame by turbulence but rather the limit of possibility of ignition by a spark. In RSF modelling study, no such extinction has been found even for u' = 4.0 *m/s*, as shown in Fig. 5.10(b).

It should be noted that for modelling study, there is a transient flame size which turbulent burning velocity reached its maximum value, then turbulent burning velocity drastically decreased with flame growth as shown in Fig. 5.10(b). The stronger the turbulence intensity, the smaller size of this transient flame radius. The reason for this is the influence of wall on the turbulent convection. In fact, at stronger turbulence, the presence of the wall during one time step Δt is "felt" by the flame at distance of $\Delta r \sim u'\Delta t$. This presence is numerically reduced to limiting the linear dependency for the conditionally averaged velocity, thus reducing the effective value of u', henceforth producing a drop in u_t.

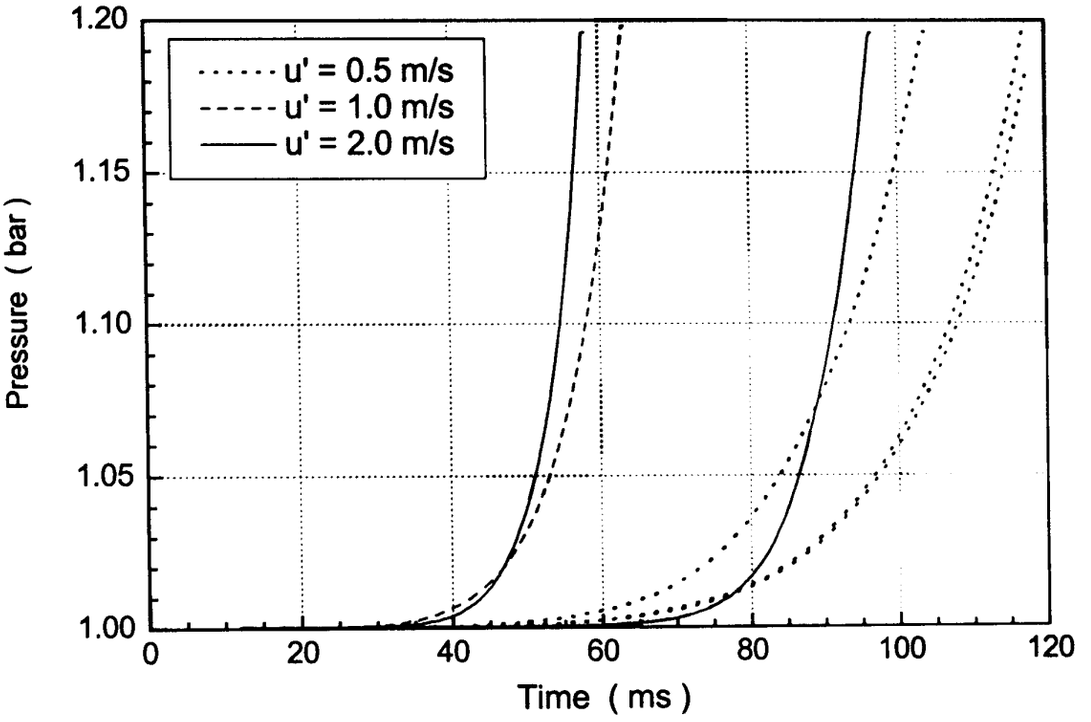

(a) Measurements

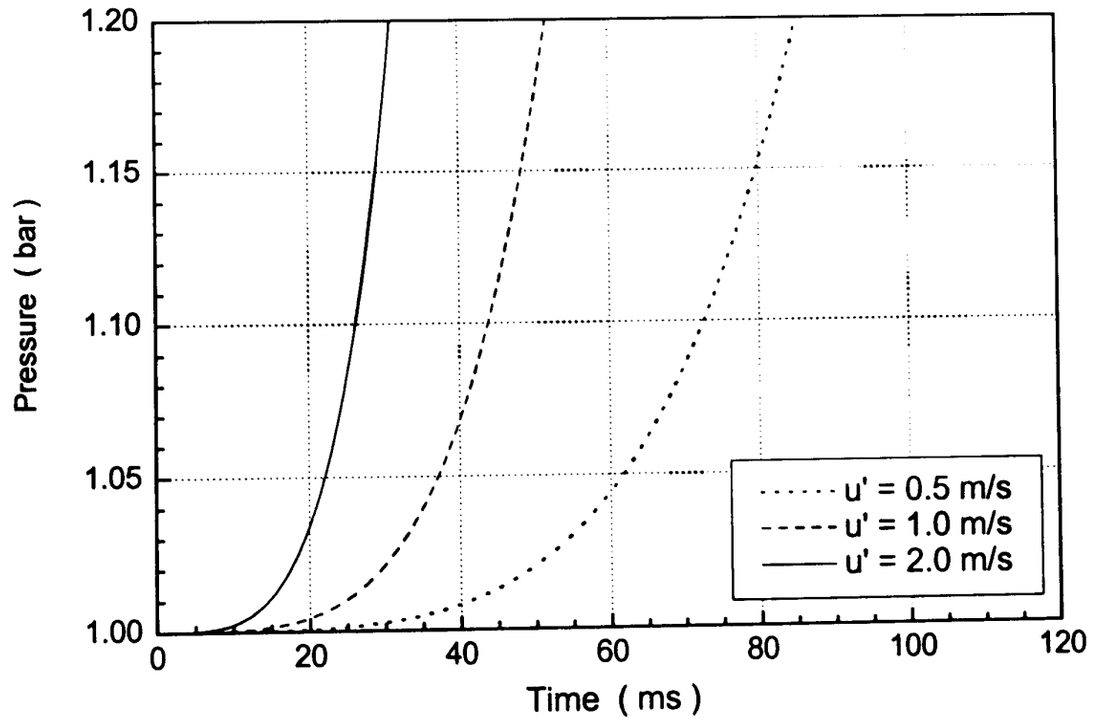

(b) RSF simulations

Fig. 5.8 Pressure records for turbulent flame propagation

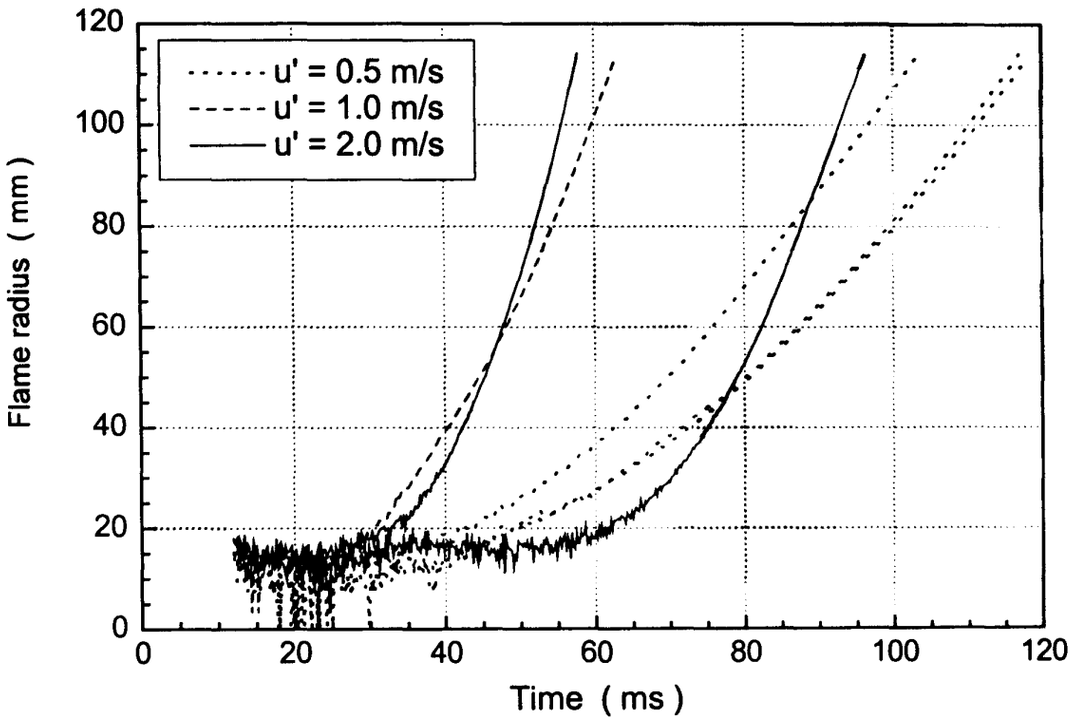

(a) Measurements

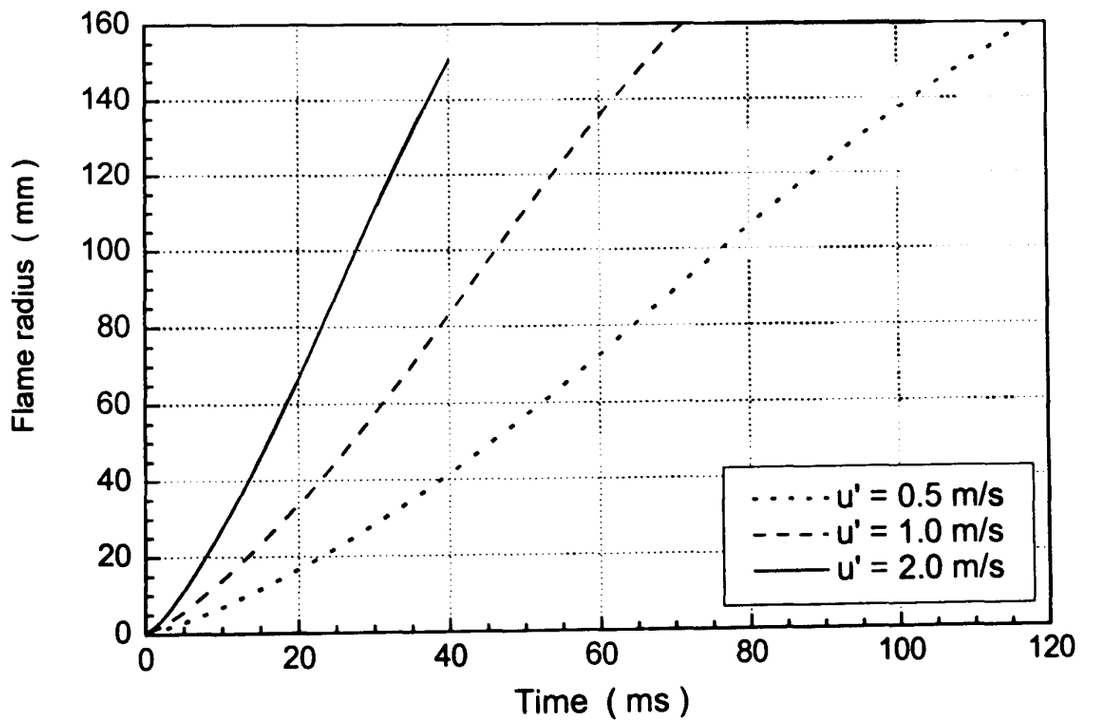

(b) RSF simulations

Fig. 5.9 Flame radius *vs.* time

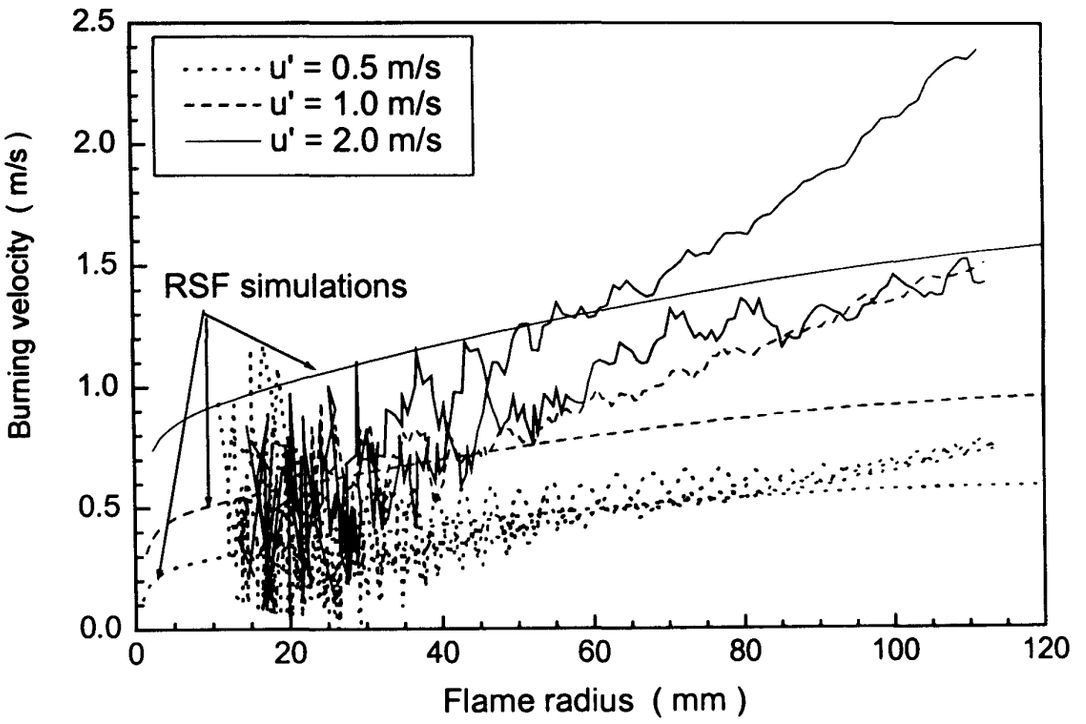

(a) Comparisons of RSF predictions with measurements

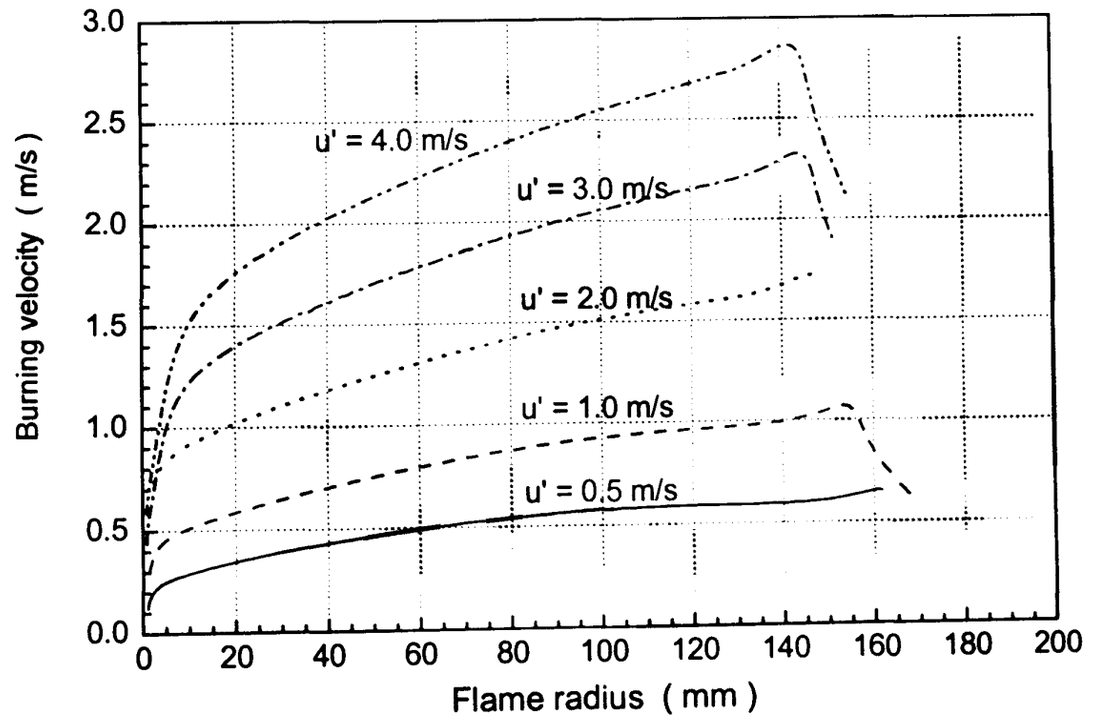

(b) Turbulent burning velocities predicted by RSF

Fig. 5.10 Turbulent burning velocity *vs.* flame radius

The unsteady flame develepment clearly visible in Fig. 5.10 makes it difficult to compare current RSF model predictions directly with the numerical values of turbulent burning velocity reported in the literature, such as Nakahara *et al.* (1998) and Karpov *et al.* (1980) which are averaged values. However, recent development on unsteady flame propagation based on Taylor's turbulent diffusion theory (Abdel-Gayed, Bradley *et al.*, 1987) gives the possibility to compare RSF model predictions with the unsteady development of turbulent flame: KLe correlation of Bradley *et al.* (2000) and Lipatnikov-Zimont model (Lipatnikov *et al.*, 2000), introduced in more details previously in *Chapter 4*. Presented in Fig. 5.11 is the comparison for three different turbulence intensities. The predictions of the RSF model are in much better agreement with these two models rather than they agree with the measurements.

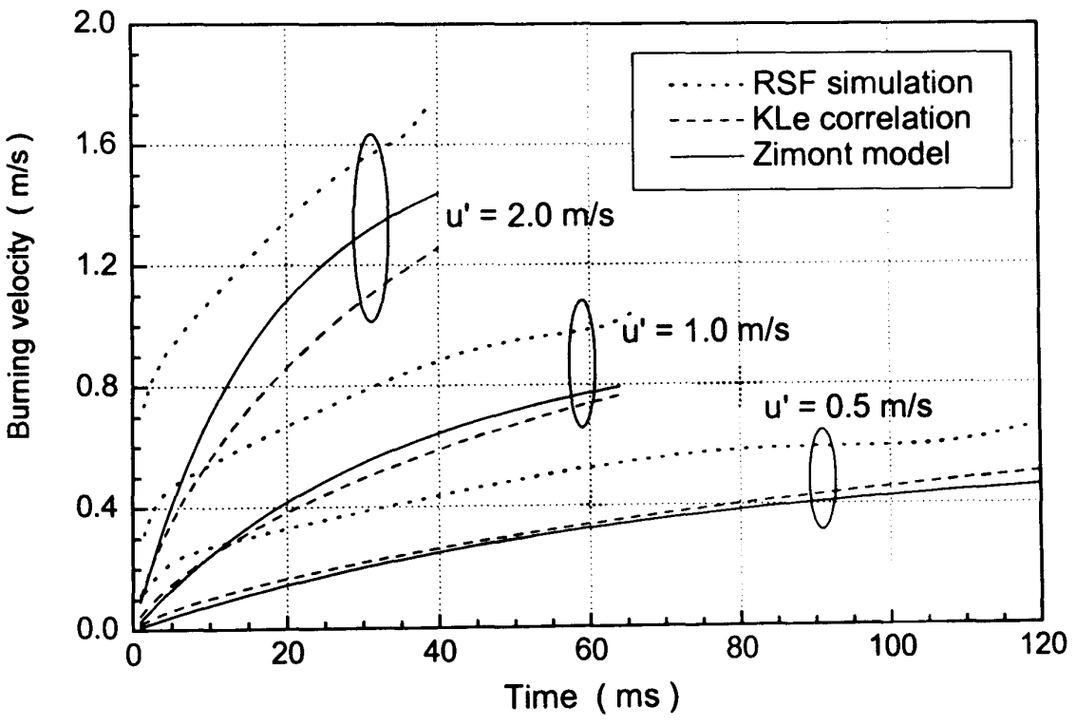

Fig. 5.11 Comparison of turbulent burning velocity predicted by RSF, KLe correlation and Lipatnikov-Zimont model

For the sake of completeness, the profiles of mean values of temperature, DTBP and acetone concentrations are shown in Fig. 5.12, while their *rms* variance is presented in Fig. 5. 13, for different turbulence intensities.

Upon comparison of Fig. 5.13(a) and (b) one may draw a conclusion that increase in turbulence results in lowering values of maximum *rms* fluctuations. This corresponds to

a broadening of the instantaneous reaction zone in qualitative agreement with the ideas underlying Borghi's diagram. Corresponding micro-scale structure of the instantaneous reaction zone can be deduced from the pdf of temperature Figs. 5.14 and 5.15. It can be seen that mostly these pdfs are close to a bimodal shape which signifies a thin reaction zone. Substantial broadening and motion of the "δ peak" corresponding to the fresh mixture is clearly visible. This means that the temperature of the fresh gas immediately in front of the flame front is already risen. It is at present unclear whether such an extended preheating is a true reflection of the enhancement of the transport within the preheat zone by the small-scale turbulence (a phenomenon which should exist at the least under certain conditions when *Da* approaches unity) or it is an artifact caused by LMSE-like samll-scale mixing model in Eq. (4.11).

At the same time, stronger turbulence also results in greater average flame brush thickness which is several times the integral length scale of turbulence. This is due to the increased large-scale turbulent diffusivity which amplifies the dispersion of the reacting gas.

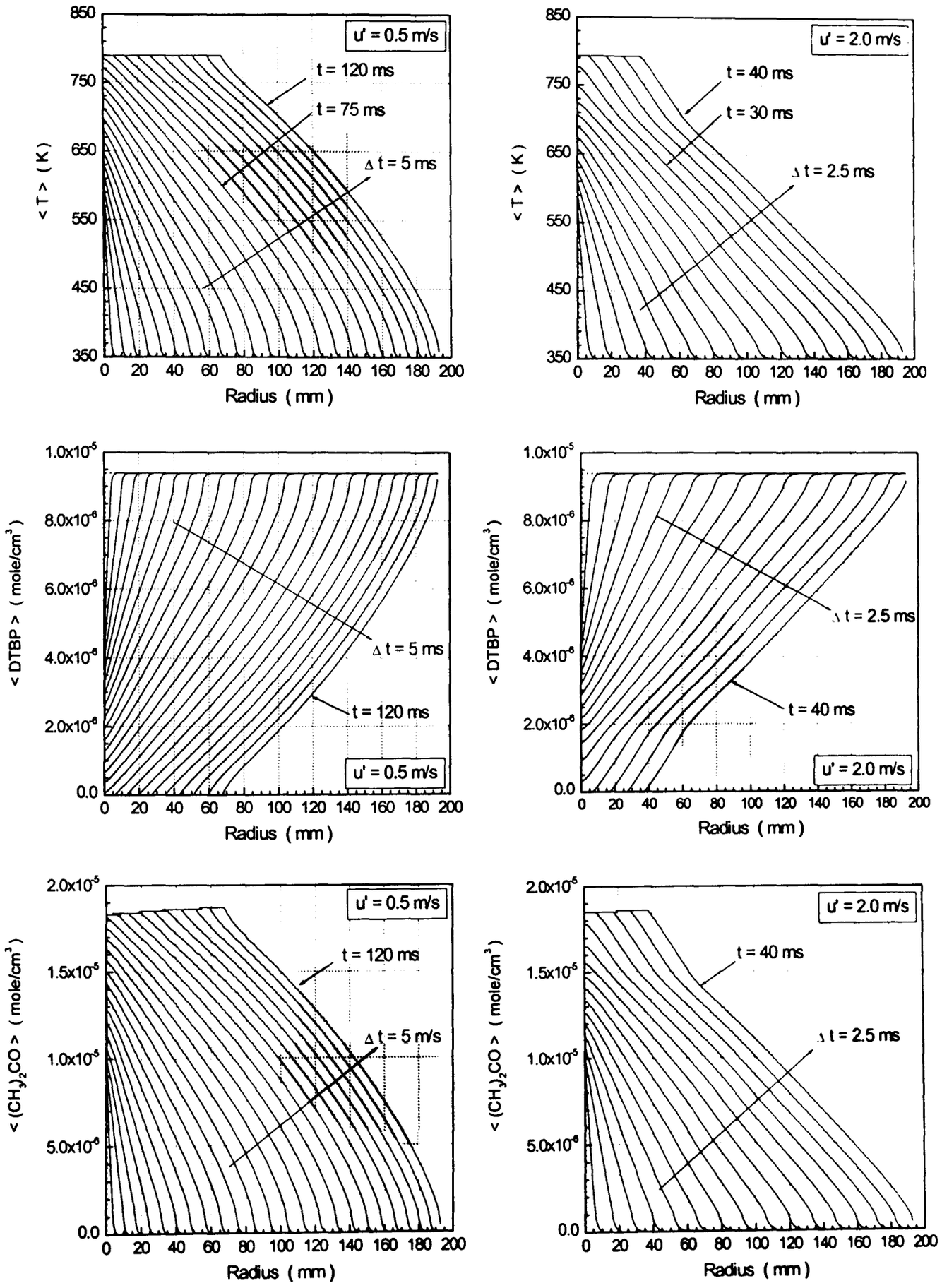

(a) $u' = 0.5\ m/s$ (b) $u' = 2.0\ m/s$

Fig. 5.12 Temporal evolution of mean scale values

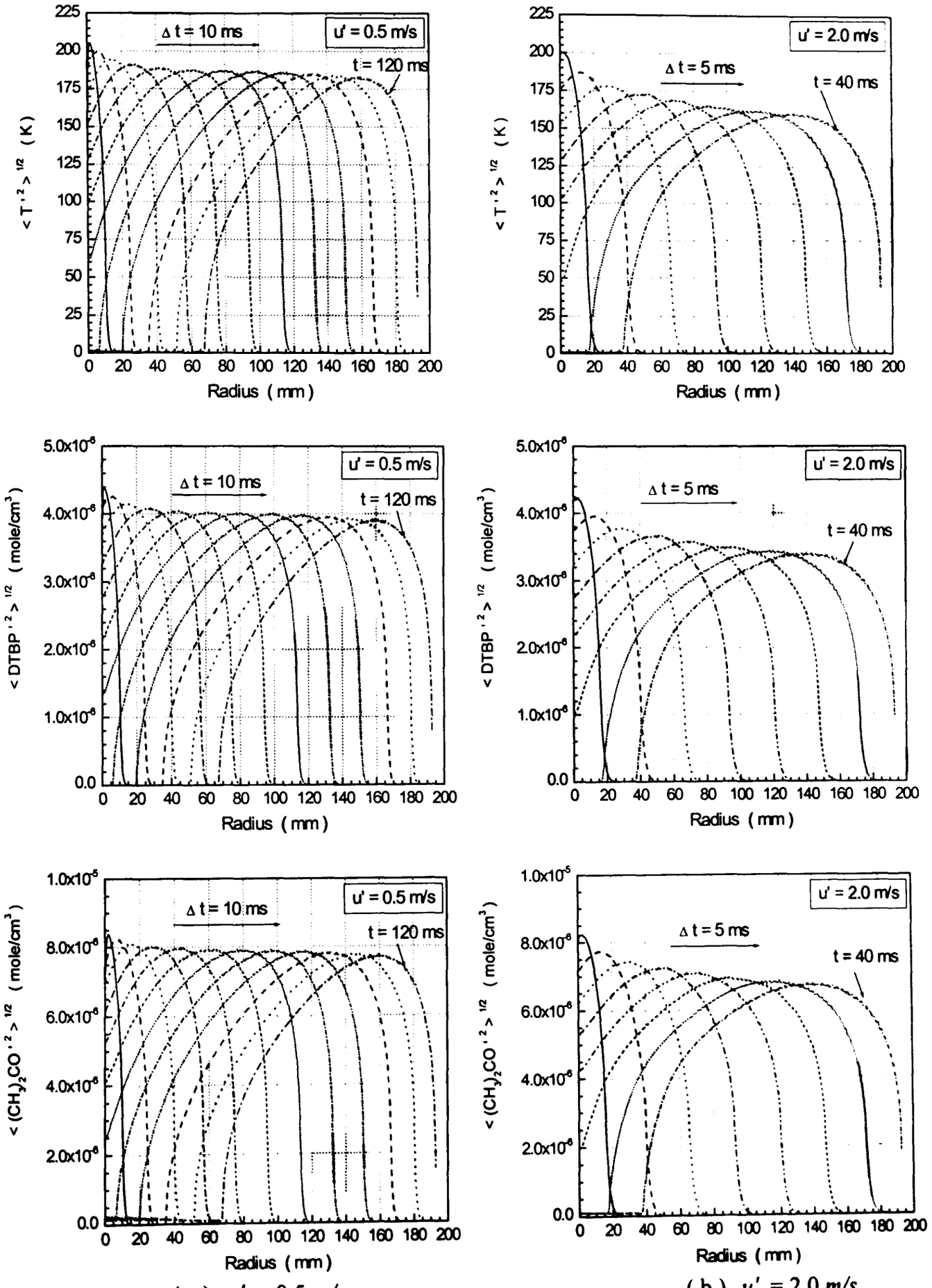

(a) $u' = 0.5$ *m/s* (b) $u' = 2.0$ *m/s*

Fig. 5.13 Temporal evolution of *rms* fluctuations

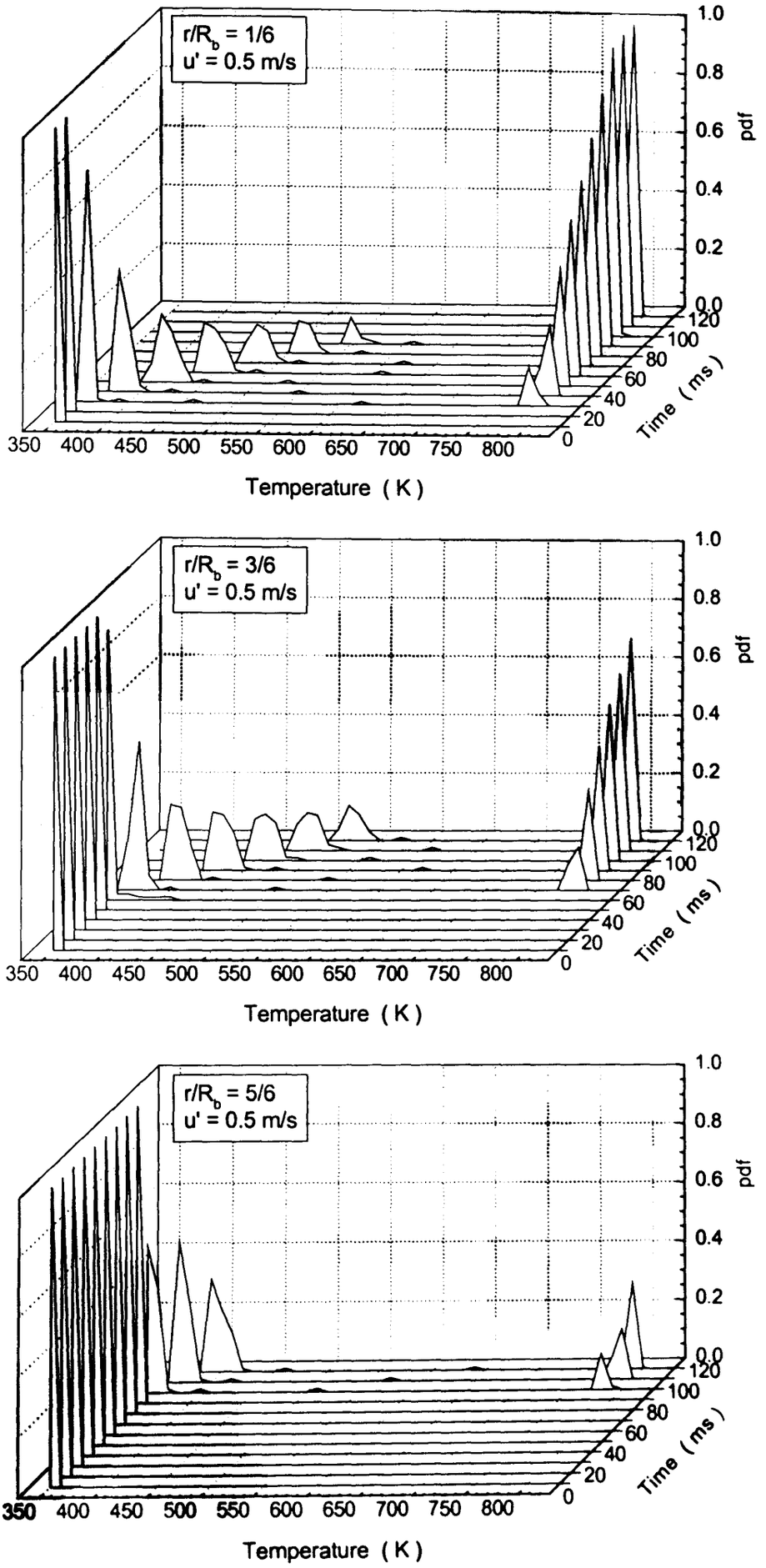

Fig. 5.14 Temperature pdf evoulation, u' = 0.5 *m/s*

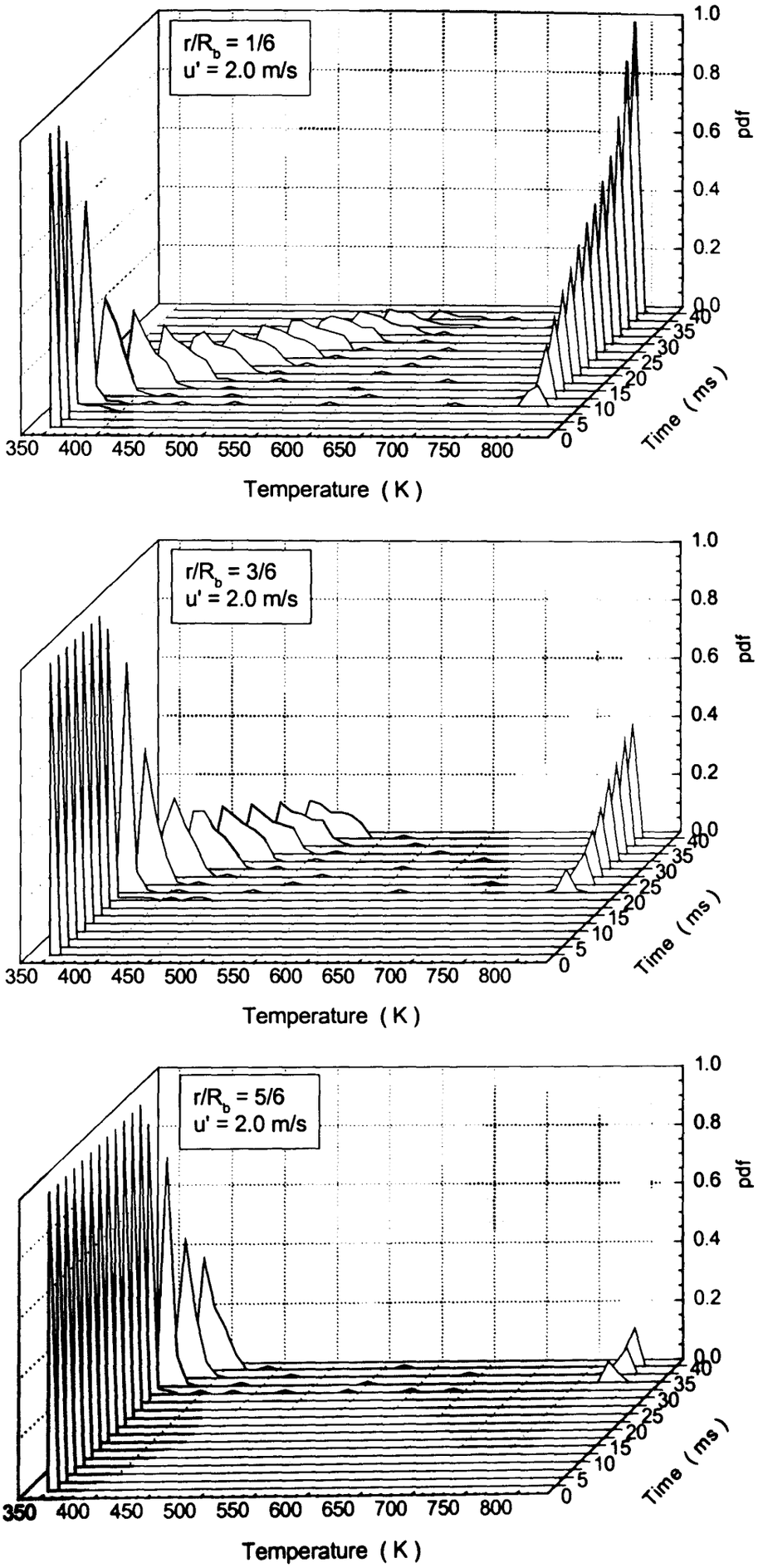

Fig. 5.15 Temperature pdf evoulation, u' = 2.0 *m/s*

5.5 Conclusions

The attractive feature of DTBP decomposition in an inert gas is that it has very simple chemical kinetics, and chemical reaction rate constants have been measured accurately elsewhere. For this reason 3.76DTBP/N_2 flame propagation in a spherical bomb was experimentally and numerically studied.

For laminar flame simulation, pressure rise in the bomb, flame speed and Markstein length were simulated. The simulation results in an unstretched laminar flame speed and Markstein length of $S_s = 0.485$ *m/s* and $L_b = 0.379$ *mm*, which compares favourably with measured values of $S_s = 0.52$ *m/s* and $L_b = 0.352$ *mm* as shown in Fig. 5.4. Laminar flame structure was also studied, the laminar flame thickness from simulation is about $\delta_L = 0.5$ *mm*, which is close to the thermal flame thickness calculated as $\delta_L = 0.39$ *mm*. This means that laminar flame propagation is well-predicted with the one-step kinetics and the evaluated thermo-chemical properties of DTBP.

Similarly to methane-air flames, for turbulent flame propagation the measurements showed a relatively long initial "incubation" period during which the flame propagated slowly. The duration of this initial period seems to increase for stronger turbulence. However, the simulations again failed entirely to reproduce this observation. Both simulations and measurements showed that turbulent burning velocity increased with increasing *rms* turbulent velocity u' see Fig. 5.10. Both measurement and RSF showed that burning velocity was approximately linearly proportional to flame radius except the very early and very late stages, see Fig. 5.10. In addition to this, turbulent burning velocities predicted by the RSF model were compared with those given by KLe and Lipatnikov-Zimont model. As shown in Fig. 5.11, the comparison showed that the predictions of these three models were quite close.

In general, the increase in turbulent burning velocity with u' is well-predicted with RSF, although, quantitatively, the turbulent burning velocity predicted with RSF is slower than measurements. The broadened δ peak in the bimodal evolution temperature pdf in Fig. 5.14 and 5.15 reveals the deficiency of the micro-scale mixing caused by the simple IEM-like term in Eq. (4.1).

Chapter 6

Study of KPP Theory as a Test for Turbulent Combustion Modelling

6.1 Introduction

Turbulent burning velocity is one of the most important parameters in turbulent premixed flames. It provides information for analysis and comparisons between modelling predictions and measurements. Since the pioneering work of Kolmogorov, Petrovskii, and Piskunov (1937) (KPP) devoted to propagation of biological species, KPP theorem has been widely used in studies of flame propagation. For example, Zel'dovitch (1980) applied KPP theorem for laminar flame study, Hakberg and Gosman (1984) applied it to premixed turbulent flames with classical gradient transport assumption for turbulent diffusion.

KPP theorem provides an analytical tool to study flame speed, particularly, for turbulent flame. In turbulent premixed flames, the distribution of average chemical reaction rate across a turbulent flame brush is likely to satisfy the requirements of the KPP theory. The lower boundary of the KPP velocity spectrum is often cited as an estimation of the turbulent burning velocity to be compared with modelling predictions, *i.e.* Bray (1990) and Libby (1989) applied the KPP theory to the so-called BML description of turbulent premixed flames (see *Chapter 1*) and obtained some quite plausible results. KPP theorem and its solution (KPP velocity) also provide the possibility to compare different numerical modelling predictions, *e.g.* Duclos *et al.* (1993) studied turbulent flame speed produced by 5 different flamelet models for planar premixed turbulent combustion. It is interesting to note that in that work the reference datum for the flame speed came from KPP theory and the measurements of Abdel-Gayde and Bradley (1987). Having an exact solution to some very simple "academic" problem is thus very helpful in both trivial check-ups of the algorithm and computer codes used as well as in less trivial analysis of the validity of the assumptions underpinning the theory used here.

This chapter is devoted to analysis of the RSF model "behaviour" in conditions for which the exact results of the KPP theory may be applied.

6.2 KPP Theory and its Application for Combustion Study

KPP theory is a description of propagating reaction waves in a system which can be characterised with a single progress variable c, with constant density and constant diffusion coefficient D. So the system may be described by a diffusion-reaction equation:

$$\frac{\partial c}{\partial t} = D\frac{\partial^2 c}{\partial x^2} + w(c) \tag{6.1}$$

where $w(c)$ is the reaction rate. If $w(c)$ satisfies the following requirements:

$$\begin{cases} w(c=0) = w(c=1) = 0 \\ w(c) > 0, \quad for \quad 0 < c < 1 \\ \left.\dfrac{dw(c)}{dc}\right|_{c=0} = \alpha > 0 \\ \dfrac{dw(c)}{dc} < a, \quad for \quad 0 < c \le 1 \end{cases} \tag{6.2}$$

and the initial spatial distribution of c is a step function, then it can be shown that there exists a lower bound of the propagation velocity spectrum. It is this lower bound velocity that is selected as propagation velocity and it is often cited as the KPP velocity:

$$u(KPP) = 2\sqrt{D\alpha} \tag{6.3}$$

This lower value is obviously defined by α which is the property related to the point c = 0. The conditions of initial step distribution of c and subsequent formation of a propagating reaction wave is similar to a flame generated by a spark propagating through a premixed combustible mixture. Because it is defined by the boundary condition c = 0, KPP velocity for a flame propagation through a combustible mixture is determined by the leading edge of the flame (Bray, 1990). The study of Zel'Dovitch (1980) demonstrated importance of the leading edge of the flame in determining laminar flame speed. KPP theorem may also provide a useful tool to analyse a turbulence combustion model. Particularly, for the laminar flamelet models, such as those of Cant *et al.* (1990) and Boudier *et al.* (1992), the KPP theorem can be applied

for analysis of the flame surface density equation. More details about this application are presented in the papers of Fichot *et al.* (1993), and Duclos *et al.* (1993).

For the application to the turbulent case, density must be assumed constant and turbulent diffusion coefficient described by a gradient transport model must also be constant everywhere in the flame, and not only at the leading edge (Bray, 1990). A spectrum of possible burning velocity then exists with the lower bound value of:

$$u_t(KPP) = 2\sqrt{D_T \alpha} \tag{6.4}$$

where D_T is the turbulent diffusivity determined as:

$$D_T = c_2 l_t u' \tag{6.5}$$

c_2 is a constant and Bray (1990) recommends $c_2 = 0.547$ as a standard value.

Hakberg and Gosman (1984) derived Eq. (6.4) using series expansion of dependent variables at the leading edge of the flame and assuming turbulent diffusion to be described with a conventional gradient transport model. Later, Libby (1989) used expanding dependent variables in powers of $\tilde{c}$ (Farve mean of c) at the leading edge, and obtained a lower limit burning velocity, $u_t(Limit)$. Bray (1990) demonstrated that the u_t(Limit) given by Libby was in the same form as Eq. (6.4) but with different diffusion coefficient D_{BML} as:

$$u_t(Limit) = 2\sqrt{D_{BML} \alpha} \tag{6.6}$$

where D_{BML} is the effective diffusion coefficient and in the leading edge it is expressed as (Bray (1990):

$$D_{BML} = u'(1 + \lambda)/w^* \tag{6.7}$$

where λ is empirical constant, w^* is the characteristic chemistry time scale. In both Hakberg and Gosman, and Libby's works it was noted that u_t must be greater than or equal to the minimum value u_t(KPP) or $u_t(Limit)$.

Bray (1990) showed that in the case of scalar fluctuation $\sqrt{\langle c'^2 \rangle} \to 0$, D_{BML} should reduce to the normal turbulent diffusion coefficient D_T at the leading edge of the flame. Then he concluded that the KPP burning velocity predicts the unique burning velocity at which the leading edge of the flame propagates into a uniform turbulent medium. It is

this burning velocity, u_t(KPP), which is often cited as KPP burning velocity in turbulent flame and which provides an estimation for comparisons between modelling predictions and measurements. So, at the leading edge, u_t may be expressed as:

$$u_t \geq u_t(KPP) = 2\sqrt{D_{BML}\alpha} \tag{6.8}$$

6.3 Cases for Simulations

The cases selected in this session are supposed to reflect two aspects: one is to study the RSF model in the situation where KPP theory holds in order to assess the model; the other one is to fully check the procedures and the computer codes described in *Chapter 2* for laminar and *Chapter 4* for turbulent flames. For those purposes, spherical flames propagating in the same bomb as described in *Appendix A* and in *Chapters 4* and *5* for RSF simulation are studied in both laminar and turbulent media. Assumptions were: no heat release (constant density), constant molecular diffusivity, constant pressure, unity Lewis number, Le = 1, and Prandtl number Pr = 1. From these assumptions the gas velocity in front of the flame front is zero.

Chemical reaction rate is taken:

$$w(c) = \frac{c(1-c)}{\tau_c} \tag{6.9}$$

which exactly matches the requirements formulated in Eq. (6.2) with $\alpha = 1/\tau_c$, τ_c may be considered as "chemistry" time scale.

For numerical calculations molecular diffusivity, and chemistry time scale were set as D = 0.2 cm^2/s, τ_c = 1 ms in the present study. For these values KPP theory results in the laminar burning velocity, u_L equal to 0.283 *m/s*.

For turbulent simulations, two different turbulent integral length scalars, l_t = 20 and 0.5 *mm* were selected, *rms* turbulence velocity were varied from u' = 0.25 up to 4.0 *m/s*. The reasons for such selections are: 1) with l_t = 20 mm, the parameters for simulations are exactly the same as that of *Chapters 4* and *5*; *2*) with those two different length scales, two different mechanisms of turbulence effects on combustion are studied: large

scale and small scale. It is often said that the large scale turbulence wrinkles the flame front and promotes combustion by enlarged flame surface, while small scale turbulence enhances the heat and mass transfer then effectively increases molecular and turbulent diffusivity. As a sequence of this choice, RSF model is applied here for two different combustion regimes, flamelet and distributed regime, see their representation in Borghi's diagram presented in Fig. 6.1. The simulations for flamelet combustion regime with parameters of $l_t = 20\ mm$, $u_L = 0.283\ m/s$, $D = 0.2\ cm^2/s$, would also be a close match to the bomb measurements of Abdel-Gayed and Bradley (1987) for propane-air explosions with equivalence ratio $\phi = 0.8$, $u_L = 0.29\ m/s$, $D = 0.18\ cm^2/s$. It should be noticed that their comparison is somewhat questionable, because in measurement heat release induces thermal expansion and thermal expansion may increase u_t. However, the effect of thermal expansion on u_t is complex and it still remains an open issue in premixed turbulent combustion (Ronney, 1995). However, it may be argued that for the purpose of this Chapter, such a comparison may be justified.

Listed in Table 6.1 are some relevant parameters, such as turbulent diffusivity calculated from Eq. (6.5), turbulent Reynolds number *etc.*, which were used to determine the location of current simulations in Fig. 6.1, where the Karlovitz number was calculated from Eq. (4.14).

Table 6.1 Parameters for simulations

(a) $l_t = 20\ mm$

u' (m/s)	τ_t (ms)	D_T (cm^2/s)	Da	Re_t	K
0.25	80	27.35	80	250	0.008
0.5	40	54.70	40	500	0.022
1.0	20	109.40	20	1000	0.062
2.0	10	218.00	10	2000	0.176
4.0	5	437.60	5	4000	0.496

(b) $l_t = 0.5\ mm$

u' (m/s)	τ_t (ms)	D_T (cm^2/s)	Da	Re_t	K
0.25	2	0.684	2	6.25	0.049
0.5	1	1.368	1	12.5	0.139
1.0	0.5	2.735	0.5	25	0.393
2.0	0.25	5.470	0.25	50	1.110
4.0	0.125	10.940	0.125	100	3.140
6.0	0.083	16.410	0.083	150	5.769
8.0	0.063	21.880	0.062	200	8.881

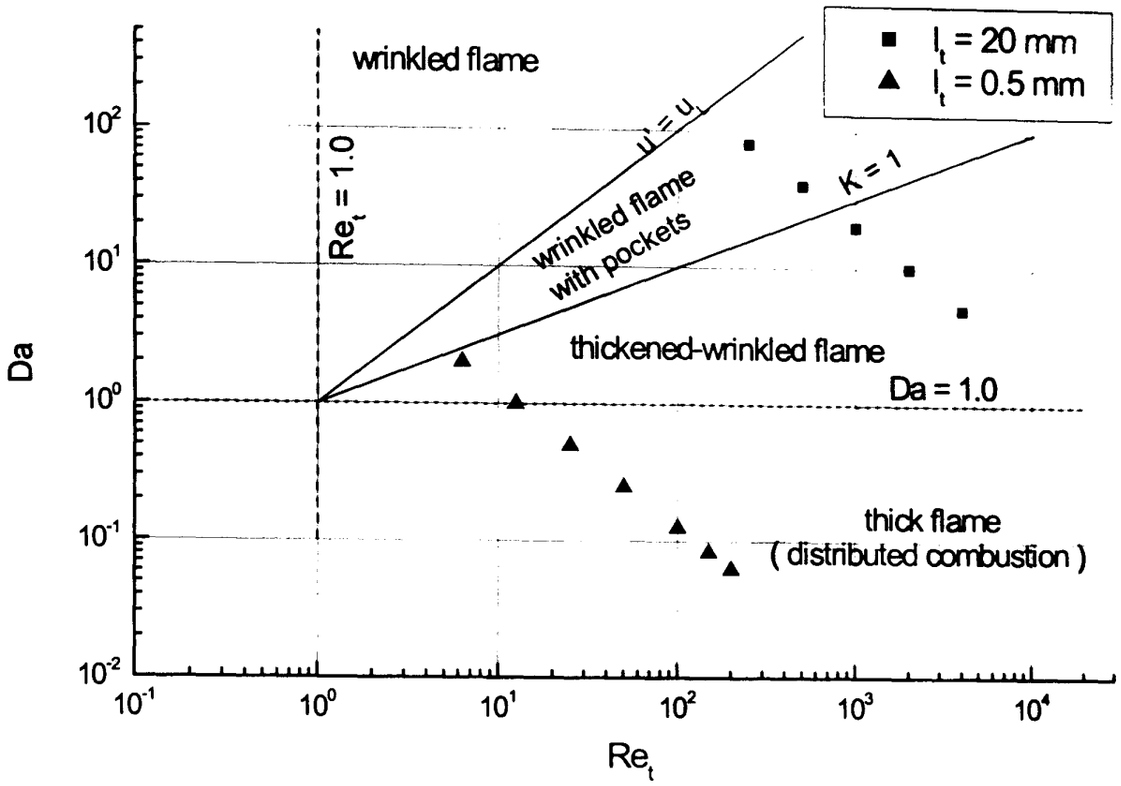

Fig. 6.1 Simulations located in Borghi's diagram

6.4 Simulation Results and Discussions

For both laminar and turbulent flame simulations, flame was initiated by numerically setting a hot flame kernel of 2 *mm* radius; the boundary conditions and the solution procedures were the same as those previously described in *Chapters 2* and *4* for laminar and RSF simulations, respectively.

For both laminar and turbulent simulations, the time step and grid size were set same as those in *Chapters 2* and *4*: time step, 1.0×10^{-4} *s*; 5000 nodes in *r* direction for laminar, 500×200 in *r* and X directions for turbulent simulations.

For laminar simulation, the evolution of spatial scalar distribution is shown in Fig. 6.2, laminar burning velocity was 0.286 *m/s* determined as dr/dt at $c = 0.4$, compared to the value of 0.283 *m/s* calculated by Eq. (6.3). The agreement between the two values is quite good. The profiles in Fig. 6.2 being steady, so the particular value of the iso-line at which the flame speed is calculated is irrelevant.

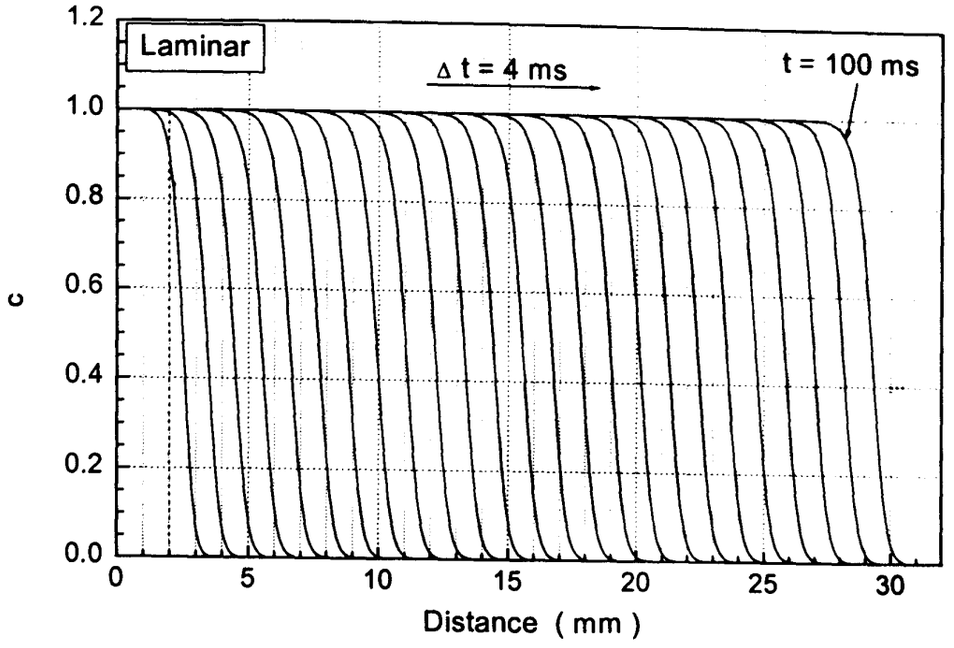

Fig. 6.2 Laminar flame propagation

Shown in Fig. 6.3 are RSF predictions for turbulent flame. In that figure RSF predictions are compared with KPP velocity (Eq. (6.4)), the predictions of KLe correlation (Bradley *et al.*, 2000) (Eq. (4.13)), Zimont model (1979) (Eq. (4.15)) and the measurements of Abdel-Gayed and Bradley (1987). In Eq. (4.13) u_k' is taken as if the flame would be fully developed, that is $u_k' = u'$.

As shown in Fig. 6.3, the scatter between different models is quite large and the predictions of RSF, KLe and Zimont are between the two limit values, where the lower limit is the Abdel-Gayed and Bradley's bomb measurements for propane-air explosion with ϕ = 0.8; the upper limit is the KPP velocity calculated by Eq. (6.4) and (6.5). In the bomb measurements the Lewis number for ϕ = 0.8 is Le = 1.78. The predictions of KLe correlation and Zimont model were close to measurement but far below the KPP velocity, and RSF predictions for lower turbulence were close to measurements, but far away from measurements and closer to KPP velocity for higher turbulence.

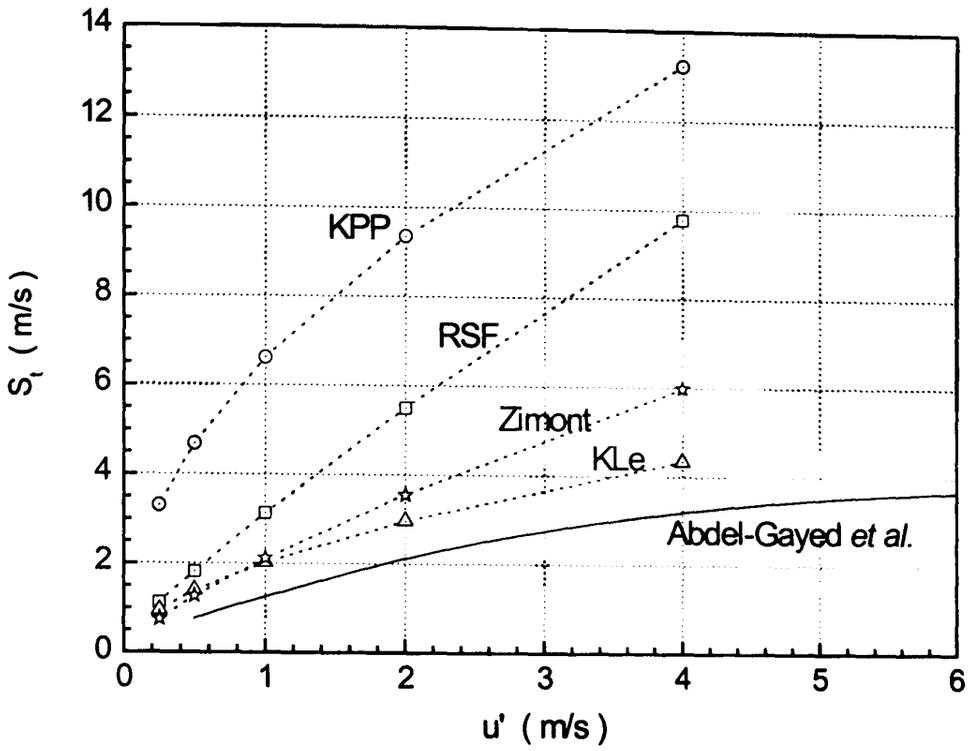

Fig. 6.3 Comparison of RSF predictions with KPP velocity , KLe correlation, Zimont model and measurements, $l_t = 20\ mm$

It is interesting to compare this with the results of Duclos *et al.* (1993), where they calculated the KPP velocities for 5 different flame surface density equations, *i.e.* laminar flamelet models, for one dimensional frozen turbulence combustion. This comparison of the KPP velocity predicted by different laminar flamelet models and the bomb measurements of Abdel-Gayed and Bradley (1987) is presented in Fig. 6.4. The scatter is again quite large between the results of different models. One of the reasons that there exists such a large scatter in Fig. 6.4 is that different flame stretch models were used in different flame surface density equations. In the flamelet combustion regime, flame stretch has strong effect on turbulent burning velocity. It may be inferred from Fig. 6.4 that the so-called CFM2b model is quite close to measurements, but as discussed in Duclos *et al.* (1993) this model has good agreement with measurement only at $\phi = 1.1$ and the agreement is not so good at $\phi = 0.7$. So it would not be surprising that in Fig. 6.3 the scatter between KPP velocity, RSF model and measurements is also large. The KPP velocity calculated with Eqs. (6.4) and (6.5) neglects the flame stretch effects thus overestimating the burning velocity.

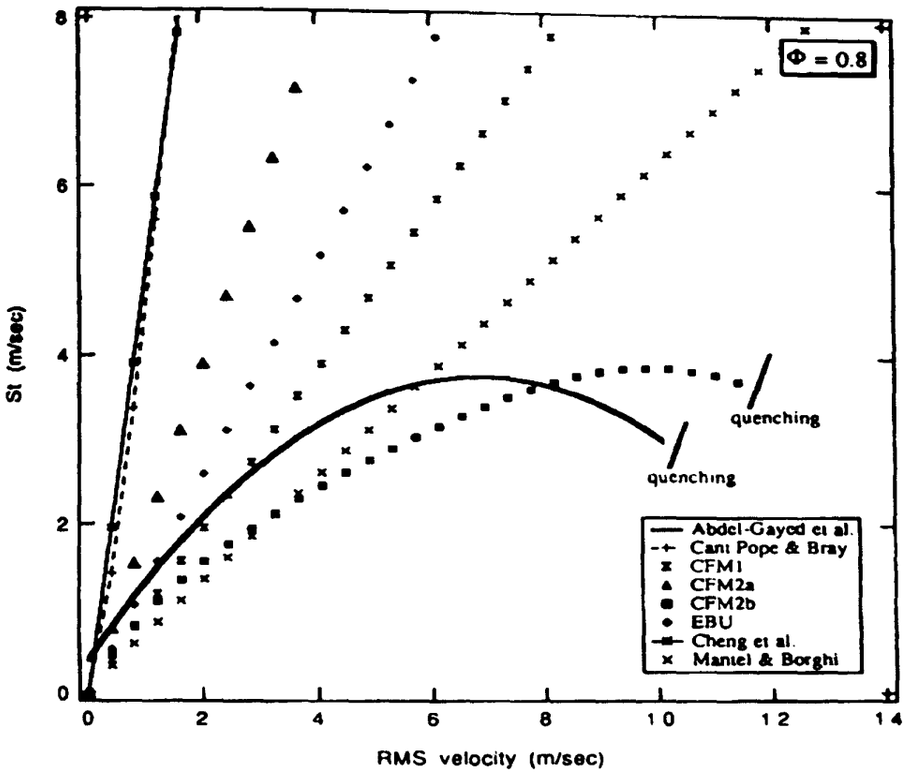

Fig. 6.4 Comparison between KPP velocities obtained by flame surface density equations and the measurements of Abdel-Gayed and Bradley (1987), figure taken from Duclos *et al.* (1993)

For $l_t = 0.5\ mm$, when $u' > 0.5\ m/s$, combustion will happen in the so-called distributed reaction regime with Damköhler number $Da < 1.0$ as shown in Fig. 6.1. In this regime, all the turbulence length-scales are smaller than laminar flame thickness. The mechanism of turbulence influence on combustion is different in this regime and it may be reduced simply to an enhancement of the laminar transport processes within the flame as suggested by Damköhler (1940). Damköhler reasoned that the transport properties within the flame are altered, so instead of laminar viscosity ν_L turbulent exchange coefficient ν_T has to be used. Then the relationship between laminar and turbulent burning velocity is expressed as:

$$u_t / u_L = \sqrt{\nu_T / \nu_L} \tag{6.10}$$

If turbulent Prandtl number is unity for both laminar and turbulent situation Damköhler's r relationship of Eq. (6.10) is equivalent to:

$$u_t / u_L = \sqrt{D_T / D_M} \tag{6.11}$$

Eq. (6.11) is consistent with KPP theory, as it can also be obtained from Eqs. (6.4) and (6.5).

Turbulent burning velocity predicted by RSF is presented in Fig. 6.5. In that figure, Zimont model (1979) which has been derived for Da >> 1 was extrapolated to Da < 1, and the predictions by this "extended" Zimont model is also shown in that figure. One can see for the small scale turbulence, the scatter is reduced as compared to Fig. 6.3. The predictions of turbulent burning velocity from three methods are in good agreement for lower turbulence intensity. For RSF predictions, the rate of turbulent burning velocity increase with increasing *rms* turbulence velocity is reduced. In particular, when $u' \geq 3$ *m/s*, turbulent burning velocity does not increase with increasing u' but remains approximately constant. No such trend is revealed by either Zimont model or KPP theory results.

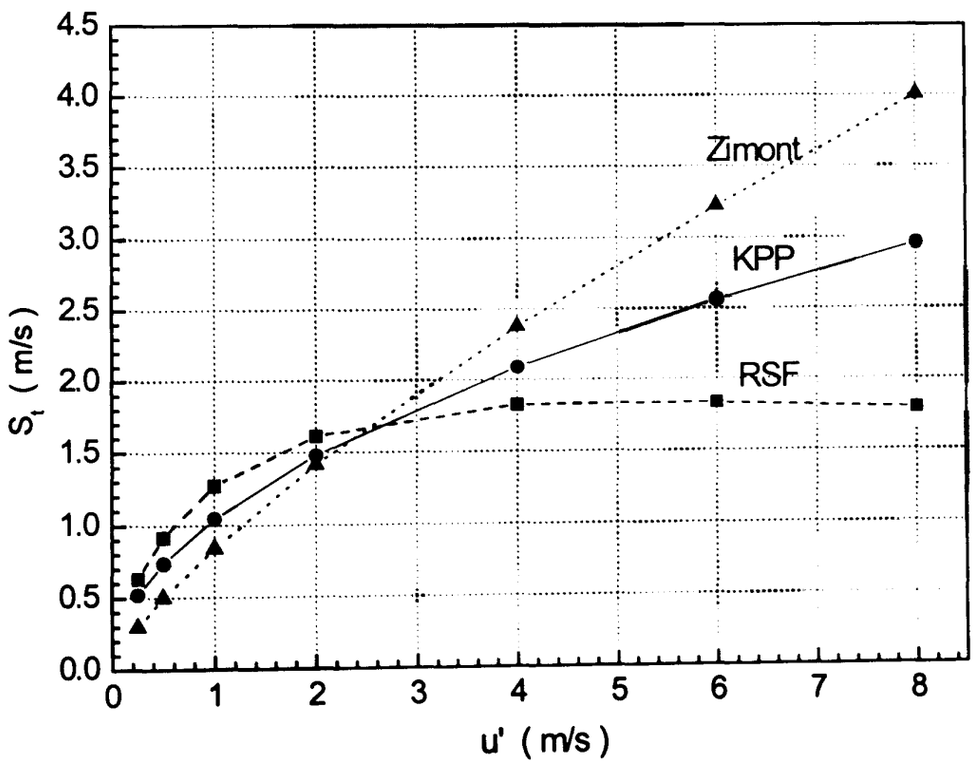

Fig 6.5 Comparison of RSF predictions with KPP velocity and Zimont model predictions, $l_t = 0.5$ *mm*

Shown in Figs. 6.6 and 6.7 are the profiles of scalar mean value for different turbulence length scales l_t = 20 and 0.5 *mm*. As shown in these figures, flame propagation attains a steady regime very soon.

6.5 Summary

In this Chapter, an "acadamic" case of one dimensional flames without heat release propagating in a spherical bomb was simulated. This served as a tool of validation for both numerical procedures and the computer codes were justified by comparing the predictions with KPP theory and KLe and Zimont models. The simulation of laminar flame propagation gave good agreement with KPP theory. Also turbulent flames were simulated with the RSF model for two different integral length scales. For larger integral scale the RSF model predictions lied between KPP velocity and the predictions of KLe correlation and Zimont model as presented in Fig. 6.3; for smaller integral scale and weak turbulence the RSF predictions were in good agreement with KPP velocity as shown in Fig. 6.5. In the latter case RSF predictions also showed that there is a limiting turbulence intensity above which any increase in u' does not result in faster combustion, see Fig. 6.5.

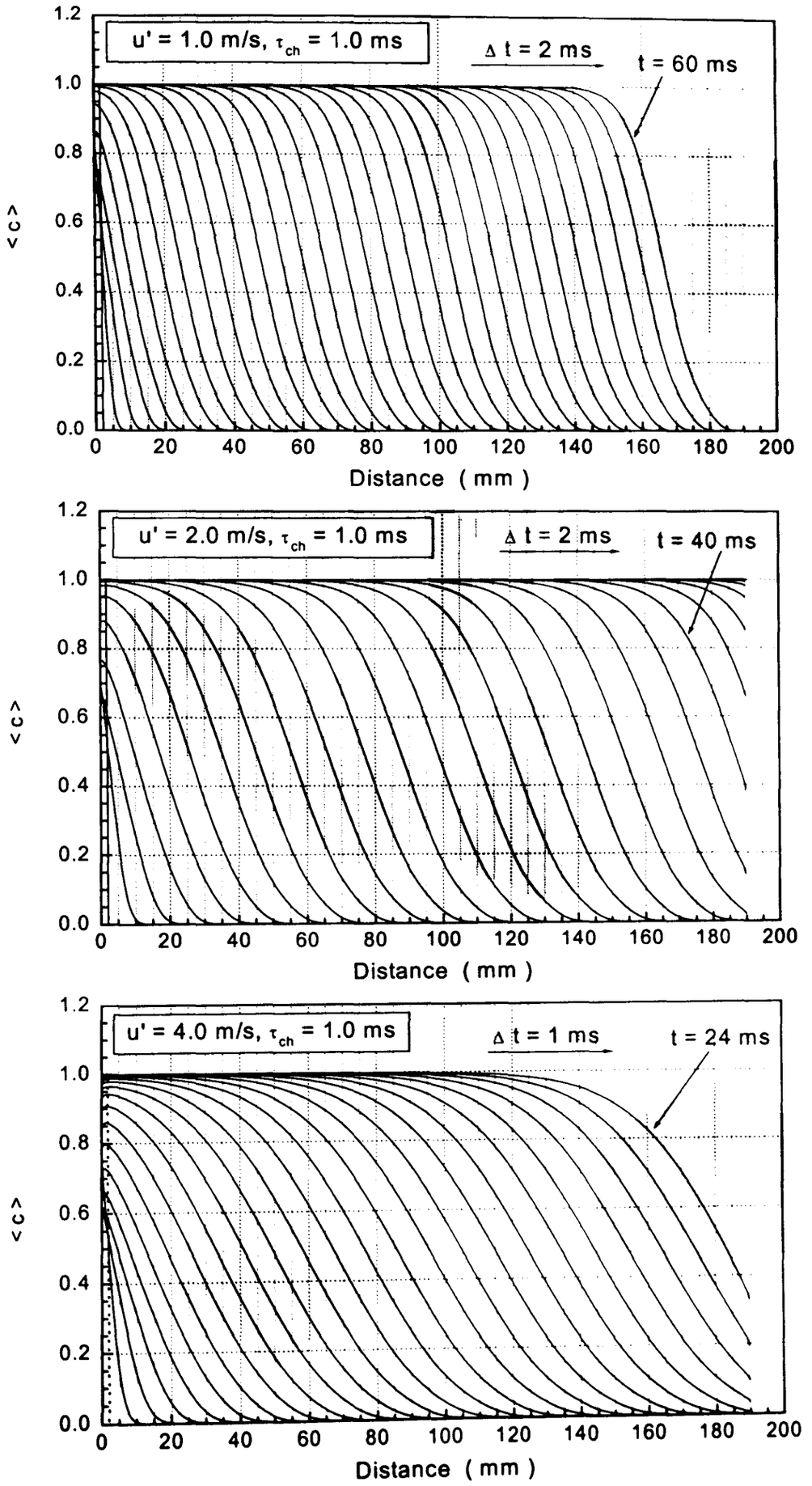

Fig. 6.6 Evolutions of scalar spatial distribution, l_t = 20 *mm*

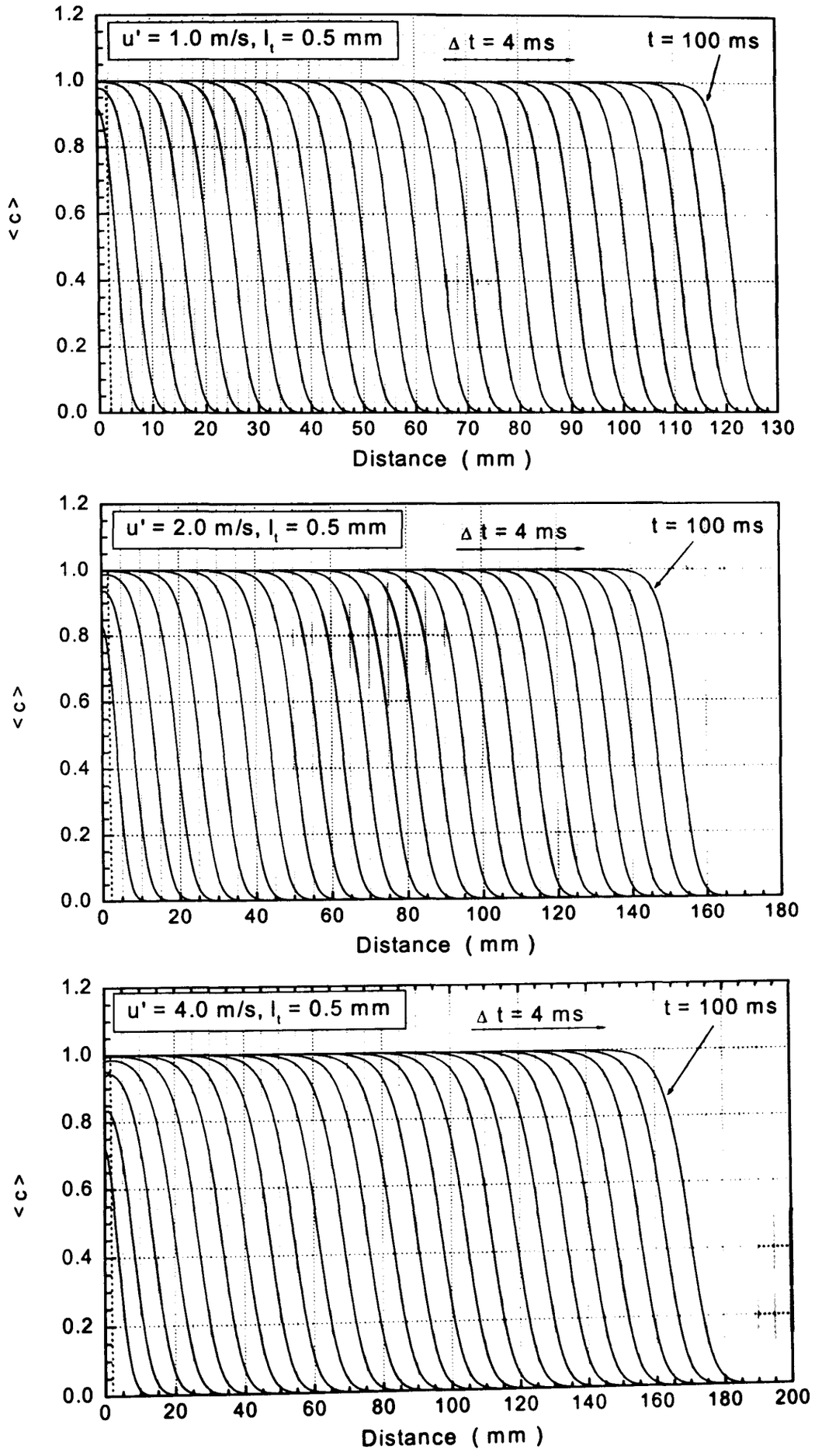

Fig. 6.7 Evolutions of scalar spatial distribution, l_t = 0.5 *mm*

Conclusions and Recommendations

Summary and conclusions

The present work assesses the recently proposed reference scalar field (RSF) model of turbulent combustion on the test cases of self-ignition and flame propagation.

In the simulations of self-ignition and flame propagation of CH_4/air mixtures, a finite rate chemical reaction scheme, a reduced two-step scheme, was used to study the turbulence-chemistry interaction. The reduced two-step chemical reaction scheme reflects the fact that there exists a two-stage structure for hydrocarbon oxidation, the first stage being fuel consumption where fuel is converted to CO and H_2, and the second stage being the oxidation layer of CO and H_2, where the final products such as CO_2 and H_2O are formed. The constants for the chemical kinetics were "tuned" and tested in a laminar situation. In the self-ignition study, ignition delays and the profiles of temperature and species for various initial temperatures in a homogenous stagnant medium were obtained. The ignition delays were compared with an empirical correlation based on shock tube measurements. The comparison shows a quite good agreement as shown in Fig. 2.3. In the flame propagation study, spherical flame propagation in a bomb was simulated for different fuel/air equivalence ratios. Pressure rise during gas explosions was simulated. Laminar burning velocity and flame radius were calculated from the pressure simulation. Simulation results were compared with measurements, and comparisons showed good agreements in terms of pressure and flame radius as shown in Figs. 2.18, 2.19, 2.20. Two-stage combustion could be clearly distinguished in the simulated flame structures for different equivalence ratios and different initial pressures as presented in Figs. 2.10 to 2.15. Prediction of laminar flame structure by the present two-step kinetics was compared with the full kinetics of Dixon-Lewis, as shown in Fig. 2.16, and several common properties of the flame are captured by the two-step scheme.

After the chemical kinetics of CH_4/air had been studied, a first assessment of RSF was performed in the self-ignition study. Combined effects of temperature/concentration

inhomogeneities and turbulence on self-ignition were studied. Three types of initial condition were simulated which were formulated in terms of initial temperature pdf's as: a) Dirac's δ peak pdf, which means the initial temperature field is uniform and homogeneous, b) Rectangular pdf, which means the initial temperature gradient is uniform, c) bimodal pdf, with the mixture initially composed of burnt/unburnt gas. Simulations were performed for statistically homogeneous stoichiometic CH_4/air mixtures. The simulations showed that both initial temperature/concentration inhomogeneities affect the chemistry in a complex manner and make the ignition delay event ambiguous as shown in Fig. 3.2; strong turbulence may reduce the effects of initial temperature and concentration variations on the chemical kinetics as presented in Fig. 3.4. With the presence of initial temperature gradients, the ignition delay time is shorter than that defined in a stagnant medium. However, with the turbulence intensity increase, the ignition delay becomes longer. Predictions of the RSF model were compared with those predicted by another statistical turbulence combustion model named LEM. The trends mentioned above were predicted both with RSF and LEM; moreover the results were nearly indistinguishable for moderate and strong turbulence, as shown in Figs. 3.3. As for the computation cost, RSF is found to be less expensive than LEM. The effects of heat losses on ignition were also studied with the RSF model. As shown in Fig. 3.13, the heat losses can only affect the self-ignition delay for lower initial temperatures and make ignition delay longer, and can even make self-ignition impossible. The effect of heat loss on ignition delay is more noticeable for higher turbulence intensity. These trends are reasonable predicted with RSF, however, no definitive answer can be given at the current stage because of a lack of experimental data in a controlled turbulent environment.

A second assessment has been carried out for the problem of statistically homogeneous turbulent flame propagation. Two types of turbulent flames, CH_4/air flame and DTBP/N_2 decomposition flame, were simulated. The purpose of the selection of the DTBP/N_2 flame was to isolate the effects of inaccuracies in kinetics on the outcome of turbulence combustion modelling because this flame can be described with a single-step reaction and parameters which are well-established. Thus the study of this flame would not suffer from any ambiguity related to reaction mechanisms in hydrocarbon-air flames. Thermochemical properties of DTBP were estimated and testing for laminar DTBP/N_2 flame propagation in a spherical bomb was performed. The predictions

agreed with measurement quite well as shown in Fig. 5.1 to 5.4, in terms of pressure rise, flame radius and burning velocity.

In RSF simulations, turbulent burning rate was determined based on the pressure rise during the explosion which was simulated. Turbulence parameters, such as u' and l_t, were assumed constant and a simple linear dependency of conditionally averaged velocity (Eq. 4.5) was used to describe the process of turbulent convection. Turbulent burning velocities predicted by the RSF model were compared with those given by KLe and Lipatnikov-Zimont model. As shown in Figs. 4.18, 5.11, the comparison showed that the predictions of these three models were quite close. For measurements, as shown in Figs. 4.20, 5.9(a) and 5.10(a), both CH_4/air and DTBP/N_2 flames revealed a relatively long initial "incubation" period during which the flame propagated slowly, and the duration of this initial period seemed to increase for stronger turbulence. However, RSF simulations could not reproduce this observation. Although, quantitatively, turbulent burning velocities predicted with RSF were much slower than measurements, general trends such as burning velocity increase with increasing *rms* turbulent velocity u' were well-predicted with RSF, see Fig. 4.18, 5.9(b) and 5.10(b).

Temperature pdf evolutions were calculated from the extra statistical coordinate, X, and the results showed that the pdf remained nearly bimodal throughout, *i.e.* combustion occurs in a thin flame regime, see Figs. 4.14, 5.15. However, the motion of a broadened δ peak corresponding to the fresh mixture is also visible. This means that the fresh gas immediately in front of the flame front is already heated-up. This is a clear deficiency of the model caused by the simple IEM-like term in Eq. (4.1) for micro-scale mixing.

Finally, RSF model "behaviour" was studied in conditions for which the exact results of the KPP theory may be applied. Turbulent burning velocities for two different length scales were predicted and the results were compared with KPP predictions. The RSF model reasonably predicted that upon attaining a certain limiting turbulence intensity any further increase in turbulence intensity does not result in faster combustion, see Fig. 6.5. However, KPP and Zimont model cannot predict this trend.

Recommendation for Future Work

Recommendations for future work may be given as:

(1) One can deduce that a better small-scale-mixing model for RSF is vital before it could be recommended for wider use.

(2) In the study of self-ignition and flame propagation of CH_4/air mixtures, the coefficients for the reaction rate of the two-step scheme were fixed at an initial pressure of 1.0 *bar*. In the study of self-ignition, it was found that these kinetics could not be used for higher pressure situations. Future work should consist of modifications of the two-step kinetics, or looking at other better chemical kinetics for the assessment of the RSF model.

(3) Direct modelling of the conditionally averaged velocity, as suggested in *Chapter 4*, is worthy of future study.

(4) There is clearly a requirement for further experimental data for flame propagation in the fan-stirred bomb, with regard to both CH_4/air combustion and DTBP/N_2 decomposition flames. In the case of CH_4/air flame there is required to explain differences between the present and earlier results. For DTBP/N_2 decomposition flame more detailed measurements are required.

Appendix A

Experimental Study of Flame Propagation in a Fan-Stirred Bomb

A.1 Introduction

In practical combustion devices, would it be an internal combustion engine or a stationary power generator, turbulent combustion is of particular interest. This is because turbulence increases the mass consumption rate and henceforth increases the volumetric power output.

In many approaches to turbulent combustion, it is important to characterise the turbulent burning velocity, Lipatnikov *et al.* (2001). However, the definition of the turbulent burning velocity is not as clear as it is in the laminar case. Various definitions of turbulent burning rate are used in the literature, making it difficult to analyse the available experimental data. One can sometimes find a paper in which the comparison is carried out between, *e.g.* mass burning rate and propagation speed. Also, it seems that even for the same definition, there exists a big discrepancy in the numerical values for the same mixtures and conditions. That is why it was judged necessary to supplement the studies of the new modelling approaches with the purpose-made experiments, in order to have data of which processing and collection procedure is known entirely.

Reported in this Session is the experimental studies of flame propagation in a fan-stirred bomb. Pressure history during gas explosion in the bomb, flame radius and turbulent mass burning velocity were obtained for pre-mixed methane and air at different equivalence ratios from lean to rich. These results also provide experimental data to assess the modelling results which are the primary objective of this thesis.

A.2 Experimental Setup

Experiments were carried out in a constant volume fan-stirred bomb. The experimental setup is shown in Fig. A.1. The system consisted of five components: constant volume combustion chamber, ignition system, optical visualisation system, pressure recording system and control system, and which are briefly introduced below, while more details may be found in the PhD thesis of Ali (1995) and Scott (1992).

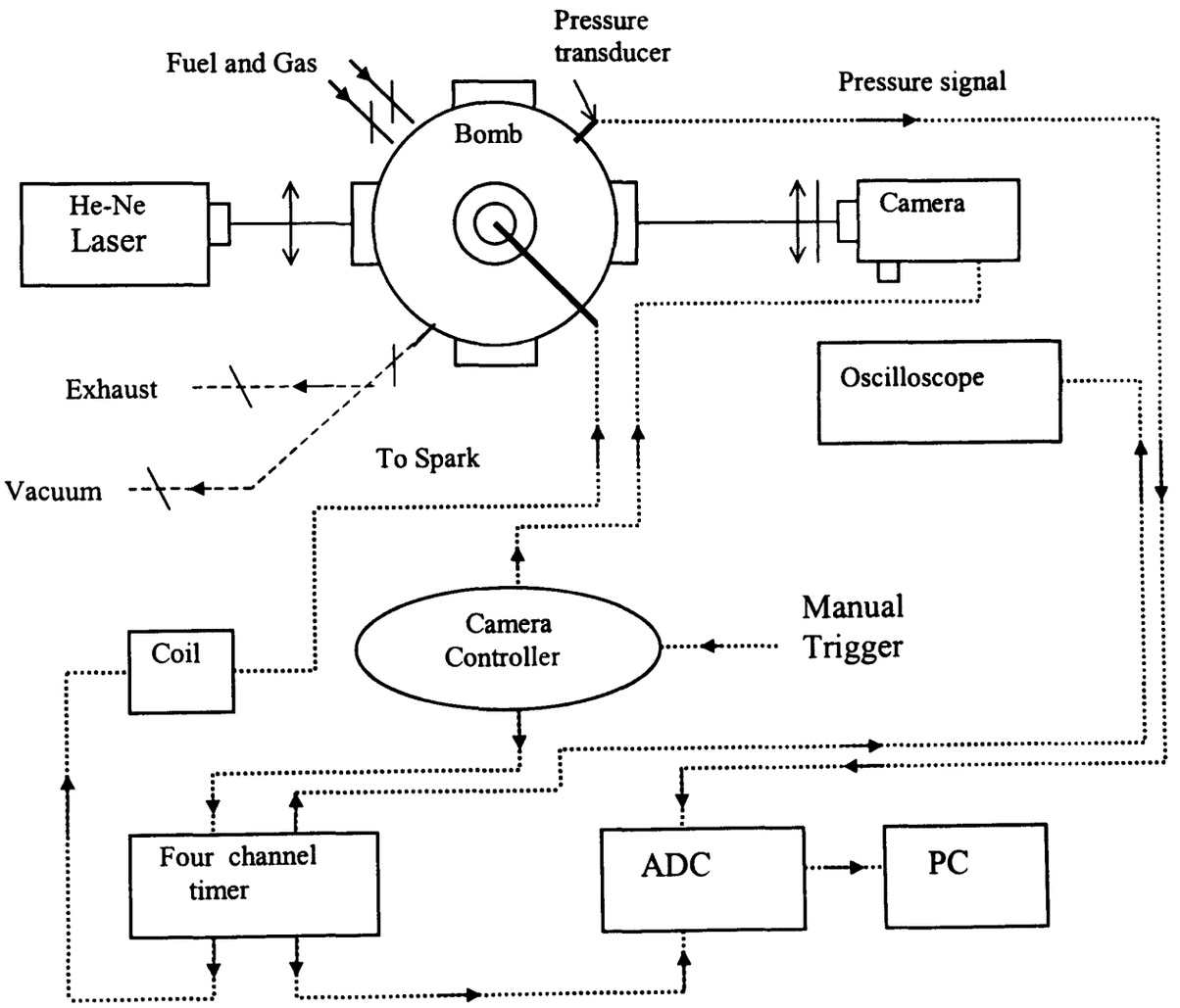

Fig. A.1 Experimental setup

The constant volume combustion chamber is a quasi-spherical, fan stirred bomb, with volume of 0.0301 m^3 and its equivalent radius is 193 *mm*. The bomb has three pairs of orthogonal windows of 150 *mm* diameter which provide an extensive optical access for the laser Schlieren technique. Isotropic turbulence can be created by the four identical, separately controlled fans which are symmetrically mounted in a regular tetrahedron configuration.

Turbulence parameters were measured with laser doppler velocimetry (LDV). The turbulence within the central region of the chamber has been found uniform and isotropic with very low mean velocities. The *rms* turbulence intensity u' can be derived from the fan speed as $u' = c^{st} \times f$, where c^{st} is a constant, and f is the fan speed in *rpm*. The calibration of 1993 gave c^{st}=0.0011799 and calibration of 1996 (Bradley *et al.*, 1996a) gave the value of 0.00119, the difference of the two values lies within 1%. Present study adopts the latter value of c^{st} = 0.00119. The fan speed can be accurately adjusted between 200*rpm* to 10000*rpm*, corresponding to turbulence intensities ranging from 0.238 *m/s* to 11.9 *m/s*. The integral length scale, l_t = 20 *mm*, has been determined from a two point correlation in a cold flow measurements and is independent of fan speed and pressure (Bradley, *et al.*, 1992).

Before the mixture was filled into the chamber, the chamber was evacuated and flushed twice with dry cylinder air to remove any residual products from previous explosions, especially the water vapour. After third evacuation, methane with 99% purity was added first until the required partial pressure was reached, then dry cylinder air was filled in until required initial pressure. Both methane and dry cylinder air were supplied by BOC Ltd. For laminar explosions, the fans were kept running during the process of gas filling to ensure the reactants well-mixed but before igniting the mixture the fans were stopped and the chamber was left at least 1 *min* to ensure the mixture had become quiescent.

Ignition was achieved with a standard 6.35 *mm* Miningag spark plug mounted in the centre of the chamber through a stainless steel tube inside which a PTFE insulated high voltage lead was fitted. A Lucas 12 *V* transistorised automotive ignition coil system was connected to the spark electrode.

For the present work the Schlieren image technique for visualizing the propagating flames was used to study only laminar flame propagation, it was not used for turbulent flame studies. For the Schlieren imaging, the laser beam was produced by a Spectral-Physics 10 *mW* He-Ne laser with a beam diameter of 0.65 *mm* and wavelength of 632.8*nm* and expanded by a microscope Olympus A40 and a 1000 *mm* focus lens with 150 *mm* diameter. When the laser beam passed through the lens, a parallel beam of 150 *mm* diameter was produced. After the passage of this parallel beam through the bomb windows, it was focused by another 150 *mm* diameter, 1000 *mm* focus lens. Then this

focused beam passed through a 0.65*mm* pinhole which was placed in front of the Hitachi 16 *HM* high speed camera, and was received by the camera set at speed of 5000 frames per second. Thus the flame propagation was recorded on 16 *mm* high speed film.

Pressure rise during combustion was measured with a quartz pressure transducer Kistler 701 H, which was mounted flush with the inner surface of the bomb. The signal from the transducer was amplified by a Kisler Charge Amplifier 5007, and sent to a personal computer through an Analogue Digital Converter (ADC) board, DAS-50.

The role of the control system is to trigger the spark and to start the measurements synchronously. As shown in Fig. A.1, after the manual trigger was switched on, the signal was sent to the camera controller, then the camera controller sent a signal to control the camera and a four-channel timer simultaneously. The timer sent three signals, one was to the coil to trigger the spark, one to the ADC to record the response from the pressure transducer, and one to the oscilloscope. Before the oscilloscope received the signal from the timer, the screen of the oscilloscope had a bright dot. When the oscilloscope was triggered, the dot jumped out of the screen and this event was recorded on the film. As a sequence, before the spark was triggered, there was a line on the margin of the film, when the spark was triggered, the dot jumped out of the screen and on the film that line disappeared, so the instant that the line disappears defines exactly the moment of trigging the spark. Usually, the spark delayed the ADC by a few micro-seconds, this delay was accurately measured with the oscilloscope and used in the post-processing of the recorded pressure.

A.3 Data Processing

A.3.1 Schlieren Image

Schlieren photography has an advantage of providing a readily definable flame surface as the image of a certain isotherm (Glassman,1996). Weinberg (1955) suggested that the isotherm of Schlieren edge is 460 *K*, and recently Rankin & Weinberg (1997) found that the isotherm of Schlieren edge is a function of flame radius and varies from 850 to 900 *K*. From the Schlieren image the flame radii can be easily determined, as a

consequence, flame speed and burning velocity can be obtained and the effect of flame strength and curvature can be studied (Bradley *et al.*, 1998).

Time interval between each frame on the film can be determined with the help of the timing mechanism built in the high-speed camera. Inside the camera, a light emitting diode flashed at 1KHz producing a timing mark on the film at intervals of 1 *ms*. The distance between each timing mark was measured to determine the framing rate at that time. As reported above the instant at which that spark was triggered was determined by the moment when the signal from the oscilloscope disappeared.

The flame image diameter was measured at three different directions. The averaged value of these three measurements was then taken as the "real" flame diameter for further processing. For this aim a channel-shaped metal marker, with 50 *mm* gap, was fixed on the bomb window so it could be seen clearly on the films. Just measuring the length of the marker on the image, one can obtain the scale for the diameter of the flame on the image.

From the dependency of flame radius against time so obtained, laminar burning velocity can be derived.

A.3.2 Pressure Processing

The pressure rise was measured until its value reached 0.5 *bar*. The pressure signal reveals usually a substantial level of noise and a low-bandwith pass Fourier filter was used to remove the noise. An example of this procedure is illustrated in Fig. A.2 in which original and filtered signals are presented.

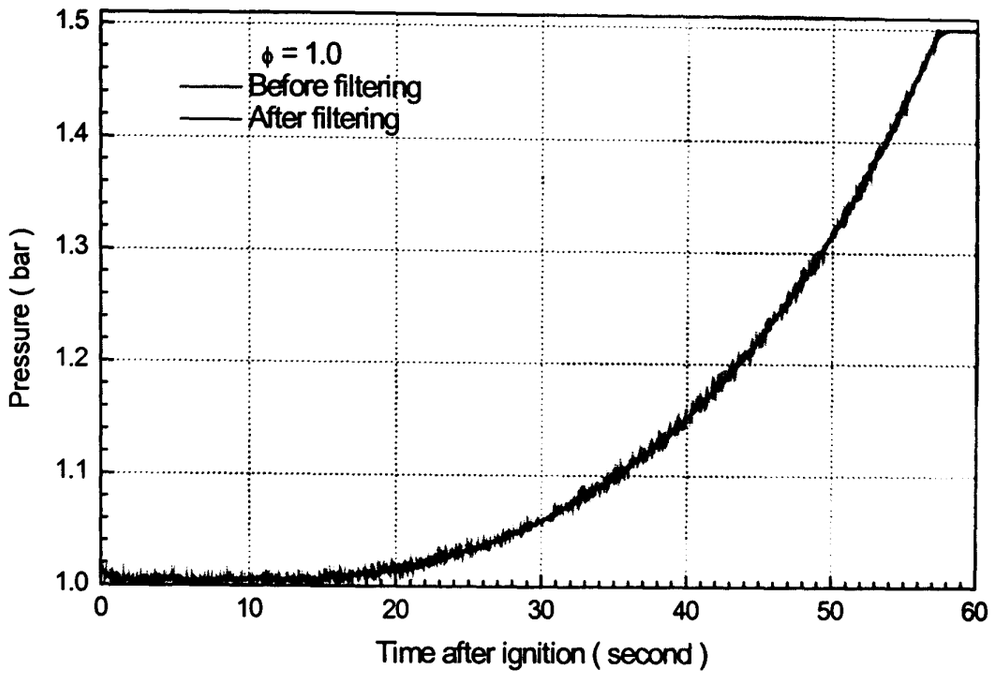

Fig. A.2 An example of pressure data filtering

A.3.3 Calculation of Flame Radius and Burning Velocity

For the combustion in a closed vessel, numerous relationships between pressure rise and flame radius have been suggested in the literature as early as twenties of last century. For the pre-pressure period of small pressure rise during combustion in a spherical vessel probably the most well known is the procedure of Lewis and von Elbe (1951).

The basic assumptions of Lewis and von Elbe procedure are that the fresh mixture is compressed adiabatically by the flame and the pressure rise is proportional to the mass fraction burnt m_b , $m_b = \frac{P - P_0}{P_{eq} - P_0}$. After these assumptions, the flame radius is found as Eq. (A.1b) and the flame speed is given by Eq. (A.1).

$$u_n = \frac{dr_i}{dt}\left(\frac{r_i(t)}{r(t)}\right)^2\left(\frac{P_{ini}}{P(t)}\right)^{1/\gamma_u} \qquad (A.1)$$

$$\frac{r_i(t)}{R_b} = \left[\frac{P(t) - P_{ini}}{P_{eq} - P_{ini}}\right]^{1/3} \qquad (A.1a)$$

$$\frac{r(t)}{R_b}=\left[1-\left(\frac{P_{ini}}{P(t)}\right)^{1/\gamma_u}\frac{P_{eq}-P(t)}{P_{eq}-P_{ini}}\right]^{1/3} \qquad \text{(A.1b)}$$

where, γ_u is the ratio of the mixture specific heats for the unburned gas remaining constant during processing, $P(t)$ is pressure at time t, P_{ini} is initial pressure, R_b is the combustion vessel radius, $r(t)$ is the flame radius at time t, r_i is an imaginary flame radius that would exist in absence of the burnt gas thermal expansion. In the formulae above Lewis and von Elbe recommend to use the thermodynamically calculated value P_{eq} for the final pressure rather than the observed value, in other words an assumption is made that combustion is adiabatic.

In 1940, Fiock *et al.* (1940) derived another expression for u_n that would employ a pressure record simultaneous with flame imaging as:

$$u_n=\left[1-\frac{R_b^3-r_{sch}^3}{3P\gamma_u r_{sch}^2}\frac{dP(t)}{dt}\right]\frac{dr_{sch}}{dt} \qquad \text{(A.2)}$$

where, r_{sch} is the spherical flame radius taken from Schlieren images at the moment when the pressure is $P(t)$. However, this method makes use of product of two time derivatives and in the presence of experimental noise the possible error would be thus be amplified. Another source of inaccuracy in this method lies in the fact that the second term in the bracket, during most of the explosion, is only slighly less than unity, ranging from 0.85 to 0.95 (Linnett, 1953). The present experiment confirms Linnett's conclusion and yields this value ranging from 0.683 to 0.816. This means that an inaccuracy of 1% in this term leads to an inaccuracy of about 10% in the value deduced for u_n. Thus one can argue that Lewis and von Elbe procedure allows to obtain higher accuracy.

One can express the derivative $\frac{dr_i}{dt}$ and $r(t)$ in terms of the current pressure and substitute it directly into Eq. (A.1). Then one can obtain an expression, directly expressing flame radius and u_n in terms of the pressure derivative, see Schetinkov (1970), as:

$$u_n = \frac{R_b^3 - r^3(t)}{3r^2(t)(P_{eq} - P(t))} \frac{d\,P(t)}{d\,t} \qquad \text{(A.3a)}$$

$$\frac{r(t)}{R_b} = \left[1 - \frac{P_{eq} - P(t)}{P_{eq} - P_{ini}} \left(\frac{P_{eq}}{P(t)} \right)^{1/\gamma_u} \right]^{1/3} \qquad \text{(A.3b)}$$

A.4 Results and Discussions

A.4.1 Laminar Flame Propagation

Laminar flame propagation was studied in three methane-air mixtures, lean (ϕ = 0.8), stoichiometric and rich (ϕ = 1.2). The pressure histories after filtering for all three mixtures are shown in Fig. A.3.

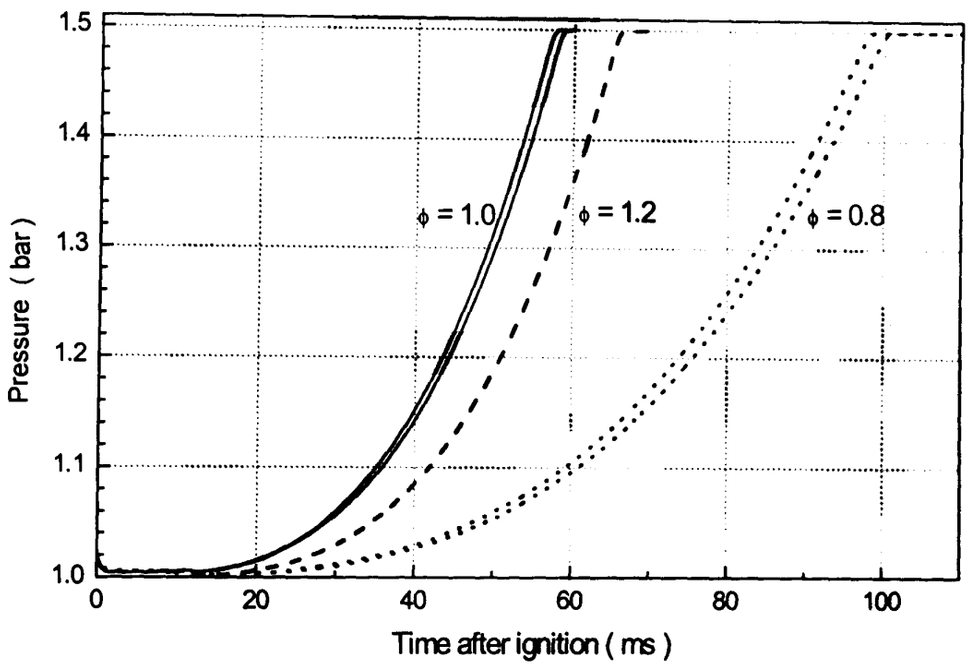

Fig. A.3 Pressure histories for laminar flame propagation in the bomb

At zero time corresponding to spark discharge, one can notice a peak in the pressure signal, after which there is a prolonged (longer for lean mixtures) period during which the pressure is slightly above the nominal initial level. This most probable explanation to this observation is that the spark discharge induced a shock wave, trace of which is seen as the pressure peak. Because of the pressure transducer finite relaxation time, or time-lag for the transducer, there will be a period of inaccurate pressure reading. In

other words, the pressure transducer exhibits a hysterisis phenomena somewhat similar to semi-conductor devices. Once the pressure rise due to the burnt gas expansion becomes greater than the sensitivity threshold, the pressure reading will become accurate again, the conclusion supported by analysis of Fig. A.4(a). However, this means that flame radius derived from pressure will exhibit unphysical behaviour for some initial period, and one can rely on its values only for $r_b \geq 20\,mm$. Advocating the present set-up, one can notice that the similar studies reported in the literature the flame speeds taken at the instants of quite substantial (*i.e.* the sensitivity of the present apparatus being superior to them) pressure rise, *e.g.* for Karpov *et al.* (1980), $\Delta P =$ 5~140 *mbar*, Nakahara and Kido (1998), $\Delta P = 10\sim30\% P_0$.

Flame kernel development for three mixture from lean to rich mixture is shown in Fig. A.4. Presented in Fig. A.4(a) is flame radii determined with both the Schlieren imaging and pressure rise. From analysis of this figure, the advantages and drawbacks of the two methods are obvious. The advantage of Schlieren image is that it can study the early development of flame kernel, but it is limited to the size of optical access window and the later stages of flame kernel development could not be observed. On the contrary, the method using pressure rise can study the later stages of flame kernel development, but it is not well suited for studying the very early flame kernel development during which the pressure rise is small and its detection is hindered with effects of shock wave from the spark discharge. But usually, as it is in Fig. A.4(a), there exist some time where the results form both methods overlap, and then one can see the results from the Schlieren imaging agree well with those derived from the pressure rise for all three mixtures. Comparison of flame kernel development with other's work is presented in Fig. A.4(b). Presented in this figure are measurements of Haq (1998) performed in the same bomb for the same initial conditions. The difference between the present data may be attributed to the data post-processing employed by Haq where an attempt was made to deduce the position of 305 *K* isotherm from the film. This post-processing systematically increased flame radius compared with the directly observed value. In spite of that, the results of present work still agree quite well with the results of Haq (1998).

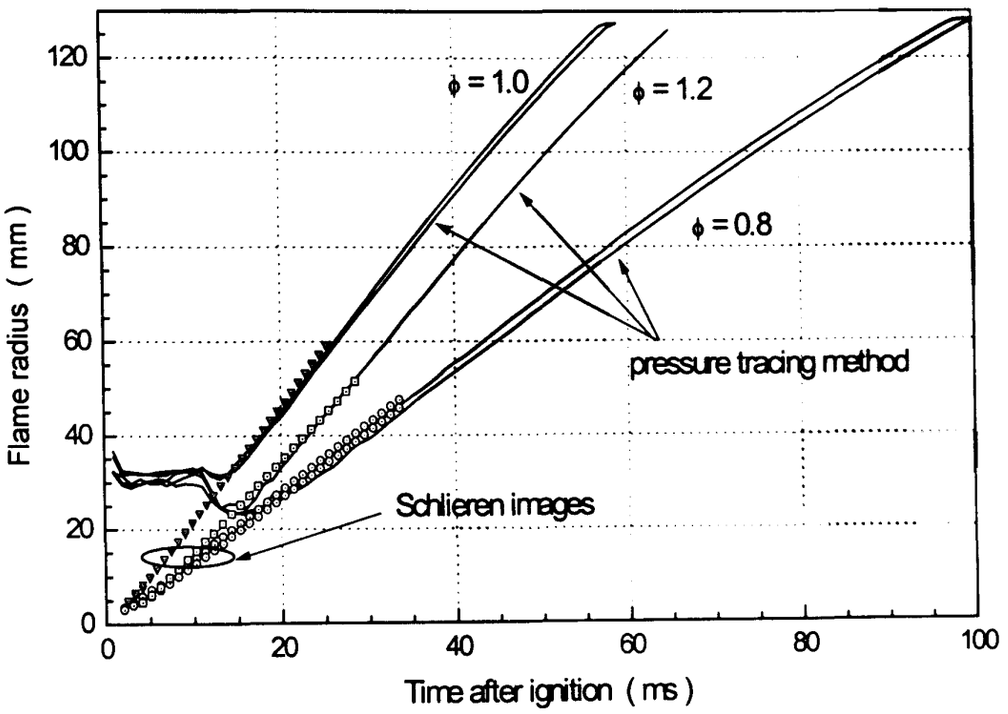

Fig. A.4(a) Flame radius determined by Schlieren image and by pressure history

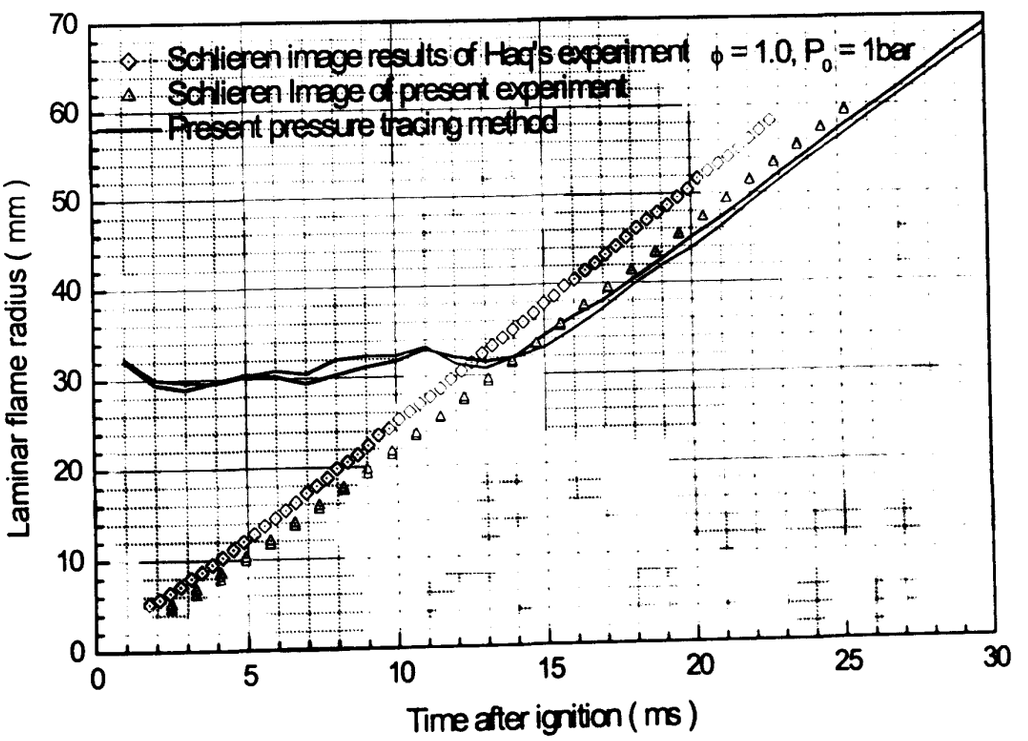

Fig. A.4(b) Comparison of flame radius with other works

Fig. A.4 Laminar flame radius

Inferred from these flame radii burning velocities are shown in Fig. A.5. In this figure burning velocities for the three mixtures are presented. The results of burning velocity determined by pressure rise includes the effects of flame curvature and stretch. Following Bradley *et al.* (1998), the unstretched laminar burning velocities u_L determined from Schlieren images are 22.83 *cm/s* for $\phi = 0.8$, 34.21 *cm/s* for $\phi = 1.0$ and 27.93 *cm/s* for $\phi = 1.2$. These values are within the variation of reported values of laminar burning velocity reviewed by Gu *et al.* (2000).

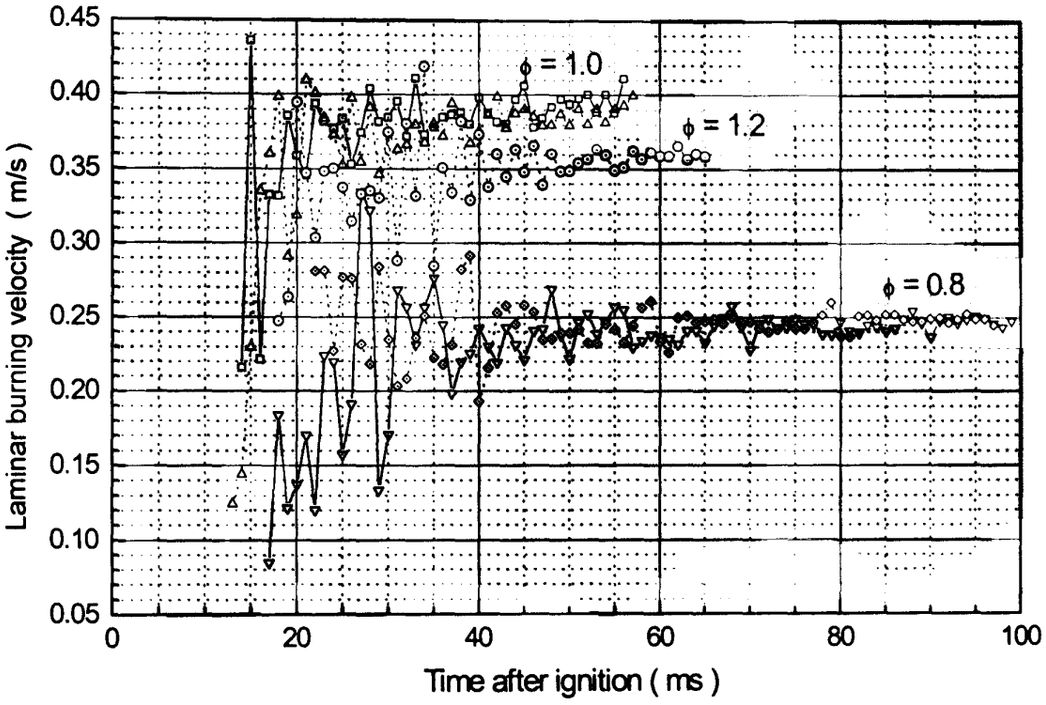

Fig. A.5 Laminar burning velocities determined by pressure histories

A.4.2 Turbulent Flame Propagation

Turbulent explosions were studied for the same three mixtures, lean (ϕ = 0.8), stoichiometric and rich (ϕ = 1.2). The turbulence intensities for stoichiometric, lean and rich mixture were 9.52 *m/s*, 4.76 *m/s* and 2.76 *m/s*. However, turbulence intensity of 9.52 *m/s* for lean mixture and 4.76 *m/s* for rich mixture were tried but the mixture could not be ignited.

Pressure signals after application of the low bandwith pass filter are shown in Fig. A.6(a), (b) and (c) for stoichiometric, lean and rich mixture at different turbulence intensities. As it can been seen in these figures, there exists a long initial period during which the pressure rise is quite small, or cannot be discerned within the hysterisis effects discussed above, after that period pressure rise is visibly much faster. This long initial period is particularly pronounced for stronger turbulence, for example, for ϕ=1.0, $u'=9.52\,m/s$, for ϕ=0.8, $u'=4.76\,m/s$, the initial period shown in Fig. A6(a) and (b) lasts more than half of the total explosion duration.

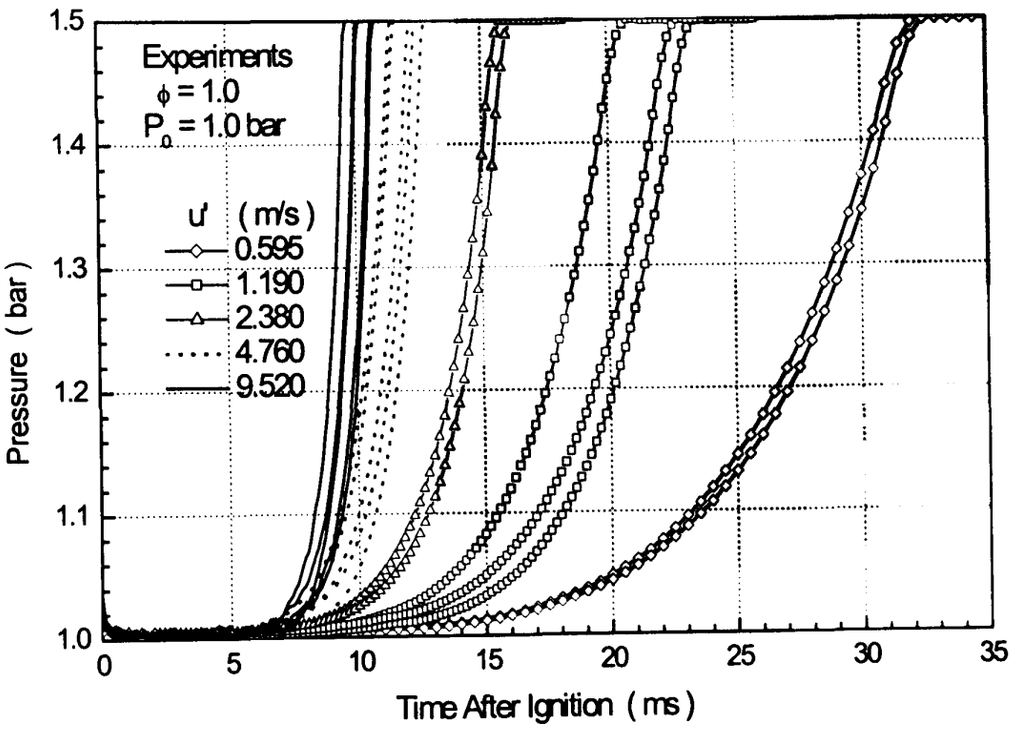

Fig. A.6(a) Pressure histories of turbulent flame propagation for different turbulent intensities at ϕ= 1.0, P_0= 1.0 *bar*, T_0= 300 *K*

Fig. A.6 Pressure histories of turbulent flame propagation

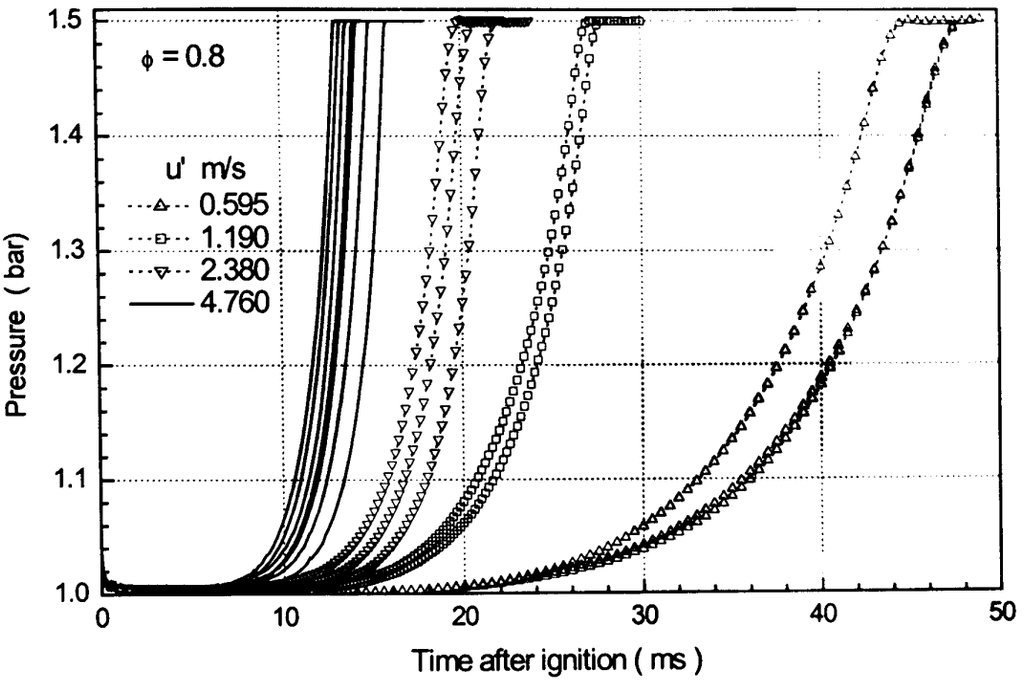

Fig. A.6(b) Pressure histories of turbulent flame propagation for different turbulent intensities at $\phi = 0.8$, $P_0 = 1.0$ *bar*, $T_0 = 300$ *K*

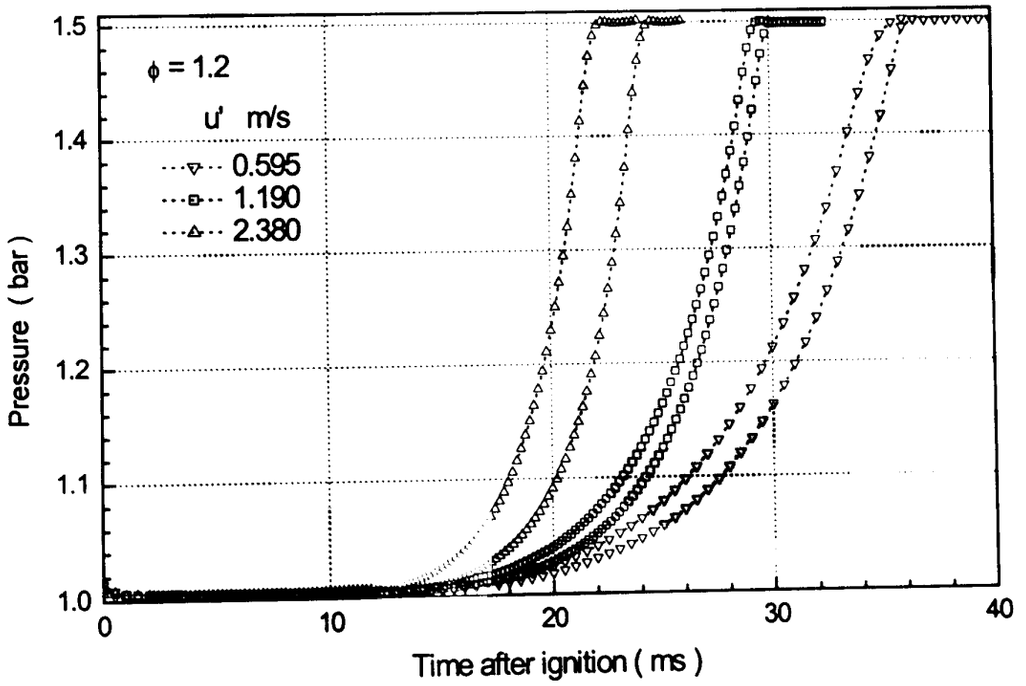

Fig. A.6(c) Pressure histories of turbulent flame propagation for different turbulent intensities at $\phi = 1.2$, $P_0 = 1.0$ *bar*, $T_0 = 300$ *K*

Fig. A.6 Pressure histories of turbulent flame propagation

It has to be noticed that Carmen *et al.* (1998) used Monte Carlo method to study the turbulence effects on the early phase of ignition and found that there existed laminar portion during turbulent flame propagation, and the duration of the laminar portion was approximately 2.5 *ms* and it was not sensitive to turbulence intensity as shown in Fig. A.7. This results clearly contradicts observations of Fig. A.6.

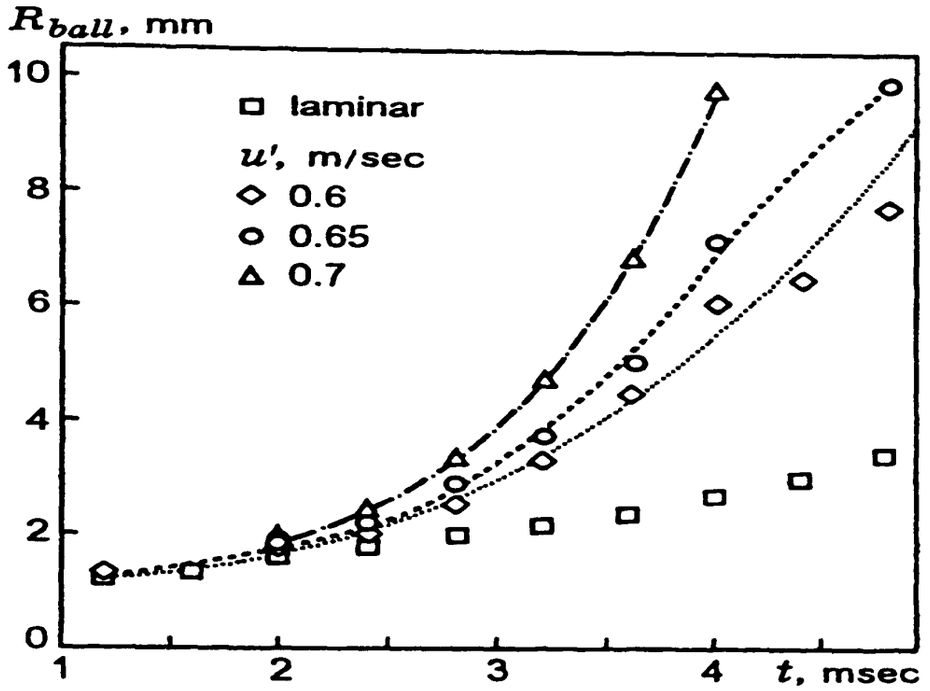

Fig. A.7 "Laminar period" during turbulent flame propagation, Carmen *et al.* (1998)

The pressure signals shown in these figures also reveal a phenomena similar to SI engine run-to-run variations. This SI engine run-to-run variations subsequently can be seen in turbulent flame radius and mass burning velocities development derived from the pressure signal, shown in Figs. A.8 to A.11. For lower turbulence intensities, scatter in temporal development of mass burning velocity is visibly less than that for stronger turbulence. It is interesting to note that the curves of burning velocity *vs* flame radius exhibit much less scatter than the curves of burning velocity *vs* time for the same set of conditions. This leads to a conclusion, that similar to an engine, these run-to-run variations are provoked by the different local instantaneous conditions at the instant of the spark discharge. However, the insufficient experimental data preclude any quantitative conclusions to be drawn.

Pressure signals were processed similarly to the laminar flame explosions, obviously, the meaning of flame radius so obtained for turbulent explosions is different and its direct comparison with *e.g.* Schlieren image size would be impossible without making some additional hypothesis. Indeed, the flame radius derived from pressure signal in turbulent explosion may be understood as a radius of some imaginary sphere filled with combustion products (of which the composition and temperature are at thermodynamic equilibrium) which would create the same pressure rise as the observed one. If one assumes that a laminar flame thickness is zero, then, at the same pressure rise, the flame radii derived from pressure are equal in turbulent and laminar explosion, and the following formula:

$$\frac{u_t}{u_n} = \frac{(dp/dt)_{turb}}{(dp/dt)_{lam}}\bigg|_{\Delta P} \qquad (A.4)$$

is a convenient measure of mass burning rate in turbulent combustion in a closed vessel. Indeed, this definition of turbulent burning velocity was adopted in works of Checkel *et al.* (1994), Nakahara and Kido (1998). Comparison of different ways calculating turbulent burning velocity is not the objective of this thesis, so it is limited to employing only Lewis and von Elbe procedure adopted in both laminar and turbulent situations. The last thing to note in this connection is that both Eq. (A.4) and the present procedure should yield identical values for turbulent burning velocity, once all other thermodynamical parameters are taken the same.

Shown in Figs. A.8(a) to A.8(c) are flame radii derived by Eq. (A.1a) based on pressure records for different mixtures with various turbulence intensities. One can notice a substantial deviation of the curves from the straight lines, which indicate non-constant burning velocity. Also, in Fig. A.8(d), a comparison is represented with the flame radii obtained with the same rig but with planar Mie scattering (PMS) by Haq (1998).

Once the flame radius is found, turbulent mass burning rate may be found with Eq. (A.1), the values obtained are shown in Figs. A.9, A.10 and A.11. For the same mixture, two graphs are presented, one is burning velocity *vs.* time, the other one is burning velocity as a function of flame radius. It can be seen that the scatter between different explosions is greatly reduced when burning velocity is expressed in terms of flame

radius, especially for stronger turbulence. There exists a long initial period where turbulent flame propagation is very slow, especially at high turbulent intensity, during this period no reliable measurement of turbulent burning velocity can be done with the present apparatus. After that period turbulent flame propagates much faster and burning velocity seems to increase nearly linearly with time or flame radius.

Finally, turbulent burning velocity is compared with two models, one is KLe correlation of Abdel-Gayed and Bradley *et al.* (1987), the other one is due to Zimont (1979) and Lipatinikov *et al.* (2000). Further discussion of these models is presented in *Chapter 4*. This comparison is shown in Fig. A.12. The two models give the same trends, however, they yield faster turbulent flames in early stages and slower in the later stages.

Several reports about turbulent burning velocity measurements are available in the literature, *e.g.* Karpov *et al.* (1980) and Nakahara and Kido (1998). Karpov *et al.* (1980) measured turbulent burning velocity for the flame radius at the interval of 15 $mm \leq r \leq 45$ *mm* where the best fit linear approximation was obtained and pressure rise was in the range of $1.005 \leq P(t)/P_{ini} \leq 1.16$. The combustion vessel volume they used was 3800 cm^3, so for the same pressure range the flame radius in present study is in the range of 25 $mm \leq r \leq$ 95 *mm*. However, the values of turbulent burning velocity reported there are substantially lower than obtained in the present work. For example, for stoichiometric mixture at $u' = 4.76$ *m/s*, $\phi = 1.0$ and 0.8, at $u' = 2.38$ *m/s*, $\phi = 1.2$, Karpov *et al.* (1980) reported turbulent burning velocities are 1.32, 0.6, and 1.0 *m/s*, while, present work gives the values growing up from 0 to 4.0±0.5, 2.2±0.5 and 2.0±0.3 *m/s*. Similarly, present work gives much higher values than those given by Nakahara and Kido (1998). Such difference persists over the whole range of equivalence ratios and turbulence intensities, and the reasons for this are not entirely clear at this moment. Several physical mechanisms may be responsible for this transient behaviour, such as different turbulent length scales, flame curvature, etc, for more details one can refer to Lipanikov and Chomiak (2000).

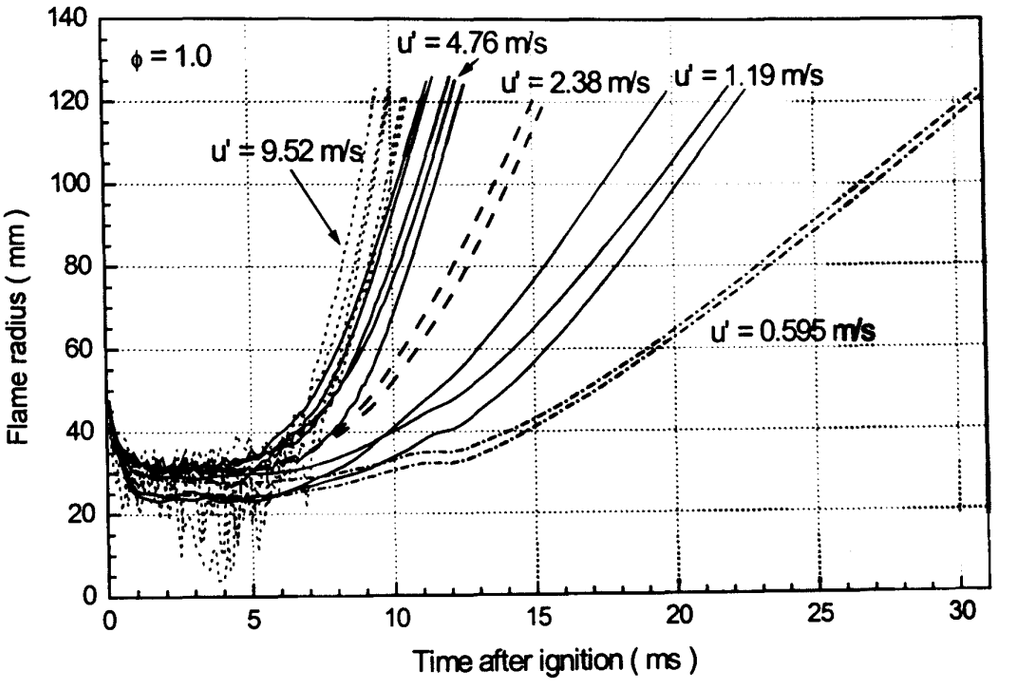

Fig. A.8(a) Flame radius for turbulent flame propagation

for $\phi = 1.0$, $T_0 = 300\ K$, $P_0 = 1.0\ bar$

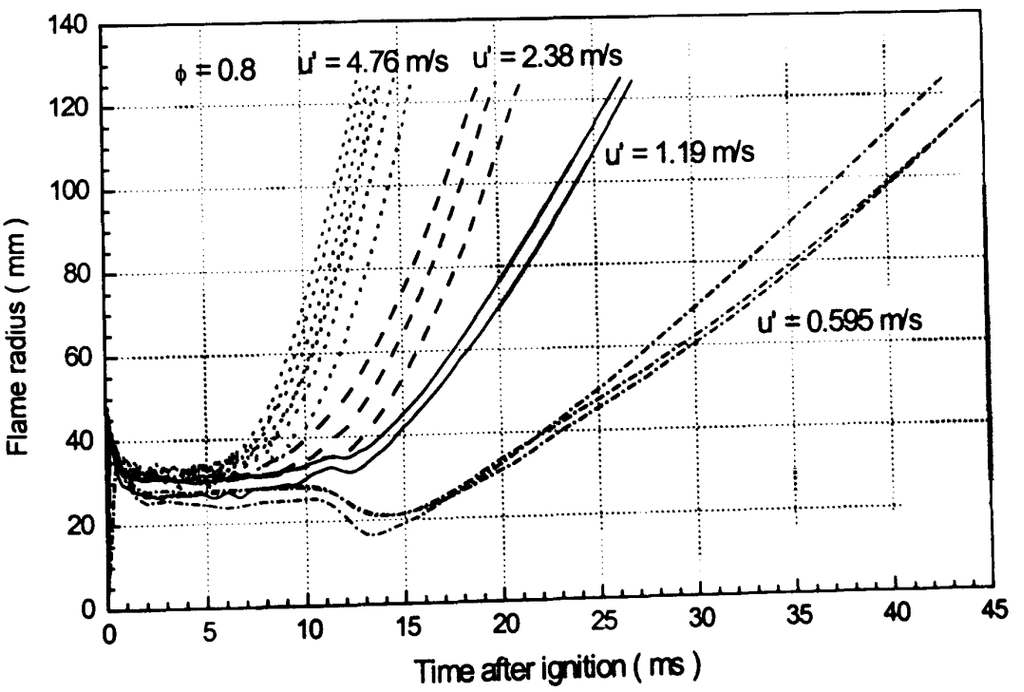

Fig. A.8(b) Flame radius for turbulent flame propagation

for $\phi = 0.8$, $T_0 = 300\ K$, $P_0 = 1.0\ bar$

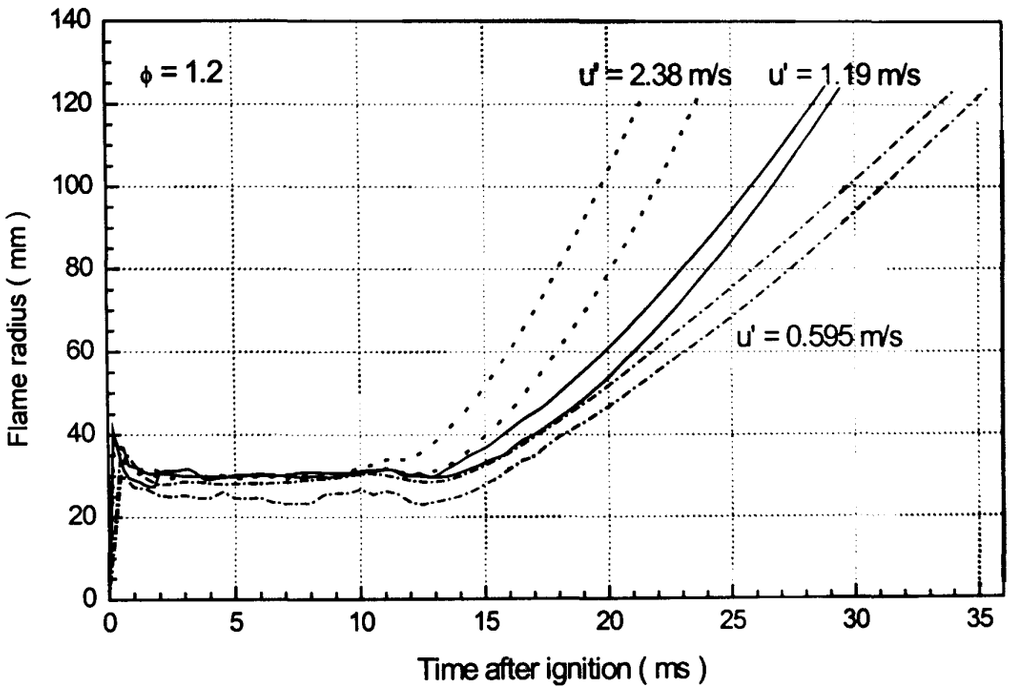

Fig. A.8(c) Flame radius for turbulent flame propagation for $\phi = 1.2$, $T_0 = 300\ K$, $P_0 = 1.0\ bar$

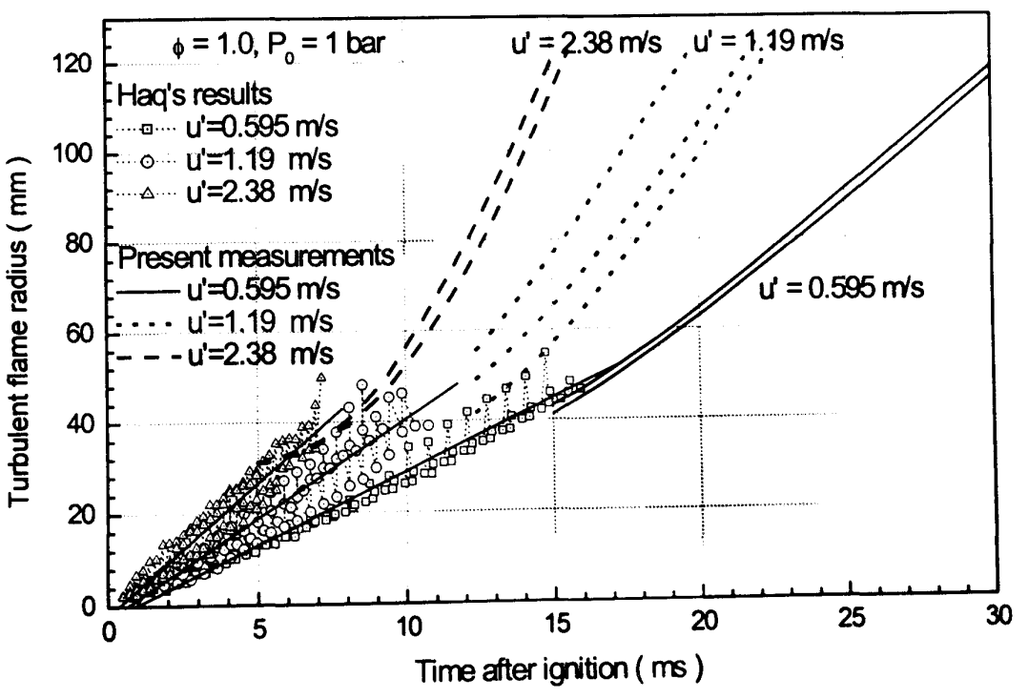

Fig. A.8(d) Comparison of flame radius with experiments of Haq (1998) for turbulent flame propagation for $\phi = 1.0$, $T_0 = 300\ K$, $P_0 = 1.0\ bar$

Fig. A.8 Turbulent flame radius for various mixtures at $T_0 = 300\ K$, $P_0 = 1.0\ bar$

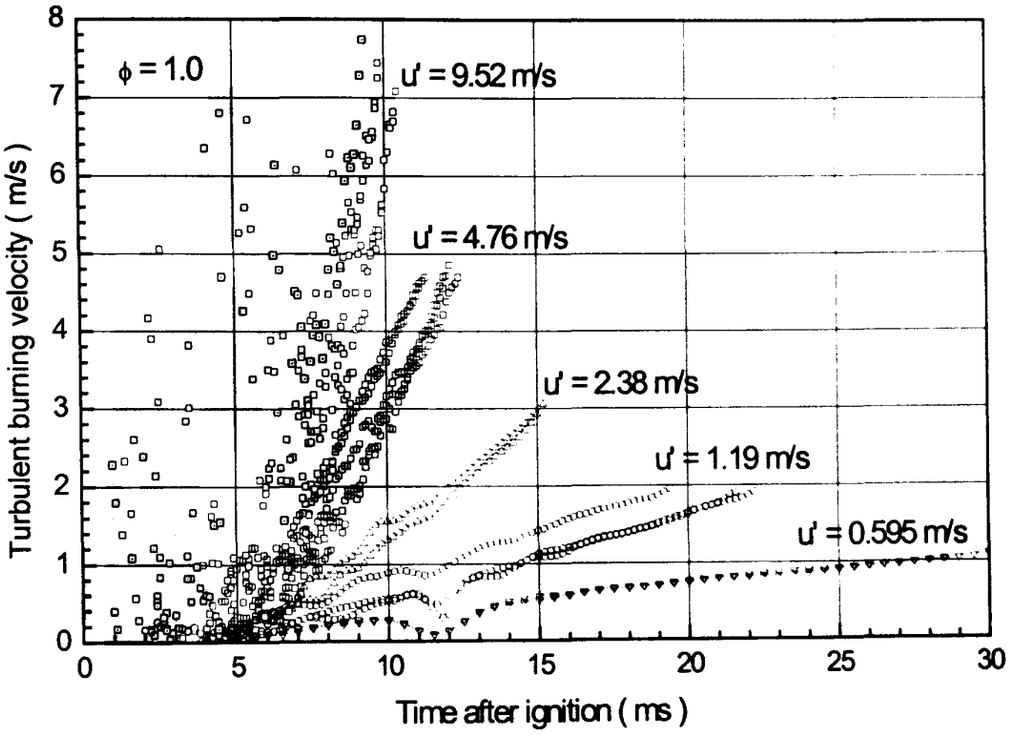

Fig. A.9(a) Turbulent burning velocities *vs.* time

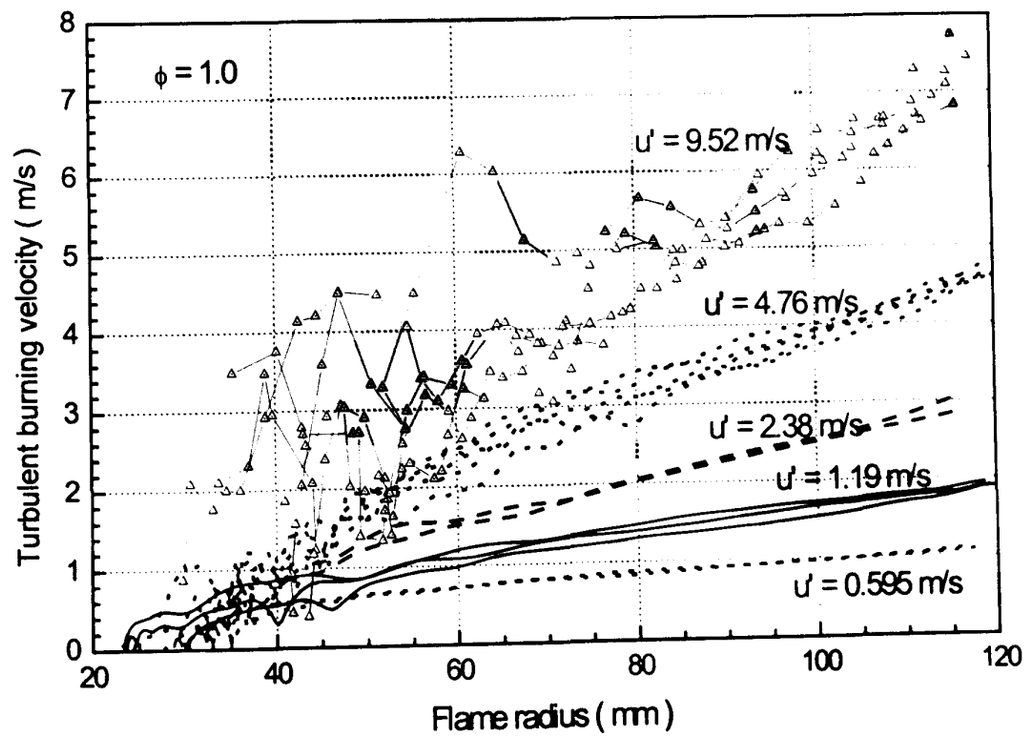

Fig. A.9(b) Turbulent burning velocities *vs.* flame radius

Fig. A.9 Turbulent burning velocities for $\phi = 1.0$, $T_0 = 300\ K$, $P_0 = 1.0\ bar$

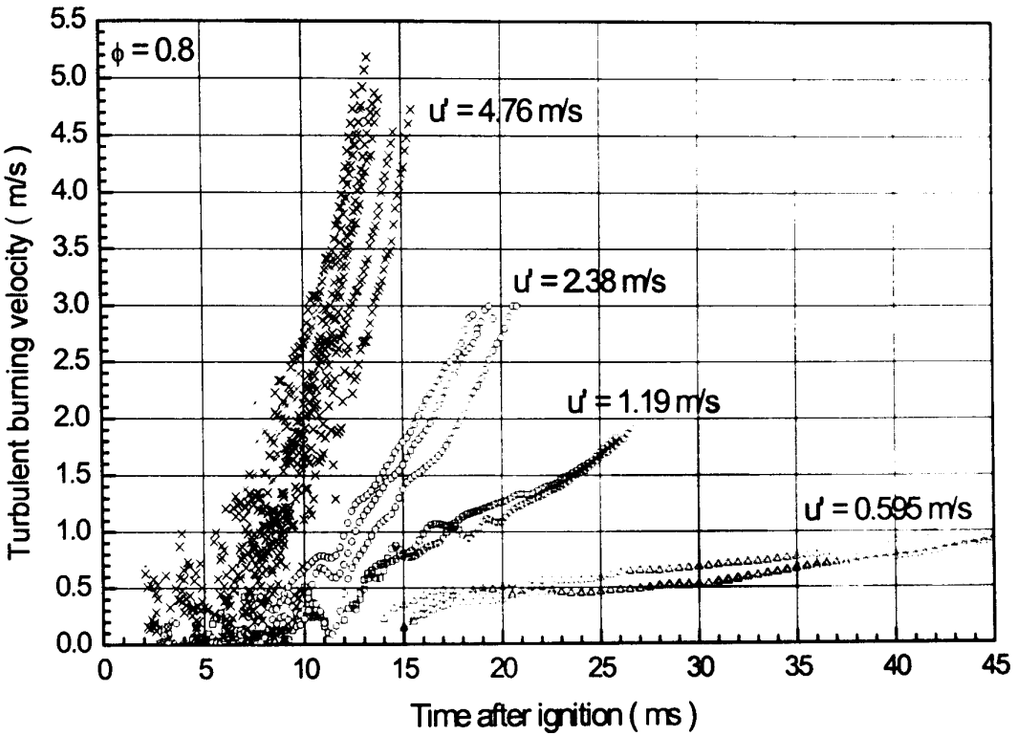

Fig. A.10(a) Turbulent burning velocities *vs.* time

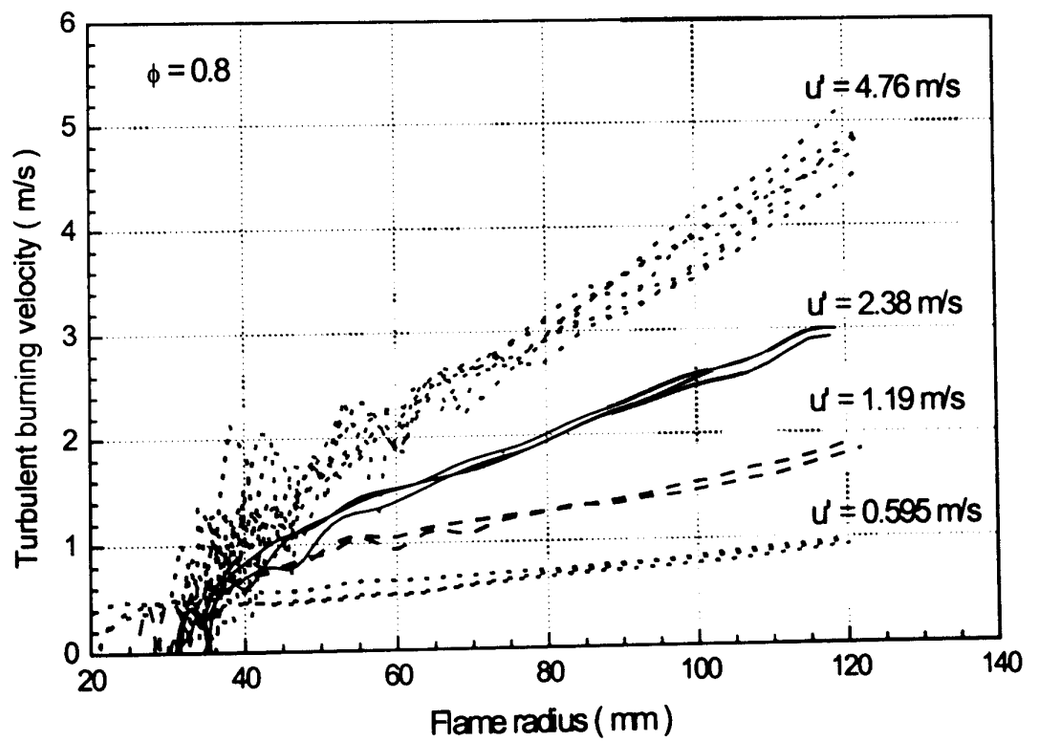

Fig. A.10(b) Turbulent burning velocities *vs.* flame radius

Fig. A.10 Turbulent burning velocities for ϕ = 0.8, T_0 = 300 *K*, P_0 = 1.0 *bar*

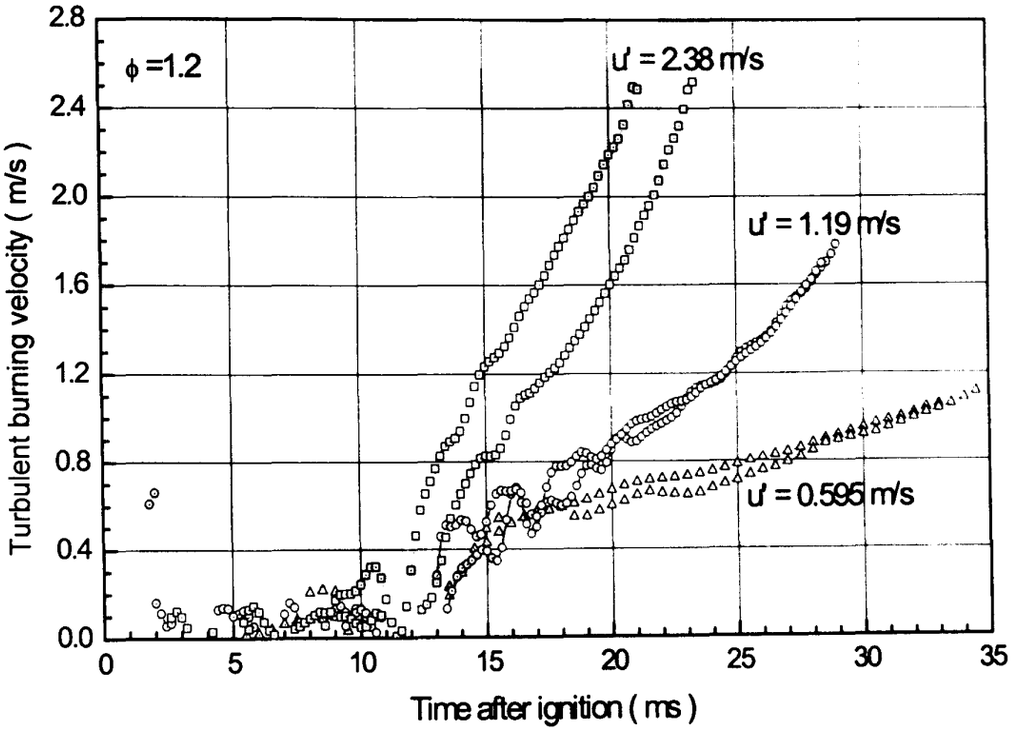

Fig. A.11(a) Turbulent burning velocities *vs.* time

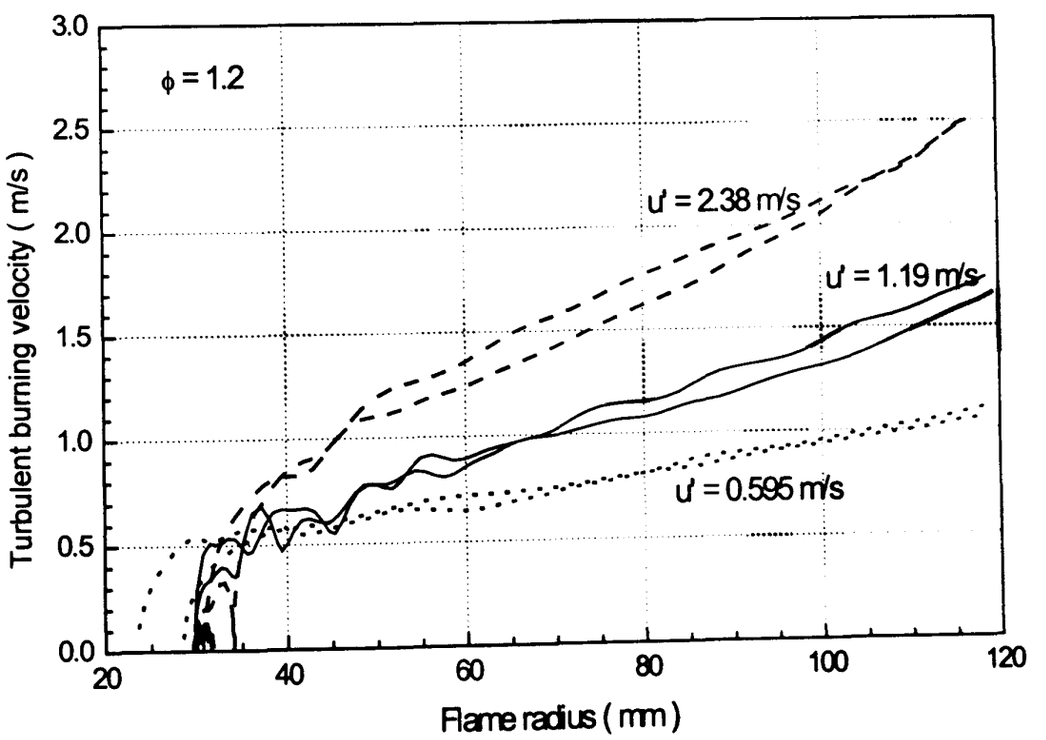

Fig. A.11(b) Turbulent burning velocities *vs.* flame radius

Fig. A.11 Turbulent burning velocities for $\phi = 1.2$, $T_0 = 300\ K$, $P_0 = 1.0\ bar$

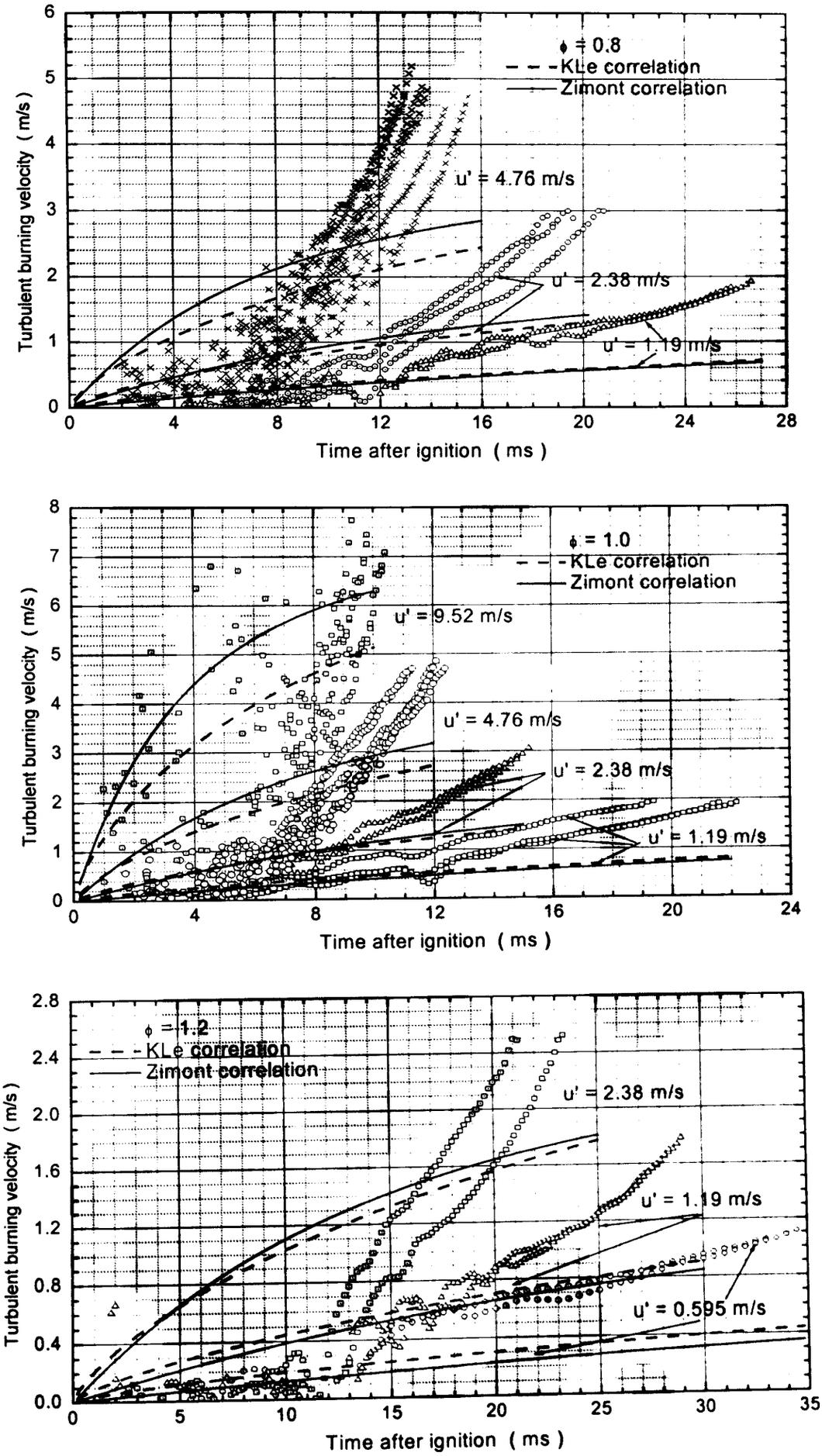

Fig. A.12 Comparisons of experimental results with models of Bradley & co-workers and Lipatnikov-Zimont

Appendix B

Determination of Pressure During Explosion

Consider a spherical bomb of radius R_b, initially filled with a gaseous mixture of mass m. The mass contained in the element of volume between r and r+dr, as shown in Fig. B.1, is $\rho(r)4\pi r^2 dr$, where $\rho(r)$ is the gas density at radius r. Then the total mass within the bomb can be obtained by integration of the masses elements of volume:

$$m = \int_0^{R_b} \rho(r)\, 4\pi r^2 dr \tag{B.1}$$

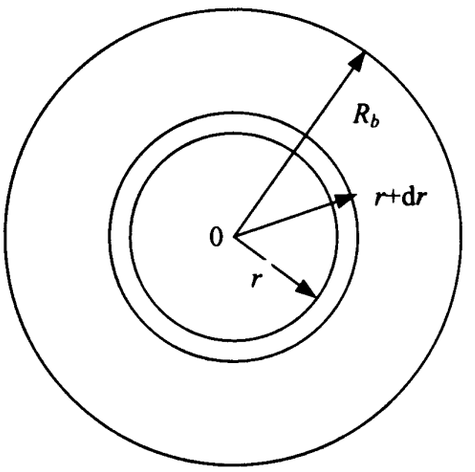

Fig.B.1 Illustration of determination of pressure in the bomb

The mass inside the bomb is a conservative variable, it does not change with time. If both sides of Eq. (B.1) are differentiated with respect to time, then

$$\frac{dm}{dt} = \frac{d}{dt}\left(\int_0^{R_b} \rho(r)4\pi r^2 dr \right) = \int_0^{R_b} \frac{d\left(\rho(r)4\pi r^2\right)}{dt} dr = \int_0^{R_b} \frac{d\,\rho(r)}{dt} 4\pi r^2 dr = 0 \tag{B.2}$$

$d\rho(r)/dt$ may then be expressed by finite differences as:

$$\frac{d\,\rho(r)}{dt} = \frac{\rho^{n+1}(r) - \rho^n(r)}{\Delta t} \tag{B.3}$$

where $n+1$ and n are the two consecutive time instants. Density of instant $n+1$ $\rho^{n+1}(r)$ can be found from:

$$\rho^{n+1}(r)=\frac{P^{n+1}}{R_u T^{n+1}(r)} W_{mix}^{n+1} \tag{B.4}$$

Where R_u is universal gas constant, W_{mix}^{n+1} is the mixture molecular weight.

Substituting $d\rho(r)/dt$ from Eq. (B.3) and $\rho^{n+1}(r)$ from Eq. (B.4), one can get, after some arrangement, the following expression:

$$\int_0^{R_b}\left(\frac{P^{n+1}}{R_u T^{n+1}(r)} W_{mix}^{n+1}\right) 4\pi r^2 dr = \int_0^{R_b} \rho^n(r) 4\pi r^2 dr \tag{B.5}$$

If the pressure is uniform, P^{n+1} is independent of radius, one can finally obtain:

$$\begin{aligned} P^{n+1} &= \frac{\int_0^{R_b} \rho^n(r) r^2 dr}{\int_0^{R_b}\left(\frac{1}{R_u T^{n+1}(r)} W_{mix}^{n+1}\right) r^2 dr} \\ &= \frac{mR_u}{4\pi \int_0^{R_b}\left(\frac{1}{T^{n+1}(r)} W_{mix}^{n+1}\right) r^2 dr} \end{aligned} \tag{B.6}$$

Appendix C

Simulation of Spark Ignition

One may assume that the spark action is equivalent to an instantaneous creation of a flame kernel filled up with adiabatically equilibrium combustion products. The radius of this initial flame kernel, usually of order of a few millimeters, is somewhat arbitrary. In the present work this has been used and initial flame size is put to $r_0 = 2\ mm$.

However, the spark action may also be represented as a deposit of a certain amount of the thermal energy within given time, thus allowing development of chemical reactions at their own pace. This method is probably somewhat more realistic and it has been used in, *e.g.* Vincent *et al.* (1996) and Carmen (1998). The exact amount of heat released by the spark is related to the nominal electrical energy of the spark, usually varying between 1 to 100 *mJ*, and the spark "efficiency", usually of order of a few percent, see Vincent *et al.* (1996) for more details. Also, the energy deposit is not necessarily instantaneous, and may follow some prescribed dependency on time.

In the present work, following source term in the equation for RSF of temperature has been added to describe the spark effects:

$$q(r,t) = A e^{-t/t_0} e^{-(r/r_0)^2} \qquad \text{(C.1)}$$

The purpose of the present appendix is to compare the results obtained with use of Eq. (C.1) and the method where flame is initiated with a hot spot of adiabatic combustion products.

For practical application, the parameters in Eq. (C.1) have to be chosen to correspond to the spark used in the measurements: that is the spark plug gap of $r_0 = 1\ mm$, and the time of electrical energy of discharge $t_0 = 1\ ms$. To obtain the full discharge energy, one needs to integrate Eq. (C.1) with respect to time and space obtaining :

$$e = \int_0^{t_0} \int_0^{r_0} q(r,t) 4\pi r^2 \rho C_p \, dr dt \qquad \text{(C.2)}$$

It has been found that mixture could not be ignited if spark discharge energy is smaller than 4 *mJ*.

The results of calculations are shown in Figs. C.1 and C.2. Shown in Fig. C.1 is the pressure and flame radius obtained with different spark energies of 10, 5 and 4 *mJ* for stiochiometric laminar flame at 1.0 *bar*, 300 *K*. Presented in Fig. C.2 are the pressure, turbulent burning velocity and flame radius for turbulent lean mixture ($\phi = 0.8$), turbulence intensity $u' = 1$ *m/s*, initial pressure and temperature are 1.0 *bar* and 358 *K*, respectively, with different spark energies of 4, 8, 16 *mJ*. The results shows that the initially flame propagation is faster for higher spark energy, while the difference disappears soon afterwards. Hence variation in spark energy can only affect the initial period of combustion, after which, combustion is independent on spark energy. This conclusion is in agreement with the computational study of Bradley *et al.* (1996b) for methane/air flame, as well as with the measurements of Bradley *et al.* (1998).

Similar comparison is shown in Figs. C.3 and C.4 for the stoichiometric mixtures, parameters of calculations being: Fig. C.3, $r_0 = 2$ *mm* of "hot spot", spark energy $e = 10$ *mJ* in Eq. (D.2) ; Fig. C.4 the same spark characteristics, turbulence intensities being $u' = 2.38$ and 9.52 *m/s*. The comparison shows that the two methods to initiate flame agree quite well; even for stronger turbulence, after some short initial period, the method chosen to initiate combustion does not affect the results.

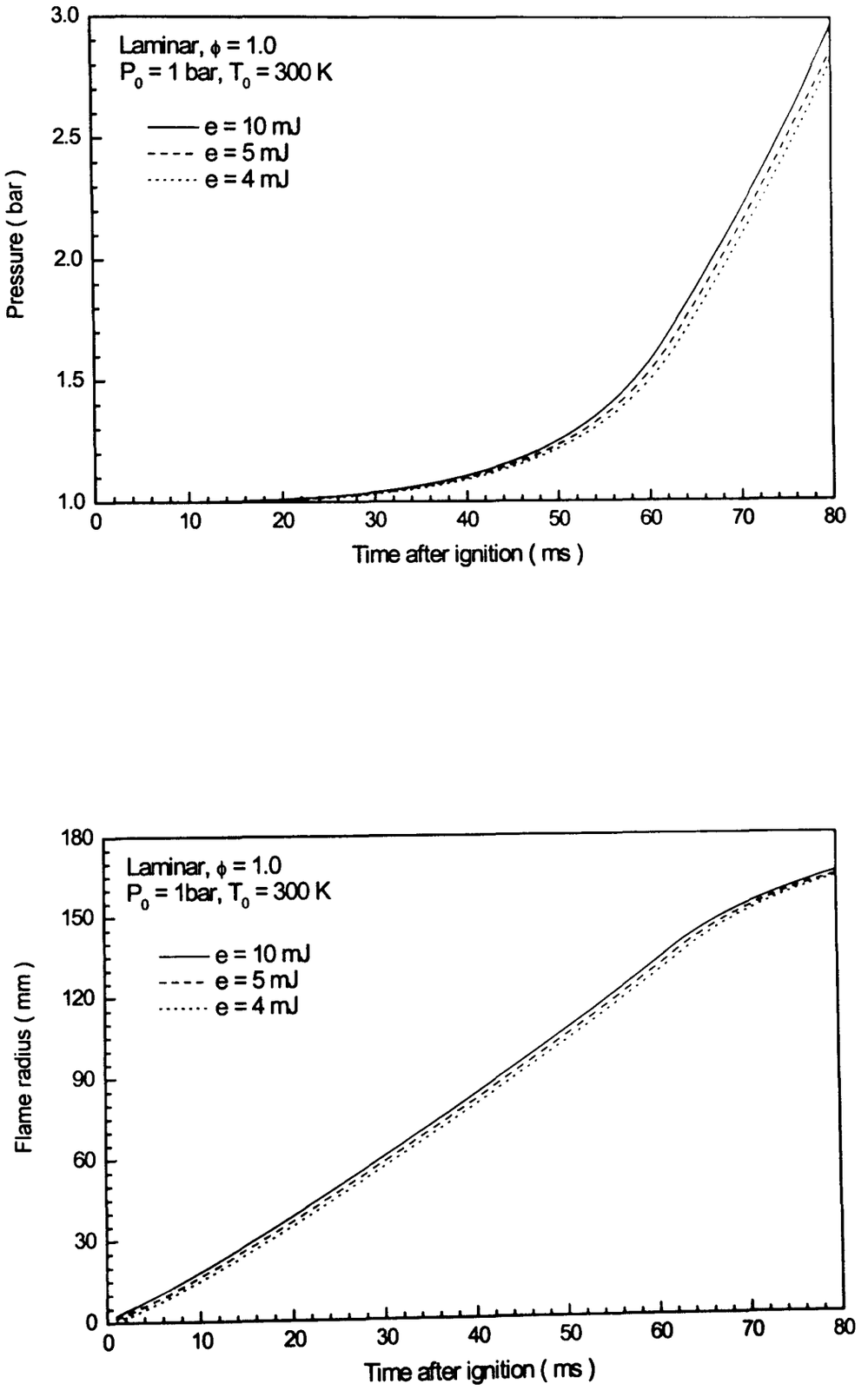

Fig. C.1 Effect of spark energy on laminar flame propagation

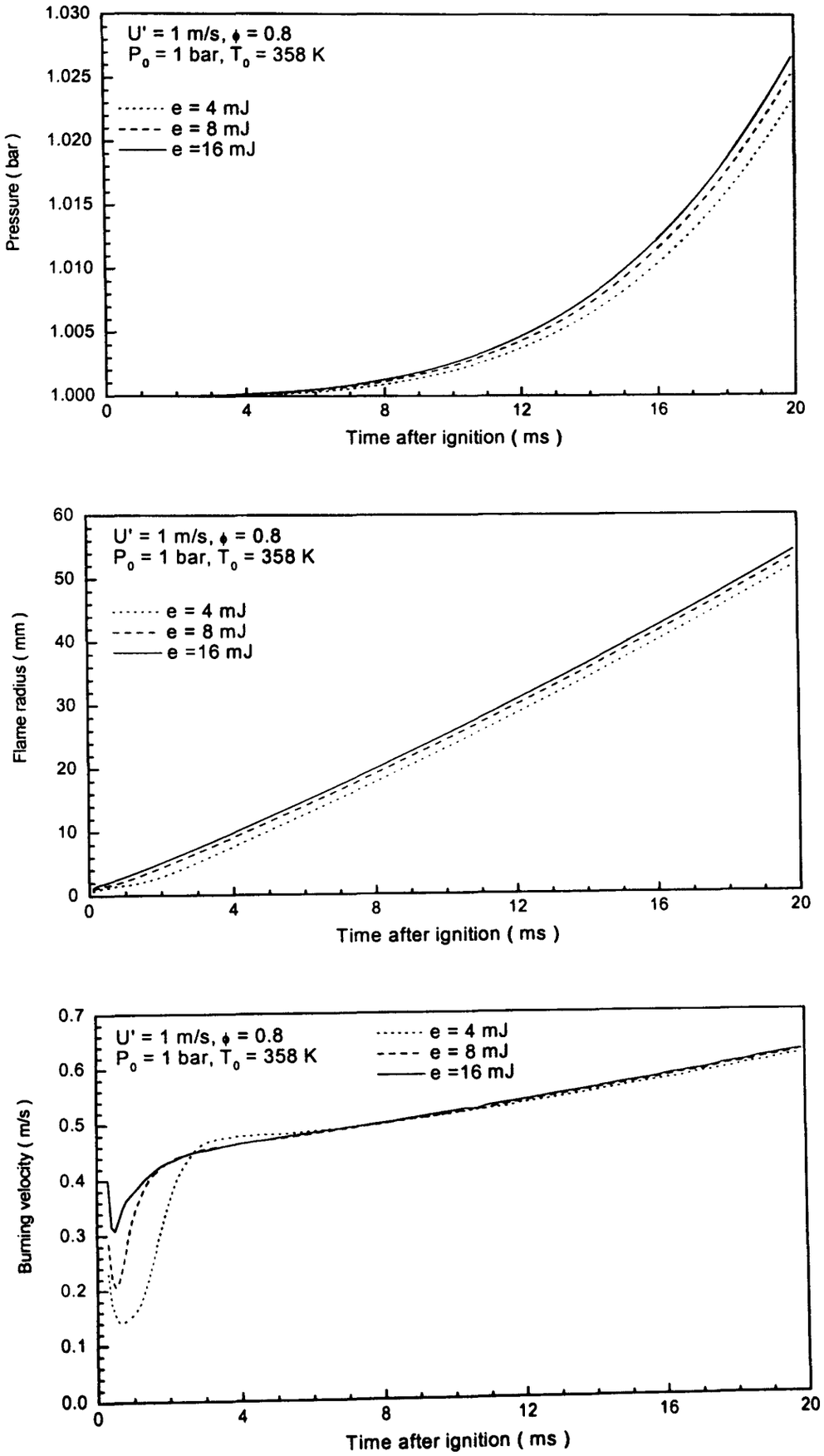

Fig. C.2 Effect of spark energy on turbluent flame propagation

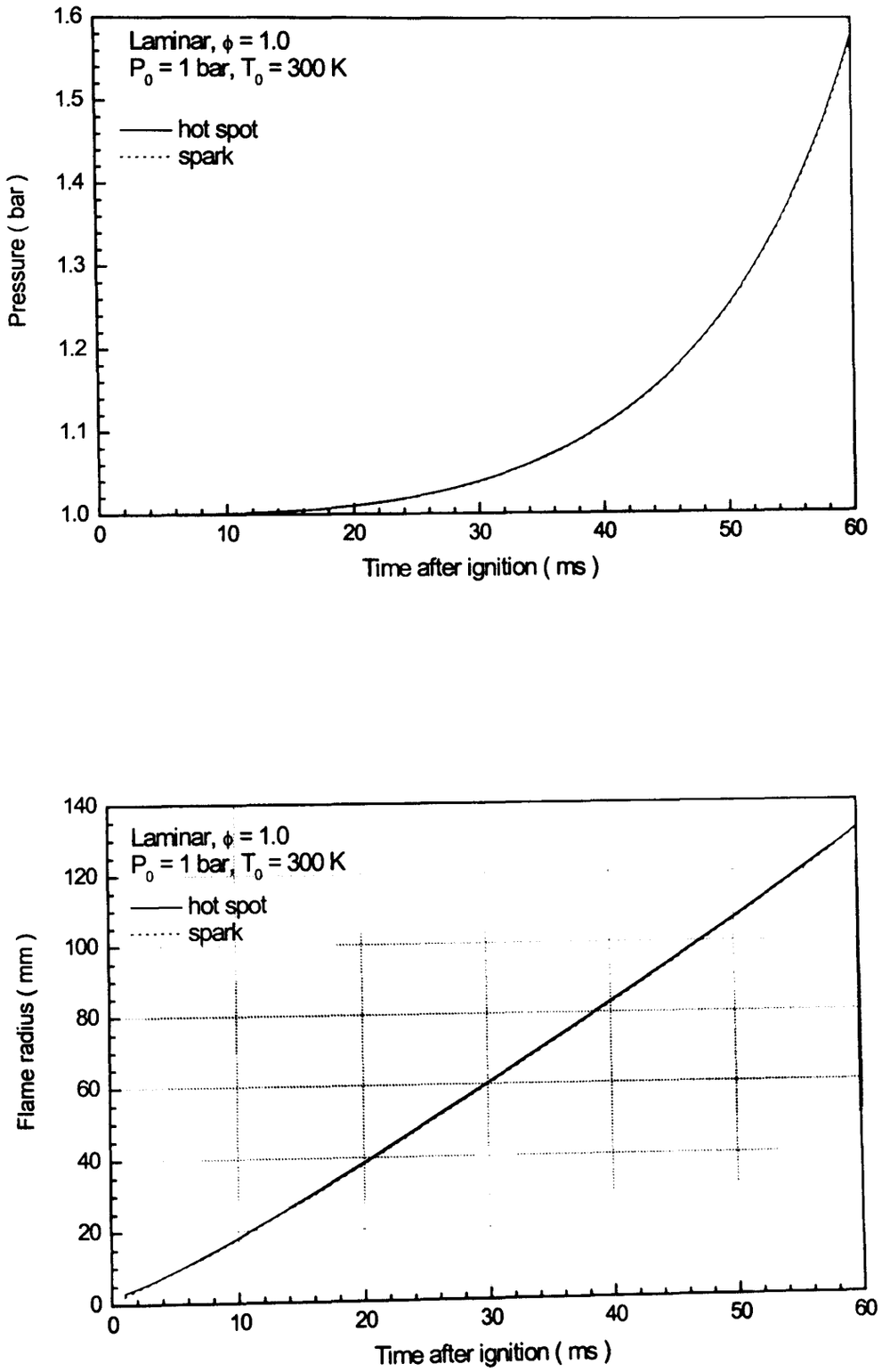

Fig. C.3 Comparison of flame initiated by hot spot and spark for laminar flame

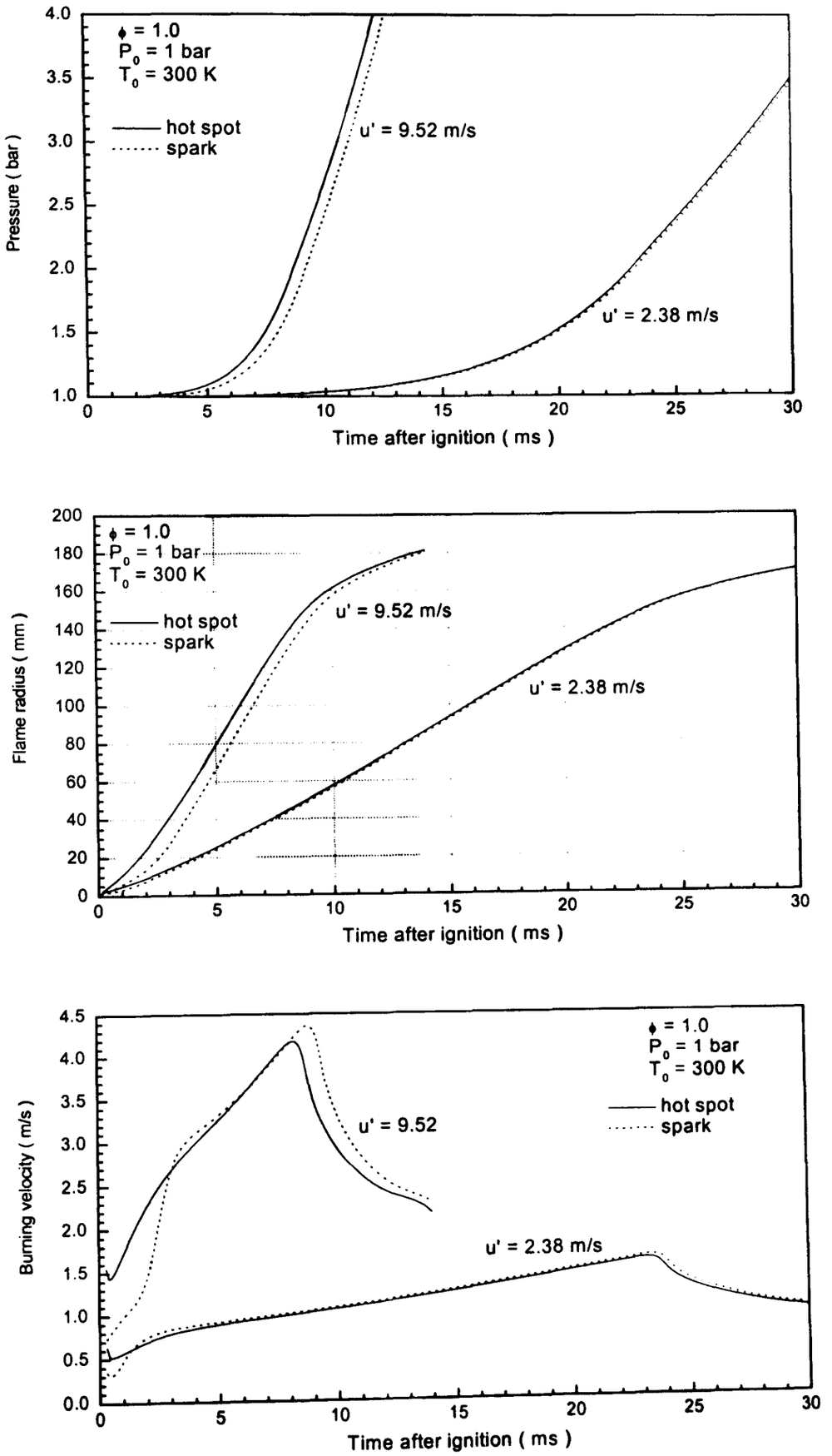

Fig. C.4 Comparison of flame initiated by hot spot and spark for turbulent flame

Appendix D

Effects of Molecular Diffusivity Modelling

For the simulations of laminar flame propagation in *Chapter 2*, the molecular diffisivity considered there was assumed to depend only on temperature. Also all the species were assumed to have the same diffusivity, *i.e.* all Lewis numbers equal to one. Temperature dependency of the molecular diffusivity is given by Eq. (2.22), and it has been found that laminar burning velocity obtained with use of Eq. (2.22) was not steady but the flame accelerated with time, see the dashed line in Fig. D.1. The reason for this is that Eq. (2.22) overestimated the molecular diffisivity by neglecting the very important parameter: pressure. According to Reid *et al.* (1977) molecular diffisivity has the dependency of $1/P$ with pressure. With flame size growth pressure inside the bomb increases and molecular diffusivity decreases. As it is well-known laminar burning velocity is sensitive to transport properties of the mixture.

By this reason, it was found necessary to employ more realistic calculations of heat and mass diffusivities using the formulae from the compilation of Reid *et al.* (1977) as described in *Appendix E*. Presented in Fig. D.1 is the comparison of how different calculations of molecular diffusivity affect the burning velocity.

In this figure the curves labelled "Model 1" are obtained with use of Eq. (2.22); it has to be stressed that all the calculations presented in *Chapter 2* employed it. The results obtained using much more accurate (and time consuming) dependencies are labelled "Model 2". Indeed, the difference between these two sets is quite large, moreover, the latter approach resulted in laminar flame speed first increasing, in line with the experimental observations, but decreasing after some period for the stoichiometric and rich mixture, contrary to the experiments. For the lean mixture, u_n attains a constant value of order of 18 *cm/s* which experiments produced $u_n \approx 23$ *cm/s*.

It has to be noticed that the discrepancy between the calculations of "Model 2" and measurements may be ascribed to deficiencies in the chemical kinetics. However, the

similar discrepancy between the measurements and calculations is observed for the DTBP flames for which the chemical kinetics details are unambiguous. This invokes the potentially very important question of the role of various flames instabilities and their contribution to the observed flame speed.

Even with this "real" diffusivity, much work still needed for this two-step kinetics, and it is left for the future work.

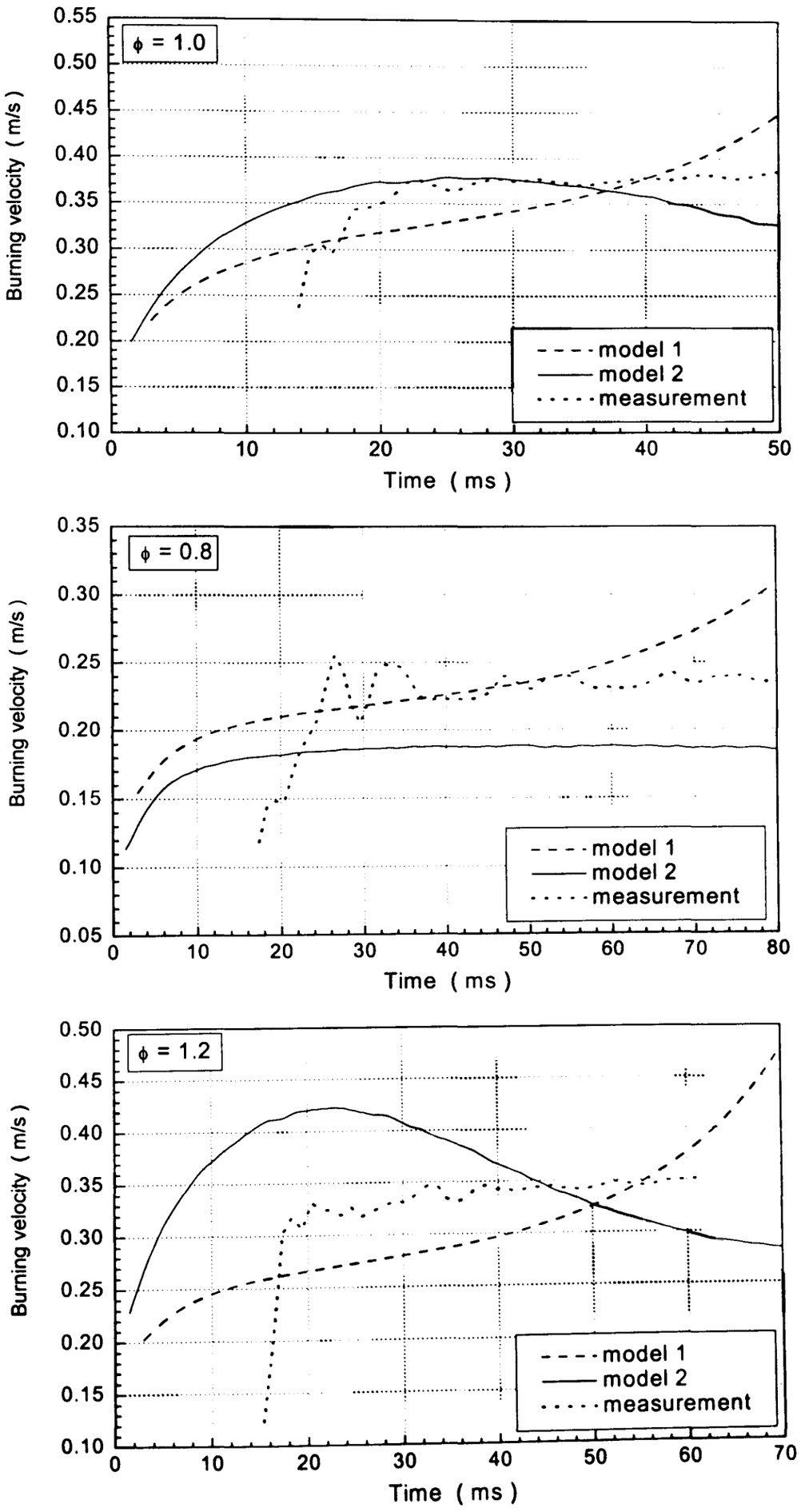

Fig. D.1 Effect of molecular diffusivity modelling on laminar burning velocity

Appendix E

Estimation of Molecular Transport Properties

E.1 Estimation of Mass Diffusivity

The theory describing mass diffusion in binary gas mixtures has been well established, for details one should refer to, *e.g.* Reid *et al.* (1977). Following is a brief description of the currently implemented calculations of mass diffusion coefficients. Binary mass diffusion D_{ij} is calculated as:

$$D_{ij} = \frac{10^{-3} T^{3/2} W_{ij} (2.14 - 0.49 W_{ij})}{P \sigma_{ij}^2 \Omega_{Dj}} \tag{E.1}$$

where

W:	Molecular weight, in *g/mole*
T:	Temperature, in K
P:	Pressure, in *atm*
Ω_D:	Diffusion collision integral, dimensionless
σ :	Characteristic collision cross-section, in $\dot{A}$

and

$$W_{ij} = \frac{W_i + W_j}{W_i W_j} \tag{E.2}$$

$$\sigma_{ij} = \frac{\sigma_i + \sigma_j}{2} \tag{E.3}$$

The key issue in Eq. (E.1) is the selection of an intermolecular force law for evaluation of Ω_D and σ. One of the most popular is the Lennard-Jones "12-6" (see Reid *et al.*, 1977) intermolecular force correlation. Based on this "12-6" intermolecular force law Ω_D is a function of kT/ε, where k is Boltzmann's constant, ε is Lennard energy so Ω_D can be calculated as:

$$\Omega_{Dj} = \sum_{n=1}^{6} f_{2,n} \left(1.4 + \ln\left(kT/\varepsilon_j \right) \right)^{n-3} \tag{E.4}$$

where the coefficients $f_{2,n}$ are listed in Table E.1.

Table E.1 Coefficients for $f_{2,n}$

$f_{2,1}$	$f_{2,2}$	$f_{2,3}$	$f_{2,4}$	$f_{2,5}$	$f_{2,6}$
-2.25768×10^{-2}	0.19779	-0.16845	0.64373	-9.26718×10^{-2}	7.1131×10^{-3}

The values of k/ε and σ for various materials can be found in Reid *et al.* (1977). However, for DTBP such data are not available in literature, so they have been estimated by Lydersen's method (see Reid *et al.*, 1977) as following.

The critical values of temperature T_c, pressure P_c and volume V_c can be determined by Lydersen's method as:

$$T_c = T_b\left(0.567 + \sum\Delta_T - \left(\sum\Delta_T\right)^2\right)^{-1} \tag{E.5}$$

$$P_c = W\left(0.34 + \sum\Delta_P\right)^{-2} \tag{E.6}$$

$$V_c = 40 + \sum\Delta_V \tag{E.7}$$

where T_b is boiling point at 1 *atm* and T_b = 384.3 *K* for DTBP from the measurement of Indritz *et al.* (1978), V_c is in $cm^2/g\text{-}mole$, Δ is group contributions and evaluated by summing contributions for various bonds, and for DTBP:

$$\Delta = 6(CH_3) + 2(C) + 2(O) \tag{E.8}$$

The values of Δ are listed in Table E.2.

Table. E.2 Contributions of Δ

	Δ_T	Δ_P	Δ_V
CH_3	0.02	0.227	55
C	0	0.21	41
O	0.021	0.16	20

The typical error of T_c from Lydersen's method does not usually exceed 2% but may be as high as 5% for compounds of higher molecular weight (>100), the relative error in estimation of P_c, V_c, equals approximately that of T_c (Reid *et al.*, 1977).

Once critical values for DTBP are found then k/ε and σ can be determined from the best correlation as:

$$\sigma\left(\frac{P_c}{T_c}\right)^{1/3} = 2.3551 - 0.087\omega \tag{E.9}$$

$$\varepsilon/kT_c = 0.7915 + 0.1693\omega \tag{E.10}$$

where ω is the acentric factor which can be evaluated as:

$$\omega = \frac{3}{7}\frac{T_b}{T_c - T_b}\log(P_c) - 1 \tag{E.11}$$

For DTBP this method yields $\omega = 0.4075$, $\sigma = 6.5319\,\dot{A}$, $\varepsilon/k = 470.34\,K$.

Obviously Eq. (E.1) results in self-diffusivity coefficient D_{ii} if $j = i$.

E.2 Estimation of Mixture Thermal Diffusivity

Mixture thermal conductivity can be calculated as:

$$\lambda_{mix} = \sum_{i=1}^{n} \frac{Y_i \lambda_i}{1 + \sum_{\substack{j=1 \\ j \neq i}}^{n} 1.065 f_j Y_j} \tag{E.12}$$

where

$$f_j = \frac{\left(1 + \left(\frac{\nu_i}{\nu_j}\right)^{1/2}\left(\frac{W_j}{W_i}\right)^{1/4}\right)^2}{2\left(2\left(1 + \frac{W_i}{W_j}\right)\right)^{1/2}} \tag{E.13}$$

and Y_i is mole fraction, ν is the pure substance dynamic viscosity, *g/cm-s*, estimated as:

$$\nu_i = \frac{2.67 \times 10^{-5}(W_i T)^{1/2}}{\sigma_i^2 \Omega_{vi}} \tag{E.14}$$

Ω_v is dimensionless collision integral which can be determined as:

$$\Omega_{vi} = \sum_{n=1}^{6} f_{1,n} \left(1.5 + \ln\left(Tk/\varepsilon_i\right)\right)^{n-3} \tag{E.15}$$

The coefficients $f_{1,n}$ in Eq. (E.15) are listed in Table E.3.

Table E.3 Coefficients for $f_{1,n}$

$f_{1,1}$	$f_{1,2}$	$f_{1,3}$	$f_{1,4}$	$f_{1,5}$	$f_{1,6}$
-5.08552×10^{-2}	0.3401	-0.40811	0.70375	-0.10699	7.62686×10^{-3}

In Eq. (E.12) λ_i is thermal conductivity for component i calculated as:

$$\lambda_i = 19.89 \frac{v_i}{W_i} \left(0.115 + 0.354 \frac{c_{pi}}{R_u}\right) \tag{E.16}$$

where c_p is constant pressure specific heat, R_u is universal gas constant.

So mixture thermal diffusivity is finally determined as:

$$\kappa = 4.18 \frac{\lambda_{mix} W_{mix}}{\rho c_{pmix}} \tag{E.17}$$

where κ is in cm^2/s.

The methods introduced above have been used to test the transport properties of N_2 for different temperatures and good agreement has been found with the measurements.

Reference

Abdel-Gayed, R.G., Al-Khishali, K.J. and Bradley, D., 1984, *Turbulent Burning Velocities and Flame Straining in Explosions*, Proc. R. Soc. Lond. A, Vol.391, pp.393-414.

Abdel-Gayed, R.G., Bradley, D., 1985, *Criteria for Turbulent Propagation limits of Premixed Flames*, Combustion and Flame, Vol.62, pp.61-68.

Abdel-Gayed, R.G., Bradley, D., and Lawes, M., 1987, *Turbulent Burning Velocities: A General Correlation in Terms of Straining Rates*, Proc. Royal Soc., London A, Vol. 414, pp.389-413.

Ali, Y.B., 1995, *Fundamentals of Turbulent Combustion Related to Gasoline Engines*, PhD Thesis, School of Mechanical Engineering, The University of Leeds.

Amielh, M., Pietri, L., Lucas, J.F., and Anselmet, F., 2000, *Statistical Properties of the Velocity and Scalar Fields in Variable Density Jets*, The international Conference on Variable Density Turbulent Flows, 22-23 June, Banyuls, France.

Barrere, M., 1974, *Modèles de combustion turbulente, Revue générale de thermique*, Tome XIII, Vol.148, pp.295.

Batchelor, G.K., 1953, *The Theory of Homogeneous Turbulence*, Cambridge, Cambridge University.

Baum, M., Poinsot, T.J., Haworth, D.C., and Darabiha, N., 1994, *Direct Numerical Simulation of $H_2/O_2/N_2$ flames with complex chemistry in two-dimensional turbulent flames*, J. Fluid Mech. Vol.281, pp.1-32.

Beeley, J.F. and Gray, P., 1980, *Rapid Compression Studies on Spontaneous Ignition of Isoproyl Nitrate*, Combustion and Flame, Vol.39, pp.255-281.

Benson, S.W., 1976, *Thermochemical Kinetics*, Second Edition, Wiley & Son, New York.

Bilger, R.W., 1993, *Conditional Moment Closure for Turbulent Reacting Flows*, Physics of Fluids, A.5, pp.436-444.

Bilger, R.W., 2000, *Future Progress in Turbulent Combustion Research*, Progress in Energy and Combustion Science, Vol.26, pp.367-380.

Borghi, R., 1984, *Mise au point sur la structure des flammes turbulentes*, Journal de Chimie physique, Vol.81, pp.361-370.

Borghi, R., 1985, *On the Structure and Morphology of Turbulent Premixed Flames*, Recent Advances in the Aerospace Science, Plenum, New York, pp.117-138.

Borghi, R. and Gonzalez, M., 1986, *Application of Lagrangian Models to Turbulent Combustion*, Combustion and Flame, Vol.63, pp.239-250.

Borghi, R., 1988, *Turbulent Combustion Modelling*, Progress in Energy and Combustion Science, Vol.14, pp.245-292.

Boudier, P., Henriot, S., Poinsot, T., and Baritaud, T., 1992, *A Model for Turbulent Flame Ignition and Propagation in Spark Ignition Engines*, Twenty-fourth Symposium (International) on Combustion, The Combustion Institute, Pittsburgh, pp.503-510.

Bradley, D., Lau, A.K.C., and Lawes, M., 1992, *Flame Stretch Rate as a Determination of Turbulent Burning Velocity*, Philos. Trans. R.Soc. Lond.A pp.339-359.

Bradley, D., Lawes, M., Scott, M.J., and Mushi, E.M.J., 1994, *Afterburning in Spherical Premixed Turbulent Explosions*, Combustion and Flame, Vol.99, pp.581-590.

Bradley, D., Hicks, R.A., Lawes, M. and Sheppard, C.G.W., 1996a, *Study of Turbulent and Combustion Interaction: Measurement and Prediction of the Rate of Turbulent Burning*, Technical Report, School of Mechanical Engineering, The University of Leeds.

Bradley, D, Gaskell, P.H. and Gu, X.J., 1996b, *Burning Velocities, Markstein Lengths, and Flame Quenching for Spherical Methan-Air Flames: A Computational Study*, Combustion and Flame, Vol.104, pp.176-198.

Bradley, D., Hicks, R.A., Lawes, M., Sheppard, C.G.W., and Woolley, R., 1998, *The Measurement of Laminar Burning Velocities and Markstein Numbers for Iso-octane-air and Iso-octane-n-Heptane-Air Mixtures at Elevated Temperatures and Pressures in an Explosion Bomb*, Combustion and Flame, Vol.115, pp.126-144.

Bradley, D., Lawes, M. and Sheppard, C.G.W., 2000, *Combustion and the Thermodynamic Performance of Spark Ignition Engines*, Proc. Instn. Mech. Engrs, Part C, Vol.214, pp.257-268.
Bray, K.N.C. and Moss, J.B., 1977, Acta Astronauctica, Vol.4, pp.291-320.

Bray, K.N.C., Libby, P.A., Masuya, G. and Moss, J.B., 1981, *Turbulent Production in Premixed Turbulent Flames*, Combustion Science and Technology, Vol.25, pp.127-140.

Bray, K.N.C., 1985, *Laminar Flamelet Modelling of Turbulent Combustion*, Lecture Notes in Physics, Numerical Simulation of Combustion Phenomena, Proceedings of the Symposium Held at INRIA Sophia-Antipolis, France, pp.3-19.

Bray, K.N.C, Libby, P.A. and Moss, J.B., 1985, *Unified Modelling Approach for Premixed Turbulent Combustion, Part I: General Formulation*, Combustion and Flame, Vol.61, pp.87-102.

Bray, K.N.C., 1990, *Studies of the Turbulent Burning Velocity*, Proc. R. Soc. Lond. A, Vol.431, pp.315-335.

Bray, K.N.C. and Peters, N., 1994, *Laminar Flamelets in Turbulent Flames*, Turbulent Reacting Flows, Edited by Libby, P.A., and Williams, F.A., Academic Press, pp.63-113.

Bray, K.N.C. and Libby, P.A., 1994, *Recent Developments in the BML Model of Premixed Turbulent Combustion*, Turbulent Reacting Flows, Edited by Libby, P.A., and Williams, F.A., Academic Press, pp.115-151.

Bui-Pham, M., Seshadri, K. and Williams, F.A., 1992, *The Asymptotic Structure of Premixed Methane-Air Flames with Slow CO Oxidation*, Combustion and Flame, Vol.89, pp.343-362.

Burluka, A.A. and Borghi, R, 1995, *Studies of New Model for Small Scale processes in Turbulent Premixed Flames*, Archivum combustionis, Vol.15, No.3-4.

Burluka, A.A., 1996, *Améliorations des modèles de combustion turbulente en milieu prémélangé*, Thèse de doctorat de l'Université de Rouen.

Burluka, A.A., Gorokhovski, M.A. and Borghi, R., 1997, *Statistical Model of Turbulent Premixed Combustion With Interacting Flamelets*, Combustion and Flame, Vol.109, pp.173-187.

Cant, R.S. and Bray, K.N.C., 1988, *Strained Laminar Flamelet Calculations of Premixed Turbulent Combustion in a Closed Vessel*, Twenty-second Symposium (International) on Combustion/The Combustion Institute, Pittsburgh, pp.791-799.

Cant, R.S. and Bray, K.N.C., 1989, *A Theoretical Model of Premixed Turbulent Combustion in Closed Vessels*, Combustion and Flame, Vol.76, pp.243-263.

Cant, R.S., Pope, S.B., and Bray, K.N.C., 1990, *Modelling of Flamelet Surface-to-Volume Ratio in Turbulent Premixed Combustion*, Twenty-third Symposium (International) on Combustion, The Combustion Institute, Pittsburgh, pp.809-815.

Carmen, C.L., Feikema, D.A., 1998, *Monte Carlo Computation of Turbulent Premixed Methane-Air Ignition*, Combustion, Explosion, and Shock Waves, Vol.34, pp.253-259.

Checkel, M.D., Thomas, A., 1994, *turbulent Combustion of Premixed Flames in Closed Vessels*, Combustion and Flame, Vol.96, pp.351-370.

Chen, H., Chen, S. and Kraichnan, R.H., 1989, *Probability Distribution of a Stochastically Advected Scalar Field*, Phys. Rev. Lett., Vol.63, pp.2657-2660.

Ciezki, H.K. and Adomeit, G., 1993, *Shock-Tube Investigation of Self-Ignition of n-heptane-air Mixtures under Engine Relevant conditions*, Combustion and Flame, Vol.93, pp.421-433.

Clarkson, J., Griffiths, J.F., Macnamara, J.P. and Whitaker, B,J., 2001, *Temperature Fields During the Development of Combustion in a Rapid Compression Machine*, Combustion and Flame, Vol.125, pp.1162-1175.

Colucci, P.J., Jaberi, F.A., Givi, P. and Pope, S.B., 1998, *Filtered Density Function for Large Eddy Simulation of Turbulent Reacting Flows*, Physics of Fluids, Vol.10, pp.499-515.

Curl, R.L., 1963, *Dispersed Phase Mixing: I, Theory and Effects in Simple Reactors*, AIChE J,. Vol.9, pp.175-181.

Daeyup, L. and Simone, H., 1998, *Rapid Compression Machines: Heat Transfer and Suppression of Corner Vortex*, Combustion and Flame, Vol.114, pp.531-545.

Damokhler, G.Z., 1940, Elektrochemie Angewandte Phys. Chem., Vol.46, pp.601-626. English Translation: NACA TM 1112, 1947.

Debruynkops,S.M. and Riley, J.J., 1998, *Scalar Transport Characteristics of the Linear-Eddy Model*, Combustion and Flame, Vol.112, pp.253-260.

Desgroux, R., Minetti, R. and Sochet, L.R., 1996, *Temperature Distribution Induced by Pre-Ignition Reactions in a Rapid Compression Machine*, Combustion Science and Technology, Vol.113, pp.193-203.

Desjardin, P.E. and Frankel, S.H., 1996, *Assessment of Turbulent Combustion Submodels Using the Linear Eddy Model*, Combustion and Flame, Vol.104, pp.343-357.

Deuflhard., P., Nowak, U. and Poehle, U., 1989, *Integrator for Stiff System of Ordinary Differential Equations.*

Dixon-Lewis, G., 1990, *Structure of Laminar Flames*, Twenty-third Symposium (International) on Combustion, The Combustion institute, pp.305-324.

Dopazo, C., 1975, *Probability Density Function Approach for a Turbulent Axisymmetric heated Jet. Centerline Evolution*, Physics of Fluids, Vol.18, pp.397-404.

Dopazo, C. and O'Brien, E.E., 1976, *Statistical Treatment of Non-Isothermal Chemical Reactions in Turbulence*, Combustion Science and Technology, Vol.13, pp.99-122.

Dopazo, C., 1979, *Relaxation of initial Probability Density Functions in the Turbulent Convection of Scalar Fields*, Phys. Fluids Vol.22, pp.20-30.

Dopazo, C., 1994, *Recent Developments in pdf Methods*, Turbulent Reacting Flows, Edited by Libby, P.A., and Williams, F.A., Academic Press, pp.375-474.

Dryer, F.L. and Glassman, I., 1973, *High temperature oxidation of CO and CH_4*, 14th Symposium (international) on combustion, The Combustion Institute, Pittsburgh, pp.987-1003.

Duclos, J.M., Veynante, D., and Poinsot, T., 1993, *A Comparison of Flamelet Models for Premixed Turbulent Combustion*, Combustion and Flame, Vol.95, pp.101-117.

Duterque, J., Borghi, R. and Tichtinsky, H., 1981, *Study of Quasi-Global Schemes for Hydrocarbon Combustion*, Combustion Science and Technology, Vol.26, pp.1-15.

Edelman, R.B. and Fortune, O., 1969, *A Quasi Global Chemical Kinetic Model for Finite Rate Combustion of Hydrocarbon fuels*, AIAA Paper pp. 69-86.

Fichot, F., Lacas, F., Veynante, F., and Candel, S., 1993, *One-Dimensional Propagation of a Premixed Turbulent Flame with a Balance Equation for the Flame Surface Density*, Combustion Science and Technology, Vol.89, pp.35-60.

Fiock, E.F., Marvin, C.F., Caldwell, F.R., and Roeder, C.H., 1940, Natl. Advisory Comm. Aeronaut. Repts., Bo.682.

Frank, J., Griffiths, J.F. and Nimmo, W., 1986, *The Control of Spontaneous Ignition under Rapid Compression*, Twenty-first Symposium (International) on Combustion, The Combustion Institute, Pittsburgh, pp.447-454.

Frankel, S.H., Mcmurtry, P.A. and Givi, P., 1995, *Linear Eddy Modelling of Reactant Conversion and Selectivity in Turbulent Flows*, AIChE J., Vol.41, pp.258-266.

Friedman, R. and Cyphers, J.A., 1956, *On the Burning Rate of Carbon Monoxide*, Journal of Chemical Physics, Vol.25, pp.448-457.

Fristrom, R.M., and Westenberg, A.A., 1965, *Flame Structure---Its Measurement and Interpretation*, McGraw Hill.

Frost, V.A., 1960, *A Mathematical Model of Turbulent Combustion*, Third All-Union Conf. On Combustion Theory, Vol.1, pp.121-125, Press of Academy of Sciences USSR.

Frost, V.A., 1975, *Model of a Turbulent Diffusion-Controlled Flame Jet*, Fluid Mech. Soviet. Res. 4(2), 124-133.

Glarborg, P., Miller, J.A. and Kee, R.J., 1986, *Kinetics Modelling and Sensitivity Analysis of Nitrogen Oxide Formation in Well-Stirred Reactors, Combustion and Flame*, Vol.65, pp.177-202.

Glassman, I., 1996, *Combustion*, Third Edition, Academic Press.

Green, R.M. and Cloutman, L.D., 1997, *Planar LIF Observation of Unburned Fuel Escaping the Upper Ring-Land Crevice in a SI Engine*, SAE Paper, 970823.

Griffiths, J.F., and Singh, H.J., 1982, J. Chem. Soc. Farady. Trans. 1, Vol.78, pp.747-760.

Griffiths, J.F., 1985, *Thermokinetic Interactions in Simple Gaseous Reactions*, Ann. Rev. Phys. Chem., Vol.36, pp.77-104.

Griffiths, J.F., Rose, D.J., Schreiber, M., Meyer, J. and Knoche, K.F., 1992, *Novel Features of End-Gas Autoignition Revealed by Computational Fluid Dynamics*, Combustion and Flame, Vol.91, pp.209-212.

Griffiths, J.F., Jiao, Q., Kordylewski, W., Schreiber, M., Meyer, J. and Knoche, F., 1993, *Experimental and Numerical Studies of Ditertiary Butyl Peroxide Combustion at High Pressures in a Rapid Compression Machine*, Combustion and Flame, Vol.93, pp.309-321.

Gu, X.J., Haq, M.Z., Lawes, M., and Woolley, R., 2000, *Laminar Burning Velocity and Markstein Lengths of Methane-air Mixtures*, Vol.121, pp.41-58.

Hakgerg, B., and Gosman, A.D., 1984, *Analysis Determination of Turbulent Flame Speed From Combustion Models*, Twentieth Symposium (International) on Combustion, The Combustion Institute, pp.225-232.

Haq, M.Z., 1998, *Fundamental Studies of Premixed Combustion*, PhD Thesis, School of Mechanical Engineering, The University of Leeds.

Haworth, D.C., and Poinsot, T.J., 1992, *Numerical Simulations of Lewis Number Effects in Turbulent Premixed Flames*, J. Fluid Mech. Vol.244, pp.405-436.

Hayase, T., Humphrey, J.A.C. and Greif, R., 1992, *A Consistently Formulated QUICK Scheme for Fast and Stable Convergence Using Finite-Volume Iterative Calculation Procedures*, J. Comput. Phys., Vol.98, pp.108-118.

Howard, J.B., Williams, G.C. and Fine, D.H., 1973, *Kinetics of Carbon Monoxide Oxidation in Postflame Gases*, 14th Symposium (international) on combustion, The Combustion Institute, Pittsburgh, pp.975-985.

Hottel, H.C., Williams, G.C., Nerheim, N.M. and Schneider, G.P.,1965, *Kinetic Studies in Stirred Reactors: Combustion of Carbon Monoxide and Propane*, 10th Symposium (international) on Combustion, The Combustion Institute, Pittsburgh, pp.111-121.

Indritz, D., Stone, J., and Williams, F., 1978, *Vapour Pressure of Di-tert-butyl peroxide*, J. Chem. Eng. Data, Vol.23, pp.6-7.

Jones, W.P. and Whitelaw, J.H, 1982, *Calculation Methods for Reacting Turbulent Flows: A Review*, Combustion and Flame, Vol.48, pp.1-26.

Jones, W.P. and Kollmann, W., 1987, Turb. Shear Flows. 5, Springer Verlag.

Jones, W.P. and Lindstedt, R.P., 1988, *Global reaction schemes for hydrocarbon combustion*, Combustion and Flame, Vol.73, pp.233-249.

Karpov, V.P., and Severin, E.S., 1980, *Effects of Molecular-Transport Coefficients on the Rate of Turbulent Combustion*, Combustion, Explosion and Shock Waves, Vol.16, pp.41-46.

Kee, R.J., Grcar, J.F., Smooke, M.D. and Millier, J.A., 1985, *Sandia Report SAND85-8240.*

Kerstein, A.R., 1988, *A Linear-Eddy Model of Turbulent Scalar Transport and Mixing*, Combustion Science and Technology, Vol.60, pp.391-421.

Kerstein, A.R., 1989, *Linear-Eddy Modelling of Turbulent Transport, II: Application to Shear Layer mixing*, Combustion and Flame, Vol.75, pp.397-413.

Kerstein, A.R., 1990, *Linear-Eddy Modelling of Turbulent Transport, Part 3, Mixing and Differential Molecular Diffusion in a Round Jet*, J. Fluid Mech, Vol.216, pp.411-435.

Kerstein, A.R., 1991, *Linear-Eddy Modelling of Turbulent Transport, part 6, Microstructure of Diffusive Scalar Mixing Fields*, J. Fluid Mech, Vol.231, pp.361-394.

Kerstein, A.R., 1992, *Linear-Eddy Modelling of Turbulent Transport, part 4, Structure of Diffusion Flames*, Combustion Science and Technology, Vol.81, pp.75-96.

Khitrin, L.N., 1963, *Combustion in Turbulent Flow: Proceedings of the Moscow Seminar on Combustion Held at the Energetics Institute of the U.S.S.R.* Academy of Sciences; Edited by Khitrin, L. N.

Klimenko, A.Y., 1990, *Multi-Component Diffusion of Various Scalars in Turbulent Flows*, Fluid Dyn., Vol.25, pp.327-334.

Klimenko, A.Y. and Bilger, R.W., 1999, *Conditional Moment Closure for Turbulent Combustion*, Progress in Energy and Combustion Science, Vol.25, pp.595-687.

Kobayashi, H., Kawabata, Y., and Maruta, K., 1998, *Experimental Study on General Correlation of Turbulent Burning Velocity at High Pressure*, The Twenty-Seventh Symposium (International) on Combustion, The Combustion Institute, pp.941-948.

Kolmogorov, A., Petrovskii, I., and Piskunov, N., 1937, *Study of the Diffusion Equation with Growth of the Quantity of Matter and its Application to a Biology Problem*, Bull. MGU, Moscow State University, USSR A 1(6).

Kozlov, G.I., 1959, *On High Temperature Oxidation of Methane*, Seventh Symposium (international) on combustion, The Combustion Institute, Pittsburgh, pp.142-149.

Kuznetsov, V.R., 1972, *Passive Contaminant Concentration Probability in Turbulent Flows with Transverse Shear*, Izv. AN SSSR, MZhG, No.5, pp.86-91.

Kuznetsov, V.R. and Sabel'nikov, V.A., 1990, *Turbulent and Combustion*, Revised and Augmented for the English Edition, Hemisphere Publishing Corporation.

Lavrov, N.V. and Karbirnichi-Kuznetsuv, V.B., 1968, *Experimental Study of Overall Kinetics of CO Combustion*, Nank, Uzb SSR, 25, 9.

Leisenheimer, B, and Leuckel, W., 1996, *Self-Generated Acceleration of Confined Deflagrative Flame Fronts*, Combustion Science and Technology, Vol.118, pp.147-164.

Lewis, B., and von. Elbe, G., 1951, *Combustion, Flame and Explosions of Gases*, New York. Academic Press.

Libby, P.A., 1989, *Theoretical Analysis of the Effect of Gravity on Premixed Turbulent Flames*, Combustion Science and Technology, Vol.68, pp.15-33.

Linnett, J.W., 1953, *Methods of Measuring Burning Velocities*, Fourth Symposium (International) on Combustion (Combustion and Detonation Waves), The Combustion Institute, Pittsburgh, pp.21-35.

Lipatnikov, A.N., and Chomiak, J., 2000, *Transient and Geometrical Effects in Expanding Turbulent Flames*, Combustion Science and Technology, vol.154, pp.75-117.

Lipatnikov, A.N., and Chomiak, J., 2001, *Turbulent Flame Speed and Thickness: Phenomenology, Evaluation, and Application in Multi-Dimensional Simulations*, Progress in Energy and Combustion Science, Vol.28, pp.1-74.

Liu, K., Burluka, A.A., Woolley, R., Sheppard, C.G.W., and Lipatnikov, A.N., 2001, *On the development of the turbulent mass burning rate*, The third Asia-Pacific Conference on Combustion, June 24-27, Seoul, Korea.

Lyon, R.K., Hardy, J.E. and William von Holt, 1985, *Oxidation Kinetics of Wet CO in Trace Concentrations*, Combustion and Flame, Vol.61, pp.79-86.

Mantel, T., and Samaniego, J.M., 1999, *Fundamental Mechanisms in Premixed Turbulent Flame Propagation via Vortex-Flame Interactions, Part II: Numerical Simulation*, Combustion and Flame, Vol.118, pp.557-582.

Mcmurtry, P.A., Menon, S. and Kerstein, A.R., 1992, *A Linear Eddy Sub-Grid Model for Turbulent Reacting Flows: Application to Hydrogen-Air Combustion*, Twenty-fourth Symposium (International) on Combustion, The Combustion Institute, Pittsburgh, pp.1445-1460.

Miller, J.A., Mitchell, R.E., Smooke, M.D., and Kee, R.J., 1982, *Toward A Comprehensive Chemical Kinetic Mechanism for the Oxidation of Acetylene: Comparison of Model Prediction with Results From Flame and Shock Tube Experiments*, Nineteenth Symposium (International) on Combustion, The Combustion Institute, pp.181-196.

Mullins, B.P., 1953, *Studies on the Spontaneous Ignition of Fuels Injected into a Hot Air Stream*, Fuel, Vol.32, pp.211-252.

Nakahara, M., and Kido, H., 1998, *A Study of the Premixed Turbulent Combustion Mechanism Taking the Preferential Diffusion Effect into Consideration*, Memoires of the Faculty of Engineering Kyushu Univ., Vol.58,pp.55-82.

O'Brien, E.E., 1980, *The Probability Density Function (pdf) Approach to Reacting Turbulent Flows*, Turbulent Reacting Flows (Topics in Applied physics, Vol.44), Springer-Verlag, pp.185-218.

Pasquill, F. and Smith, F.B., 1983, *Atmosphere Diffusion*, Third Edition, Wiley, New York.

Patankar, S.V., 1980, *Numerical Heat Transfer and Fluid Flow*, Hemisphere Publishing Corporation, McGraw-Hill Book Company.

Peeters, J. and Mahnen, G., 1973, *Reaction Mechanisms and Rate Constants of Elementary Steps in Methane-Oxygen Flame*, Fourteenth Symposium (international) on combustion, The Combustion Institute, Pittsburgh, pp.133-146.

Peters, N., 1986, *Laminar Flamelet Concept in turbulent combustion*, Twenty-first Symposium (International) on Combustion/The Combustion Institute, Pittsburgh pp.1231-1250.

Peters, N and Williams, F.A., 1987, *The Asymptotic Structure of Stoichiometric Methane-Air Flames*, Combustion and flame, Vol.68, pp.185-207.

Peters, N., 2000, *Turbulent Combustion*, Cambridge University Press.

Pope, S.B., 1976, *The Probability Approach to the Modelling of Turbulent Reacting Flows*, Combustion and Flame, Vol.27, pp.299-312.

Pope, S.B., 1981, *A Monte-Carlo Method for the pdf equations of turbulent reactive flow*, Combustion Science and Technology, Vol.25, pp.159-174.

Pope, S.B., 1982, *An improved Turbulent Mixing Model*, Combustion Science and Technology, Vol.28, pp.131-145.

Pope, S.B., 1985, *PDF Methods for Turbulent Reactive Flows*, Progress in Energy and Combustion Science, Vol.11, pp.119-192.

Pope, S.B., 1990, *Computations of Turbulent Combustion: Progress and Challenges*, Twenty-third Symposium (International) on Combustion/The Combustion Institute, Pittsburgh, pp.591-612.

Pope, S.B. and Chen, Y.L., 1990, *The Velocity-Dissapation Probability density Function Model for Turbulent Flows*, Physics of Fluids, A: Fluid Dynamics, pp.1437-1449.

Pope, S.B., 1991, *Application of the Velocity-Dissipation Probability Density Function Model to Inhomogeneous Turbulent Flow*, Physics of Fluids, A: Fluid Dynamics, pp.1947-1957.

Rankin, D.D., Weinberg, F.J., 1998, *Location of the Schlieren Image in a Premixed Flames: Axially Symmetrical Refractive Index Fields*, Combustion and Flame, Vol.113, pp.303-311.

Reid, R.C., Prausnitz, J.M., and Sherwood, T.K., 1977, *the Properties of Gases and Liquids*, Forth Edition, McGraw-Hill, New York.

Ronney, P.D., 1985, *Some Open Issures in Premixed Turbulent Combustion*, Lecutre Notes in Pyhsics, Edited by T.Takeno, J.Buckmaster, Springer-Verlag, New York, pp.1-22.

Sabel'nikov, V., and Gorokhovski, M, 2001, TSFP-2, June, 2-29, Stokholm, pp.6.

Schetinkov, V.M., 1970, *Physics of Gaseous Combustion*, Izdvo Nauka, Moscow.

Scott, M.J., 1992, *Distributions of Strain Rate and Temperature in Turbulent Combustion*, PhD Thesis, School of Mechanical Engineering, The University of Leeds.

Seshadir, K. and Peters, N., 1990, *The Inner Structure of Methane-Air Flames*, Combustion and Flame, Vol.81, pp.96-118.

Seshadri, K, Williams, F.A., 1994, *Reduced Chemical Systems and Their Application in Turbulent Combustion*, Turbulent Reacting Flows, Edited by Libby. P.A., and Williams, F.A., Academic Presss.

Shcherbina, Yu, A., 1982, *Statistical Characteristics of Turbulent Transport*, Dolgoprudnyi, MFTI.

Shinjin, K. and Tetsunori, S.,1993, *Autoignition-Delay Measurement over Lean to Rich Mixtures of n-butane/air under Swirl Conditions*, Combustion and Flame, Vol.92, pp.254-265.

Smoot, L.D, Hecker, W.C. and Williams, G.A., 1976, *Prediction of Propagating Methane-Air Flames*, Combustion and Flame, V01.26, pp.323-342.

Snyder, W.H. and Lumley, J.L., 1971, *Some Measurements of Particle Velocity Autocorrelation Functions in a Turbulent Flow*, J. Fluid Mech., Vol.48, pp.41-71.

Sobolev, G.K., 1959, *High Temperature Oxidation and Burning of Carbon Monoxide*, Seventh Symposium (international) on combustion, The Combustion Institute, Pittsburgh, pp.386-391.

Spadaccini, L.J. and Colket III, M.B., 1994, *Ignition Delay Characteristics of Methane Fuels*, Prog. Energy Combust. Sci., Vol.20, pp.431-460.

Spalding, D.B., 1971, *Mixing and Chemical Reaction in Steady Confined Turbulent Flames*, Thirteenth Symposium (International) on Combustion, The Combustion Institute, Pittsburgh, pp.649- 657.

Spalding, D.B., 1998, *Turbulent Mixing and Chemical Reaction; the Multi-Fluid Approach*, London, see lectures at the web site: *http://www.cham.co.uk.*

Subramaniam, S. and Pope, S.B., 1998, *A Mixing Model for Turbulent Reactive Flows Based on Enclidian Minimum Spanning Trees*, Combustion and Flame, Vol.115, pp.487-514.

Swaminathan, N. and Bilger, R.W., 2001, *Analyses of Conditional Moment Closure for Turbulent Premixed Flames*, Combustion Theory and Modelling, Institute of Physics Publishing, Vol.5, pp.241-260.

Tabaczynski, R.J., Hoult, D.P., and Keck.J.C., 1970, *High Reynolds Number Flow in a Moving Corner*, J. Fluid Mech., Vol.42, pp.249-255.

Tavoularis, S. and Corrsin, S., 1981, *Experiments in Nearly Homogeneous Turbulent Shear Flow with Uniform Mean Temperature Gradient, Part 1*, J. Fluid Mech., Vol.104, pp.311-347.

Valiño, L., and Dopazo, C., 1991, *A Binomial Langevin Model for Turbulent Mixing*, Phys. Fluid A, Vol.3, pp-3034-3037.

Versteeg, H.K. and Malalasekera, W., 1995, *An Introduction to Computational Fluid Dynamics: The Finite Volume Method.* Longman Group Ltd.

Vincent, S., Burluka, A., Said, R., and Borghi, R., 1996, *Modelling of Spark Ignition in a Premixed Turbulent Medium*, SAE Paper, 961193.

Villermaux, J. and Devillon, J.C., 1972, *Représentation de la coalescence et de la redispersion des domaines de ségrégation dans un fluide par un modèle d'interaction phénoménologique*, proceedings of the second international symposium on chemical reaction engineering, Elsevier, New York, pp.1611-1621.

Walker, D.W., Diehl, L.H, Strauss, W.A. and Edse, R., 1969, *Investigation of the Ignition Properties of Flowing Combustible Gas Mixtures*, USAF Reprot AFAPL-TR-69-82.

Walker, R.E. and Westenberg, A.A., 1960, *Molecular Diffusion Studies in Gases at High Temperature, III. Results and Interpretation of the He---A System*, Journal of Chemical Physics., Vol.31, pp.436-519-525.

Warnatz, J., 1981, *The Structure of Laminar Alkane-, Alkene-, and Acetylene Flame*, Eighteenth Symposium (International) on Combustion, The Combustion Institute, pp.369-381.

Weinberg, F.J., 1955, *Location of the Schlieren Image in a Flame*, Fuel, Vol.34, pp.84-87.

Westbrook, C.K., Creighton, J., Lund, D. and Dryer, F.L., 1977, *A numerical model of chemical kinetics of combustion in a turbulent flow reactor*, Journal of Physical Chemistry, Vol.81, pp.2542-2554.

Westbrook, C.K. and Dryer, F.L., 1979, *A Comprehensive Mechanism for methanol Oxidation, Combustion Science and Technology*, Vol.20, pp.125-140.

Westbrook, C.K. and Dryer, F.L., 1980a, *Prediction of Laminar Flame Properties of Methane-Air Mixtures*, Combustion and Flame, Vol.37, pp.171-192.

Westbrook, C.K. and Dryer, F.L., 1980b, *Chemical Kinetics And Modelling of Combustion Progresses*, Eighteenth Symposium (international) on combustion, The Combustion Institute, Pittsburgh, pp.749-764.

Westbrook, C.K. and Dryer, F.L., 1981, *Simplified Reaction Mechanisms for the Oxidation of Hydrocarbon Fuels in Flames*, Combustion Science and Technology, Vol.27, pp.31-43.

Westbrook, C.K. and Dryer, F.L., 1984, *Chemical Kinetic Modelling of Hydrocarbon Combustion*, Progress in Energy and Combustion Science, Vol.10, pp.1-57.

Williams, G.C., Hottel, H.C. and Morgan, A.C., 1969, *The Combustion of Methane in Jet-Mixed Reactor*, Twelfth Symposium (international) on combustion, The Combustion Institute, Pittsburgh, pp.913-925.

Woolley, R., 2001, Private Communication.

Yeo, J., 1994, *Autoignition in Gasoline Engines*, PhD Thesis, School of Mechanical Engineering, The University of Leeds.

Yetter, R.A., Dryer, F.L. and Rabitz, H., 1991, *A Comprehensive Reaction Mechanism for Carbon Monoxide/Hydrogen/Oxygen Kinetics*, Combustion Science and Technology, Vol.79, pp.97-128.

Zel'dovich, Y.B., 1948, Zhur. Fizi. Khi. (USSR), Vol.22, pp.27-49, English Translation in NACA TM 1282, 1951.

Zel'dovich, Y.B., 1980, *Flame Propagation in a Substance Reacting at Initial Temperature*, Combustion and Flame, Vol.39, pp.219-224.

Zel'dovich, Y.B., 1985 *The Mathematical Theory of Combustion and Explosions*, Translated from Russian by Donald H. McNeil , New York.

Zimont, V.L., 1979, *Theory of Turbulent Combustion of a Homogeneous Fuel Mixture at High Reynolds Numbers*, Combustion, Explosion and Shock Waves, Vol.15, pp.305-311.